Laser cooling of atomic gases

Jean Dalibard
Collège de France, chair *Atoms and radiation*

Lecture series 2014-15

COLLÈGE
DE FRANCE
1530

Contents

Introduction

Can the thermodynamic equilibrium of a sample of matter be controlled by a well-chosen electromagnetic radiation? Since the seminal papers by Einstein in 1917 and Kastler in 1950, this question has accompanied the development of atomic physics and quantum optics. From the 1970s onwards, the development of tunable laser sources has renewed the subject, with proposals to cool gases of neutral atoms or ions (Hänsch & Schawlow 1975; Wineland & Dehmelt 1975). The development of this research field have gone far beyond the most optimistic initial predictions. Laser cooling of atomic particles enables the temperature of a gas to be lowered from room temperature (300 K) to a range between millikekelvin and microkelvin, or even below in certain special cases (figure 1).

Cold atoms are ubiquitous in time and frequency metrology experiments, as well as in most high-precision measurements in atomic physics. Radiative cooling has also paved the way for the production of quantum gases such as Bose-Einstein condensates, in which large numbers of particles accumulate in a single microscopic state. It allows us to approach the limit where the thermal wavelength of the gas particles, $\lambda_T \sim h/Mv$, where h is Planck's constant, M the mass of an atom and v the average velocity at thermal equilibrium, becomes comparable to the distance between particles. It should be noted, however, that radiative cooling does not generally lead directly to the condensation threshold. It is followed by a phase of evaporative cooling, which lowers the temperature by one or two orders of magnitude (figure 1).

Radiative cooling has been applied to many atomic species, more than thirty to date (see figure 2). The only determining factor is the availability of sufficiently reliable, intense (and relatively inexpensive) continuous laser sources to resonantly excite an atomic transition. The aim of this course is to present the evolution of the main ideas behind radiative cooling, and to discuss their performance and limitations. We will not attempt to describe here all the methods that have been proposed, but will concentrate on a few important principles:

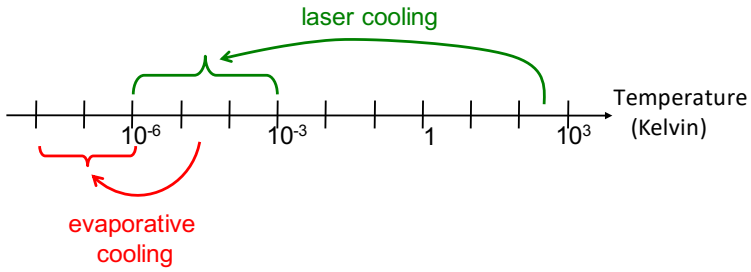

Figure 1. *Temperature scale showing the gain resulting from laser cooling of atomic gases and the additional gain from evaporative cooling.*

- The Doppler effect, which provides an atomic response to the light wave that depends on the atomic velocity.
- The Sisyphus mechanism, which forces the atom to climb more potential hills than it descends.
- The use of dark states, which involves hiding atoms in the shadow, i.e. accumulating them in states where they are effectively decoupled from light.

As a preliminary, it is probably worth clarifying what we mean by *cooling*, a sometimes subtle notion that may concern filtering, temperature lowering or even an increase in phase-space density.

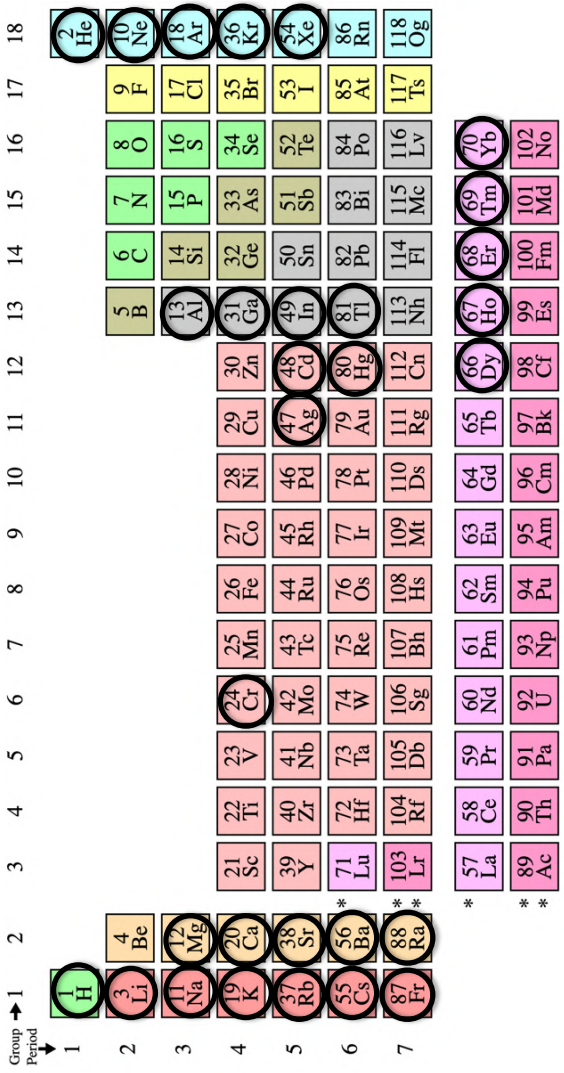

Figure 2. *Atomic species that have been laser cooled [periodic table from wikipedia].*

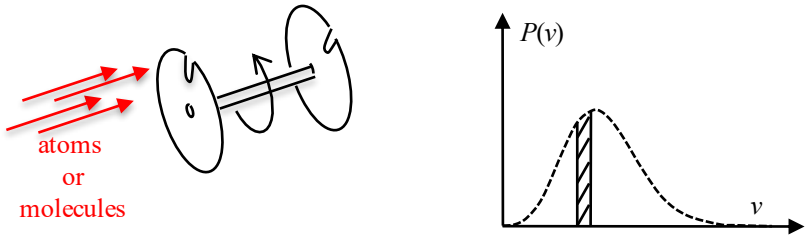

Figure 3. *Velocity selection of an atomic or molecular beam by means of a rotating wheel. There is no increase in the density of a given velocity class.*

Let us look at two examples. Starting from an atomic beam with a wide velocity distribution Δv, we can filter a slice of width $\delta v \ll \Delta v$ by a rotating wheel (figure 3). The gas is not cooled, but separated into two parts, one consisting of the desired velocity range, which is transmitted by the wheel, and the other, which sticks to the walls of the wheel. This filtering is very different from accumulating all the atoms of the beam in the slice δv, as is done when slowing down an atomic beam using the radiation pressure force. The gain in brightness can be several orders of magnitude in the latter case.

A second example will enable us to distinguish between *lowering temperature* and *increasing phase-space density*. Let us consider an assembly of particles of mass M in a 1D harmonic trap of frequency ω, at thermodynamic equilibrium at temperature T:

$$\frac{1}{2}M\omega^2\Delta x^2 = \frac{1}{2}M\Delta v^2 = \frac{1}{2}k_{\mathrm{B}}T, \tag{1}$$

where Δx and $\Delta v = \omega\,\Delta x$ are the standard deviations of the position and velocity distributions. Let us suppose we open this trap by modifying its frequency. This opening, if sufficiently slow, maintains thermal equilibrium with a temperature T' which can be deduced from T via the adiabatic theorem:

$$\frac{T'}{\omega'} = \frac{T}{\omega} \quad \Rightarrow \quad T' = T\frac{\omega'}{\omega} < T. \tag{2}$$

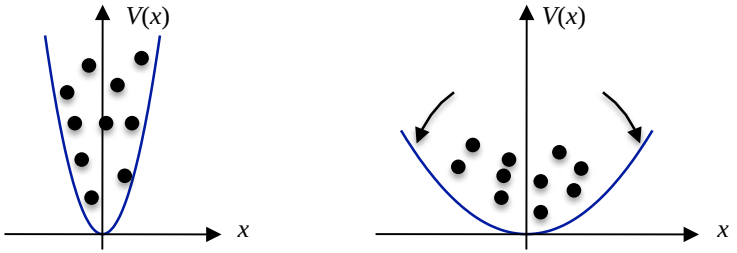

Figure 4. *Adiabatic opening of a harmonic trap, the frequency changing from ω to $\omega' < \omega$.*

So we do have cooling. The new widths in position and velocity are:

$$\Delta x' = \Delta x \left(\frac{\omega}{\omega'}\right)^{1/2}, \qquad \Delta v' = \Delta v \left(\frac{\omega'}{\omega}.\right)^{1/2} \tag{3}$$

We therefore divided the width of the velocity distribution by the factor $(\omega/\omega')^{1/2}$, and multiplied the width of the position distribution by the same factor. The phase space density, proportional to $(\Delta x \Delta v)^{-1}$, is unchanged in this process: we have simply exchanged a good knowledge of position and a bad knowledge of velocity by its inverse.

In this second example, we can see that cooling does not necessarily lead to an increase in phase-space density, nor – to put it in quantum terms – to an increase in the population of an individual quantum state. Yet this increase is essential for many laser-cooling experiments on atoms, since one of the aims of these experiments is to approach, or even reach, the quantum degeneracy threshold and Bose-Einstein condensation.

In fact, for a system of N independent particles (i.e. an ideal gas), we can easily show that this increase can never be obtained in a Hamiltonian evolution of the gas. The reasoning is simple : let us start with the one-body density operator $\hat{\rho}$ characterizing the state of the gas. This operator can be diagonalized and its eigenvalues $\pi_1, \pi_2, \ldots$, all real positive or zero with $\sum_j \pi_j = 1$, give us the occupation probabilities of the different quantum states. Suppose the evolution of the gas of particles between t_i and t_f is governed by the Hamiltonian

$$\hat{H}(t) = \sum_{n=1}^{N} \hat{H}^{(n)}(t), \tag{4}$$

where $\hat{H}^{(n)}$ is the Hamiltonian of the n-th particle. At time t_f, the single-particle density operator will simply be

$$\hat{\rho}(t_f) = \hat{U}(t_i \to t_f)\ \hat{\rho}(t_i)\ \hat{U}^{\dagger}(t_i \to t_f), \tag{5}$$

where the single-particle evolution operator $\hat{U}(t_i \to t_f)$ is calculated from $\hat{H}^{(n)}$. We do not need an explicit expression for $\hat{U}$ here. The only important point is that this operator is unitary: the eigenvalues of $\hat{\rho}(t_f)$ are always identical to the eigenvalues of $\hat{\rho}(t_i)$. We cannot therefore hope to accumulate particles in a given state via a purely Hamiltonian process (such as the opening of the trap in figure 4) when these particles are independent.

Examination of the assumptions required to arrive at this somewhat negative conclusion gives us the approach we need to take to move forward:

(i) We have considered a Hamiltonian process. The system considered above was not necessarily isolated since $\hat{H}$ can be time-dependent, but we have made the assumption that our assembly of N particles is not coupled to another quantum system that could act as a reservoir. This is precisely what will happen in laser cooling. Each atom is coupled to all modes of the electromagnetic field, notably via spontaneous emission processes: the evolution of the atom's reduced density matrix is therefore non-Hamiltonian, and we may well increase one of its eigenvalues to the detriment of the others.

(ii) We have considered a system of independent particles. If the particles interact with each other, then it is possible to change the occupation of the single-particle energy levels by an appropriate variation of the Hamiltonian $\hat{H}(t)$. In particular, it is possible to produce a Bose-Einstein condensate by modifying only the potential confining the N particles, without introducing any coupling with an external quantum system, or evaporating any particles. The total entropy of the gas is unchanged (or even increased if the process is irreversible), but the number of particles occupying the ground level of the trap can nevertheless increase dramatically during this transformation. We will see an example of this below.

The course will run as follows.

- Chapter 1 will be devoted to the seminal approach of Einstein (1916) and Einstein (1917). Einstein showed how the motion of atoms coupled to electromagnetic radiation is analogous to Brownian motion, and why the Doppler effect leads to the thermalization of an atom coupled to blackbody radiation.
- The second chapter will also be devoted to Doppler cooling, now with lasers; we will also describe its equivalent in position space, the magneto-optical trap, and encounter the first signature of an effective atom-atom interaction created by light.
- In the third chapter, we will look at the possibility of manipulating narrow-line atoms, and we will discuss the possibility of accumulating atoms in velocity classes that are weakly coupled to light.
- This notion of atoms accumulating in darkness will be explored further in Chapter 4, with the use of dark states and discussion of the very special statistical laws (Lévy's laws) that can arise.
- Chapter 5 will focus on the Sisyphus effect, which is at work in most cooling experiments and leads very simply to velocity distributions limited only by the recoil associated with a single photon. We will focus in particular on recent developments in grey molasses, which extend the concept of Sisyphus cooling.
- Finally, Chapter 6 will be devoted to sideband cooling, and will give us the opportunity to review the maximum phase-space density that can be expected in this type of radiative cooling experiment.

Let us stress once again that our aim is not to make an exhaustive review of all the devices that have been proposed or studied since the initial articles by Hänsch & Schawlow (1975) and by Wineland & Dehmelt (1975). Rather, it is to outline the principles of the mechanisms currently in use, and to illustrate them with recent experiments, in the hope of stimulating the exploration of new avenues.

Chapter I

Atoms and light in thermal equilibrium

The starting point for this course is blackbody radiation, i.e. the electromagnetic radiation emitted by a material body in thermodynamic equilibrium with its environment. The spectral distribution of this radiation is a universal law that depends only on the body's temperature. It is given by Planck's law, proposed in 1900:

$$\rho(\omega, T) = \frac{\hbar\omega^3}{\pi^2 c^3} \frac{1}{\mathrm{e}^{\hbar\omega/k_\mathrm{B}T} - 1}, \tag{I.1}$$

where $\rho(\omega)\,\mathrm{d}\omega$ represents the electromagnetic energy per unit volume corresponding to radiation with a frequency between ω and $\omega + \mathrm{d}\omega$.

A modern version (and completely equivalent as we will see in what follows) of this law consists in giving ourselves a quantization volume of finite size and positing that the average number of photons in a mode of frequency ω is given by the Bose-Einstein law with a zero chemical potential

$$\bar{n}(\omega, T) = \frac{1}{\mathrm{e}^{\hbar\omega/k_\mathrm{B}T} - 1}\,. \tag{I.2}$$

Starting from Planck's law (I.1), Einstein (1917) studied how radiation with this spectral energy density would impose its temperature on a collection of atoms. To do this, he introduced the notion of the friction force caused by light on a moving atom, a friction force identical in every respect to that proposed almost 60 years later by Hänsch & Schawlow (1975) and at work in the Doppler molasses used in today's laboratories. Einstein's reasoning is identical to the one we will be using to deal with the motion of atoms in laser beams, with arguments based on the notion of Brownian motion, which we will also review in this chapter.

1 Einstein 1916: absorption and emission

In 1916, having just published his theory of General Relativity, Einstein returned to the study of energy and momentum exchange between atoms and radiation. To pursue this theme, which he had already addressed in 1905 in his study of the photo-electric effect, he took as his guiding principle the achievement of thermodynamic equilibrium.

Einstein considered a collection of atoms illuminated by black-body radiation at temperature T (figure I.1). His aim was to model the way in which the atom and the radiation can exchange energy. The only constraint Einstein imposes is statistical physics consistency: the average population distribution of the atom's different energy levels must be a Boltzmann distribution with the same temperature T. In a two-level model of the atom, with a ground state g and an excited state e separated by an energy $\hbar\omega_\mathrm{A}$ (figure I.2, left), the ratio of populations $P_{g,e}$ must be such that:

$$\frac{P_e}{P_g} = \exp\left(-\frac{\hbar\omega_\mathrm{A}}{k_\mathrm{B}T}\right). \tag{I.3}$$

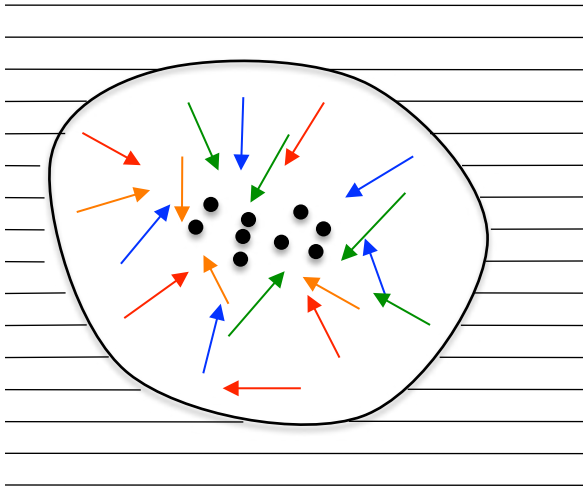

Figure I.1. *The problem considered by Einstein: an assembly of independent atoms is illuminated by radiation from a black body at temperature T. Will this assembly of atoms thermalize with the black-body radiation, in terms of both its internal and external degrees of freedom?*

1-1 Elementary processes and steady state

To explain how such a state of equilibrium can be achieved, Einstein studies the competition between photon absorption processes[1] and emission processes:

- If the atom is in its ground state, it can absorb a photon and reach its excited state (figure I.3). Einstein postulated that the probability of this process occurring over an infinitesimal time interval $\mathrm{d}t$ is proportional to $\mathrm{d}t$ and to the energy density of the radiation ρ, taken at the frequency[2] for the atomic resonance ω_A:

$$\mathrm{d}P_{g\to e} = B\ \rho(\omega_\mathrm{A})\ \mathrm{d}t, \tag{I.4}$$

[1] Einstein does not use the term photon, which will not be introduced until much later (1926) by Lewis.

[2] We will frequently use the usual denomination *frequency* for the quantity ω, although it is in fact an *angular frequency*, the frequency being $\omega/2\pi$.

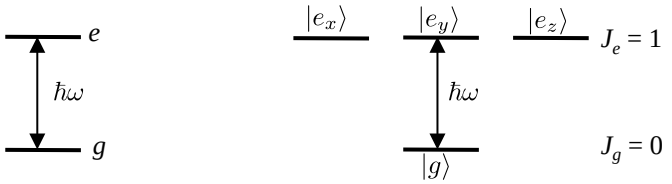

Figure I.2. *The two atomic transition models considered in this chapter. On the left, a two-level atom; on the right, a $J_g = 0 \leftrightarrow J_e = 1$ transition that correctly takes into account phenomena linked to the polarization of light. We will choose as a basis of the excited level the states $|e_j\rangle$ whose angular momentum projection on the j axis is zero ($j = x, y, z$).*

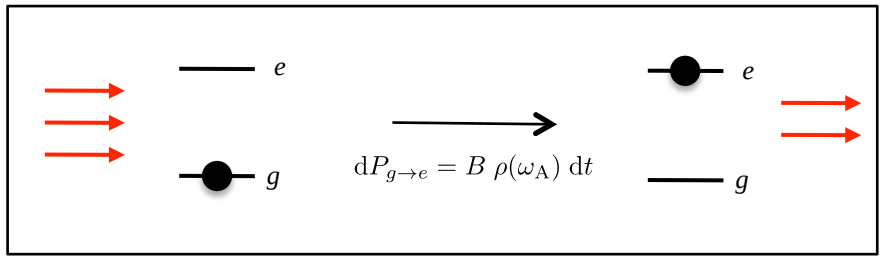

Figure I.3. *Absorption process.*

where B is an undetermined coefficient at this stage.

- If the atom is in the excited state, it can fall back to the ground state by emitting a photon. The probability of this emission occurring during $\mathrm{d}t$ is the sum of two terms. On the one hand, even if no photon is initially present, the atom can go from e to g by spontaneous emission of a photon (figure I.4) with probability:

$$\mathrm{d}P_{e\to g}|_{\mathrm{spont.}} = A\ \mathrm{d}t, \tag{I.5}$$

i.e. a law which, as Einstein points out, is identical to that of radioactive decay. On the other hand, emission can be stimulated by the radiation already present at atomic frequency, with probability

$$\mathrm{d}P_{e\to g}|_{\mathrm{stim.}} = B'\ \rho(\omega_\mathrm{A})\ \mathrm{d}t. \tag{I.6}$$

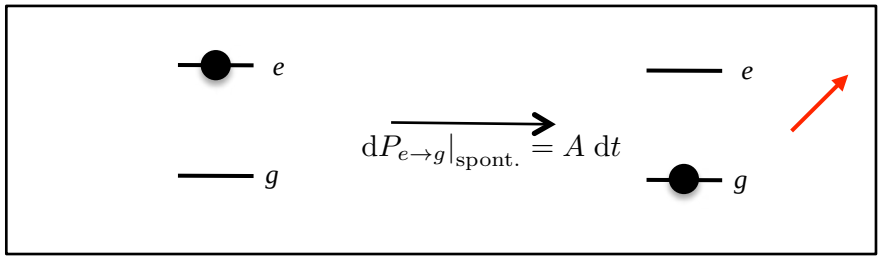

Figure I.4. *Spontaneous emission process: the photon is emitted in a random direction.*

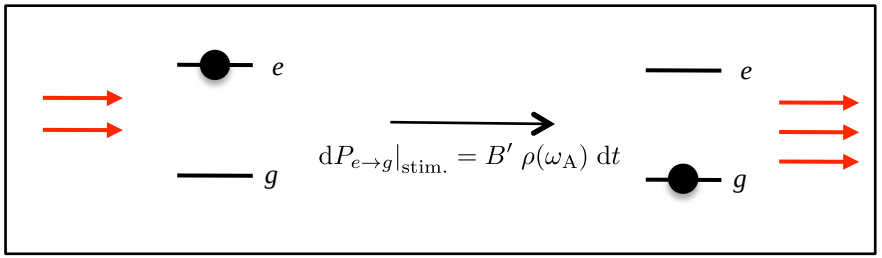

Figure I.5. *Stimulated emission process.*

The evolution of probabilities $P_{g,e}$ is then given by a rate equation:

$$\frac{\mathrm{d}P_g}{\mathrm{d}t} = -B\ \rho(\omega_{\mathrm{A}})\ P_g + [A + B'\ \rho(\omega_{\mathrm{A}})]\ P_e, \qquad P_g + P_e = 1, \tag{I.7}$$

which implies that these probabilities tend towards the stationary state

$$P_g = \frac{A + B'\ \rho(\omega_{\mathrm{A}})}{A + (B + B')\ \rho(\omega_{\mathrm{A}})}, \quad P_e = \frac{B\ \rho(\omega_{\mathrm{A}})}{A + (B + B')\ \rho(\omega_{\mathrm{A}})}, \tag{I.8}$$

with characteristic time

$$\tau_{\mathrm{int.}} = [A + (B + B')\ \rho(\omega_{\mathrm{A}})]^{-1}\,. \tag{I.9}$$

The subscript “int.” means that this is the equilibration time of the internal variables, which is different from the equilibration time of the atom’s center of mass that we will calculate later.

1-2 Constraints on Einstein coefficients

Comparing the stationary state found in (I.8) with the expected result for thermodynamic equilibrium (I.3) leads to the following constraint

$$\frac{B\ \rho(\omega_{\mathrm{A}})}{A + B'\ \rho(\omega_{\mathrm{A}})} = \exp\left(-\hbar\omega_{\mathrm{A}}/k_{\mathrm{B}}T\right), \tag{I.10}$$

which must be satisfied at any temperature T, the coefficients A, B, B' being independent of temperature.

Let us first take the high-temperature limit, for which $\rho(\omega) \to +\infty$: we immediately deduce:

$$B' = B. \tag{I.11}$$

The processes of absorption and stimulated emission are therefore intimately linked.

More generally, the constraint (I.10) can be satisfied if the energy density $\rho(\omega_{\mathrm{A}})$ of the radiation is equal to:

$$\rho(\omega_{\mathrm{A}}) = \frac{A/B'}{\exp(\hbar\omega_{\mathrm{A}}/k_{\mathrm{B}}T) - 1}. \tag{I.12}$$

This relationship is compatible with Planck’s law given in (I.1) provided that the ratio A/B' is equal to

$$\frac{A}{B'} = \frac{\hbar\omega_{\mathrm{A}}^3}{\pi^2 c^3}. \tag{I.13}$$

With the constraints (I.11) and (I.13), Einstein’s hypotheses concerning the absorption and emission of light by the atom do indeed lead to thermodynamic equilibration of the populations of atomic energy levels with blackbody radiation. Einstein concludes his 1916 paper by noting that, although the fact that thermal equilibrium is reached does not constitutea rigorous proof of the validity of the hypotheses (I.4-I.5-I.6), there is a strong chance that these processes will indeed form the basis of a future theoretical construct. Furthermore, he notes that the coefficients A, B and B' could be calculated *ab initio*, and thus the relations (I.11,I.13) tested, if one had "a modified version of electrodynamics and mechanics compatible with the quantum hypothesis". This is precisely what we will be doing in the next section.

Note: the case of degenerate levels In his study, Einstein also considers the case where energy levels can be degenerate. Noting d_e and d_g for these degeneracies, a line of reasoning similar to the previous one leads to

$$d_g B = d_e B', \qquad \frac{A}{B'} = \frac{\hbar\omega_{\mathrm{A}}^3}{\pi^2 c^3}. \tag{I.14}$$

Further on we encounter the case of a $J_g = 0 \leftrightarrow J_e = 1$ transition (see figure I.2, right), for which $d_g = 1$ and $d_e = 3$ and for which the population evolution equation P_g of level g, given in (I.7) for a two-level system, becomes using $B = 3B'$:

$$\frac{\mathrm{d}P_g}{\mathrm{d}t} = A\left\{-3\frac{B'}{A}\rho(\omega_{\mathrm{A}})P_g + \sum_j \left[1 + \frac{B'}{A}\rho(\omega_{\mathrm{A}})\right] P_{e,j}\right\}, \tag{I.15}$$

where the subscript j denotes the three sublevels forming the excited level e. We will see later [eq. (I.33)] a more compact way of writing this relationship in terms of the number of photons per mode.

2 The quantum approach

In this paragraph, we will reformulate Einstein's treatment of the absorption and emission of light by an atom in an isotropic, incoherent light field, based on the quantum formalism. We will use the notion of average number of photons per mode $\bar{n}$, slightly easier to manipulate than the energy density ρ, and we will consider a realistic atomic transition for which we will be able to treat the atom-field interaction from Fermi's golden rule.

2-1 Energy density and number of photons per mode

To translate the coefficients A and B introduced by Einstein into modern quantum language, let us start by relating the energy density $\rho(\omega)$ to the average number of photons per mode $\bar{n}$ for an electromagnetic field confined in a box of volume L^3. We consider periodic boundary conditions in this box, so that the modes of the field are identified by their wave vector $\boldsymbol{k}$ and their polarization $\boldsymbol{\epsilon}$, with

$$k_j = \frac{2\pi}{L} n_j, \quad n_j \in \mathbb{Z}, \quad j = x, y, z \tag{I.16}$$

and $\boldsymbol{\epsilon} \perp \boldsymbol{k}$. The total energy of the field is written as a function of $\rho(\omega)$ in the form

$$E = L^3 \int_0^{+\infty} \rho(\omega)\, \mathrm{d}\omega \tag{I.17}$$

and is expressed in terms of mode occupancy

$$E = \sum_{\boldsymbol{k},\boldsymbol{\epsilon}} \hbar\omega\, \bar{n}_{\boldsymbol{k},\boldsymbol{\epsilon}}, \quad \omega = ck. \tag{I.18}$$

Let us replace the discrete sum by an integral in this last expression, and assume that the population $\bar{n}_{\boldsymbol{k},\boldsymbol{\epsilon}}$ of a mode depends only on the frequency ω of this mode, and is independent of polarization. We then have

$$E = 2 \times \frac{L^3}{8\pi^3} \int_0^{+\infty} \hbar\omega\, \bar{n}(\omega)\, 4\pi k^2\, \mathrm{d}k, \tag{I.19}$$

where the factor 2 corresponds to the sum over the two independent polarizations associated with a given wave vector $\boldsymbol{k}$. Comparing (I.17) and (I.19) gives:

$$\rho(\omega) = \frac{\hbar\omega^3}{\pi^2 c^3}\, \bar{n}(\omega), \tag{I.20}$$

as could be seen directly by comparing (I.1) and (I.2).

If we go back to Einstein's reasoning in terms of the number of photons per mode $\bar{n}$ rather than the energy density ρ, we are then led to replace the coefficient B by the coefficient $\tilde{B}$ such that

$$B\,\rho(\omega_{\mathrm{A}}) = \tilde{B}\,\bar{n}(\omega_{\mathrm{A}}), \quad \text{that is} \quad \tilde{B} = B\,\frac{\hbar\omega_{\mathrm{A}}^3}{\pi^2 c^3} \tag{I.21}$$

and ditto for B'. The constraints (I.14) to reach thermodynamic equilibrium then boil down to:

$$d_g \tilde{B} = d_e \tilde{B}' \quad \text{and} \quad A = \tilde{B}'. \tag{I.22}$$

2-2 Model for an atomic transition

To satisfactorily account for the vector nature of the electromagnetic field, it is best to consider a slightly more complicated level structure than the two-level atom of the previous section. Here, we will look at a transition between a ground level with zero angular momentum, i.e. non-degenerate, and an excited level with unit angular momentum, i.e. triple degenerate (figure I.2, right). A possible basis for this excited level is obtained by choosing a reference trihedron $\boldsymbol{u}_j$, $j = x, y, z$, and considering the three orthogonal Zeeman states $|e_j\rangle$ each having a zero angular momentum projection along the j axis: $\left(\hat{\boldsymbol{J}} \cdot \boldsymbol{u}_j\right) |e_j\rangle = 0$.

The atom-radiation coupling is written in the electric dipole approximation and in the rotating field approximation

$$\hat{V} = d \left(\sum_j \boldsymbol{u}_j |g\rangle\langle e_j| \right) \cdot \hat{\boldsymbol{E}}^{(-)} + \text{H.c.} \tag{I.23}$$

where d is the reduced atomic dipole characterizing the atomic transition. The electric field operator is written in terms of the creation ($a^\dagger_{\boldsymbol{k},\boldsymbol{\epsilon}}$) and destruction ($a_{\boldsymbol{k},\boldsymbol{\epsilon}}$) operators of a photon in a given mode:

$$\hat{\boldsymbol{E}}^{(-)} = \sum_{\boldsymbol{k},\boldsymbol{\epsilon}} \mathcal{E}_k \, a^\dagger_{\boldsymbol{k},\boldsymbol{\epsilon}} \, \boldsymbol{\epsilon}, \qquad \hat{\boldsymbol{E}}^{(+)} = \left(\hat{\boldsymbol{E}}^{(-)}\right)^\dagger, \qquad \mathcal{E}_k = \sqrt{\frac{\hbar\omega}{2\epsilon_0 L^3}}. \tag{I.24}$$

2-3 Using Fermi's golden rule

We are now going to fully determine the Einstein coefficients using quantum electrodynamics. We will use Fermi's golden rule, which gives, to the lowest non-zero order, the probability per unit time of going from a given initial state to a continuum of states.

Let us take the example of a spontaneous or stimulated emission process. The initial state corresponds to the atom placed in one of its excited states $|e_j\rangle$ in the presence of a given state of the electromagnetic field. This state is characterized by the set of occupancy numbers $\{n_{\boldsymbol{k},\boldsymbol{\epsilon}}\}$ of the radiation modes:

$$|\Psi_i\rangle = |e_j, \{n_{\boldsymbol{k},\boldsymbol{\epsilon}}\}\rangle. \tag{I.25}$$

The final state corresponds to the atom in its ground state, in the presence of the field state $\{n'_{\boldsymbol{k},\boldsymbol{\epsilon}}\}$:

$$|\Psi_f\rangle = |g, \{n'_{\boldsymbol{k},\boldsymbol{\epsilon}}\}\rangle, \tag{I.26}$$

where all $n'_{\boldsymbol{k},\boldsymbol{\epsilon}}$ are equal to $n_{\boldsymbol{k},\boldsymbol{\epsilon}}$, except one which is increased by one, corresponding to the emission of a photon in this particular mode[3]:

$$n'_{\boldsymbol{k}_0,\boldsymbol{\epsilon}_0} = n_{\boldsymbol{k}_0,\boldsymbol{\epsilon}_0} + 1, \qquad n'_{\boldsymbol{k},\boldsymbol{\epsilon}} = n_{\boldsymbol{k},\boldsymbol{\epsilon}} \quad \text{if } (\boldsymbol{k},\boldsymbol{\epsilon}) \neq (\boldsymbol{k}_0,\boldsymbol{\epsilon}_0). \tag{I.27}$$

The transition probability per unit time from the state Ψ_i to the continuum of states Ψ_f is given by Fermi's golden rule:

$$\mathcal{P}_{\text{emission}} = \frac{2\pi}{\hbar} \sum_f \left| \langle \Psi_f | \hat{V} | \Psi_i \rangle \right|^2 \, \delta(E_f - E_i). \tag{I.28}$$

which is explicitly calculated in terms of a sum on the mode $\boldsymbol{k}_0, \boldsymbol{\epsilon}_0$ whose population has been increased by one unit:

$$\mathcal{P}_{\text{emission}} = \frac{2\pi}{\hbar^2} \sum_{\boldsymbol{k}_0,\boldsymbol{\epsilon}_0} d^2 \mathcal{E}_{k_0}^2 \left(\boldsymbol{\epsilon}_0 \cdot \boldsymbol{u}_j\right)^2 \left(n_{\boldsymbol{k}_0,\boldsymbol{\epsilon}_0} + 1\right) \, \delta(\omega_0 - \omega_\text{A}), \tag{I.29}$$

where we used

$$\langle \{n'_{\boldsymbol{k},\boldsymbol{\epsilon}}\} | a^\dagger_{\boldsymbol{k}_0,\boldsymbol{\epsilon}_0} | \{n_{\boldsymbol{k},\boldsymbol{\epsilon}}\} \rangle = \sqrt{n_{\boldsymbol{k}_0,\boldsymbol{\epsilon}_0} + 1}. \tag{I.30}$$

The calculation of the sum (I.29), which we replace by an integral as in (I.19), is detailed in quantum optics courses. As before, we will assume that the average population of a mode $(\boldsymbol{k},\boldsymbol{\epsilon})$ depends only on the frequency of that mode: this is the assumption of an isotropic state for the field. Let us just give the result, averaged over the initial state Ψ_i:

$$\mathcal{P}_{\text{emission}} = \left[\bar{n}(\omega_\text{A}) + 1\right] \Gamma, \qquad \Gamma = \frac{d^2 \omega_\text{A}^3}{3\pi\epsilon_0 \hbar c^3}, \tag{I.31}$$

where the quantity Γ is the natural width of the excited state, i.e. the probability per unit time that the atom will de-excite if the radiation field is initially empty.

[3] We are only interested here in the lowest order, given by Fermi's golden rule. Higher-order processes would correspond to multiple photon scattering by the atom, with several $n'_{\boldsymbol{k},\boldsymbol{\epsilon}}$ different from $n_{\boldsymbol{k},\boldsymbol{\epsilon}}$.

A similar calculation gives the probability per unit time that an atom initially in its ground state will absorb a photon and reach one of the three excited states:

$$\mathcal{P}_{\text{absorption}} = 3\ \bar{n}(\omega_{\text{A}})\,\Gamma. \tag{I.32}$$

The evolution equation for one of the populations, P_g for example, is then given by

$$\dot{P}_g = -3\bar{n}\,\Gamma\ P_g + \sum_j (\bar{n}+1)\,\Gamma\ P_{e_j}, \tag{I.33}$$

where we have posed $\bar{n} \equiv \bar{n}(\omega_{\text{A}})$. This equation is formally identical to the one we wrote in (I.15) based on Einstein's reasoning, but it is much more compact thanks to the use of the variable $\bar{n}$ instead of the energy density ρ. The stationary state

$$P_g = \frac{\bar{n}+1}{4\bar{n}+1}, \qquad P_{e_j} = \frac{\bar{n}}{4\bar{n}+1}, \tag{I.34}$$

is reached in a time of the order of

$$\tau_{\text{int}} = \frac{\Gamma^{-1}}{4\bar{n}+1}. \tag{I.35}$$

The structure of the result, with terms for absorption, stimulated emission and spontaneous emission, corresponds well to the result predicted by Einstein with

$$A = \Gamma. \tag{I.36}$$

In particular, at equilibrium, the ratio between the population of an excited state and that of the ground state:

$$\frac{P_{e_j}}{P_g} = \frac{\bar{n}}{\bar{n}+1} \tag{I.37}$$

is equal to the expected result

$$\frac{P_{e_j}}{P_g} = \exp\left(-\frac{\hbar\omega_{\text{A}}}{k_{\text{B}}T}\right) \tag{I.38}$$

if we inject the blackbody law given in (I.2):

$$\bar{n}(\omega) = \frac{1}{\exp(\hbar\omega/k_{\text{B}}T)-1}. \tag{I.39}$$

The treatment we have just given fulfills Einstein's wish when he wrote the sentence quoted above: the coefficients A and B can indeed be calculated *ab initio*, and thus the relation (I.13) tested. In other words, we have checked the proportionality relation between A and B, as well as the relation $B = 3B'$, from the first principles of quantum electrodynamics. The coherence of matter-radiation interaction and thermodynamics is thus well assured, at least as far as internal atomic dynamics is concerned.

3 Brownian motion

In the previous paragraph, we looked at how the internal atomic variables, i.e. the populations of the states g and e, reach a thermal equilibrium compatible with the temperature imposed by blackbody radiation. In the remainder of this chapter, we will consider the motion of the atom's center of mass and verify that the stationary state of this motion is also compatible with thermal equilibrium at temperature T. More specifically, we want to verify that the stationary probability distribution for the atom's momentum is the Gaussian

$$\mathcal{P}_{\text{stat.}}(\boldsymbol{p}) \propto \mathrm{e}^{-p^2/2p_0^2} \tag{I.40}$$

with

$$\frac{p_0^2}{2M} = \frac{1}{2}k_{\text{B}}T. \tag{I.41}$$

The thermalization of the atom in black-body radiation results from the succession of photon absorption and emission processes by the atom. As each process is accompanied by a change in the momentum of the atomic center of mass, the situation is similar to that of Brownian motion: the atom plays the role of the Brownian particle, and the photons of blackbody radiation play the role of the fluid molecules. The tools developed for the study of Brownian motion are therefore perfectly suited to the problem we are interested in here, and we will briefly summarize them in the following paragraphs [for more information, see Van Kampen (1992)]. We will then return to the problem of atomic thermalization in black-body radiation.

3-1 The Langevin equation approach

This approach assumes that the equation of motion of the Brownian particle has two components:

$$\frac{\mathrm{d}\boldsymbol{p}}{\mathrm{d}t} = -\alpha\boldsymbol{p} + \boldsymbol{F}(t). \tag{I.42}$$

The first, deterministic force corresponds to fluid friction, which damps the momentum over a characteristic time α^{-1}. The second force $\boldsymbol{F}(t)$, called *Langevin force*, is random and characterized by its statistical properties. The equation (I.42) is therefore a stochastic differential equation.

In practice, we impose the first two moments of the random force $\boldsymbol{F}(t)$:

$$\langle \boldsymbol{F}(t)\rangle = 0, \qquad \langle F_i(t)F_j(t')\rangle = 2D_p\,\delta_{i,j}\,\delta(t-t'), \quad i,j = x,y,z, \tag{I.43}$$

where the averages are taken over different realizations of the disorder associated with the positions and velocities of the fluid molecules. The coefficient D_p is called *momentum diffusion coefficient*, for a reason that will become clear later.

We now show that the two coefficients α and D_p entering (I.42-I.43) are related if we impose that the stationary state of the particle's momentum distribution corresponds to thermal equilibrium, i.e..:

$$\langle \frac{p_i^2}{2M}\rangle = \frac{1}{2}k_{\mathrm{B}}T, \qquad i = x,y,z. \tag{I.44}$$

To find this relationship, let us integrate the equation of motion (I.42) between the initial time $t = 0$ and an arbitrary time t:

$$\boldsymbol{p}(t) = \boldsymbol{p}(0)\,\mathrm{e}^{-\alpha t} + \int_0^t \mathrm{e}^{-\alpha(t-t')}\boldsymbol{F}(t')\,\mathrm{d}t'. \tag{I.45}$$

By averaging this equation over different realizations of disorder, we find:

$$\langle \boldsymbol{p}(t)\rangle = \langle \boldsymbol{p}(0)\rangle\,\mathrm{e}^{-\alpha t}. \tag{I.46}$$

The particle's mean momentum therefore tends towards 0 with the characteristic time α^{-1}. Let us now consider the evolution of the square of one component of the momentum and take the average over the disorder again:

$$\begin{aligned}\frac{\mathrm{d}\langle p_j^2(t)\rangle}{\mathrm{d}t} &= 2\langle p_j(t)\frac{\mathrm{d}p_j}{\mathrm{d}t}\rangle \\ &= -2\alpha\langle p_j^2(t)\rangle + 2\langle p_j(t)F_j(t)\rangle.\end{aligned} \tag{I.47}$$

The second term is calculated[4] by injecting the result (I.45):

$$\begin{aligned}\langle p_j(t)F_j(t)\rangle &= \langle p_j(0)F_j(t)\rangle\mathrm{e}^{-\alpha t} + \int_0^t \mathrm{e}^{-\alpha(t-t')}\langle F_j(t')F_j(t)\rangle\,\mathrm{d}t' \\ &= 0 \quad + \quad 2D_p\int_0^t \mathrm{e}^{-\alpha\tau}\delta(\tau)\,\mathrm{d}\tau \\ &= D_p \qquad\qquad (\text{for } t>0).\end{aligned} \tag{I.48}$$

The root-mean-square momentum evolves under the effect of two terms:

$$\frac{\langle p_j^2(t)\rangle}{\mathrm{d}t} = -2\alpha\langle p_j^2(t)\rangle + 2D_p. \tag{I.49}$$

The first term corresponds to an exponential decrease due to dissipation, and the second to a linear growth in time due to fluctuations of the Langevin force. The slope of this growth is $2D_p$, hence the name *momentum diffusion coefficient* for D_p. Equilibrium between dissipation and fluctuations is reached in a characteristic time $(2\alpha)^{-1}$ and corresponds to

$$\langle p_j^2\rangle_{\mathrm{stat.}} = \frac{D_p}{\alpha}. \tag{I.50}$$

If the bath of molecules in which the Brownian particle is immersed is at temperature T, thermodynamic equilibrium (I.44) will be reached if

$$\frac{\langle p_j^2\rangle}{2M} = \frac{1}{2}k_{\mathrm{B}}T \quad \Rightarrow \quad \frac{D_p}{M\alpha} = k_{\mathrm{B}}T. \tag{I.51}$$

In a phenomenological model of Brownian motion, we can estimate the coefficient of friction α from Stokes' law, and we impose the value of the momentum diffusion coefficient so that (I.51) is satisfied. If we have a microscopic model of the interaction between Brownian particles and fluid

[4] We use the relationship $\int_0^\infty f(x)\,\delta(x)\,\mathrm{d}x = \frac{1}{2}f(0)$.

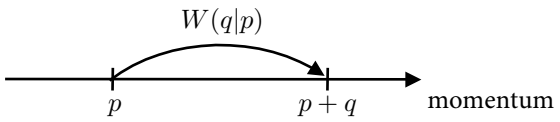

Figure I.6. *Random walk in momentum space (one-dimensional model); the quantity $W(q|p)$ represents the transition probability per unit time for a jump of amplitude q starting from momentum p.*

molecules, we can calculate α and D_p separately: verification of the relationship (I.51) is then a test of the model's consistency. This is what we will be able to do in the next paragraph for the thermalization of atomic motion in blackbody radiation.

3-2 The Fokker–Planck equation approach

The Langevin equation approach has enabled us to determine the first two moments of the momentum distribution. We could iterate this approach to obtain all the moments, thus characterizing the stationary state and verifying that it is indeed a Gaussian. However, it is quicker to use another equivalent approach, which consists in establishing the evolution equation of the momentum distribution $\mathcal{P}(\boldsymbol{p}, t)$.

To simplify writing, let us consider a one-dimensional problem so that the momentum p is now a scalar. We are interested in a class of problems for which the evolution of $\mathcal{P}(p, t)$ is described by a master equation of the type

$$\frac{\partial \mathcal{P}(p,t)}{\partial t} = -\left(\int W(q|p)\,\mathrm{d}q\right)\mathcal{P}(p,t) + \int W(q|p-q)\,\mathcal{P}(p-q,t)\,\mathrm{d}q. \quad \text{(I.52)}$$

The meaning of this equation is as follows. Since the Brownian particle is initially in the state p, it has the probability $W(q|p)\,\mathrm{d}t$ of gaining the momentum q during the time interval $\mathrm{d}t$. The quantity $W(q|p)$ is therefore *the transition probability per unit time for a jump of amplitude q starting from p* (figure I.6). The first term of (I.52) corresponds to the total departure from momentum class p by momentum gains q. The second term corresponds to feeding the momentum class p with an amplitude jump q from the initial momentum $p - q$. One can check that the normalization of $\mathcal{P}(p, t)$, $\int \mathcal{P}(p, t)\,\mathrm{d}p = 1$, is well preserved by this evolution.

All the physics of the problem is contained in the choice of the function $W(q|p)$. For example, for a problem involving fluid friction, this function should be such that, for $p > 0$, jumps with $q < 0$ will be favored over jumps with $q > 0$ (and vice versa for an momentum $p < 0$), so that the particle's momentum is on average reduced towards 0.

Let us now assume small jumps in amplitude: more precisely, we will assume that $W(q|p)$ is peaked around the value $q = 0$ with a characteristic width q_c, while varying smoothly with the momentum p. Let us further assume that the momentum distribution $\mathcal{P}$ is a slowly varying function of p on the scale of q_c. In particular, q_c must be small compared with the width $\sqrt{Mk_{\mathrm{B}}T}$ expected for $\mathcal{P}(p)$ at thermodynamic equilibrium. We will therefore develop the term involved in the second member of (I.52):

$$\begin{aligned} W(q|p-q)\,\mathcal{P}(p-q,t) &= W(q|p)\,\mathcal{P}(p,t) - q\frac{\partial}{\partial p}\left[W(q|p)\,\mathcal{P}(p,t)\right] \\ &+ \frac{q^2}{2}\frac{\partial^2}{\partial p^2}\left[W(q|p)\,\mathcal{P}(p,t)\right] + \ldots \end{aligned} \quad \text{(I.53)}$$

We can, of course, push this expansion to an arbitrarily high order (Kramers–Moyal expansion), but order two will suffice for what follows. Let us inject this expansion into the master equation (I.52). We then obtain for $\mathcal{P}(p, t)$ the partial differential equation (Fokker–Planck equation):

$$\frac{\partial \mathcal{P}(p,t)}{\partial t} = -\frac{\partial}{\partial p}\left[\mathcal{F}(p)\,\mathcal{P}(p,t)\right] + \frac{\partial^2}{\partial p^2}\left[\mathcal{D}(p)\,\mathcal{P}(p,t)\right], \quad \text{(I.54)}$$

with

$$\mathcal{F}(p) = \int q\,W(q|p)\,\mathrm{d}q, \qquad \mathcal{D}(p) = \frac{1}{2}\int q^2\,W(q|p)\,\mathrm{d}q. \quad \text{(I.55)}$$

The first term of (I.54) corresponds to the evolution of the probability density $\mathcal{P}(p, t)$ under the effect of the force $\mathcal{F}(p)$. To confirm this, we can evaluate the evolution of the average momentum $\langle p(t)\rangle = \int p\,\mathcal{P}(p, t)\,\mathrm{d}p$ for a probability distribution centered around p_0. After integration by parts, we find

$$\frac{\mathrm{d}\langle p\rangle}{\mathrm{d}t} = \int \mathcal{F}(p)\,\mathcal{P}(p,t)\,\mathrm{d}p \approx \mathcal{F}(p_0). \quad \text{(I.56)}$$

The second term in (I.54) corresponds to diffusion in momentum space. To demonstrate this, let us once again consider a distribution centered around p_0 and study the evolution of the root-mean-square momentum:

$$\frac{\mathrm{d}\langle p^2\rangle}{\mathrm{d}t} = 2\int p\,\mathcal{F}(p)\,\mathcal{P}(p,t)\,\mathrm{d}p + 2\int \mathcal{D}(p)\,\mathcal{P}(p,t)\,\mathrm{d}p, \tag{I.57}$$

$$\approx 2p_0\mathcal{F}(p_0) + 2\mathcal{D}(p_0). \tag{I.58}$$

We find a structure similar to that obtained in (I.49) by the Langevin equation approach, with the two contributions of mean force and momentum diffusion.

At this stage, the class of problems described by the Fokker–Planck equation is more general than that described by the Langevin equation (eq:Langevin), since the deterministic force $\mathcal{F}$ is not necessarily linear in momentum and the diffusion coefficient $\mathcal{D}$ is not necessarily constant. We will see in the rest of this course that this generalization can be very useful when modeling certain types of light cooling. For now, we can restrict ourselves to the simple case of

$$\mathcal{F}(p) = -\alpha p, \qquad \mathcal{D}(p) = D_p, \tag{I.59}$$

and model Brownian motion by *the linear Fokker–Planck equation*:

$$\frac{\partial\mathcal{P}(p,t)}{\partial t} = \alpha\frac{\partial\left(p\,\mathcal{P}(p,t)\right)}{\partial p} + D_p\frac{\partial^2\mathcal{P}(p,t)}{\partial p^2}. \tag{I.60}$$

A stationary solution of this equation is the Gaussian function

$$\mathcal{P}_{\mathrm{stat.}}(p) = \frac{1}{p_0\sqrt{2\pi}}\,\mathrm{e}^{-p^2/2p_0^2}, \qquad \text{with} \quad p_0^2 = \frac{D_p}{\alpha}, \tag{I.61}$$

which corresponds to the Maxwell-Boltzmann distribution expected for a particle in contact with a reservoir at temperature T, provided that $k_{\mathrm{B}}T = D_p/(M\alpha)$ [*cf.* (I.51)].

3-3 Spatial diffusion

So far we have been interested in the atom's motion in momentum space. We have seen that this motion is the resultant of a momentum diffusion characterized by D_p and a friction force characterized by α. In the rest of this course, we will also consider the atom's motion in position space. We will see here that this motion is purely diffusive and characterized by the spatial diffusion coefficient $D_x = D_p/(M\alpha)^2$.

To calculate this spatial diffusion coefficient, let us start again with Langevin's equation

$$\frac{\mathrm{d}\boldsymbol{p}}{\mathrm{d}t} = -\alpha\boldsymbol{p} + \boldsymbol{F}(t), \tag{I.62}$$

and its solution between an initial time t_i and time t.

$$\boldsymbol{p}(t) = \boldsymbol{p}(t_i)\mathrm{e}^{-\alpha(t-t_i)} + \int_{t_i}^{t}\mathrm{e}^{-\alpha(t-t')}\boldsymbol{F}(t')\mathrm{d}t'. \tag{I.63}$$

Let us look at the distance covered by the particle between t_i and t:

$$\boldsymbol{r}(t) = \boldsymbol{r}(t_i) + \frac{1}{M}\int_{t_i}^{t}\boldsymbol{p}(t')\,\mathrm{d}t'. \tag{I.64}$$

Because of the isotropy of Brownian motion, it is clear that if the particle is at point $\boldsymbol{r}(t_i)$ at initial time, its mean position will still be $\boldsymbol{r}(t_i)$ at time t. Now consider the mean square deviation

$$\Delta r^2(t) = \langle[\boldsymbol{r}(t) - \boldsymbol{r}(t_i)]^2\rangle \tag{I.65}$$

and calculate its time derivative:

$$\frac{\mathrm{d}\Delta r^2}{\mathrm{d}t} = \frac{2}{M}\langle\boldsymbol{p}(t)\cdot[\boldsymbol{r}(t) - \boldsymbol{r}(t_i)]\rangle = \frac{2}{M^2}\int_{t_i}^{t}\langle\boldsymbol{p}(t)\cdot\boldsymbol{p}(t')\rangle\,\mathrm{d}t'. \tag{I.66}$$

We therefore need to evaluate the correlation function of the momentum at two different time, which is immediately deduced from (I.63): since the Langevin force at time t is not correlated with the value of the momentum at an earlier time t', we have:

$$\langle\boldsymbol{p}(t)\cdot\boldsymbol{p}(t')\rangle = \langle\boldsymbol{p}^2(t')\rangle\,\mathrm{e}^{-\alpha(t-t')} \quad \text{for} \quad t > t'. \tag{I.67}$$

We will assume that at times t' contributing to the integral (I.66), the particle is in thermal equilibrium, so that $\langle\boldsymbol{p}^2(t')\rangle = 3p_0^2$ (three-dimensional). So, for a time interval $t - t_i \gg \alpha^{-1}$:

$$\frac{\mathrm{d}\Delta r^2}{\mathrm{d}t} = \frac{6p_0^2}{M^2\alpha}, \tag{I.68}$$

i.e. a constant increase in Δr^2, characteristic of diffusion along each component of x, y, z space:

$$\frac{\mathrm{d}\Delta x^2}{\mathrm{d}t} = 2D_x \qquad \text{with} \quad D_x = \frac{p_0^2}{M^2\alpha} = \frac{D_p}{M^2\alpha^2}. \tag{I.69}$$

This spatial diffusion coefficient can be interpreted as the result of a random walk in the position space, with the rate α and the step v_0/α, i.e. the distance covered by a particle of average velocity $v_0 = p_0/M$ during the velocity damping time α^{-1}.

4 Thermalization in black-body radiation

In his 1917 article, Einstein took up the arguments developed in 1916 to identify the three elementary processes of atom-radiation interaction: absorption, stimulated emission and spontaneous emission. He develops a line of reasoning that reinforces his 1916 conclusions: if we accept that these three processes are present, then not only do the internal atomic variables (populations $P_{g,e}$) reach the expected state of thermal equilibrium, but so does the momentum distribution $\mathcal{P}(p)$ of the atom's center of mass. To establish this result, Einstein developed a formalism that is the direct precursor of Doppler cooling as used in modern experiments. The aim of this paragraph is to present Einstein's argument, with tools that can be directly transposed to the study of laser cooling of atoms.

We use a Brownian motion approach here, decomposing the mechanical action of radiation on the atom into two parts: on the one hand, a friction force $-\alpha\boldsymbol{p}$, and on the other, a momentum diffusion characterized by the coefficient D_p. We will calculate the two coefficients α and D_p separately, then check that the equilibrium reached corresponds to what is expected, i.e. that $D_p/\alpha = Mk_{\mathrm{B}}T$, where T is the blackbody temperature. In practice, calculating the diffusion coefficient is simpler than calculating the friction coefficient, so we will start with D_p.

4-1 Atomic momentum diffusion

Let us consider an atom initially at rest ($\boldsymbol{p} = 0$). If the image of Brownian motion is correct, the evolution of its mean square momentum under the effect of the random kicks constituted by the elementary processes of absorption and emission is given by

$$\frac{\mathrm{d}\langle p_j^2(t)\rangle}{\mathrm{d}t} = -2\alpha\langle p_j^2(t)\rangle + 2D_p. \tag{I.70}$$

The root-mean-square momentum begins to grow linearly with a slope $2D_p$, saturating at long time at D_p/α.

Let us consider a time interval Δt short enough for the contribution of the friction $-2\alpha\langle p_j^2(t)\rangle$ to be negligible compared to diffusion, but long enough for several elementary processes to take place (we will verify a posteriori that such a time interval exists). The rate R at which these processes occur is:

$$R = 3\bar{n}\,\Gamma\,P_g + \sum_j (\bar{n}+1)\,\Gamma\,P_{e_j}. \tag{I.71}$$

Using the stationary population values given in (I.34), we obtain

$$R = 6\Gamma\frac{\bar{n}(\bar{n}+1)}{4\bar{n}+1}. \tag{I.72}$$

During the time interval Δt, $\Delta N = R\,\Delta t$ elementary processes will occur, each corresponding to a kick transferring to the atom a momentum of modulus $\hbar k$ in a random direction. The atom's momentum thus follows a random walk of step $\hbar k$ and rate R. At the end of the time interval Δt, the atom's mean momentum remains zero, but the root-mean-square momentum along one of the three directions in space has increased by

$$\langle p_j^2(\Delta t)\rangle = \frac{1}{3}\hbar^2k^2\,\Delta N, \tag{I.73}$$

From this we deduce the momentum diffusion coefficient

$$D_p = \frac{1}{2}\,\frac{\langle p_j^2(\Delta t)\rangle}{\Delta t} \qquad \Rightarrow \qquad D_p = \hbar^2k^2\Gamma\,\frac{\bar{n}(\bar{n}+1)}{4\bar{n}+1}. \tag{I.74}$$

4-2 Friction force

Let us now consider an atom moving at velocity $\boldsymbol{v} = \boldsymbol{p}/M$. We will assume $v \ll c$ so that the particle is non-relativistic. The origin of the friction force is the Doppler effect: in the frame of reference $\mathcal{R}$ in motion with the atom, blackbody radiation is not isotropic, unlike in the laboratory frame. Now, the atom probes the radiation in $\mathcal{R}$ at its resonant frequency $\omega_{\rm A}$; it will therefore interact with modes of the field that are not all equally populated.

For example, let us consider two modes in opposite directions, one going in the same direction as the atom, the other in the opposite direction, which are likely to interact with the atom. The frequency of the mode running in the same direction as the atom is $\omega_{\rm A}$ in the atomic frame of reference, i.e. $\omega_{\rm A}(1 + v/c)$ in the laboratory frame. The mode going in the opposite direction to the atom also has a frequency $\omega_{\rm A}$ in the atomic frame of reference, so $\omega_{\rm A}(1 - v/c)$ in the laboratory frame. The number of photons per mode $\bar{n}(\omega)$ is a decreasing function of ω for blackbody radiation. Therefore

$$\bar{n}[\omega_{\rm A}(1 - v/c)] > \bar{n}[\omega_{\rm A}(1 + v/c)]. \tag{I.75}$$

The moving atom sees more resonant photons coming towards it than going in the same direction as it: there will therefore be more kicks decreasing atomic velocity than increasing it: this is the origin of the friction force.

For a quantitative assessment of the coefficient of friction α, let us take an atom moving in one direction in space, z for example. Let us denote its velocity v_z and assume that the atom is in its electronic ground state g. The average change in momentum over an infinitesimal time interval Δt can be calculated using a formalism very similar to the one we used to evaluate absorption and emission probabilities based on Fermi's golden rule. It is obtained by considering all the momentum gains $\hbar\boldsymbol{k}$ resulting from the absorption of a photon in a given mode of the $\boldsymbol{k}_0, \boldsymbol{\epsilon}_0$ field, accompanied by the atom's passage into the state e_j, $j = x, y, z$:

$$\Delta p_z = \Delta t\, \frac{2\pi}{\hbar^2} \sum_j \sum_{\boldsymbol{k}_0, \boldsymbol{\epsilon}_0} \hbar k_z \left| \langle e_j, \{n'_{\boldsymbol{k},\boldsymbol{\epsilon}}\}| \hat{V} |g, \{n_{\boldsymbol{k},\boldsymbol{\epsilon}}\}\rangle \right|^2 \delta(\omega_0 - \omega_{\rm at}). \tag{I.76}$$

The Dirac distribution $\delta(\omega_0 - \omega_{\rm A})$ selects the modes with frequency $\omega_{\rm A}$ in the atomic frame of reference[5], i.e. frequency $\omega_{\rm A} + k_z v_z$ in the laboratory reference frame. The population of a mode corresponding to this resonance is

$$\bar{n}(\omega_{\rm A} + k_z v_z) \approx \bar{n}(\omega_{\rm A}) + k_z v_z \left.\frac{\partial \bar{n}}{\partial \omega}\right|_{\omega=\omega_{\rm A}}. \tag{I.77}$$

The calculation of the sum over the modes is then similar to that of the absorption and emission rates. After some rather tedious algebra, we find for absorption processes:

$$\frac{\Delta p_z}{\Delta t} = \hbar k^2 \Gamma \frac{\partial \bar{n}}{\partial \omega} v_z \tag{I.78}$$

and an identical result, but of opposite sign, for emission processes after averaging over the three e_j states. Finally, by weighting the momentum changes between absorption and emission by the stationary populations (I.34), we arrive at the expression for the friction force:

$$F_z = -\alpha p_z \qquad \text{with} \quad \alpha = -\frac{\hbar k^2}{M} \frac{\Gamma \frac{\partial \bar{n}}{\partial \omega}}{4\bar{n} + 1}. \tag{I.79}$$

The friction coefficient is therefore directly proportional to the frequency derivative of the mode population around the atomic resonance frequency. This result confirms the intuition based on the Doppler effect discussed above [*cf.* (I.75)]: it is the differential between the population of modes going in the same direction as the atom and those opposing its motion that creates the friction force.

4-3 Thermal balance ?

We are now in a position to apply the general results of Brownian motion theory: atomic motion is characterized by a friction coefficient α and a momentum diffusion coefficient D_p, so that the momentum distribution at equilibrium is a Gaussian to which we can associate an effective temperature

$$k_{\rm B} T_{\rm eff} = \frac{D_p}{M\alpha} = \hbar \frac{\bar{n}(\bar{n} + 1)}{\left|\frac{\partial \bar{n}}{\partial \omega}\right|}. \tag{I.80}$$

[5] The reasoning can also be done directly in the laboratory reference frame. The Dirac distribution expressing the energy conservation then selects modes of frequency ω such that $E_i - E_f = [\boldsymbol{p}^2/2M + \hbar\omega] - [(\boldsymbol{p} + \hbar\boldsymbol{k})^2/2M + \hbar\omega_{\rm A}] = 0$, which is equivalent to taking $\omega = \omega_{\rm A} + k_z v_z$, except for the recoil energy $\hbar^2 k^2/2M$, which plays a negligible role here.

If we inject the mode occupancy for blackbody radiation into this relationship:

$$\bar{n} = \frac{1}{\exp(\hbar\omega/k_{\rm B}T) - 1}, \tag{I.81}$$

we check that the model is thermodynamically consistent, i.e. that the effective temperature associated with the atom's momentum distribution coincides with the blackbody temperature:

$$T_{\rm eff} = T. \tag{I.82}$$

For Einstein, this result was a confirmation of his hypotheses on the nature of exchanges between atoms and radiation. The 1916 argument about the populations of the atom's internal states only concerned energy. On the contrary, for this thermalization problem, it is essential to posit that the atom's momentum increases or decreases by $\hbar\boldsymbol{k}$ when the atom absorbs or emits a photon. Einstein concluded his article with two prescient remarks. On the one hand, while acknowledging the weaknesses of his model, in which the instants and directions of elementary processes are left to chance, he stated that "I have full confidence in the safety of the approach followed here". He also pointed out that almost all theories of thermal radiation take into account only the exchange of energy between light and matter, but not the exchange of momenta: "We readily believe that we are authorized to do so by the fact that the momenta transferred by radiation are small, and therefore in reality almost always negligible compared with the other causes of motion". He went on to stress the importance of taking these momentum exchanges into account on a theoretical level for a justified theory. The cooling of atoms by light shows that it is also essential to take these exchanges into account on a practical level!

4-4 Orders of magnitude and validity criteria

In the above, we have obtained the value of the friction coefficient for the motion of an atom in blackbody radiation [eq. (I.79)]. Let us consider a sodium atom and model it by its resonance line at $\lambda = 589\,$nm. The temperature required to reach $k_{\rm B}T = \hbar\omega$ is considerable, on the order of 25 000 Kelvins. Although this is a rather unrealistic situation (even for our two-level atom model), we can calculate the corresponding friction coefficient and find a time α^{-1} of the order of 10 minutes. For a blackbody of more reasonable temperature, $k_{\rm B}T \ll \hbar\omega$, the thermalization time diverges exponentially:

$$\alpha^{-1} \approx \frac{M}{\hbar k^2}\,\frac{k_{\rm B}T}{\hbar\Gamma}\,{\rm e}^{\hbar\omega/k_{\rm B}T}. \tag{I.83}$$

A 6000 Kelvin blackbody (an atom close to the sun's surface) gives $\bar{n}(\omega_{\rm A}) = 0.017$ and a thermalization time of 40 minutes. The thermal velocity $v_0 = \sqrt{k_{\rm B}T/M}$ corresponds in this case to 1500 m/s, and the average distance covered during a thermalization time, i.e. the step of the random walk in position space, is 3600 km. Even in an astrophysical environment, it is likely that other thermalization processes, such as collisions with other atoms or molecules, will limit the mean free path of our sodium atom to much lower values. The advantage of using laser sources will be to produce much larger values of $\left|\frac{\partial\bar{n}}{\partial\omega}\right|$, the thermalization time then being simply the first factor in (I.83), i.e. $M/\hbar k^2$.

Finally, it should be noted that our assumption of low-amplitude jumps, essential for the Brownian motion approach, is well verified in this example. The recoil velocity of the sodium atom when it absorbs or emits a photon is $v_{\rm r} = \hbar k/M = 3\,$cm/s, which is very small indeed compared with the characteristic width of the thermal velocity distribution at 6000 K, of the order of 1500 m/s.

Chapter II

Doppler cooling and magneto-optical trap

Sixty years after Einstein's paper showing how light from a blackbody could impose a kinetic temperature on an assembly of atoms, two papers by Hänsch & Schawlow (1975) on the one hand and Wineland & Dehmelt (1975) on the other, came simultaneously to propose exploiting light from tunable lasers (a novelty in 1975) to create new thermodynamic equilibria. In the language we developed in the previous chapter, a monochromatic laser can produce a spectral distribution of light with $\frac{\partial \bar{n}}{\partial \omega}$ arbitrarily large: it is then the natural width Γ of the excited level of the atom that will replace the width of the blackbody distribution. In other words, there is no longer any temperature imposed on the exterior by incident light, and it is the parameters of the atomic transition used that determine the equilibrium temperature.

As in Einstein's paper, it is the Doppler effect that is at the root of the friction force that cools the atoms. The approach we are going to follow will therefore be very similar to what we have seen for blackbody radiation. We will use Brownian motion theory to determine both a friction coefficient and a diffusion coefficient, to arrive at the famous Doppler limit:

$$k_{\mathrm{B}} T = \frac{\hbar \Gamma}{2}. \tag{II.1}$$

Once we have established the principle of these optical molassess, we will transpose them from velocity space to position space, substituting the Zeeman effect for the Doppler effect. We will then arrive at the principle of the magneto-optical trap, which we will describe and illustrate using recent experiments with both atoms and molecules.

1 Radiation pressure force

At the root of Doppler cooling of atoms is the radiation pressure force. The simplest physical situation in which this force appears is that of an atom with two relevant electronic levels, g and e, placed in a monochromatic plane light wave, of wave vector $\boldsymbol{k}$ (figure II.1). The atom's internal state performs *absorption – emission* cycles, each of which transfers a certain momentum to the atom. More precisely:

- During a photon absorption process, the atom passes from the g state to the e state by gaining the momentum $\hbar\boldsymbol{k}$.
- During a photon emission process, the atom passes from the e state to the g state, and two cases are possible:
  1. In the case of stimulated emission, the emitted photon is identical to the photons of the incident wave; the momentum lost by the atom is therefore $\hbar\boldsymbol{k}$, so the momentum change of the *absorption–stimulated emission* cycle is zero.
  2. In the case of spontaneous emission, the photon is emitted in a random direction in space. The angular distribution of this emission is not universal and depends on the nature of the atomic transition, but it always occurs with equal probability in two opposite directions in space. The average momentum carried away by the spontaneously emitted photon is therefore always zero, so

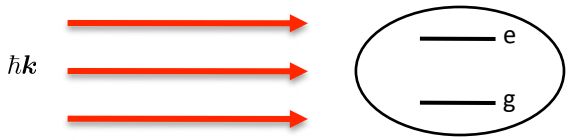

Figure II.1. *A two-level atom illuminated by a plane wave; the repetition of "absorption– spontaneous emission" cycles creates a radiation pressure force on the atom that can reach the value $\hbar k\Gamma/2$, where Γ is the natural width of the excited state e.*

that the balance of the cycle *absorption-spontaneous emission* is a gain of $\hbar\boldsymbol{k}$.

We deduce from this analysis that the radiation pressure force is equal to

$$\boldsymbol{F} = \hbar\boldsymbol{k}\,\gamma \tag{II.2}$$

where γ is the rate for the spontaneous emission of photons. Using the result from the previous chapter, this rate can be written as

$$\gamma = \Gamma P_e, \tag{II.3}$$

where Γ is the natural width of the excited state (Einstein's A coefficient) and P_e is the steady-state population of this excited state. The result will be the equivalent for a coherent field of the result $P_e = \bar{n}/(2\bar{n}+1)$ found for a two-level atom in an incoherent, isotropic field.

1-1 Optical Bloch equations

We are interested here in the internal dynamics of an atom coupled both to a monochromatic (i.e. coherent) light field and to the empty modes of the electromagnetic field, this second –incoherent– coupling being responsible for the spontaneous emission phenomenon. If we were dealing solely with the coherent coupling with the light field, we could describe the atom's internal state by a state vector $\alpha_g(t)|g\rangle + \alpha_e(t)|e\rangle$, and deduce the evolution of $\alpha_{g,e}(t)$ from Schrödinger equation to then calculate $P_e = |\alpha_e|^2$. If we were dealing solely with incoherent coupling, we could, as in the previous chapter, write rate equations for the populations $P_{g,e}$ and determine their stationary state. The simultaneous presence of both types of coupling, coherent and incoherent, necessitates recourse to the master equation formalism. We will briefly summarize this formalism, which leads to the optical Bloch equations [for more details, see for example Cohen-Tannoudji, Dupont-Roc, et al. (2012)].

We describe the atom's internal state by its density operator $\hat{\rho}$, i.e. for the case of the two-level system of interest here, a 2×2 matrix:

$$\hat{\rho} = \begin{pmatrix} \rho_{gg} & \rho_{ge} \\ \rho_{eg} & \rho_{ee} \end{pmatrix}. \tag{II.4}$$

This matrix is Hermitian and its diagonal elements, which are real, give the populations of the states concerned:

$$\rho_{gg} = P_g, \qquad \rho_{ee} = P_e, \qquad \rho_{gg} + \rho_{ee} = 1. \tag{II.5}$$

The matrix therefore has trace 1. The non-diagonal elements describe the quantum coherence between the g state and the e state and the Hermitian character of the matrix imposes:

$$\rho_{eg} = \rho_{ge}^*. \tag{II.6}$$

In the incoherent field model developed in the previous chapter, these non-diagonal elements were zero in steady state.

In the master equation description, valid if the laser excitation is not too intense[1], the evolution of ρ is written as the sum of two terms:

$$\frac{\mathrm{d}\hat{\rho}}{\mathrm{d}t} = \left.\frac{\mathrm{d}\hat{\rho}}{\mathrm{d}t}\right|_{\text{coh.}} + \left.\frac{\mathrm{d}\hat{\rho}}{\mathrm{d}t}\right|_{\text{incoh.}}. \tag{II.7}$$

The first term describes the coherent evolution under the effect of the atom's coupling with the light field. This coupling is characterized by two parameters, each having the dimension of a frequency:

- The detuning $\Delta = \omega_{\mathrm{L}} - \omega_{\mathrm{A}}$ between the frequency of the light field ω_{L} and the resonant frequency of the atom ω_{A}.

[1] The Rabi frequency κ and the detuning Δ must both be small compared to the atomic frequency ω_{A}.

- The Rabi frequency $\kappa = dE_0\,\mathrm{e}^{\mathrm{i}\phi}/\hbar$, proportional to the reduced dipole d associated with the transition $g \leftrightarrow e$ and to the complex amplitude of the electric field of the light wave: $E(t) = E_0\cos(\omega_\mathrm{L}t - \phi) = \frac{1}{2}E_0\mathrm{e}^{\mathrm{i}(\omega_\mathrm{L}t-\phi)} + \text{c.c.}$. We have assumed here that the atom is located at the origin of coordinates $\boldsymbol{r} = 0$.

In the rotating field approximation[2], the Hamiltonian characterizing the coupling is written as a 2×2 matrix in the $\{|g\rangle, |e\rangle\}$ basis:

$$\hat{H} = \frac{\hbar}{2}\begin{pmatrix}\Delta & \kappa^* \\ \kappa & -\Delta\end{pmatrix}. \tag{II.8}$$

In particular, the non-diagonal terms of this Hamiltonian, $\kappa|e\rangle\langle g|$ and $\kappa^*|g\rangle\langle e|$, describe the photon absorption and emission processes in the monochromatic laser wave. In the density operator formalism, the atom-coherent field coupling is then deduced from the Schrödinger equation:

$$\mathrm{i}\hbar\left.\frac{\mathrm{d}\hat{\rho}}{\mathrm{d}t}\right|_{\text{coh.}} = [\hat{H}, \hat{\rho}]. \tag{II.9}$$

Incoherent coupling related to spontaneous emission processes is given by the simple evolution (Cohen-Tannoudji, Dupont-Roc, et al. 2012):

$$\left.\frac{\mathrm{d}P_g}{\mathrm{d}t}\right|_{\text{incoh.}} = \Gamma P_e, \qquad \left.\frac{\mathrm{d}P_e}{\mathrm{d}t}\right|_{\text{incoh.}} = -\Gamma P_e \tag{II.10}$$

$$\left.\frac{\mathrm{d}\rho_{eg}}{\mathrm{d}t}\right|_{\text{incoh.}} = -\frac{\Gamma}{2}\rho_{eg}, \qquad \left.\frac{\mathrm{d}\rho_{ge}}{\mathrm{d}t}\right|_{\text{incoh.}} = -\frac{\Gamma}{2}\rho_{ge} \tag{II.11}$$

The first line is identical to what we established in the previous chapter from Fermi golden rule. The second line shows that the coherence between g and e decreases with the rate $\Gamma/2$, i.e. half the population decay rate $P_e = \rho_{ee}$.

By adding the two contributions, coherent and incoherent, we arrive at the equation of motion of the density operator, constituting the set of *optical Bloch equations*:

$$\dot{P}_e = -\Gamma P_e + \frac{\mathrm{i}}{2}\left(\kappa^*\rho_{eg} - \kappa\rho_{ge}\right), \tag{II.12}$$

$$\dot{\rho}_{eg} = \left(\mathrm{i}\Delta - \frac{\Gamma}{2}\right)\rho_{eg} - \frac{\mathrm{i}\kappa}{2}\left(\rho_{gg} - \rho_{ee}\right), \tag{II.13}$$

[2]This approximation was detailed in the 2013-14 course, chapter 4.

to which we add the two other equations for $\dot{P}_g$ and $\dot{\rho}_{ge}$ deduced from $P_g + P_e = 1$ and $\rho_{ge} = \rho_{eg}^*$.

1-2 Stationary state of optical Bloch equations

The characteristic time to equilibrium for the system of equations (II.12-II.13) is of the order of Γ^{-1}. The stationary value of populations and coherences is given by

$$P_e = \frac{1}{2}\frac{s}{1+s}, \qquad \rho_{eg} = \frac{\kappa}{2\Delta + \mathrm{i}\Gamma}\,\frac{1}{1+s}, \tag{II.14}$$

where we have introduced the *saturation parameter*:

$$s = \frac{2|\kappa|^2}{\Gamma^2 + 4\Delta^2}. \tag{II.15}$$

Note. We often introduce the notion of saturation intensity I_sat for an atomic line, measured in $\mathrm{W{\cdot}m^{-2}}$, and characterize the strength of laser excitation by the ratio I/I_sat, where I is the intensity of light at the atomic location. This ratio is related to the parameters introduced above by:

$$\frac{I}{I_\mathrm{sat}} = \frac{2|\kappa|^2}{\Gamma^2}, \qquad s = \frac{I/I_\mathrm{sat}}{1 + 4\Delta^2/\Gamma^2}. \tag{II.16}$$

Our saturation parameter therefore coincides with the ratio I/I_sat for a laser beam in resonance with the atom. The advantage of using s is that it directly characterizes the atom's excitation rate:

- if $s \ll 1$, which can be obtained with low laser intensity or high detuning, the population of the excited state is negligible compared to that of the ground state:

$$s \ll 1: \qquad P_g \approx 1, \qquad P_e \approx \frac{s}{2}. \tag{II.17}$$

- if $s \gg 1$, the atom occupies the ground state and the excited state with equal probabilities

$$s \gg 1: \qquad P_g \approx P_e \approx \frac{1}{2}. \tag{II.18}$$

Knowing the stationary population of the excited state, we can now return to the expression for the radiation pressure force (II.2-II.3):

$$\gamma = \frac{\Gamma}{2}\frac{s}{1+s}, \qquad \boldsymbol{F} = \hbar\boldsymbol{k}\frac{\Gamma}{2}\frac{s}{1+s}. \tag{II.19}$$

The maximum value of this force is reached in the limit of strong saturation, $s \gg 1$, for which the atom performs on average $\Gamma/2$ absorption–spontaneous emission cycles per second. The corresponding acceleration is

$$a_{\max} = \frac{F_{\max}}{M} = v_{\mathrm{r}}\frac{\Gamma}{2} \tag{II.20}$$

where we have introduced the recoil velocity

$$v_{\mathrm{r}} = \frac{\hbar k}{M}, \tag{II.21}$$

i.e. the change in velocity of an atom when it absorbs or emits a photon. For a sodium atom illuminated on its resonance line, the recoil velocity is 3 cm/s and the maximum acceleration is $10^6\,\mathrm{m/s^2}$.

1-3 Using Ehrenfest's theorem

In the foregoing, we have adopted an intuitive approach (II.2-II.3) to relate the radiation pressure force to the spontaneous emission rate and thus to the excited state population. This result can be rigorously justified by starting from the complete Hamiltonian describing the coupling between the atom and the radiation, i.e. the Hamiltonian taking into account both the atom's internal variables and those describing the motion of its center of mass.

Noting $\hat{\boldsymbol{r}}$ and $\hat{\boldsymbol{p}}$ as the operators for the position and momentum of the center of mass, this Hamiltonian can be written as follows

$$\hat{H}_{\mathrm{tot.}} = \frac{\hat{\boldsymbol{p}}^2}{2M} + \frac{\hbar}{2}\begin{pmatrix}\Delta & \kappa^*\,\mathrm{e}^{-\mathrm{i}\boldsymbol{k}\cdot\hat{\boldsymbol{r}}}\\ \kappa\,\mathrm{e}^{\mathrm{i}\boldsymbol{k}\cdot\hat{\boldsymbol{r}}} & -\Delta\end{pmatrix}. \tag{II.22}$$

The force operator acting on the atom is calculated using the Heisenberg picture(Gordon & Ashkin 1980):

$$\hat{\boldsymbol{F}} = \frac{\mathrm{d}\hat{\boldsymbol{p}}}{\mathrm{d}t} = \frac{\mathrm{i}}{\hbar}[\hat{H}_{\mathrm{tot}}, \hat{\boldsymbol{p}}] \tag{II.23}$$

$$= \frac{1}{2}\hbar\boldsymbol{k}\begin{pmatrix}0 & i\kappa^*\mathrm{e}^{-\mathrm{i}\boldsymbol{k}\cdot\hat{\boldsymbol{r}}}\\ -\mathrm{i}\kappa\mathrm{e}^{\mathrm{i}\boldsymbol{k}\cdot\hat{\boldsymbol{r}}} & 0\end{pmatrix}. \tag{II.24}$$

We take the average of this operator on a wave packet localized in the vicinity of $\boldsymbol{r} = 0$ and of small extension in front of the optical wavelength:

$$\langle\hat{\boldsymbol{F}}\rangle = \mathrm{Tr}(\hat{\boldsymbol{F}}\hat{\rho}) = \hbar\boldsymbol{k}\,\frac{\mathrm{i}}{2}\left(\kappa^*\rho_{eg} - \kappa\rho_{ge}\right). \tag{II.25}$$

In steady state, the term in the right-hand side is none other than ΓP_e [*cf.* (II.12)], hence the announced result (II.2-II.3).

1-4 Doppler effect and the broad line condition

In the preceding paragraphs, we have outlined the notion of an average radiation pressure force. This average force, applied to the atom, will change its velocity. Taking this velocity into account in the formalism we have just established is simple: just use the fact that for a moving atom, the effective frequency of the laser is not ω_{L} but $\omega_{\mathrm{L}} - \boldsymbol{k}\cdot\boldsymbol{v}$ due to the Doppler effect. The saturation parameter is then a function of velocity:

$$s(\boldsymbol{v}) = \frac{2|\kappa|^2}{4(\Delta - \boldsymbol{k}\cdot\boldsymbol{v})^2 + \Gamma^2}, \tag{II.26}$$

as well as the radiation pressure force $\boldsymbol{F}(\boldsymbol{v})$. The evolution of the atom's velocity in a light wave is therefore given by the equation of motion

$$M\frac{\mathrm{d}\boldsymbol{v}}{\mathrm{d}t} = \boldsymbol{F}(\boldsymbol{v}), \tag{II.27}$$

an expression we will generalize in what follows to the case where several plane waves simultaneously illuminate the atom.

However, we must first examine the validity of the notion of average force. We have already used the fact that the average momentum carried

away by a spontaneously emitted photon is zero. The notion of force can be deduced from this if the value of this force changes only by a small amount in an elementary change in velocity $v \to v \pm v_{\rm r}$. It is this necessary condition that we now propose to examine.

For low light intensity ($s \ll 1$), the width of the resonance curve giving P_e as a function of the detuning Δ is equal to Γ (total width at half-height). The change in detuning in an elementary absorption or emission process is equal to $kv_{\rm r} = 2\omega_{\rm r}$, where $\omega_{\rm r} = \hbar k^2/(2M)$ is the recoil frequency. We can therefore distinguish two limiting situations:

- If $\Gamma \gg \omega_{\rm r}$ (broad line), then an elementary absorption or emission process hardly changes the saturation parameter s, nor the population of the excited state. It is only by repeating a large number of such processes that $s(\boldsymbol{v})$ can be modified appreciably. This is the case that will interest us in the remainder of this chapter. It occurs for the resonance line of many atomic species, as shown in the table below. For example, we find $\Gamma/\omega_{\rm r} \sim 400$ for the sodium atom.

- If $\Gamma \ll \omega_{\rm r}$, the absorption or emission of a single photon is enough to change $s(\boldsymbol{v})$ considerably. The atom may be in resonance with the laser before a spontaneous absorption-emission cycle, and completely out of resonance after this cycle[3], so that the notion of average force for a given $\boldsymbol{v}$ velocity loses its meaning. We will explore the possibilities offered by these narrow lines in the next chapter.

	A	λ nm	$\Gamma/2\pi$ kHz	$\omega_{\rm r}/2\pi$ kHz	$\Gamma/\omega_{\rm r}$	$T_{\rm min}$ μK	$v_{\rm r}$ cm/s	v_0 cm/s	$\delta v_{\rm res}$ cm/s	ℓ μm
He	4	1083	1600	42.3	38	38	9.16	28.2	173	3.3
Li	6	671	5910	73.5	80	142	9.86	44.2	397	4.3
Na	23	589	9800	24.9	394	235	2.93	29.1	577	18.5
Mg	24	285	80000	101.8	786	1922	5.80	81.3	2280	17.8
K	39	770	6000	8.6	699	144	1.32	17.5	462	42.8
Ca	40	423	34600	27.7	1248	831	2.35	41.4	1464	42.0
Cr	52	426	5020	21.1	238	121	1.79	13.8	214	8.1
Rb	87	780	6100	3.8	1627	147	0.59	11.8	476	101.0
Sr	84	461	30500	11.1	2743	733	1.03	26.8	1406	100.6
Cs	133	852	5200	2.1	2529	125	0.35	8.8	443	171.5
Er	168	401	27500	7.3	3743	661	0.59	18.0	1103	119.4
		583	190	3.5	55	5	0.41	1.5	11	2.5
Dy	170	421	32000	6.6	4857	769	0.55	19.3	1347	162.7
		626	135	3.0	45	3	0.37	1.3	8	2.3
Yb	174	399	29100	7.2	4061	699	0.57	18.2	1161	128.9
		556	183	3.7	50	4	0.41	1.4	10	2.2
Hg	202	254	1300	15.2	85	31	0.77	3.6	33	1.7

Table II.1. *Characteristics of some chemical elements with a broad resonance line ($\Gamma/\omega_{\rm r} \gg 1$) that can be laser-cooled. For certain atoms with two outer electrons, the main line ${}^1S_0 \leftrightarrow {}^1P_1$ and the intercombination line ${}^1S_0 \leftrightarrow {}^3P_1$ are indicated. The minimum temperature shown, and the root-mean-square velocity v_0, correspond to the Doppler cooling studied in this chapter. For some of these elements, Sisyphus-type cooling is also possible, leading to lower temperatures than those indicated here.*

[3] We can nevertheless recover a broad-line situation even if $\Gamma \ll \omega_{\rm r}$. To do this, we need to choose a value for the Rabi frequency $|\kappa| \gg \Gamma$, so that the population of the excited state

$$P_e = \frac{1}{2}\frac{s}{1+s} = \frac{|\kappa|^2}{4(\Delta - \boldsymbol{k}\cdot\boldsymbol{v})^2 + 2|\kappa|^2 + \Gamma^2} \tag{II.28}$$

has an broadened resonance:

$$\Gamma \longrightarrow \sqrt{\Gamma^2 + 2|\kappa|^2} = \Gamma\sqrt{1 + I/I_{\rm sat}}, \tag{II.29}$$

which can be considerably larger than Γ for realistic values of $I/I_{\rm sat}$.

2 Doppler cooling

We now turn to the description of Doppler cooling with lasers. The mechanism involved is very similar to that seen in the previous chapter for blackbody radiation. The theoretical description will also be very similar, with a Brownian motion-type approach to evaluating a friction coefficient and a momentum diffusion coefficient, and finally deducing the cooling limit temperature.

2-1 Optical molasses and low saturation assumption

We aim to achieve a Doppler cooling situation, in which an atom with a non-zero initial velocity experiences a friction force that drives its velocity towards 0. To achieve this, we illuminate the zone of interest with one, two or three pairs of waves, depending on the number of directions in space we wish to cool (figure II.2). As initially proposed by Hänsch & Schawlow (1975), we choose a detuning $\Delta < 0$, i.e. $\omega_{\rm L} < \omega_{\rm A}$, so that a moving atom is closer to resonance with a counter-propagating wave ($\boldsymbol{k}\cdot\boldsymbol{v} < 0$) than with a co-propagating wave ($\boldsymbol{k}\cdot\boldsymbol{v} > 0$). This is the cooling phenomenon we are looking for. Now let us be more quantitative and calculate the total force acting on the atom.

To calculate this force, it is tempting to add the radiation pressure forces created by the 2, 4 or 6 waves illuminating the atom. In the case of the single plane wave studied in paragraph 1, the absorption-stimulated emission cycles played no role, as they were not associated with any momentum transfer, the atom returning to the wave the momentum it had borrowed from it during absorption. If several plane waves are simultaneously incident on the atom, the atom can absorb a photon in wave 1, then make a stimulated emission in wave 2, thus gaining the momentum $\hbar(\boldsymbol{k}_1 - \boldsymbol{k}_2)$. Of course, the reverse process is also possible, but it is unclear that both processes occur with the same amplitude, for a given atomic velocity and position.

There is one situation in which taking the sum of the radiation pressures is a good approximation: this is the case where the saturation parameter s_0 associated with each travelling wave is much smaller than 1, and where we

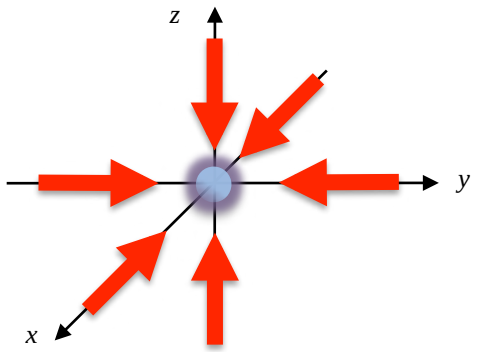

Figure II.2. *Basic diagram of a three-dimensional optical molasses. The atoms are illuminated by 3 pairs of monochromatic waves, with negative detuning* $\Delta = \omega_{\rm L} - \omega_{\rm A}$.

can therefore neglect the processes of stimulated emission in comparison with those of spontaneous emission. Note, however, that this approximation ignores the periodic structure of the standing waves created by the superposition of traveling waves. The calculated force must therefore be understood as the spatial average (over one standing-wave period) of the force $\boldsymbol{F}(\boldsymbol{r},\boldsymbol{v})$ calculated by a more sophisticated method, such as numerical resolution of the optical Bloch equations at any point $(\boldsymbol{r},\boldsymbol{v})$ in phase space.

Once this approximation has been made, the force acting on the atom is easy to calculate:

$$\boldsymbol{F}(\boldsymbol{v}) = \frac{\Gamma}{2}\sum_j \hbar\boldsymbol{k}_j s_j(\boldsymbol{v}), \tag{II.30}$$

where the sum relates to all running plane waves illuminating the atom, with

$$s_j(\boldsymbol{v}) = \frac{2|\kappa|^2}{4(\Delta - \boldsymbol{k}_j\cdot\boldsymbol{v})^2 + \Gamma^2}, \qquad s_j(0) \equiv s_0. \tag{II.31}$$

To apply the theory of Brownian motion, we consider the case of velocities small in front of the interval $\delta v_{\rm res}$ quasi-resonant with a monochromatic light wave:

$$|kv| \ll \Gamma \qquad \Rightarrow \qquad |v| \ll \delta v_{\rm res} \equiv \Gamma/k, \tag{II.32}$$

which allows us to calculate the force at order 1 in velocity:

$$\boldsymbol{F}(\boldsymbol{v}) = -M\alpha\,\boldsymbol{v}, \qquad \text{with} \quad M\alpha = \hbar k^2 s_0\,\frac{2(-\Delta)\Gamma}{\Delta^2+\Gamma^2/4}, \tag{II.33}$$

where we used $\sum_j \boldsymbol{k}_j = 0$ for the geometry considered, which cancels out the 0-order term in v. We have also used for the term of order 1:

$$\sum_j \boldsymbol{k}_j\,(\boldsymbol{k}_j\cdot v) = 2k^2\,\boldsymbol{v} \tag{II.34}$$

in the geometry of figure II.2. It is clear from (II.33) that a negative detuning Δ must be chosen to generate friction ($\alpha > 0$).

If we fix a given value of the saturation parameter s_0, chosen in particular such that $s_0 \ll 1$ so that the approximation consisting in summing the forces created by the different plane waves is valid, we see that the coefficient of friction α is maximum when $|\Delta|/(\Delta^2+\Gamma^2/4)$ is maximum, which occurs for $\Delta = -\Gamma/2$:

$$\text{Maximum friction coefficient at fixed } s: \quad \alpha = 2\,s_0\,\frac{\hbar k^2}{M} \ \text{ for } \Delta = -\frac{\Gamma}{2}.$$

2-2 Momentum diffusion and equilibrium temperature

As in the previous chapter, an analysis in terms of Brownian motion also requires the knowledge of the momentum diffusion coefficient (Gordon & Ashkin 1980). The treatment developed for the blackbody radiation can be directly transposed. We found that this coefficient can be written as $D_p = \hbar^2 k^2 R/6$, where R is the rate of elementary processes, absorption or emission, for an atom at rest. In this case, the scattering rate for an atom illuminated by six waves of saturation parameter s_0 is $R = 6\times\Gamma s_0$, i.e.

$$D_p = \hbar^2 k^2 s_0\,\Gamma. \tag{II.35}$$

The final step is to determine the equilibrium temperature of the atoms illuminated by these light beams:

$$k_{\mathrm{B}}T = \frac{D_p}{M\alpha} = \frac{\hbar}{2}\frac{\Delta^2+\Gamma^2/4}{|\Delta|}. \tag{II.36}$$

First, we note that this quantity is independent of the power of the light waves. In fact, the coefficients of friction α and diffusion D_p are both linear in intensity ($\propto s_0|\kappa|^2$). We then see that this temperature is minimal for :

$$\Delta_{\min} = -\frac{\Gamma}{2}, \qquad k_{\mathrm{B}}T_{\min} = \frac{\hbar\Gamma}{2}, \tag{II.37}$$

which constitutes the Doppler limit announced in the introduction to this chapter. These temperatures are located in the $1-1000$ μK range. The values corresponding to certain atomic species commonly used in radiative cooling experiments are given in table II.1.

As we saw in the previous chapter, a Fokker–Planck equation approach shows that the stationary velocity distribution is a Gaussian, identical to a Maxwell-Boltzmann distribution of velocity width v_0 given by

$$\frac{1}{2}Mv_0^2 = \frac{1}{2}k_{\mathrm{B}}T_{\min}, \qquad \text{i} \quad v_0 = \sqrt{\frac{\hbar\Gamma}{2M}}. \tag{II.38}$$

2-3 Validity of the Brownian motion approach

Since we have used a Brownian motion approach here, we need to check that the underlying assumption of small steps is verified. Furthermore, we have used a linear approximation to calculate the force as a function of the velocity, and we need to ensure that this approximation is satisfied for the predicted mean-square velocity v_0 at equilibrium.

Let us show that the broad-line criterion ensures that these two conditions are met. For our problem, the elementary step of the random walk in velocity space is the recoil velocity $v_{\mathrm{r}} = \hbar k/M$. This velocity is indeed small compared to v_0:

$$\frac{v_{\mathrm{r}}}{v_0} = \frac{\hbar k/M}{\sqrt{\hbar\Gamma/2M}} = 2\sqrt{\frac{\omega_{\mathrm{r}}}{\Gamma}} \ll 1. \tag{II.39}$$

Regarding the validity of the linear approximation, we check that v_0 is small compared to the velocity range δv_{res} :

$$\frac{v_0}{\delta v_{\mathrm{res}}} = \frac{\sqrt{\hbar\Gamma/2M}}{\Gamma/k} = \sqrt{\frac{\omega_{\mathrm{r}}}{\Gamma}} \ll 1. \tag{II.40}$$

We therefore have three velocity scales in the problem:

$$v_{\mathrm{r}} \ll v_0 \ll \delta v_{\mathrm{res}}, \tag{II.41}$$

which guarantees the validity of our approach. For the sodium atom, these three velocities are 3 cm/s, 30 cm/s and 600 cm/s (see table).

Time constants. The model we have just presented can also be used to estimate the typical cooling time for $\Delta = \Delta_{\min}$:

$$\alpha^{-1} = \frac{M}{\hbar k^2}\,\frac{1}{2s_0}. \tag{II.42}$$

In the limit of low saturation, this time can of course be arbitrarily long. Let us take $s_0 = 0.1$ as a typical upper bound for our perturbative treatment. We then find $\alpha^{-1} \sim 20\,\mu$s for the sodium atom, which is short: for an initial velocity $v_i = \delta v_{\mathrm{res}} = 6$ m/s (at the limit of the linearity range), the atom only travels about a hundred microns before its mean velocity becomes negligible.

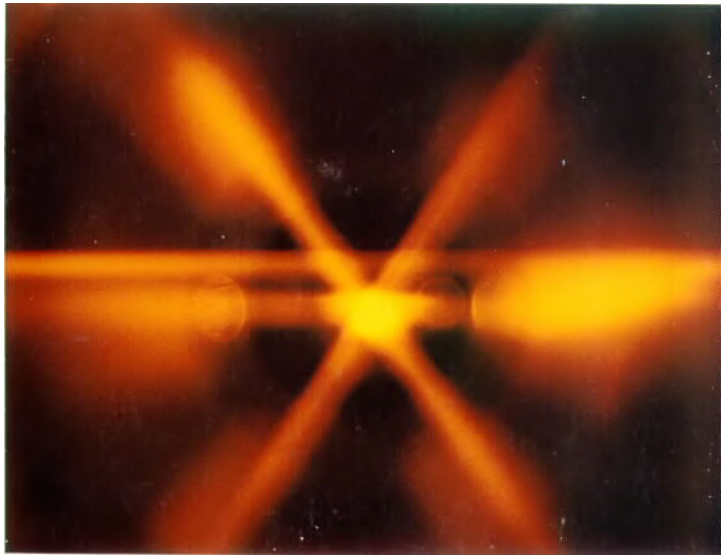

Figure II.3. *Sodium molasses made in W.D. Phillips' group (NBS-NIST).*

3 Optical molasses in practice

The first optical molasses was produced by Chu, Hollberg, et al. (1985) shortly after atoms were successfully stopped by radiation pressure (Ertmer, Blatt, et al. 1985; Prodan, Migdall, et al. 1985). Figure II.3 shows an image of an optical molasses obtained in 1987 in Bill Phillips' group, with sodium atoms (Lett, Watts, et al. 1988a). The central volume, of the order of a cubic centimetre, contains 10^8 atoms. We are showing this image now, but we will see later that another cooling mechanism, based on the Sisyphus effect, was also at work in this gas of sodium atoms.

3-1 How to take saturation into account?

Our description in the previous paragraph was based on an assumption of low saturation, allowing the radiation pressure forces created by all the traveling waves making up the optical molasses to be added together. But in this low-saturation hypothesis, the cooling time varies as $1/s_0$ and is therefore long. In practice, it is tempting to increase the light intensity, but how can we take into account the phenomena that may then occur?

It should be pointed out at the outset that it is difficult to give an exact treatment of the problem. It is possible to calculate the force acting on an atom of velocity v in a standing light wave of arbitrarily high intensity, by searching for the steady-state regime of the optical Bloch equations (Minogin & Serimaa 1979). Let us briefly outline the principle behind this calculation: the Rabi frequency associated with a standing wave varies as $\cos(\boldsymbol{k}\cdot\boldsymbol{r})$, which creates time-modulated terms for a given trajectory $\boldsymbol{r}(t) = \boldsymbol{r}_0 + \boldsymbol{v}t$ of the atom. The system of optical Bloch equations can then be solved numerically by a Fourier series expansion (via the continued fraction approach). Going beyond the calculation of the force and evaluating the diffusion coefficient is an tedious task, which does not provide much physical intuition, especially in the three-dimensional case.

In practice, the optimal regime for optical molasses corresponds to a

saturation parameter per wave that does not exceed unity. In this case, we use a *ad-hoc* procedure, which consists of considering that the atom is simply saturated by all six incident waves, and using the response of this saturated system. Two slightly different procedures can be found in Lett, Phillips, et al. (1989) and Wohlleben, Chevy, et al. (2001). As an example, let us mention the procedure proposed by Lett, Phillips, et al. (1989), where one takes as an approximate value the total force acting on the atom:

$$\boldsymbol{F}(\boldsymbol{v}) \approx \sum_j \hbar \boldsymbol{k}_j \frac{\Gamma}{2} \frac{I/I_{\rm sat}}{1+4(\Delta - \boldsymbol{k}_j\cdot\boldsymbol{v})^2/\Gamma^2 + NI/I_{\rm sat}}. \tag{II.43}$$

where N is the total number of traveling plane waves incident on the atom. We will see later that the results obtained are in reasonable agreement with experimental observations, in particular the equilibrium temperature:

$$k_{\rm B}T = \frac{\hbar\Gamma}{2}\,\frac{\Gamma}{4|\Delta|}\left(1+\frac{4\Delta^2}{\Gamma^2}+\frac{NI}{I_{\rm sat}}\right). \tag{II.44}$$

Remember, however, that this is just one heuristic solution to a complex situation.

3-2 Capture of atoms in optical molasses

Optical molasses is formed by centimeter-sized beams intersecting in the center of a vacuum chamber (figure II.3). A key practical issue is the loading of this molasses with atoms of any velocity v. Given a finite distance L to capture an atom, what is the maximum velocity that can be brought to rest by the friction force?

Let us work with a one-dimensional version of the problem for simplicity. The equation of motion of an atom is

$$M\frac{{\rm d}v}{{\rm d}t} = F(v) \tag{II.45}$$

with

$$F(v) = \frac{\hbar k\Gamma}{2}\frac{I}{I_{\rm sat}}\left[\frac{1}{1+4(\Delta-kv)^2/\Gamma^2} - \frac{1}{1+4(\Delta+kv)^2/\Gamma^2}\right]. \tag{II.46}$$

We write this equation as

$$Mv\frac{{\rm d}v}{{\rm d}x} = F(v) \tag{II.47}$$

which can be integrated into

$$M\int_{v_i}^{v_f}\frac{v}{F(v)}{\rm d}v = \int {\rm d}x = L. \tag{II.48}$$

We wish to obtain $v_f \approx 0$ and seek to maximize v_i, for a fixed L. In practice, this optimum is obtained by taking the detuning $\Delta \approx -kv_i/2$, so that the effective detuning is initially on the blue of the atomic resonance $\Delta + kv_i \approx +kv_i/2$, and finally on the red of this resonance $\Delta + kv_f \approx \Delta \approx -kv_i/2$. We then find, keeping only the contribution of the resonant wave with the atom in (II.46)

$$\frac{1}{6}\frac{k^2v_i^4}{\Gamma^2} + \frac{v_i^2}{2} \approx \frac{\hbar k\Gamma}{2M}\frac{I}{I_{\rm sat}}L. \tag{II.49}$$

As soon as the distance L is large enough, the dominant term in the left-hand side of (II.49) is the term in v_i^4, corresponding to the variation $F(v) \propto 1/v^2$ for $|\Delta - kv| \gtrsim \Gamma$. We thus obtain the scaling law

$$\frac{kv_i}{\Gamma} \approx \left(3\frac{L}{\ell}\frac{I}{I_{\rm sat}}\right)^{1/4} \tag{II.50}$$

where $\ell = M\Gamma/\hbar k^3$ is the relevant length scale for this problem (*cf.* table II.1). The velocity that can be captured in optical molasses therefore varies only as the power $1/4$ of the available distance, which is not very favorable. We will see later how the magneto-optical trap leads to a much more promising situation.

An example of a phase portrait, i.e. the variation of velocity as a function of position, is shown in figure II.4. The distance $L = 400\,\ell$ corresponds to about one centimeter for sodium atoms. The maximum velocity that can be captured in this molasses, obtained for $\Delta \approx -3\Gamma$, is such that $kv_i/\Gamma \approx 5$, in good agreement with (II.50).

3-3 Spatial diffusion

Optical molasses is a simple way of accumulating a large number of atoms, in excess of a million, in a given volume of space, on the order of a cubic

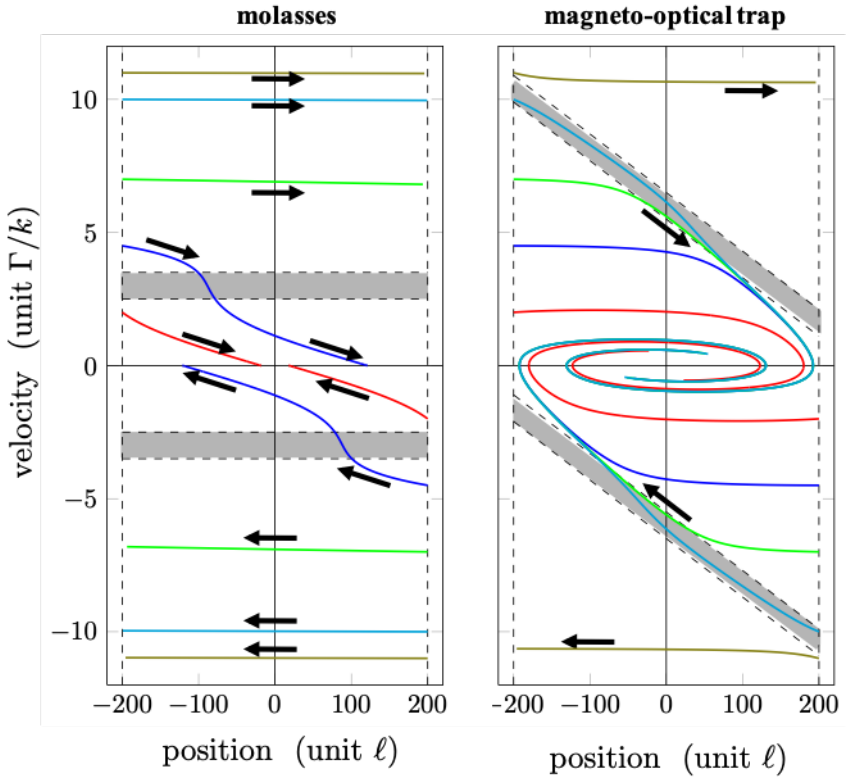

Figure II.4. *Phase portrait of 1D capture in optical molasses (left) and in a magneto-optical trap (right), with two waves of intensity $I = I_{\rm sat}/2$ and effective length $L = 400\,\ell$, with $\ell = M\Gamma/\hbar k^3$. The total force is taken to be the sum of the two individual radiation pressure forces (taking saturation into account). The shaded area represents the phase-space zone resonant with the light wave (to within $\pm\Gamma/2$). The detuning has been optimized to maximize the capture rate, as well as the magnetic field gradient in the case of the magneto-optical trap. Molasses: $\Delta = -3\,\Gamma$; Magneto-optical trap: $\Delta = -6\,\Gamma$, $\mu b'\ell/\hbar\Gamma = 0.022$. The trajectories correspond to initial velocities $k|v|/\Gamma = 2,\ 4.5,\ 7,\ 10,\ 11$. The capture velocity is of the order of $5\,\Gamma/k$ for molasses and $10\,\Gamma/k$ for the magneto-optical trap.*

centimetre. The reason why this number can be so large lies in the relatively long time it takes for an atom to find the edge of the molasses and escape. In other words, the spatial diffusion coefficient in molasses is low (and additional cooling mechanisms, such as Sisyphus cooling, lowers it further).

In the previous chapter, we obtained the general expression for the spatial diffusion coefficient D_x for Brownian motion:

$$D_x = v_0^2/\alpha. \tag{II.51}$$

Consider molasses with optimal detuning $\Delta = -\Gamma/2$:

$$v_0^2 = \frac{\hbar\Gamma}{2M}, \qquad \alpha = 2s_0\frac{\hbar k^2}{M} \qquad \Rightarrow \qquad D_x = \frac{\Gamma}{4k^2}\,\frac{1}{s_0}. \tag{II.52}$$

For a sodium atom ($\lambda = 0.59\,\mu$m, $\Gamma/2\pi = 10\,$MHz) and the choice $s_0 = 0.1$, this gives $D_x \sim 1.4\,\text{mm}^2/\text{s}$: for a centimetre-sized molasses, it takes more than ten seconds for an atom starting from the center to reach the edge of the molasses and escape. Although there is no trapping force as such, the high viscosity means that atoms accumulate in the molasses. Sub-Doppler cooling processes further reduce this spatial diffusion coefficient and thus reinforce the accumulation of atoms, the coefficient D_x in this case being of the order of tens of h/M.

3-4 Some recent experimental tests at 3D

Testing the theory of broad-line Doppler cooling is not as easy as it sounds, at least not in three dimensions. Indeed, for many atomic species, the ground level is degenerate and other cooling mechanisms are also present, such as the Sisyphus cooling we will see in a later chapter. This is notably the case for all alkali-metal species, whose ground level is degenerate due to (i) the spin of the outer electron, (ii) the spin of the nucleus. Good candidates for testing Doppler cooling theory are the bosonic isotopes of atoms with two outer electrons. Indeed, these atoms have a zero electron spin in their ground state (singlet state for the two outer electrons) and the nuclear spin can also be zero for bosonic isotopes (it is necessarily half-integer for fermionic isotopes).

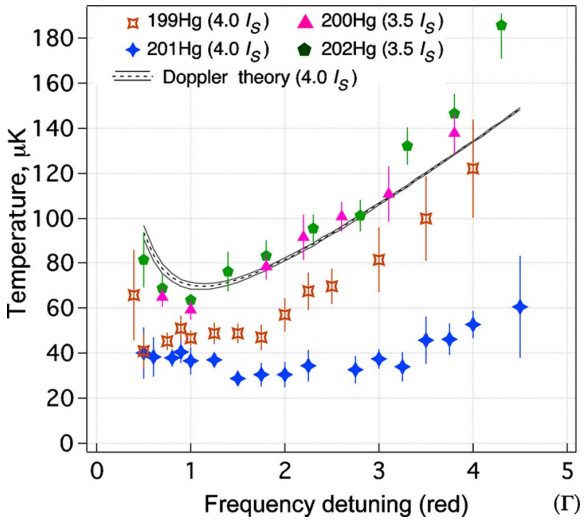

Figure II.5. *Temperature of an optical molasses of mercury atoms for different isotopes. Figure taken from McFerran, Yi, et al. (2010). The Doppler cooling prediction is shown as a solid line, heuristically taking saturation effects into account [eq. (II.44)]. Bosonic isotopes, with zero nuclear spin, give results in good agreement with Doppler cooling theory. For fermionic isotopes, sub-Doppler cooling mechanisms are also present.*

In figure II.5, we have plotted the result of McFerran, Yi, et al. (2010), obtained on isotopes 200 and 202 of the mercury atom (pink and green dots). Cooling is performed on the ${}^1S_0 \leftrightarrow {}^3P_1$ intercombination line ($\lambda = 254\,\text{nm}$ and $\Gamma/2\pi = 1.3\,\text{MHz}$). The broad-line condition is well verified in this case, since the natural width is about 100 times greater than ω_r. Temperatures are measured using the time-of-flight technique, from atoms initially captured in a magneto-optical trap (see below). The measured temperature variation reproduces well the expected Doppler cooling law, once saturation effects have been taken into account in the heuristic way described in §3-1 (in this experiment, there was a total intensity at the molasses center $\sim 4\,I_\text{sat}$, with $I_\text{sat} = 10.2\,\text{mW/cm}^2$). Temperature measurements made on fermionic isotopes of mercury are also shown on this graph, and clearly demonstrate the existence of sub-Doppler mechanisms for these isotopes.

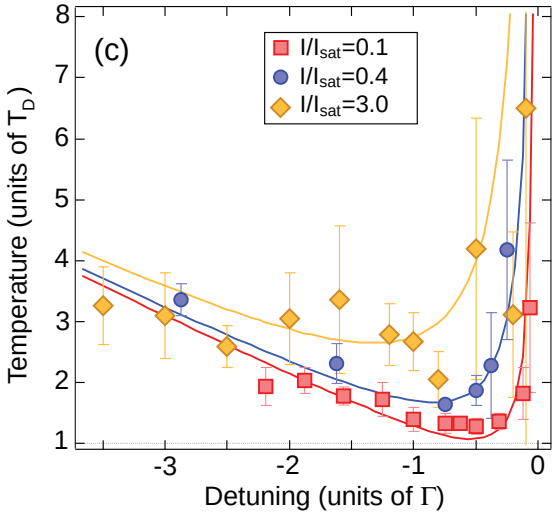

Figure II.6. *Evolution of temperature with detuning in an optical molasses of metastable helium atoms, for different values of light intensity. The lines represent the prediction (II.44). Figure taken from Chang, Hoendervanger, et al. (2014).*

Another recent result on the test of Doppler cooling theory is given by Chang, Hoendervanger, et al. (2014) and is shown in figure II.6. This time, the experiment is performed on metastable helium atoms ($\lambda = 1083\,\text{nm}$, $\Gamma/2\pi = 1.6\,\text{MHz}$), which has a degenerate ground level. However, the authors placed themselves in conditions where sub-Doppler mechanisms play a negligible role. The experiment carried out at low intensity ($I_\text{sat}/10$ for total intensity) leads to very good agreement with Doppler theory [minimum measured temperature $\sim 1.3\,T_\text{min}$ given in (II.38)]. At higher intensities, the variation in temperature with detuning is also in good agreement with the heuristic law (II.44).

3-5 Laser cooling of macroscopic bodies

Although this course is devoted to the cooling of individual atoms, let us briefly mention here that the radiation pressure force can also be used to

cool certain degrees of freedom of macroscopic objects, such as the center of mass of a mirror in an optical cavity. The corresponding field of research, optomechanics, is rapidly expanding and it is beyond the scope of this lecture series to cover it [see, for example, the recent review article by Aspelmeyer, Kippenberg, et al. (2014)]. We will just briefly describe here the initial experiments carried out some ten years ago, the principle of which is close to what we have seen so far for individual atoms (Arcizet, Cohadon, et al. 2006; Gigan, Böhm, et al. 2006; Schliesser, Del'Haye, et al. 2006).

Let us take a look at the experimental diagram shown in figure II.7, where a light beam impinges on a Fabry–Perot cavity, the second mirror of which is mounted on a spring. The light in the cavity creates a radiation pressure force on this mirror, whose equilibrium position is a certain abscissa L^*, for which the radiation pressure force F_{RP}, directed to the right, exactly compensates for the spring force F_{spring}, directed to the left:

$$\text{Mirror at rest in } L^* : \qquad F_{\mathrm{RP}} + F_{\mathrm{spring}} = 0. \tag{II.53}$$

The radiation pressure force depends on the light power stored in the cavity, which in turn depends on the cavity length L. When L is an integer multiple of $\lambda/2$, this power is maximum.

Let us assume that the position of the spring is chosen such that L^* is slightly less than $n\lambda/2$, and let us consider an oscillation of the mirror around its equilibrium position. When the mirror passes through L^* on its way to the right, the number of photons in the cavity is increasing. Because of the time constant required for this photon number to reach its stationary value, it will be lower than it would be if the mirror were stationary at L^*. The radiation pressure force is therefore weaker than it would be for a stationary mirror, and the force felt by the mirror as it passes the point L^* is therefore directed to the left:

$$\text{Mirror passing in } L^* \text{ to the right : } \qquad F_{\mathrm{RP}} + F_{\mathrm{spring}} < 0, \tag{II.54}$$

therefore opposite to the motion of the mirror. Similarly, when the atom passes through L^* coming from the right, the cavity contains a few more photons than if the mirror were stationary and

$$\text{Mirror passing in } L^* \text{ to the left : } \qquad F_{\mathrm{RP}} + F_{\mathrm{spring}} > 0. \tag{II.55}$$

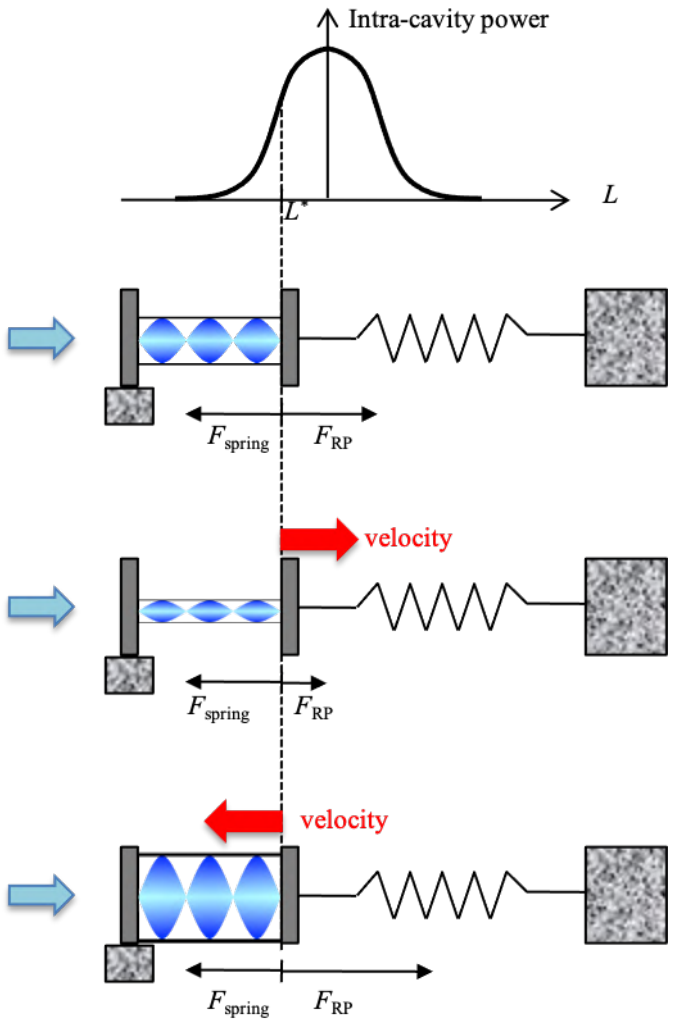

Figure II.7. *Fabry–Perot cavity with a moving mirror. For a suitable choice of equilibrium position L^*, the radiation pressure force dampens the motion of the mirror's center of mass. The damping comes from the non-zero time it takes for the intracavity power to adjust to the mirror position as it oscillates around its equilibrium position.*

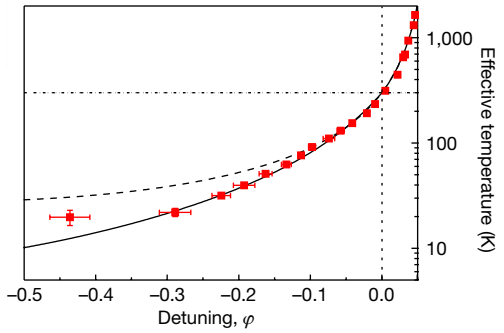

Figure II.8. *The effective temperature associated with the motion of the center of mass of the moving mirror of a Fabry–Perot cavity, as a function of the detuning of this cavity. The dotted line is the prediction obtained by considering only one mode of the mechanical micro-resonator, while the solid line takes into account the contribution of the other modes. Figure taken from Arcizet, Cohadon, et al. (2006).*

So, in addition to the static forces acting on the mirror at rest, we find a velocity-dependent force opposing the motion of the mirror's center of mass and cooling this degree of freedom (figure II.8). This friction force, analogous to the Doppler friction force for an atom, lowers the temperature associated with this degree of freedom. Note that friction is obtained only if L^* is chosen slightly to the left of the resonance $n\lambda/2$ of the Fabry–Perot cavity. Had we chosen L^* slightly to the right of this resonance, we would have found an accelerating force. The quantity $L^* - n\lambda/2$ (denoted φ in figure II.8) therefore plays the role of detuning $\Delta = \omega_L - \omega_A$ for free atoms.

4 The magneto-optical trap

Optical molasses based on the Doppler effect provides a simple means of slowing down atoms and maintaining their velocity around 0, with a temperature of the order of $\hbar\Gamma/k_B$. In addition to Doppler cooling, the magneto-optical trap provides a means of confining atoms around a given point. The only additional ingredient is a magnetic field gradient, which

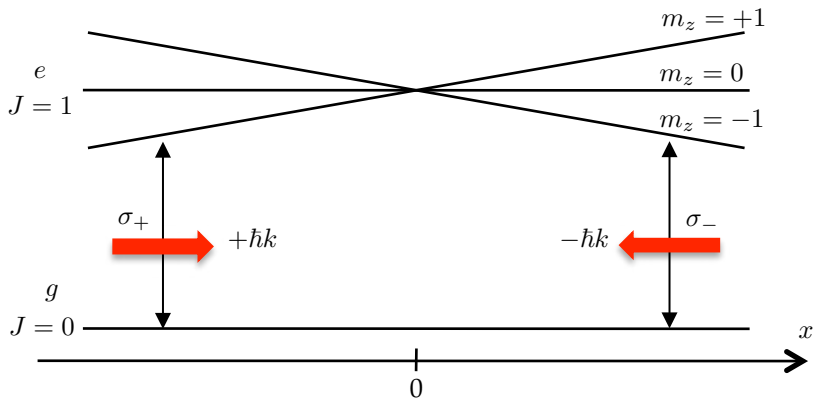

Figure II.9. *Basic principle of the magneto-optical trap (one-dimensional version). The radiation pressure force created by each light wave is position-dependent, due to the presence of a magnetic field gradient. The resultant of the two radiation pressure forces is a restoring force towards the origin.*

acts differently on the ground and excited levels of the atom, and introduces a spatial dependence of the radiation pressure force. This principle was first put into practice by Raab, Prentiss, et al. (1987).

4-1 Equilibrium size for small atom numbers

The basic principle of the magneto-optical trap is illustrated in figure II.9, in a one-dimensional geometry (generalization to 3D poses no problem of principle). Consider a transition between a ground level with zero angular momentum and an excited level with angular momentum $J_e = 1$. A magnetic field gradient lifts the degeneracy between the three Zeeman states of the excited level. If we take a circular polarization for each of the beams making up the molasses, we achieve the desired situation: for a negative detuning (the one required for Doppler cooling), an immobile atom at $x > 0$ will feel a greater radiation pressure force from the wave coming from the right than from the one coming from the left: it will therefore be pushed towards the central point. Similarly, an atom at $x < 0$ will feel a greater force from the wave propagating to the right, and will also be

pushed towards the center.

To be more quantitative, we introduce the magnetic moment μ associated with the excited atomic level, so that the Zeeman displacement of a sublevel m is $m\mu B$, where B is the amplitude of the magnetic field at the atom's location. For the magnetic field gradient shown in figure II.9, the field amplitude is written $B = b'x$, so the force felt by an atom located at point x with velocity v is written:

$$F(x,v) = \frac{\hbar k\Gamma}{2}\frac{I}{I_{\rm sat}}\Big[\frac{1}{1+4(\Delta - kv - \mu b'x/\hbar)^2/\Gamma^2} - \frac{1}{1+4(\Delta + kv + \mu b'x/\hbar)^2/\Gamma^2}\Big]. \quad \text{(II.56)}$$

Let us restrict ourselves to Doppler (kv) and Zeeman ($\mu b'x/\hbar$) shifts that are small compared to the natural width Γ. At lowest non-zero order, we obtain a force which is linear in position and velocity:

$$F(x,v) = -Kx - M\alpha v, \quad \text{(II.57)}$$

which gives rise to damped harmonic motion. The coefficient of friction α is identical to that found for molasses. The stiffness K of the restoring force is:

$$K = k\mu b' s_0 \frac{2\Gamma|\Delta|}{\Delta^2 + \Gamma^2/4}. \quad \text{(II.58)}$$

Let us move on to determining the equilibrium size of the trapped atom cloud. The momentum diffusion coefficient is unchanged, so the equilibrium state is always a thermal state, with temperature determined by $k_{\rm B}T = D_p/M\alpha$. The equilibrium distribution is a Gaussian in position, with standard deviation x_0 given by

$$\frac{1}{2}Kx_0^2 = \frac{1}{2}Mv_0^2 = \frac{1}{2}k_{\rm B}T, \quad \text{(II.59)}$$

which gives

$$x_0 = \left(\frac{\hbar\Gamma}{4k\mu b' s_0}\right)^{1/2} \quad \text{(II.60)}$$

if we choose the detuning $\Delta = -\Gamma/2$ providing the minimum temperature $k_{\rm B}T = \hbar\Gamma/2$. To obtain an order of magnitude for x_0, let us take again the case of sodium atoms, with $s_0 = 1/10$ and a typical magnetic field gradient $b' = 10\,{\rm G/cm}$ (0.1 Tesla per meter). We find $x_0 = 40\,\mu$m for the detuning $\Delta = -\Gamma/2$.

In practice, two antagonistic effects modify this prediction:

- For a degenerate ground level, the Sisyphus processes that increase the friction coefficient will also increase the stiffness K of the magneto-optical trap, thus reducing its size (Cooper, Hillenbrand, et al. 1994; Townsend, Edwards, et al. 1995).
- Collective effects, related to the multiple scattering of photons within the cloud of atoms, increase the equilibrium size of the trapped gas, as we will see below (4-3).

The aforementioned article by Chang, Hoendervanger, et al. (2014) measured this size for helium atoms in a metastable electronic level. The spatial density in the magneto-optical trap they made was low (limited by Penning collisions), so the collective effects we will discuss below were negligible in their case. The measured sizes are in good agreement with the prediction (II.60), as shown in figure II.10.

4-2 Capture in a magneto-optical trap

In addition to bringing all atoms to the same point in space, the magneto-optical trap has the advantage of capturing atoms at a significantly higher velocity than optical molasses. This point is illustrated in the phase portrait in figure II.4. The resonance of an atom with the laser beams occurs for all "position-velocity" pairs satisfying:

$$\pm\Delta = kv + \mu b'x/\hbar. \quad \text{(II.61)}$$

If we have a total distance L to capture the atoms, the optimal configuration is obtained when an atom at rest at the point $x = L/2$, on the right edge of the capture zone, is resonant with the beam pushing it towards the center, i.e.:

$$|\Delta| \approx \frac{\mu b'}{\hbar}\frac{L}{2}. \quad \text{(II.62)}$$

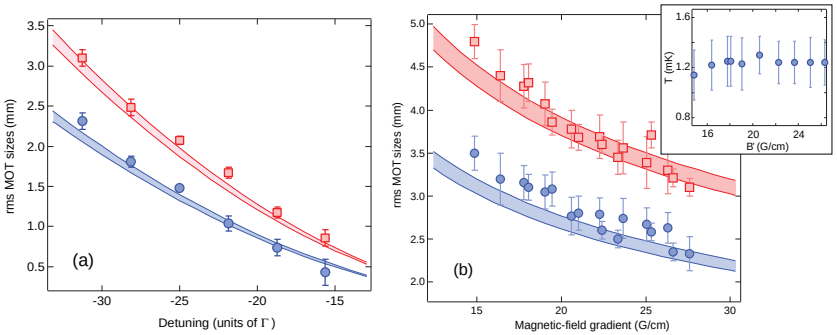

Figure II.10. *Equilibrium size of a magneto-optical trap of metastable helium atoms as a function of the detuning Δ and the magnetic field gradient b'. The two sets of points correspond to two different axes of the quadrupole magnetic field. The solid lines are the predictions of the theory presented in this chapter, taking saturation effects into account. Figures taken from Chang, Hoendervanger, et al. (2014).*

At the other end of the capture zone ($x = -L/2$), the same beam is resonant with atoms of velocity v_i satisfying the resonance condition (II.61):

$$|\Delta| = kv_i + \frac{\mu b'}{\hbar}\frac{(-L)}{2} \qquad \Rightarrow \qquad kv_i = 2\,|\Delta| = \mu b' L/\hbar. \tag{II.63}$$

It remains to choose the largest possible magnetic field gradient b', compatible with the available radiation pressure force. This problem is similar to that of a "Zeeman slower" for an atomic beam, in which the resonance condition must be maintained at all points in space, taking into account the Doppler effect variation. In this case, the points (x, v) in phase space at which the resonance condition (II.61) is satisfied must be such that

$$F = M\frac{\mathrm{d}v}{\mathrm{d}t} = Mv\frac{\mathrm{d}v}{\mathrm{d}x} \;<\; F_{\max} \tag{II.64}$$

where $F_{\max} = \hbar k\frac{\Gamma}{2}\frac{I}{I_{\mathrm{sat}}}$ is the maximum force created by each beam. By injecting the value $\frac{\mathrm{d}v}{\mathrm{d}x} = \mu b'/\hbar k$ deduced from the resonance condition and the initial velocity (II.63) into this relationship, we deduce the capture velocity and the corresponding magnetic field gradient:

$$\frac{kv_i}{\Gamma} = \frac{\mu b' L}{\hbar\Gamma} \approx \left(\frac{L}{\ell}\,\frac{I}{2I_{\mathrm{sat}}}\right)^{1/2}. \tag{II.65}$$

We can see that this capture rate varies as $L^{1/2}$ instead of the $L^{1/4}$ law found for molasses. In practice, for reasonable parameters, this capture velocity in a magneto-optical trap is two to three times greater than for optical molasses (see figure II.4). This translates into a considerable gain in terms of the number of atoms cooled if one starts with a vapor at thermal equilibrium at room temperature. In this case, the "low velocity" part of the thermal distribution is captured and the flux of atoms entering the capture region with a velocity $v \lesssim v_i$ varies as v_i^4. A gain of a factor of 2 in the capture velocity (as shown in figure II.4) translates into a gain of a factor of 16 in the flux of cooled atoms.

4-3 Equilibrium size for large atom numbers

In practice, the sizes measured for clouds of atoms confined in a magneto-optical trap are generally well above prediction (II.60), the result shown in figure II.10 being an exception. This is due to collective effects between atoms, specifically the repulsion caused by the radiation pressure from fluorescence light (Walker, Sesko, et al. 1990). The situation is similar to that of a star like the sun, where the force of gravity that tends to contract the star in on itself is offset by radiation pressure.

In practice, the density within a magneto-optical trap is limited to a value of the order of 10^{10} atoms/cm^3, and the diameter of the trapped cloud can reach a value of the order of a cm. To find these orders of magnitude, let us start by evaluating the effective repulsion between atoms. Consider a pair of atoms separated by a distance r. Atom 1, illuminated by the six laser beams forming the magneto-optical trap, scatters photons at a rate $\gamma = 6 \times (\Gamma s_0/2)$. For simplicity's sake, we will assume that these photons are emitted isotropically. Atom 2 will absorb a fraction $\sigma_{\mathrm{abs}}/(4\pi r^2)$ of these photons, and thus feel a radiation pressure force directed along the axis joining the two atoms

$$F = \gamma\hbar k\frac{\sigma_{\mathrm{abs}}}{4\pi r^2}. \tag{II.66}$$

The effective absorption cross-section of scattered photons $\sigma_{\rm abs}$ depends on their wavelength. Let us assume for the moment that these photons are emitted at the wavelength of the incident lasers (elastic Rayleigh scattering), and that [4]:

$$\sigma_{\rm abs} = \frac{3\lambda^2}{2\pi} \frac{1}{1+4\Delta^2/\Gamma^2}. \tag{II.67}$$

The equilibrium of the cloud of atoms under the combined effect of the trapping force $-K\boldsymbol{r}$ and the repulsion between atoms boils down to a well-known problem in physics. For simplicity's sake, let us assume zero temperature, which is legitimate if the equilibrium size is much larger than the single-atom prediction given in (II.60). Let us also make the assumption, which we will check later, that the atomic density is constant and equal to n inside a sphere of radius R, and zero outside, with $N = \frac{4}{3}\pi R^3 n$. In this case, the average effect of the repulsive force can be evaluated by Gauss's theorem: we have an assembly of particles repelling each other by a force in $1/r^2$ like Coulomb's force. In a spherical geometry with uniform density, we know that the electric field is radial and varies linearly with distance r from the center inside the sphere. In the case we are interested in here, the total radiation pressure force due to scattered light can be written as $\boldsymbol{F} = K'\boldsymbol{r}$ with

$$K' = \frac{1}{3}\gamma\hbar k\sigma_{\rm abs} n \tag{II.68}$$

The desired equilibrium is then obtained at any point in the cloud, provided $K' = K$, which occurs for a density

$$n = \frac{16\,\pi}{3} \frac{\mu b'}{\hbar\lambda^2} \frac{|\Delta|}{\Gamma^2}. \tag{II.69}$$

The fact that equilibrium is achieved at every point validates the initial assumption of uniform density. Taking typical magneto-optical trap parameters for alkali atoms, $b' = 0.1\,\mathrm{T/m}$, $|\Delta| = 3\,\Gamma$ and μ equal to the Bohr magneton, we find an equilibrium density of 1.7×10^{10} atoms/cm^3, leading to a radius of 2.4 mm for a cloud of one billion atoms.

Note. Our model is in fact a pessimistic version of reality. Indeed, we have neglected a similar effect, linked to the absorption of laser beams, which on the contrary reinforces the trapping effect (Dalibard 1988). To understand this effect, let us take a 1D model with an atomic cloud centered at $z = 0$. For an atom located on one edge of the cloud, for example on the right ($z > 0$), the two trapping waves do not have the same intensity. Indeed, the wave propagating towards $z > 0$, which tends to move the atom further away from the center, has crossed the entire cloud before reaching the atom; it is therefore significantly attenuated, due to absorption by the cloud. On the other hand, the wave propagating towards $z < 0$, which tends to bring the atom back towards the center, has hardly been attenuated at all. This absorption effect increases the stiffness of the magneto-optical trap. It can be shown that if the scattered photons had exactly the same frequency as the laser photons, the multiple scattering effect discussed above and this absorption effect would exactly offset each other. It is because some of the scattered photons are emitted with a frequency close to atomic resonance that the multiple scattering effect (which tends to explode the cloud) outweighs the absorption effect (which tends to compress it) (Walker, Sesko, et al. 1990). For a quantitative account of the competition between these two effects, see for example Townsend, Edwards, et al. (1995).

The magneto-optical trap with a large number of atoms is in fact a very rich non-linear system, which can lead to bistability effects, parametric instabilities and chaotic dynamics [see for example Sesko, Walker, et al. (1991), Wilkowski, Ringot, et al. (2000), Stefano, Fauquembergue, et al. (2003), Kim, Noh, et al. (2004), and Terças, Mendonça, et al. (2010) and refs. in]. In particular, the $1/r^2$ repulsive force between two atoms leads to effects similar to those seen in charged plasmas, such as the coulombic explosion (Pruvost, Serre, et al. 2000). We should also mention the dark magneto-optical trap (*dark MOT*) technique, in which optical pumping at the centre of the trap in the center of the trap to reduce the fluorescence light, thereby increasing the spatial density (Ketterle, Davis, et al. 1992).

4-4 Molecules enter the game

The magneto-optical trap can capture a large number of atomic species, opening the way to numerous applications ranging from metrology to quantum gas physics. Extending this technique to molecules is a consid-

[4] We will come back to the subtleties concerning the effective scattering cross-section of a photon by an atom when the latter is "dressed" by laser light

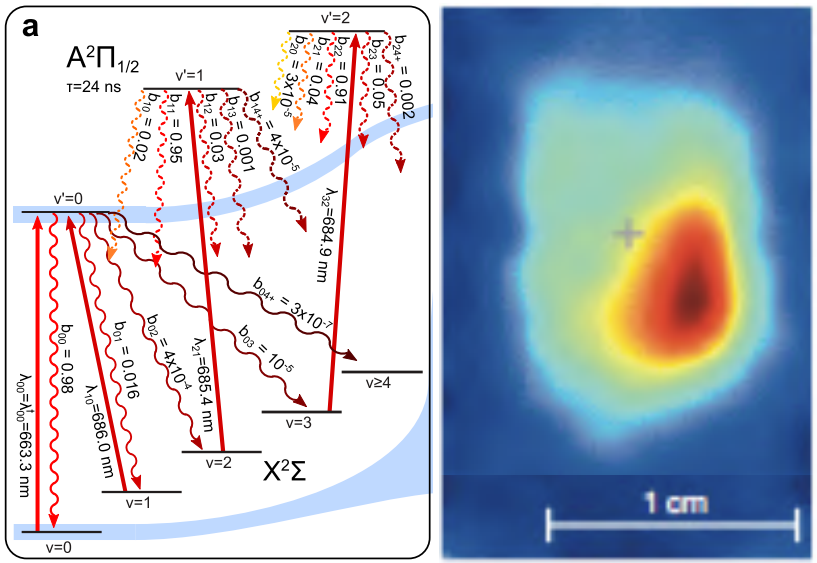

Figure II.11. *Schematic diagram of the SrF molecular levels used for magneto-optical trapping of this molecule. Four laser sources and several electro-optical modulators are needed to interact with the molecule for* $\sim 1s$ *(*10^6 *photons exchanged). Right, magneto-optical trap with* $\sim$ 300 *molecules,* $T \sim 2\,mK$*, and a lifetime of 60 ms, limited by the depth of the trap. Figure taken from Barry, McCarron, et al. (2014).*

erable challenge, but one that could lead to even more applications, given the wealth of observable phenomena, in conjunction with with quantum chemistry and with the possibility to induce an electric dipole moment in these molecules.

Very recently, the first 3D magneto-optical trap for molecules was achieved by Barry, McCarron, et al. (2014). Shortly before, 1D and 2D trapping had been observed by Hummon, Yeo, et al. (2013). These are complex experiments, as the level structure of a di-atomic molecule makes it impossible to isolate a single transition over which a sufficient number of photons could be exchanged. The experiment by Barry, McCarron, et al. (2014), carried out on strontium monofluoride (SrF), involves 7 different molecular vibrational levels (figure II.11), each of which is split into sublevels due to the molecule's rotation and hyperfine structure (the line representing the ground level $v = 0$ corresponds to 12 states). 4 laser sources are required (the straight lines in figure II.11), each electro-optically modulated to excite the different sublevels. Thanks to these multiple lasers, a given molecule can exchange an average of $\sim 10^6$ photons before falling onto a level not shown in the figure and not excited by one of the light beams. This exchange of 10^6 photons makes it possible to interact with the molecule and exert a force on it for about one second.

The difficulty of the experiment is further increased by the fact that the transition considered is not a simple $J_g = 0 \leftrightarrow J_e = 1$ transition, but includes dark states (we will come back to this notion in a later chapter). Once in a dark state, the molecule ceases to feel a force and risks escaping the trap. The polarizations of the light beams and the direction of the magnetic field must therefore be periodically switched to recycle these dark states. Once all these precautions have been taken, the trap can be observed! The newborn contains around 300 molecules (still a small number compared with the billions of atoms a magneto-optical trap can accumulate), at a temperature of around 2 millikelvin. This temperature is ten times higher than the Doppler limit, which the authors interpret as a consequence of the existence of dark states. The trap's lifetime is 60 ms, which again is well below the result measured for atoms (which can reach several minutes). The probable reason for this short lifetime is the limited depth of the trap, estimated at only $5\,k_B T$. Molecules therefore evaporate from the trap, limiting their residence time.

Chapter III

The virtues of narrow lines

In the previous chapter, we studied broad-line Doppler cooling, i.e. cooling that operates on an atomic line with a natural width Γ of the excited level that is large compared with the recoil frequency $\omega_{\rm r} = \hbar k^2/2M$. We then found a temperature proportional to the natural width Γ . It is natural to wonder what happens to the temperature limit when we try to use narrower and narrower lines, approaching the $\Gamma \sim \omega_{\rm r}$ situation, or even going beyond it. Does the law $T \propto \Gamma$ remain valid, or is it replaced by another limit?

This question may have seemed academic some fifteen years ago, but it is now highly relevant experimentally: there is a great deal of interest in atoms with two outer electrons, particularly in terms of metrology and degenerate quantum gases. These atoms naturally have narrow resonance lines, which couple the sector where the total spin of the two outer electrons is $S = 0$ (spin singlet) and the sector where $S = 1$ (spin triplet). For example, for strontium, the line at 689 nm coupling the ground state $^1S_0$ and the excited state $^3P_1$ has a width $\Gamma/2\pi = 7.5\,$kHz, which is comparable to the recoil frequency $\omega_{\rm r}/2\pi = 4.7\,$kHz (see table III.1). The cooling of this atom is of considerable metrological interest, since it was with it that Jun Ye's group in Boulder recently demonstrated the operation of an optical clock with an accuracy at the record level of 2×10^{-18} (Bloom, Nicholson, et al. 2014; Nicholson, Campbell, et al. 2015).

As we pointed out in the previous chapter, the absorption or emission of a single photon is enough in this case to significantly change the atom's saturation parameter. We can therefore no longer adopt a Fokker-Planck approach, since the small-step approximation is no longer valid. We need to return to a description of motion in which the discrete nature of each jump is taken into account. For simplicity's sake, we will deal with the one-dimensional case first; the extension to three dimensions will then be straightforward, via a numerical treatment. Using this approach, we will show that the stationary distribution has a minimum width given by the recoil velocity $v_{\rm r} = \hbar k/M$.

In the second part of this chapter, we describe some recent experiments. We will see that this cooling method makes it possible to reach submicrokelvin temperatures, we will tackle the problem of heating linked to multiple scattering in the sample, and we will discuss the possibility of obtaining a degenerate quantum gas from clouds of atoms that are cooled on

	A	λ nm	$\Gamma/2\pi$ kHz	$\omega_{\rm r}/2\pi$ kHz	$E_{\rm r}/k_{\rm B}$ nK	$v_{\rm r}$ cm/s
Mg	24	457	0.031	40	1.9	3.6
Ca	40	657	0.40	12	0.55	1.5
Zn	64	309	6.0	32	1.6	2.0
Sr	84	689	7.6	5.0	0.24	0.69
Cd	114	326	70	16	0.79	1.1

Table III.1. *Narrow intercombination lines $^1S_0 \leftrightarrow {}^3P_1$ for some atomic species with two outer electrons (data taken from Zeb Barber's doctoral thesis, Boulder, and refs. in).*

a narrow line. We will conclude with the scheme developed by Stellmer, Pasquiou, et al. (2013) to obtain a Bose-Einstein condensate without any evaporation, in a continuous laser-cooled cloud.

1 Single-frequency cooling

In this section, we develop a simple model of narrow-line cooling, adding one by one the ingredients that will bring us closer to a real-life situation. First, we will deal with a one-dimensional situation along a given direction in space (z), assuming that spontaneous photons carry no momentum along this axis. We will then see how to take this momentum into account, before moving on to the 3D case.

1-1 A model with no "spontaneous recoil"

We consider here a two-level atom g, e, mobile along the z axis, and we assume that this atom is illuminated by two waves propagating along the z axis, of wave vector $\pm k\boldsymbol{u}_z$. We assume that these waves are of low intensity, so that the probability per unit time that the atom absorbs a photon is, to a good approximation, given by the sum of the probabilities associated with each of the two waves. In this first paragraph, we also assume that spontaneous photons are emitted perpendicular to the axis considered[1].

Consider an atom initially in the internal state g with velocity v. This atom can absorb a photon in the $+z$ direction or in the $-z$ direction, its velocity increasing or decreasing by v_r (figure III.1). We saw in previous chapters that the rates for these two processes are given by $\Gamma s_\pm(v)/2$ with

$$s_\pm(v) = \frac{2|\kappa|^2}{\Gamma^2 + 4\Delta_v^2}. \tag{III.1}$$

In this equation, the quantity κ corresponds to the Rabi frequency of each wave, characterizing the electric dipolar coupling of the atom with the electromagnetic field. The detuning Δ_v is calculated by comparing the energy E_i of the initial state (before absorption, atom in state g in the presence of N laser photons) and the energy E_f of the final state (after absorption, atom in state e in the presence of $N-1$ laser photons):

$$E_i = E_g + \frac{1}{2}Mv^2 + N\hbar\omega_\mathrm{L}, \tag{III.2}$$

$$E_f = E_e + \frac{1}{2}M(v \pm v_\mathrm{r})^2 + (N-1)\hbar\omega_\mathrm{L}, \tag{III.3}$$

that is, posing $\Delta = \omega_\mathrm{L} - \omega_\mathrm{A}$ with $\hbar\omega_\mathrm{A} = E_e - E_g$:

$$\Delta_v = \Delta \mp kv - \omega_\mathrm{r}. \tag{III.4}$$

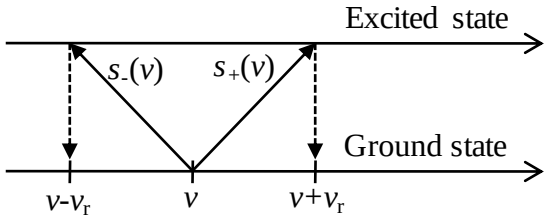

Figure III.1. *Discrete model for narrow-line Doppler cooling. Absorption of a photon changes the atomic velocity by $\pm v_\mathrm{r}$. Spontaneous emission is assumed to take place in the plane perpendicular to the cooling axis, so the atomic velocity is unchanged during this process.*

Once in the excited state, the atom falls back into the ground state, spontaneously emitting a photon. As mentioned above, we first assume that this photon propagates in the plane orthogonal to the z axis, which does not modify the velocity v along this axis.

Denoting $\mathcal{P}(v,t)$ the velocity distribution at time t, we have the evolution equation:

$$\begin{aligned}\frac{\partial\mathcal{P}(v,t)}{\partial t} = &- \frac{\Gamma}{2}\left[s_+(v) + s_-(v)\right]\mathcal{P}(v) \\ &+ \frac{\Gamma}{2}s_+(v-v_\mathrm{r})\mathcal{P}(v-v_\mathrm{r}) + \frac{\Gamma}{2}s_-(v+v_\mathrm{r})\mathcal{P}(v+v_\mathrm{r}).\end{aligned} \tag{III.5}$$

[1] Our model is therefore optimistic, since it completely neglects heating due to recoil during spontaneous emission processes. Another version, pessimistic but equally simple to handle analytically, would be to assume that spontaneously emitted photons all propagate along the z axis.

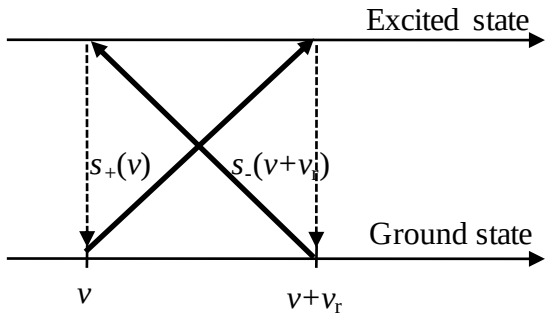

Figure III.2. *To find the stationary regime of (III.5), we write the equality of flows crossing a fictitious boundary located at $v + v_r/2$.*

In this model, we couple an infinite, but discrete, chain of velocity classes:

$$\ldots \leftrightarrow \quad v - 2v_r \quad \leftrightarrow \quad v - v_r \quad \leftrightarrow \quad v \leftrightarrow \quad v + v_r \quad \leftrightarrow \ldots \tag{III.6}$$

1-2 Stationary state

To evaluate the stationary state of this 1D narrow-line cooling model, the simplest way is to consider a virtual boundary located between v and $v+v_r$ and to write the equality of flows crossing this boundary from right to left and from left to right (figure III.2):

$$s_+(v)\ \mathcal{P}(v) = s_-(v + v_r)\ \mathcal{P}(v + v_r). \tag{III.7}$$

which gives

$$\frac{\mathcal{P}(v + v_r)}{\mathcal{P}(v)} = \frac{(\Delta + \omega_r + kv)^2 + \Gamma^2/4}{(\Delta - \omega_r - kv)^2 + \Gamma^2/4}. \tag{III.8}$$

Let us start with the special case $\Delta = -\omega_r$ and consider the family $v_n = (n - \frac{1}{2})v_r$:

$$\ldots \leftrightarrow \quad -\frac{3}{2}v_r \quad \leftrightarrow \quad -\frac{1}{2}v_r \quad \leftrightarrow \quad \frac{1}{2}v_r \quad \leftrightarrow \quad \frac{3}{2}v_r \quad \leftrightarrow \ldots \tag{III.9}$$

The relationship (III.8) becomes in the limit $\Gamma \to 0$:

$$\frac{\mathcal{P}(v_{n+1})}{\mathcal{P}(v_n)} = \frac{(n - \frac{1}{2})^2}{(n + \frac{1}{2})^2}, \qquad \text{soit} \quad \mathcal{P}(v_n) \propto \frac{1}{(n - \frac{1}{2})^2} \propto \frac{1}{v_n^2}. \tag{III.10}$$

This particular case reveals an important point: in the limit of a narrow line, the velocity distribution is no longer Gaussian, unlike in the case of a broad line, for which the Fokker-Planck equation was valid. This velocity distribution decreases as a power law $v^{-\alpha}$, in this case $\alpha = 2$ for the choice $\Delta = -\omega_r$.

As we shall see in what follows, this power-law decay raises new questions compared with the Gaussian case: on what condition is the second-order moment $\langle v^2 \rangle$ which enters into the definition of kinetic energy defined [this is clearly not the case for (III.10)]? Is the distribution $\mathcal{P}(v)$ always normalizable?

To answer these questions, let us now take an arbitrary detuning Δ. There is no exact solution as for the special case $\Delta = -\omega_r$, but we can show that the behavior at high velocities remains a power-law behavior

$$\mathcal{P}(v) \propto |v|^{-\alpha}. \tag{III.11}$$

To determine α, we use the expansion at high velocities

$$\frac{\mathcal{P}(v + v_r)}{\mathcal{P}(v)} \approx 1 - \alpha \frac{v_r}{v}. \tag{III.12}$$

An expansion in powers of $1/v$ of the right-hand side of (III.8) gives the dominant term:

$$1 + 4\frac{\Delta}{kv} = 1 + 2\frac{\Delta}{\omega_r}\,\frac{v_r}{v} \tag{III.13}$$

from which we deduce the exponent of the power law for $\mathcal{P}$.

$$\mathcal{P}(v) \propto |v|^{-\alpha} \qquad \text{with} \quad \alpha = 2\frac{|\Delta|}{\omega_r}, \tag{III.14}$$

where Δ is negative. The necessary condition for this treatment to make sense is that the distribution $\mathcal{P}$ is normalizable, i.e.:

$$\mathcal{P} \text{ normalizable:} \quad |\Delta| > \frac{1}{2}\omega_r. \tag{III.15}$$

If we want $\int v^2\,\mathcal{P}(v)\;\mathrm{d}v$ to converge so that the mean kinetic energy is finite, the constraint is stronger:

$$\text{Well defined kinetic energy:}\quad |\Delta| > \frac{3}{2}\omega_\mathrm{r}. \tag{III.16}$$

The special case $\Delta = -\omega_\mathrm{r}$ studied above corresponds to a distribution varying as $1/v^2$, i.e. normalizable but with infinite mean kinetic energy.

Before discussing the precise value of the width of the velocity distribution and the mean kinetic energy, the lesson we can draw is that when the linewidth Γ becomes very small, we cannot expect the broad-line Doppler limit $k_\mathrm{B}T = \hbar\Gamma/2$, obtained for $\Delta = -\Gamma/2$, to remain valid. The detuning should be chosen no smaller than the recoil frequency, to within a multiplicative factor of the order of unity. The velocity classes $v = 0$, $v = \pm v_\mathrm{r}$ then have comparable populations according to (III.8) and the kinetic energy obtained is therefore at least of order E_r.

1-3 Recoil due to spontaneous emission

The 1D model developed earlier, in which we neglected the momentum carried away by the fluorescence photons, enabled us to solve the evolution equation (III.5) very simply. However, this model is too optimistic, since it neglects an important heating source. We now propose to go beyond this approximation and take into account the random recoil due to spontaneous emission phenomena. We will do this first in a 1D model, then generalize our results to 3D.

To begin with, let us consider narrow-line cooling along the z axis. The projection on this axis of the momentum $\hbar k$ of a spontaneously emitted photon is a continuous variable between $-\hbar k$ and $\hbar k$ (figure III.3). To take this variable into account, we modify the population feeding terms for the velocity class v [second line of (III.5)] as follows:

$$s_+(v-v_\mathrm{r})\mathcal{P}(v-v_\mathrm{r}) \;\longrightarrow\; \int_{-v_\mathrm{r}}^{-v_\mathrm{r}} \mathcal{N}(v')\,s_+(v-v_\mathrm{r}+v')\,\mathcal{P}(v-v_\mathrm{r}+v')\;\mathrm{d}v'$$

$$s_-(v+v_\mathrm{r})\mathcal{P}(v+v_\mathrm{r}) \;\longrightarrow\; \int_{-v_\mathrm{r}}^{-v_\mathrm{r}} \mathcal{N}(v')\,s_-(v+v_\mathrm{r}+v')\,\mathcal{P}(v+v_\mathrm{r}+v')\;\mathrm{d}v'$$

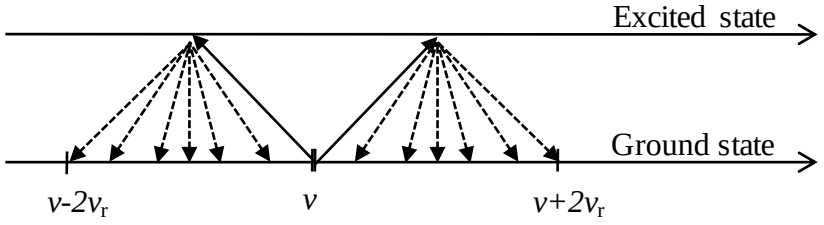

Figure III.3. *Continuous model for narrow-line Doppler cooling. Absorption of a photon (solid line) changes the atomic velocity by $\pm v_\mathrm{r}$. A spontaneously emitted photon (dotted line) has a non-zero momentum component along the cooling axis, with a probability density given by (III.17).*

where $\mathcal{N}(v')$ is the probability density for a spontaneously emitted photon to have an momentum $\hbar k_z = Mv'$ along the z axis. This quantity can be calculated from classical electromagnetic formulas for the radiation of an oscillating dipole. Taking (for example) the case of circular polarization along the z axis:

$$\mathcal{N}(v') = \frac{3}{8v_\mathrm{r}}\left(1+\frac{v'^2}{v_\mathrm{r}^2}\right). \tag{III.17}$$

Figure III.4 shows the result of the evolution found for the evolution of the distribution $\mathcal{P}(v)$, calculated for $\omega_\mathrm{r} = \Gamma$. A few salient facts emerge from this evolution:

- As expected, the final distribution obtained has a width of the order of the recoil velocity.
- This distribution is not a monotonic function of v for $v > 0$. Holes appear for the velocities at which resonance occurs with one of the two laser waves, and for multiples of these velocities.
- A detailed examination of the long-time solution shows that the wings of this distribution vary like a power law, $\mathcal{P}(v) \propto |v|^{-\alpha}$, as in the discrete model developed earlier.

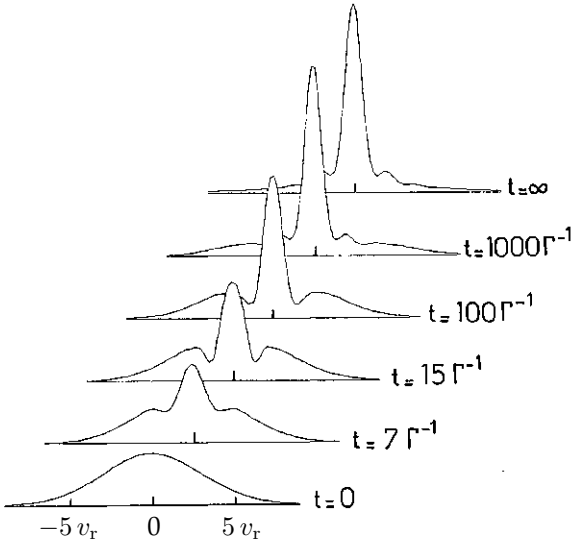

Figure III.4. *Evolution of the one-dimensional velocity distribution for Doppler cooling on a narrow line $\Gamma = \omega_{\rm r}$. The detuning is $\Delta = -1.5\,\omega_{\rm r}$ and the Rabi frequency $\kappa = \omega_{\rm r}$. The atomic transition is of type $J_g = 0 \leftrightarrow J_e = 1$ and the two beams propagating along $\pm z$ are polarized $\sigma_\pm$. Figure extracted from Castin, Wallis, et al. (1989).*

1-4 Steady state and scaling laws

Within the framework of the continuous model of the previous paragraph, we can numerically search for the detuning that minimizes the mean kinetic energy

$$E_c = \frac{1}{2} M \langle v^2 \rangle \equiv \frac{1}{2} k_{\rm B} T_{\rm eff} \tag{III.18}$$

for each value of the ratio $\Gamma/\omega_{\rm r}$, and then study how this minimum effective temperature $T_{\rm eff,\,min}$ varies with $\Gamma/\omega_{\rm r}$. Note that the definition of a temperature in this situation is debatable, since we have seen that stationary distributions are not Gaussian, but vary as a power law for high velocities.

The result for $T_{\rm eff,\,min}$ as a function of $\Gamma/\omega_{\rm r}$ is shown in figure III.5, taken

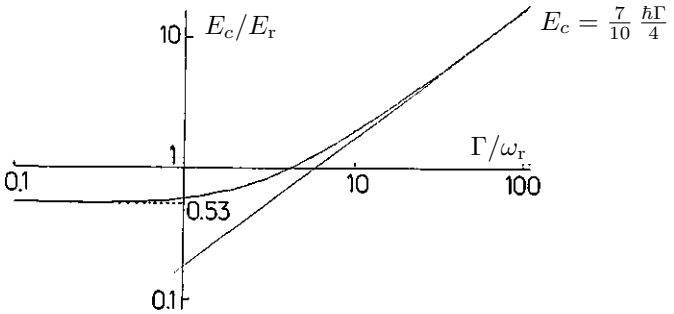

Figure III.5. *Minimum kinetic energy as a function of the ratio $\Gamma/\omega_{\rm r}$. Figure extracted from Castin, Wallis, et al. (1989).*

from Castin, Wallis, et al. (1989). For a narrow line, this minimum temperature is obtained for $\Delta \approx -3.4\,\omega_{\rm r}$ and leads to $E_c \approx 0.53\,E_{\rm r}$, which gives

$$\text{narrow line cooling in 1D:} \qquad k_{\rm B} T_{\rm eff,\,min} \approx 1.06\,E_{\rm r}, \quad \sqrt{\langle v^2 \rangle} \approx 0.73\,v_{\rm r}. \tag{III.19}$$

For a broad line, we recover the Doppler limit found in the previous chapter. It reads in the one-dimensional model studied here:

$$\text{broad-line cooling in 1D:} \qquad k_{\rm B} T_{\rm eff,\,min} = \frac{7}{10}\,\frac{\hbar\Gamma}{2}. \tag{III.20}$$

The $7/10$ coefficient found in this 1D model compared with the 3D result can be explained simply: the heating associated with the recoil of spontaneously emitted photons corresponds to $\langle p^2 \rangle = \frac{2}{5}\hbar^2 k^2$. Whereas at 3D, the momentum diffusion coefficient due to recoil during spontaneous emission is equal to that arising from the randomness of the direction of absorbed photons, its contribution is reduced here by a factor of $2/5$, resulting in an overall reduction in scattering by a factor of

$$\frac{1+\frac{2}{5}}{1+1} = \frac{7}{10}. \tag{III.21}$$

Finally, we can extrapolate these results to three dimensions, by multiplying the 1D results by the factor $10/7$. We then obtain an estimate of the

expected minimum temperature:

narrow line cooling in 3D: $k_{\mathrm{B}}T_{\mathrm{eff,\,min}} \approx 1.5\,E_{\mathrm{r}}, \qquad \sqrt{\langle v^2\rangle} \approx 0.9\,v_{\mathrm{r}}.$ (III.22)

In conclusion, the minimum temperature obtained by narrow-line Doppler cooling is limited by the recoil of a single photon. The regime leading to this minimum temperature is very different from that found for a broad line: the optimum detuning is of the order of $-3\,\omega_{\mathrm{r}}$, the total excitation rate of an atom

$$s_{\mathrm{tot}}(v) = s_+(v) + s_-(v) \tag{III.23}$$

is weak in the vicinity of $v = 0$ and only takes on appreciable values for $v \approx \pm 2\,v_{\mathrm{r}}$. This gives rise to the idea that atoms are accumulated in a dark region of velocity space (figure III.6): when the atom is in this dark region, it remains at the same velocity for a long time, as the photon scattering rate $\Gamma s_{\mathrm{tot}}/2$ is very low. When photon scattering occurs, the atom may approach one of the two bright regions $v \approx \pm 2\,v_{\mathrm{r}}$. Photon scattering then occurs at a high rate, and absorption takes place with virtual certainty in the wave propagating away from the atom: for example, if $v \approx +2\,v_{\mathrm{r}}$, then $s_-(v) \gg s_+(v)$. This last point is essential to ensure that the atom almost never crosses the bright wall: if it does, and the atom acquires a velocity of 3 or $4\,v_{\mathrm{r}}$, then it will take a considerable time to return to the vicinity of zero velocity. This is why we need to choose a detuning Δ significantly greater than ω_{r}. We will see in the next paragraph how the use of multiple-frequency beams can relax this constraint.

2 How to structure the resonance line

From the above, narrow-line cooling provides a means of cooling atoms to a temperature of the order of the recoil associated with a single photon. But the disadvantage associated with a narrow line is clear from figure III.6: for an atom of any velocity v to be cooled, this velocity must be close to the resonant velocity class with lasers, $kv \sim \Delta$ to within Γ. Since Γ is assumed to be small, of the order of the recoil frequency ω_{r}, only a narrow velocity class (of the order of v_{r}) will be concerned. How can we remedy this inefficiency?

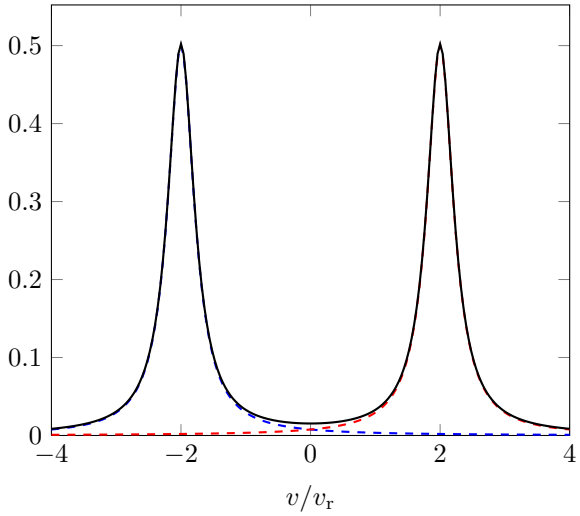

Figure III.6. *Variation of $s_+(v)$ (blue dashes), $s_-(v)$ (red dashes) and $s_{\mathrm{tot}}(v)$ (black solid line) for a narrow line, $\Gamma = \omega_{\mathrm{r}}$, $\Delta = -3\,\omega_{\mathrm{r}}$ and $\kappa = \omega_{\mathrm{r}}/2$.*

A first solution is to broaden the line by saturation. We have seen that when the Rabi frequency characterizing the atom-laser coupling becomes greater than the natural width Γ, the effective width of the resonance is increased:

$$\Gamma \longrightarrow \Gamma_{\mathrm{eff}} = \sqrt{\Gamma^2 + 2|\kappa|^2}. \tag{III.24}$$

We can therefore choose $|\kappa|$ to be large in front of the recoil frequency ω_{r}, to ensure that the capture range of optical molasses is large in front of v_{r}. But then we lose the benefit of a narrow line: everything happens as if we were using a resonance line of width $\Gamma_{\mathrm{eff}} \gg \omega_{\mathrm{r}}$, and the temperature we will reach will be given by $k_{\mathrm{B}}T \sim \hbar\Gamma_{\mathrm{eff}}$, which is large compared with the recoil energy.

2-1 Line broadening by phase modulation

It makes much more sense to broaden the line using polychromatic excitation, which can be achieved by introducing sidebands through phase

modulation of the light wave:

$$e^{i\omega_L t} \rightarrow e^{i[\omega_L t+\phi(t)]}. \qquad \text{(III.25)}$$

Consider, for example, a phase modulation $\phi(t)$ of period T for which the phase varies locally quadratically with time. Let us assume $T_0 < T$ and for the period $-T_0/2 < t < T - T_0/2$:

$$\begin{aligned} \phi(t) &= \alpha(t^2 - T_0^2/4) \quad \text{if } |t| < T_0/2, \qquad \text{(III.26)} \\ \phi(t) &= -\beta(t - T_0/2)(t - T + T_0/2) \quad \text{if } T_0/2 < t < T - T_0/2, \end{aligned}$$

which are then reproduced periodically. We impose $\alpha T_0 = \beta(T - T_0)$ to ensure the continuity and derivability of $\phi(t)$ in T_0. The frequency of the wave, equal to the derivative of the phase, then has a sawtooth variation and covers a frequency interval between $\omega_L - \Omega/2$ and $\omega_L + \Omega/2$, with $\Omega = 2\alpha T_0$. Fourier analysis shows that the light spectrum is made up of harmonics separated by the frequency $2\pi/T$, with comparable weights if the sawtooth is sufficiently asymmetrical (T_0 close to T). An example is shown in figure III.7. Harmonics outside the range $[\omega_L - \Omega/2, \omega_L + \Omega/2]$ have negligible weights compared to those inside.

To obtain a significant, uniform excitation of the atom over a wide range of velocities, we choose a harmonic spacing $2\pi/T$ of the order of the natural width Γ. An example of the profile obtained by independently summing the contributions of the various Fourier components is shown in figure III.8 for a very narrow line ($\Gamma = 0.2\,\omega_r$).

In the following, we will model this profile using the rectangular shape shown in figure III.9. We are discussing the 1D case here, but this model can be extended to three dimensions without difficulty. Let us divide velocity space into three zones:

- The central zone A corresponds to low velocities $|v| < v_0$. These atoms are almost in the dark, i.e. they have a low probability of absorbing a photon. We denote γ_a the probability per unit time for an absorption process, which proceeds in a random direction.
- The intermediate zone B corresponds to $v_0 < |v| < v_1$. In this zone, atoms absorb photons at a high γ_b rate. This absorption is directive: it takes place in the light beam propagating in the opposite direction to the atom, and therefore tends to bring the atom back to zero velocity.

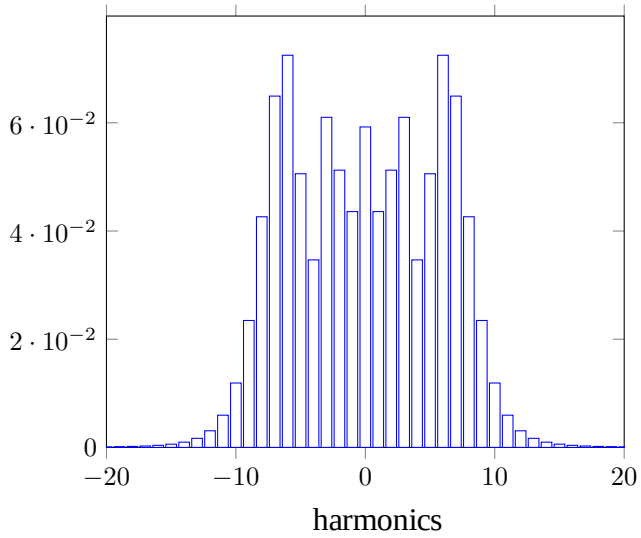

Figure III.7. *Example of spectrum obtained by quadratic phase modulation (III.26) with $T_0 = 0.99\,T$ and $\alpha = 20\pi/(TT_0)$ (i.e. 20 significantly populated harmonics).*

- The zone C corresponds to atoms with high velocity $|v| > v_1$. These atoms have a negligible probability of absorbing a photon. The velocity v_1 can in principle be chosen arbitrarily large in front of the recoil velocity, and these velocity classes $|v| > v_1$ will play a negligible role in the following.

2-2 Scaling laws for a broadened resonance line

Broadening the excitation line by phase modulation can have two benefits. The first is to accelerate the decay of the velocity distribution $\mathcal{P}(v)$ at high velocities. We have seen that for monochromatic excitation, this decay takes place with a power law $|v|^{-\alpha}$, with $\alpha = 2|\Delta|/\omega_r$. For the broadened line we are considering here, the effective detuning corresponds to the center of the rectangular excitation profile and can therefore be large compared

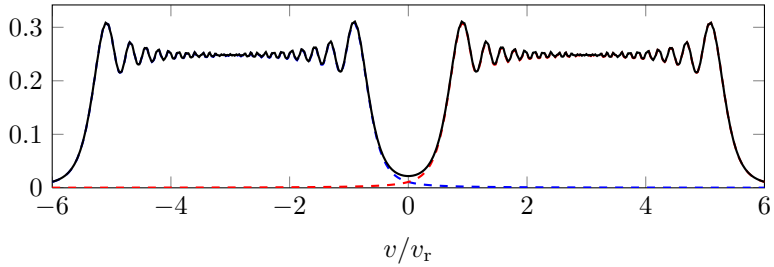

Figure III.8. *Saturation parameter $s_+(v)$ (blue dashed line), $s_-(v)$ (red dashed line) and $s_\mathrm{tot}(v)$ (black solid line) as a function of velocity v. Parameters for this figure: $\Gamma = 0.2\,\omega_\mathrm{r}$, $\kappa = 0.4\,\omega_\mathrm{r}$, average Δ equal to $-5\,\omega_\mathrm{r}$, 100 significantly populated harmonics with a harmonic spacing $0.1\,\omega_\mathrm{r}$.*

to ω_r. The exponent of the power law is therefore large in front of 1, ensuring convergence of all relevant moments of this velocity distribution.

The second virtue is to lower the average energy of cooled atoms, at least in the case of $\Gamma \ll \omega_\mathrm{r}$. To clarify this point, we will do some simple statistical reasoning, based on the absorption rate model shown in figure III.9. Let us denote P_a and P_b as the respective populations of zones A and B, and let us assume that the boundary velocity v_0 is significantly smaller than the recoil velocity v_r. In steady state, there is equilibrium between the flows into and out of each zone:

- The outflow from zone A is simply given by

$$\Phi_{A\to B} \approx P_a \gamma_a. \tag{III.27}$$

  Since $v_0 \ll v_\mathrm{r}$, an atom initially located in zone A and which undergoes photon scattering generally leaves this zone due to the random recoil associated with spontaneous emission.

- The flux entering zone A corresponds to atoms from zone B which have undergone an absorption – spontaneous emission process, and which by chance have arrived in a velocity class $|v| < v_0$. Since atoms in zone B have a velocity of the order of the recoil velocity v_r, the flux entering zone A is:

$$\Phi_{B\to A} \approx P_b \gamma_b \left(\frac{v_0}{v_\mathrm{r}}\right)^D \tag{III.28}$$

  where D is the dimension of the velocity space to be cooled. Note immediately that the factor $(v_0/v_\mathrm{r})^D$ makes three-dimensional cooling much trickier than its 1D equivalent, at given v_0 and v_r; this point will be confirmed later.

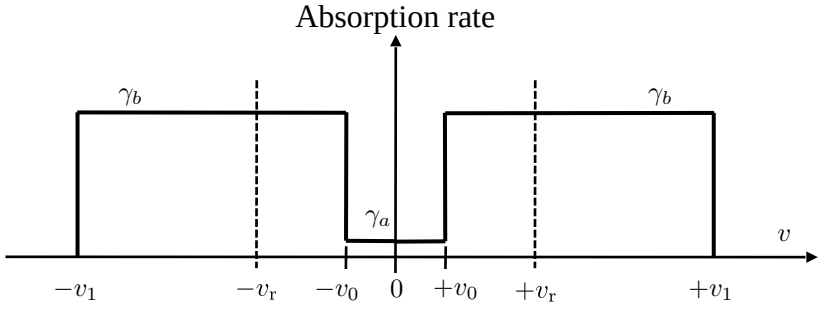

Figure III.9. *Modeling the absorption rate: a central zone with a low rate γ_a and a peripheral zone with a much higher rate γ_b. The width of the central zone v_0 is smaller than the recoil velocity.*

The equality of the two flows corresponding to steady-state conditions therefore leads to:

$$\frac{P_a}{P_b} = \frac{\gamma_b}{\gamma_a}\left(\frac{v_0}{v_\mathrm{r}}\right)^D. \tag{III.29}$$

It remains to evaluate the ratio γ_b/γ_a. Assuming a resonance line broadened by phase modulation as shown in figure III.8, the residual absorption rate around zero velocity corresponds to the sum of the wings of the different Lorentzians corresponding to each harmonic of the broadened line. Up to a numerical coefficient, we find:

$$\gamma_a \approx \gamma_b \frac{\Gamma}{|\Delta_\mathrm{min}|} \qquad \text{where we assume} \quad \gamma_a \approx \gamma_b \frac{\Gamma}{|\Delta_\mathrm{min}|} \tag{III.30}$$

where Δ_min is the detuning value for the harmonic closest to resonance. This value is directly linked to the boundary velocity v_0: $kv_0 = |\Delta_\mathrm{min}|$ so

that we arrive at

$$\frac{P_a}{P_b} = \frac{v_0^{D+1}}{v_\mathrm{r}^D\ \delta v_\mathrm{res}} \qquad \text{with} \quad \delta v_\mathrm{res} = \Gamma/k \ll v_\mathrm{r}. \tag{III.31}$$

The nature of the possible optimization is then clear: we want to have at least a fraction of the atoms (those in zone A) as cold as possible, and therefore a boundary velocity v_0 as low as possible. At the same time, we want this fraction to be significant, so that P_a is not too small compared with P_b.

For the sake of clarity, let us impose $P_a = P_b$. This fixes the value of v_0:

$$\frac{v_0}{v_\mathrm{r}} = \left(\frac{\Gamma}{\omega_\mathrm{r}}\right)^{\frac{1}{D+1}}. \tag{III.32}$$

In one dimension, the gain is significant compared with monochromatic cooling if $\Gamma \ll \omega_\mathrm{r}$. We have $v_0 = \sqrt{v_\mathrm{r}\ \delta v_\mathrm{res}} \ll v_\mathrm{r}$ (Wallis & Ertmer 1989). In three dimensions, on the other hand, the gain is only marginal compared to v_r, since the Γ/ω_r ratio only comes into play to the power of $1/4$. The main advantage of broadening the line in this case is to increase the optical molasses capture zone (this is the first argument we mentioned).

3 Experiments on narrow-line cooling

3-1 Temperature measurements

The first narrow-line cooling experiments were carried out on the strontium atom (isotope 88) in H. Katori's group in Japan (Katori, Ido, et al. 1999; Ido, Isoya, et al. 2000).

The strontium atom has two relevant resonance lines (figure III.10); the first, a broad line, corresponds to the $5s^2\ {}^1S_0 \leftrightarrow 5s5p\ {}^1P_1$ transition, with wavelength $\lambda_1 = 461\,\mathrm{nm}$ and width $\Gamma_1/2\pi = 32\,\mathrm{MHz}$. This line is used to pre-cool atoms in a magneto-optical trap. The second, narrow line corresponds to the $5s^2\ {}^1S_0 \leftrightarrow 5s5p\ {}^3P_1$ intercombination transition, $\lambda_2 = 689\,\mathrm{nm}$ and $\Gamma_2/2\pi = 7.6\,\mathrm{kHz}$. Katori, Ido, et al. (1999) showed that they could transfer atoms pre-cooled on the broad line into a magneto-optical trap

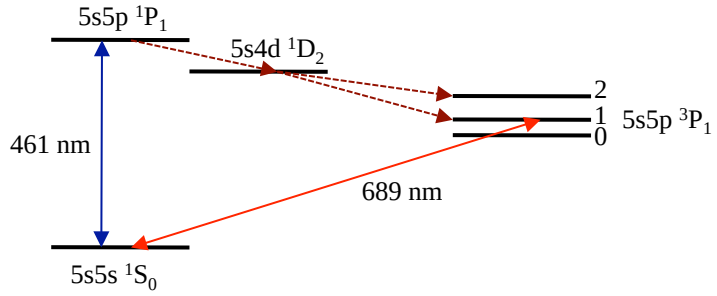

Figure III.10. *Relevant energy levels for the strontium atom. The excited state for the 5s5p ${}^1P_1$ broad line transition can de-excite to the 5s4d ${}^1D_2$ level. A repumping scheme may thus be required.*

for the narrow line, by broadening this line through phase modulation. They then switched off this phase modulation to obtain a sample cooled in monochromatic light. By reducing the laser power as much as possible (to the threshold at which the radiation pressure force no longer compensates for gravity), they were able to reach a temperature of 400 nK, i.e. $1.7\,E_\mathrm{r}/k_\mathrm{B}$. The corresponding root-mean-square velocity is

$$v_0 = \sqrt{\frac{k_\mathrm{B}T}{M}} = 6.1\,\mathrm{mm/s} = 0.9\,v_\mathrm{r}. \tag{III.33}$$

Katori, Ido, et al. (1999) also measured the phase-space density of the cooled cloud, and showed that it could reach 10^{-2}, exceeding by several orders of magnitude that measured in a broad-line magneto-optical trap ($\sim 10^{-6}$). They attribute the observed limit for this phase-space density to heating due to multiple photon scattering, to which we will return a little later. For the geometry of their sample, they observe an increase in temperature with increasing spatial density:

$$\frac{\mathrm{d}T}{\mathrm{d}n} = 400\,\mathrm{nK}/(10^{12}\,\mathrm{cm}^{-3}) \tag{III.34}$$

over the range $n = 0.1 - 0.5\,10^{12}\ \mathrm{cm}^{-3}$. Since phase-space density varies as $n/T^{3/2}$, this law favors the low-density and low-temperature regime.

Ido, Isoya, et al. (2000) then improved on this result by applying

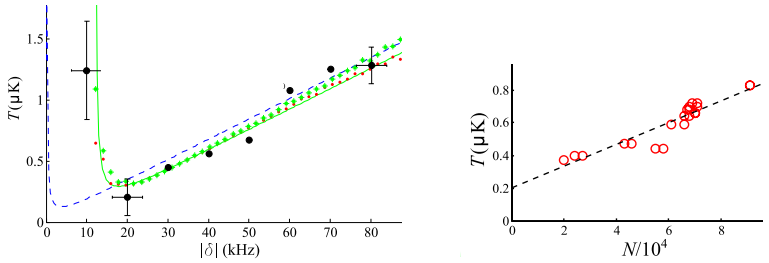

Figure III.11. *Left: Evolution of temperature versus detuning for a cloud of ^{88}Sr atoms confined in a dipole trap. The temperatures shown result from extrapolation to low atom numbers of the temperatures actually measured. Right: influence of atom number on temperature [figure taken from Chalony, Kastberg, et al. (2011)].*

narrow-line cooling to strontium atoms confined in a dipole trap. By reducing the power of the dipole trap, they achieved a phase-space density of 0.1 (within a factor of 20 of Bose-Einstein condensation). Note that the equilibrium obtained probably corresponded to a combination of laser and evaporative cooling.

A detailed study of the temperature obtained by narrow-line cooling has also been carried out by the Nice group for ^{88}Sr (Chalony, Kastberg, et al. 2011). This study was performed both with atoms confined in a dipole trap and with free atoms. For trapped atoms, the variation in temperature with detuning is in good agreement with the theoretical models presented above (Castin, Wallis, et al. 1989). The minimum temperature measured is $\sim 400\,$nK as for Katori, Ido, et al. (1999), and the minimum temperature deduced from extrapolation to a very low number of atoms is $\sim 200\,$nK (figure III.11). Here, too, the increase of temperature with the number of atoms was clearly observed: the temperature is doubled for a number of atoms corresponding to an optical thickness of the cloud of the order of unity (in its transverse direction). We will come back to this result in the next paragraph. For free atoms, the measured velocity profile is in good agreement with that shown in figure III.4, with holes corresponding to resonant velocity classes and notable non-Gaussian wings.

3-2 The role of collective effects

In the theory-experiment comparison we have just described, collective effects play an important role. The theoretical models we presented earlier focused on the case of a single atom coupled to radiation. In the experiments, a large number of particles are cooled (from 10^4 to 10^7), and it is important to specify the conditions under which we can expect the predictions made for a single atom to be valid.

The most important problem, already encountered in the broad-line magneto-optical trap, is the multiple scattering of photons. In the case of the magneto-optical trap, we reported that this multiple scattering was responsible for a repulsive force between the atoms, which increased the equilibrium size of the trapped cloud. Multiple scattering also creates heating, due to the random recoil it causes. In what follows, we estimate the parameters of the atom cloud at which these effects become significant.

To be cooled to the desired temperature, the atoms are continuously illuminated by the cooling light beams, and each atom scatters the incident photons at a rate γ. The emitted photons have approximately the same wavelength as the incident photons, so they can also be scattered, with an effective cross-section close to the resonant scattering cross-section.

$$\sigma = \frac{3}{2\pi}\lambda^2. \qquad \text{(III.35)}$$

Note the very large value of this effective resonant cross-section (a micron-square), far greater than the geometric dimension of an atom (an angström-square).

The mean free path of a photon in the atomic assembly is given by $1/(n\sigma)$. Reabsorption becomes significant when this mean free path is of the order of the size L of the cloud, i.e. using $\sigma \sim \lambda^2$:

$$\text{significant reabsorption if :} \quad n\lambda^2 L \gtrsim 1. \qquad \text{(III.36)}$$

This criterion can be recovered by looking for the situation where the scattering rate γ' due to reabsorption becomes comparable to the scattering rate γ of incident laser photons: there are $N\gamma$ laser photons scattered per second, and the probability that a given atom will reabsorb a photon scattered by another atom at an average distance $\sim L/2$ is $\sim \sigma/L^2$. The rate γ'

is therefore

$$\gamma' \sim \frac{\sigma}{L^2} N\gamma \tag{III.37}$$

so that $\gamma' \sim \gamma$ when $n\sigma L \sim 1$. Note that when this criterion is met, the absorption of incident laser beams becomes significant: the atomic medium is optically thick.

As we wrote above, as soon as γ' becomes of the order of γ, the cooling dynamics is altered: the random recoil that accompanies multiple scattering phenomena generates additional heating of the trapped atoms, and the equilibrium temperature rises. In a later chapter, we will discuss some of the possibilities that have been envisaged to counteract this heating associated with multiple scattering. In this chapter, we will just mention one that has been used in the experiments presented here: one takes a cloud of high anisotropy (cigar or pancake), so that at least one of the cloud's linear dimensions is small, of the order of just a few optical wavelengths. Photons can then easily escape in this direction, even though the trap may contain a large number of atoms.

Note. The collective effects that occur when an atomic cloud interacts with resonant light are not limited to multiple scattering. The atomic densities actually reached correspond to an average distance between atoms of the order of the optical wavelength. When an excited atom and an atom in the ground state are separated by such a small distance, the dipole-dipole interaction between atoms must be taken into account (Julienne, Smith, et al. 1992). This gives rise to multiple potential curves, attractive or repulsive, and the corresponding acceleration can also contribute very significantly to the heating of the gas, or even to atom loss via light-assisted inelastic collisions [see for example Fuhrmanek, Bourgain, et al. (2012) and refs. in].

3-3 Narrow line magneto-optical trap

The operation of a narrow-line magneto-optical trap is significantly different from that of the traditional broad-line trap. This operation has been studied in detail by the Boulder group (Loftus, Ido, et al. 2004), and we summarize their analysis here. Consider an atomic transition

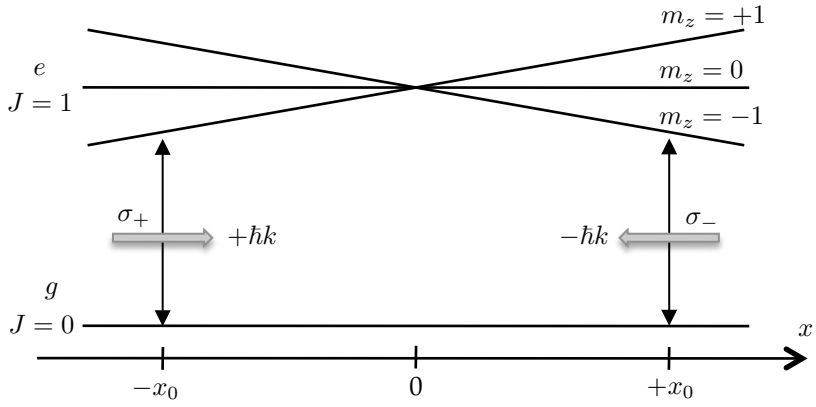

Figure III.12. *Basic diagram of the magneto-optical trap. We are interested here in the case where the radiation pressure force only takes on significant values in the vicinity of* $\pm x_0$.

$J_g = 0 \leftrightarrow J_e = 1$, a magnetic field gradient b' along the x axis, illuminate the atoms with a pair of counter-propagating monochromatic waves (figure III.12), and assume that the following inequalities are satisfied:

$$\omega_\mathrm{r} \lesssim \Gamma\sqrt{1 + \frac{2|\kappa|^2}{\Gamma^2}} \ll |\Delta|. \tag{III.38}$$

The first inequality allows us to use a semi-classical calculation for the force acting on an atom at rest:

$$F = F_+ + F_- \qquad \text{with} \quad F_\pm(z) = \pm\hbar k\Gamma \frac{|\kappa|^2}{4(\Delta \mp \mu b' x)^2 + \Gamma^2 + 2|\kappa|^2} \tag{III.39}$$

The second inequality indicates that the force will only take on significant values in two well-localized regions of the x axis (figure III.13): $F_\pm$ is nonzero at $x = \mp|\Delta|/\mu b'$. We then realize the equivalent of "walls" for atoms, with an almost square potential well[2]. Along the vertical axis, we must

[2]The notion of potential well is to be taken with care: in one dimension, knowing a force $F(x)$, we can always define the potential $V(x) = -\int^x F(x')\,\mathrm{d}x'$. In several dimensions, it is not guaranteed that the radiation pressure force of the magneto-optical trap derives from a potential (it would require that $\partial_i F_j = \partial_j F_i$ for the three i, j components of space).

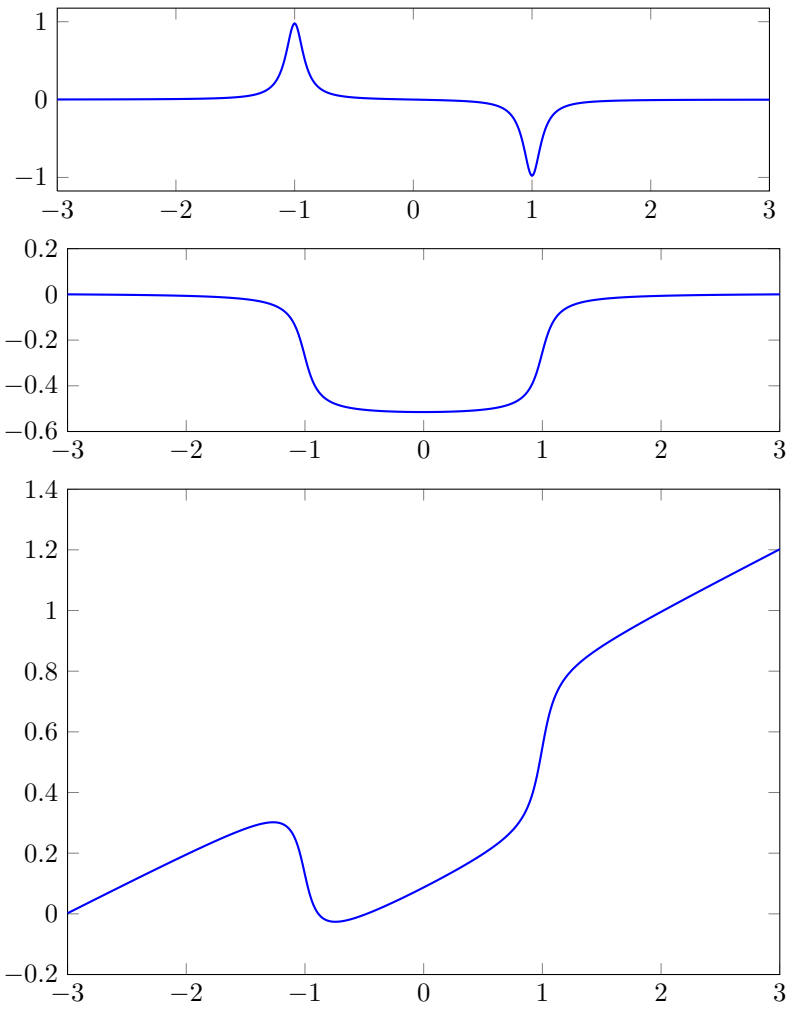

Figure III.13. *Magneto-optical trap with a narrow line. Top: radiation pressure force (in units of $F_{\max} = \hbar k\Gamma/2$) for highly detuned excitation: $\Delta = -40\,\Gamma$, $\kappa = 5\,\Gamma$, as a function of position measured in units of $x_0 = |\Delta|/\mu b'$. Middle: potential corresponding to this radiation pressure force on a horizontal axis. Bottom: total light+gravity potential on the vertical axis, calculated for $Mg = 0.1\,F_{\max}$.*

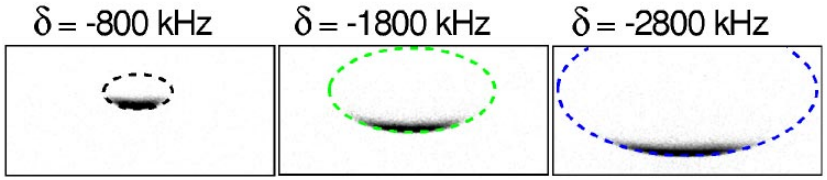

Figure III.14. *Images* in situ *of a strontium magneto-optical trap operating in the narrow-line regime. The dotted lines correspond to the contours along which the radiation pressure force is maximal ($|\kappa| \approx 11\,\Gamma \approx 2\pi \times 83\,kHz$, $\Delta = 2\pi \times \delta$). Figure taken from Loftus, Ido, et al. (2004).*

also take into account gravity, which is not negligible compared to the radiation pressure force for a narrow line: for the strontium atom, the maximum radiation pressure force $\hbar k\Gamma/2$ is only 16 times the atom's weight. The combined light+gravity potential is then shaped like a tilted box, and the atoms accumulate below the zero-magnetic-field point. The images in figure III.14, taken from Loftus, Ido, et al. (2004), clearly illustrate the asymmetry of the trap in this regime.

4 Towards Bose-Einstein condensation

We have just seen that narrow-line cooling experiments can produce very cold gases (sub-microkelvin), with relatively high spatial densities since the average distance between particles, $n^{1/3}$, is only two to three times greater than the thermal wavelength.

$$\lambda_T = \frac{\hbar\sqrt{2\pi}}{\sqrt{Mk_{\mathrm{B}}T}}. \tag{III.40}$$

These gases (made up of zero-spin atoms, i.e. bosons) are at the threshold of the quantum degeneracy regime and are good candidates for producing a Bose-Einstein condensate, with a "small" additional step. This step was taken in the experiment by Stellmer, Pasquiou, et al. (2013), which was inspired by a method proposed by Pinkse, Mosk, et al. (1997) and developed experimentally by Stamper-Kurn, Miesner, et al. (1998).

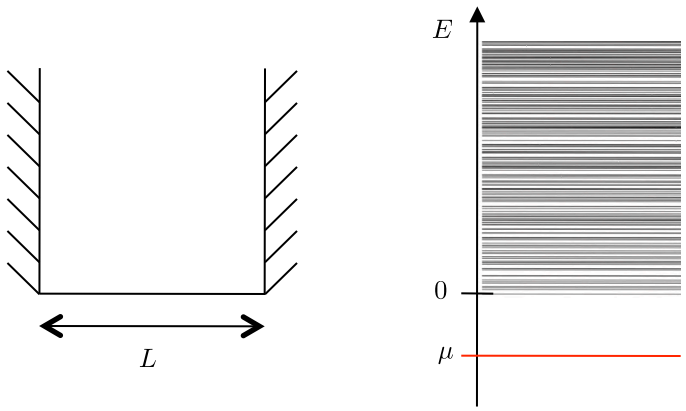

Figure III.15. *Left, cubic potential well with side L. Right, single-particle energy levels $\epsilon_p = p^2/2M$, where the momentum $\boldsymbol{p}$ is quantized according to (III.42). The red line represents the position of the chemical potential μ for an ideal gas contained in this box. For Maxwell-Boltzmann statistic, μ can take any value, but only sufficiently negative values are physically relevant, since they correspond to occupancy probabilities $n(\boldsymbol{p}) \ll 1$ for all $\boldsymbol{p}$. For Bose-Einstein statistic, the only mathematically acceptable values of μ are negative. Bose-Einstein condensation (macroscopic accumulation of atoms in the $\boldsymbol{p} = 0$ state) occurs when μ is sufficiently close to 0.*

The remarkable feature of the Stellmer, Pasquiou, et al. (2013) experiment is that at no point does it require the evaporation or loss of atoms. Insofar as this condensation without evaporation is based on the particular properties of Bose-Einstein statistic, we will begin by recalling the main properties of this statistic, comparing it with Maxwell-Boltzmann statistic. We will not describe here the standard mechanism of Bose-Einstein condensation at the thermodynamic limit [see for example Huang (1987)], but we will develop a simplified model of the method of Stamper-Kurn, Miesner, et al. (1998) and Stellmer, Pasquiou, et al. (2013). We will see how macroscopic particle accumulation can occur by changing the shape of the confinement potential, and then present the main features of the experiment of Stellmer, Pasquiou, et al. (2013).

4-1 Maxwell-Boltzmann statistics

In what follows, we consider a gas of non-interacting particles, confined in a cubic box of side L (figure III.15). We assume periodic boundary conditions, so that the eigenstates of the single-particle Hamiltonian are plane waves

$$\psi_{\boldsymbol{p}}(\boldsymbol{r}) = \frac{\mathrm{e}^{\mathrm{i}\boldsymbol{r}\cdot\boldsymbol{p}/\hbar}}{L^{3/2}} \qquad \text{with energy } \epsilon_p = \frac{p^2}{2M}, \tag{III.41}$$

with the quantization condition in the box

$$p_j = \frac{2\pi\hbar}{L} n_j, \qquad j = x, y, z, \quad n_j \in \mathbb{Z}. \tag{III.42}$$

In thermodynamics, the state of the gas in the box of volume $V = L^3$ is determined by two independent thermodynamic variables. Knowing these two variables, we can then deduce the other thermodynamic quantities, such as pressure ($P = Nk_{\mathrm{B}}T/V$), internal energy ($\frac{3}{2}k_{\mathrm{B}}T$), entropy, and so on. In what follows, we will take the temperature T and the chemical potential μ as a pair of variables, well suited to calculating the occupancy of single-particle states.

In Maxwell-Boltzmann statistics, the average number of particles occupying an momentum state $\boldsymbol{p}$ is written as

$$n^{(\mathrm{Boltz.})}(\boldsymbol{p}) = \mathrm{e}^{(\mu-\epsilon_p)/k_{\mathrm{B}}T}. \tag{III.43}$$

The total number of particles N is obtained by summing the contribution of all states, and replacing this discrete sum by an integral in the large-box limit:

$$N = \sum_{\boldsymbol{p}} n^{(\mathrm{Boltz.})}(\boldsymbol{p}) = \left(\frac{L}{2\pi\hbar}\right)^3 \int \mathrm{e}^{(\mu-\epsilon_p)/k_{\mathrm{B}}T}\, \mathrm{d}^3p, \tag{III.44}$$

which gives

$$N = Z\,\frac{L^3}{\lambda_T^3} \tag{III.45}$$

where the fugacity Z of the gas is defined as:

$$Z = \mathrm{e}^{\mu/k_{\mathrm{B}}T}. \tag{III.46}$$

In Maxwell-Boltzmann statistics, the chemical potential can take on any value, positive or negative. However, we can see from (III.43) that for $\mu > 0$ (or more generally μ greater than the energy of the ground level), the occupation of the lowest energy levels becomes greater than 1. In the case of indistinguishable particles, using Maxwell-Boltzmann statistic for $\mu > 0$ is incorrect, even if it does not lead to a mathematical singularity: the statistical nature of the particles plays an important role when $n(\boldsymbol{p})$ approaches unity, and we have to turn to Bose-Einstein or Fermi-Dirac statistics, depending on whether we are dealing with bosons (particles with integer spin) or fermions (particles with half-integer spin). In what follows, we will concentrate on Bose-Einstein statistic.

4-2 Bose-Einstein statistics

In Bose-Einstein statistics, the average occupancy of a state is given by

$$n^{(\mathrm{Bose})}(\boldsymbol{p}) = \frac{1}{\mathrm{e}^{(\epsilon_p-\mu)/k_\mathrm{B}T}-1}. \tag{III.47}$$

A remark can immediately be made about this expression. For the population of each state to be defined and positive, the value of the chemical potential μ must always be strictly smaller than the energy of the ground state of the system, in this case zero energy for our particles in a box. Unlike Maxwell-Boltzmann (and Fermi-Dirac) statistics, there is therefore a mathematical constraint on the chemical potential for the Bose-Einstein statistics (figure III.15):

$$\mu < E_\mathrm{ground}, \quad \text{i.e. for } \epsilon_p = \frac{p^2}{2M}: \quad \mu < 0. \tag{III.48}$$

A second remark concerns the link between Bose-Einstein and Maxwell-Boltzmann statistics. In the context of Bose-Einstein statistics, let us consider a sparsely populated state, i.e. $n(\boldsymbol{p}) \ll 1$. This means that the denominator of (III.47) is much greater than 1, and so $\mathrm{e}^{(\epsilon_p-\mu)/k_\mathrm{B}T} \gg 1$. So for these sparsely populated levels:

$$n(\boldsymbol{p}) \ll 1: \qquad n^{(\mathrm{Bose})}(\boldsymbol{p}) \approx n^{(\mathrm{Boltz.})}(\boldsymbol{p}) = Z\mathrm{e}^{-\epsilon_p/k_\mathrm{B}T}. \tag{III.49}$$

This approximation will be valid for all levels, including the ground level, if we take $Z \ll 1$, i.e. negative μ with $|\mu| \gg k_\mathrm{B}T$.

The total number of atoms for Bose-Einstein statistic is obtained as for Maxwell-Boltzmann statistic by the sum

$$N = \sum_{\boldsymbol{p}} n^{(\mathrm{Bose})}(\boldsymbol{p}). \tag{III.50}$$

Here too, it is tempting to replace the discrete sum by an integral, which yields a simple calculation:

$$N = g_{3/2}(Z)\,\frac{L^3}{\lambda_T^3} \qquad \text{with} \quad g_\alpha(Z) = \sum_{n=1}^{+\infty}\frac{Z^n}{n^\alpha} \text{ (polylogarithm function).} \tag{III.51}$$

The similarity with the result for Maxwell-Boltzmann statistic is striking. In particular, for $Z \ll 1$, we have $g_{3/2}(Z) \approx Z$ and the two results are comparable, as announced above.

However, this similarity is also misleading. For Maxwell-Boltzmann statistic, the result (III.45) always provides a value of the fugacity (or of the chemical potential) that accounts for a given number of N atoms. In contrast, for Bose-Einstein statistics, we have seen that the values of Z are limited to the interval $[0, 1[$; the function $g_{3/2}(Z)$ therefore takes values between 0 and $g_{3/2}(1) \approx 2.612$, so that the number of atoms calculated in this way cannot exceed

$$N_\mathrm{max} = 2.612\frac{L^3}{\lambda_T^3}. \tag{III.52}$$

Why is it that the number of atoms that can be placed in the gas is bounded? The answer to this question is Bose-Einstein condensation. We will not go into detail here, but let us recall its origin: the transition from the discrete sum (III.50) to the integral (III.51) is only legitimate if the chemical potential is sufficiently far from its maximum value $\mu = 0$. When μ tends towards the ground-state energy (here $E = 0$), the population of the ground level diverges [*cf.* (III.47)]. However, this divergence is neglected in the transition to the integral (III.51). As Z approaches 1, the population of this ground level needs to be treated more carefully. We then find that a macroscopic fraction of particles can accumulate there, via a mechanism that becomes a phase transition at the thermodynamic limit.

Condensation therefore occurs when the number of atoms N reaches the value (III.52), which corresponds to the phase-space density $\mathcal{D} = n\lambda_T^3$

with $n = N/L^3$: $\mathcal{D}_{\max} = 2.612$. This value is reached when the average distance between particles, $n^{-1/3}$, is of the order of the thermal wavelength λ_T.

4-3 Condensation in a micro-trapÒ

Before describing the Stellmer, Pasquiou, et al. (2013) experiment in detail, we present a simple model for understanding how it is possible to obtain a degenerate quantum gas, in this case a Bose-Einstein condensate, starting from a non-degenerate gas and with a simple transformation of the potential confining the gas.

Let us take our gas of N atoms at temperature T, confined in a cubic box of side L, with the occupancy $n(\boldsymbol{p})$ of each state given by (III.47). Let us start by recalling that a trivial deformation of the potential, consisting in increasing or decreasing the size L of the box, will not produce anything spectacular. If this deformation is carried out very slowly to achieve an adiabatic transformation, the phase-space density will remain constant; we demonstrated this point for a harmonic potential in the introductory chapter. If this deformation is carried out non-adiabatically, the situation will only get worse, as entropy will increase and phase-space density will decrease.

In what follows, we will take a look at the following non-trivial deformation: let us assume that we suddenly create a trap described by a very localized potential $V(\boldsymbol{r})$ (figure III.16). The volume ℓ^3 over which $V(\boldsymbol{r})$ is non-zero is small compared with L^3. The exact form of $V(\boldsymbol{r})$ is unimportant; the only important assumption for what follows is that there is one and only one bound state $|\phi_0\rangle$ of energy $\epsilon_0 < 0$ in this well. In the following, we will take $|\epsilon_0| \sim k_{\mathrm{B}}T$. The eigenstates in the box with this additional micro-trap are therefore the state $|\phi_0\rangle$ and the extended states $|\psi_{\boldsymbol{p}}\rangle$ formed from plane waves (III.41), but slightly distorted to ensure their orthogonality with $|\phi_0\rangle$.

As the branching of this well is sudden, and the volume involved ℓ^3 is very small, we can consider to a good approximation that the N atoms remain on the extended states $|\psi_{\boldsymbol{p}}\rangle$ at the moment of branching. However,

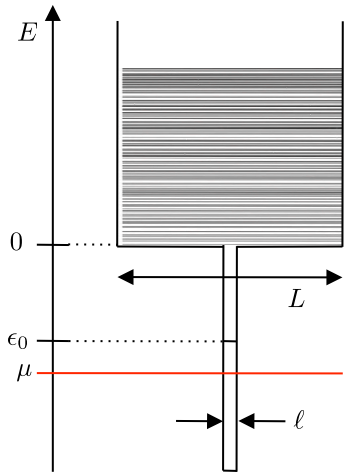

Figure III.16. *Micro-trap of size ℓ in the middle of a cubic box of much larger size L. The micro-trap is assumed to contain only one bound state $|\phi_0\rangle$, of energy $\epsilon_0 < 0$. For a gas described by Bose-Einstein statistic, the chemical potential is necessarily less than ϵ_0.*

once the branching has been made, collisions between atoms[3] will lead to thermalization of the gas.

After a sufficient time, which we will not attempt to characterize, a new thermodynamic equilibrium is reached thanks to the elastic collisions that can populate the micro-trap (figure III.17). This equilibrium is described by a temperature T' and a chemical potential μ', which are the two unknowns of the problem. This equilibrium corresponds to N_0 atoms in the state $|\phi_0\rangle$ and $N' = N - N_0$ in the states $|\psi_{\boldsymbol{p}}\rangle$. Our aim is to show that it is possible to find situations where N_0 is comparable to N: this is the definition of Bose-Einstein condensation, with an accumulation of a macroscopic number of atoms in an individual quantum state.

[3]The existence of these collisions means that the gas is not really ideal, and that there are deviations from the ideal gas model. But these deviations can be made arbitrarily small, if we accept that the relaxation time is long.

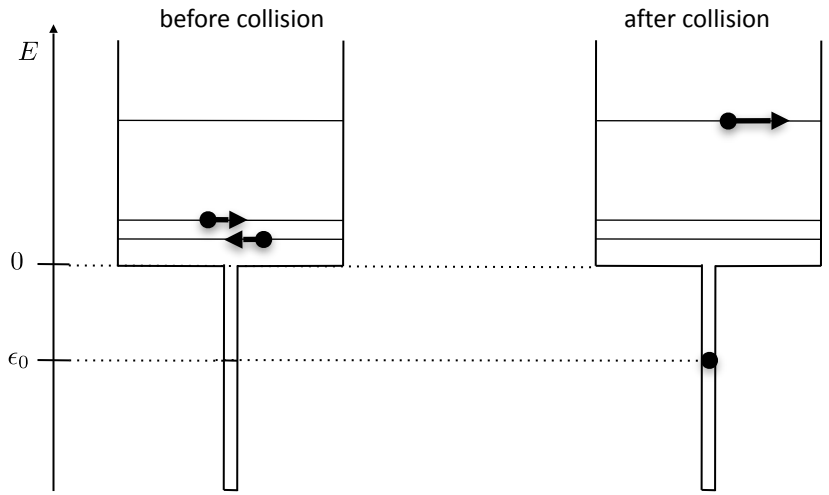

Figure III.17. *Micro-trap filling by elastic collision between two particles*

The occupancy of the extended states $|\psi_{\boldsymbol{p}}\rangle$ is given by Bose law

$$n'(\boldsymbol{p}) = \frac{1}{\mathrm{e}^{\left(\frac{p^2}{2M}-\mu'\right)/k_{\mathrm{B}}T'}-1} \tag{III.53}$$

and the occupancy of the ground state $|\phi_0\rangle$ is

$$N_0 = \frac{1}{\mathrm{e}^{(\epsilon_0-\mu')/k_{\mathrm{B}}T'}-1}. \tag{III.54}$$

Particle number conservation is written

$$N = N_0 + \sum_{\boldsymbol{p}} n'(\boldsymbol{p}), \tag{III.55}$$

which provides a first constraint on the two unknowns μ' and T'. The second constraint comes from energy conservation. Once the micro-trap is switched on, the gas is an isolated system and total energy is conserved. The initial and final energies are therefore equal

$$E_i = \sum_{\boldsymbol{p}} \frac{p^2}{2M} n(\boldsymbol{p}), \qquad E_f = N_0\epsilon_0 + \sum_{\boldsymbol{p}} \frac{p^2}{2M} n'(\boldsymbol{p}). \tag{III.56}$$

This problem with two unknowns can be easily solved using a numerical program. The input parameters are

- The initial fugacity of the gas $Z = \mathrm{e}^{\mu/k_{\mathrm{B}}T}$. We will assume that the gas is initially weakly degenerate, and we will take $Z = 0.5$, for which Bose and Boltzmann laws give similar results in terms of both atom number and energy.
- The energy of the bound state ϵ_0, measured in units of $k_{\mathrm{B}}T$.
- The ratio L/λ_T between box size and initial thermal wavelength. Here we will take $L/\lambda_T = 100$.

The conditions given above correspond to a total number of atoms $N = g_{3/2}(Z)\,(L/\lambda_T)^3 \approx 620\,000$. The results are shown in figure III.18. Take, for example, $\epsilon_0 = -3k_{\mathrm{B}}T$; the numerical resolution then indicates that, after thermalization, 23% of the atoms have accumulated on the microscopic level, and the gas temperature has become $T' \approx 1.8\,T$: the gas has warmed up (as could be anticipated from figure III.17), but a significant condensed fraction has appeared.

Note 1. The problem can be solved in an approximate, quasi-analytical way by noting (i) that in the above example, the occupancies of the extended states are given to a good approximation by Boltzmann's law, and (ii) that the chemical potential μ' is practically equal to the energy ϵ_0 of the bound state, since the latter is macroscopically occupied. We find the final fugacity

$$Z' \approx \mathrm{e}^{\epsilon_0/k_{\mathrm{B}}T'} = \mathrm{e}^{-\eta/x} \qquad \text{with} \quad \eta = \frac{|\epsilon_0|}{k_{\mathrm{B}}T}, \quad x = \frac{T'}{T} \tag{III.57}$$

and the conservation laws for the number of particles and energy give:

$$N = N_0 + N' \qquad \text{with} \quad N \approx Z\frac{L^3}{\lambda_T^3}, \quad N' \approx Z'\frac{L^3}{\lambda_T^3}, \tag{III.58}$$

$$\frac{3}{2}Nk_{\mathrm{B}}T = N_0\epsilon_0 + \frac{3}{2}N'k_{\mathrm{B}}T'. \tag{III.59}$$

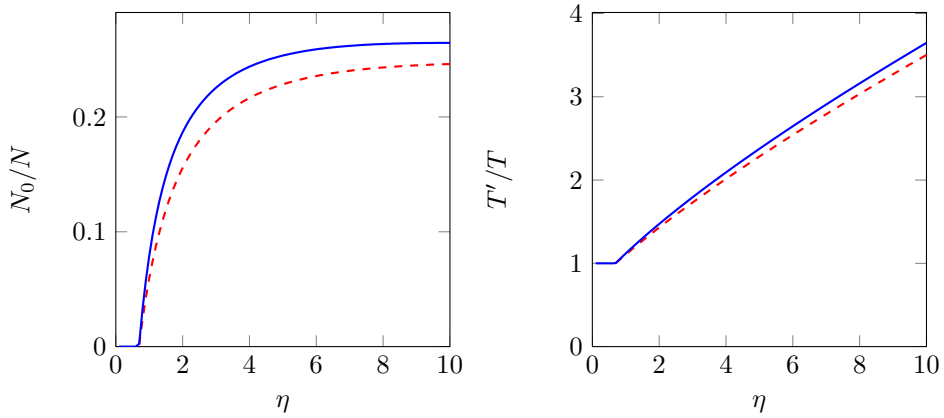

Figure III.18. *Evolution of the condensed fraction and final temperature in the box+micro-trap system as a function of the control parameter $\eta = |\epsilon_0|/k_{\rm B}T$ for a weakly degenerate initial state $Z = 0.5$. Blue solid line: exact treatment from (III.53)-(III.56), in the case $L = 100\,\lambda_T$. Red dotted line: approximate treatment (III.60).*

We choose to work with the unknowns $x = T'/T$ and the condensed fraction $f_0 = N_0/N$:

$$\begin{aligned} 1 &= f_0 + \frac{x^{3/2}\,\mathrm{e}^{-\eta/x}}{Z}, \\ 1 &= -\frac{2}{3} f_0 \eta + (1 - f_0) x. \end{aligned} \qquad \text{(III.60)}$$

Solving this system gives a result close to that obtained by exact calculation (figure III.18). In this approximation, the result no longer depends on the ratio L/λ_T, but simply on the initial fugacity Z and the choice of ratio $\eta = |\epsilon_0|/k_{\rm B}T$.

Note 2. The condensate fraction obtained here is of the order of 20% and varies slowly with the control parameter $|\epsilon_0|/k_{\rm B}T$. However, we note that the condensate formed in the $|\phi_0\rangle$ state is highly localized in space. We can then take advantage of a very efficient evaporation, consisting in evacuating all the atoms outside the ℓ^3 volume. Atoms in the state $|\phi_0\rangle$ will remain unaffected, while virtually all non-condensed atoms $[N'(1 - \frac{\ell^3}{L^3})]$ will be eliminated. The result is a quasi-pure condensate at a cost of the loss of around $4/5$ of the atoms. This method of taking advantage of the shape of the confinement potential to localize entropy in particular zones of space has been proposed in a slightly different context by various authors (see, for example, Bernier, Kollath, et al. (2009) and refs. in).

Note 3. We have neglected the interactions between atoms here, except for gas thermalization. In practice, these interactions can play an important role, as the N_0 atoms are accumulated in a very small region of space, corresponding to a high spatial density. The mean field energy will therefore shift the position of the level ϵ_0, and inelastic collisions, via three-body recombination leading to molecule formation, can play an important role. Our limiting case of an extremely narrow well should therefore be regarded as a simple model to analyze, but not necessarily an optimal situation in practical terms.

4-4 The Innsbruck experience (2013)

In their experiment, Stellmer, Pasquiou, et al. (2013) started with a gas of $N \approx 10^7$ atoms of ^{84}Sr, cooled to $T = 0.9\,\mu$K thanks to the narrow line at 689 nm we have already mentioned. This gas is confined in an optical tweezer (dipole trap) formed by a strongly focused Gaussian beam with wavelength $\lambda = 1065$ nm. The beam is elliptical with radii at $1/e^2$ (waists) $w_y = 300\,\mu$m and $w_z = 17\,\mu$m. Oscillation frequencies in the trap are 6, 35 and 600 Hz along the three axes of space x, y, z. The depth of the trap is $9\,\mu$K, well above atomic temperature, so evaporation losses are negligible. This optical tweezer plays the role of the L^3 volume box in our model.

To create the micro-well that will induce condensation, Stellmer et al. superimpose a second optical tweezer (dimple), much more focused than the first (figure III.19ab). This second tweezer propagates almost vertically, creating a potential trough in the horizontal plane with radius $\sim 20\,\mu$m, characterized by oscillation frequencies of 250 Hz. To help the atoms accumulate in this dimple, Stellmer et al. add an additional beam, similar in size and direction to the micro-tweezer, to make the atoms transparent to the cooling lasers. This beam, with a wavelength of 688 nm, creates a

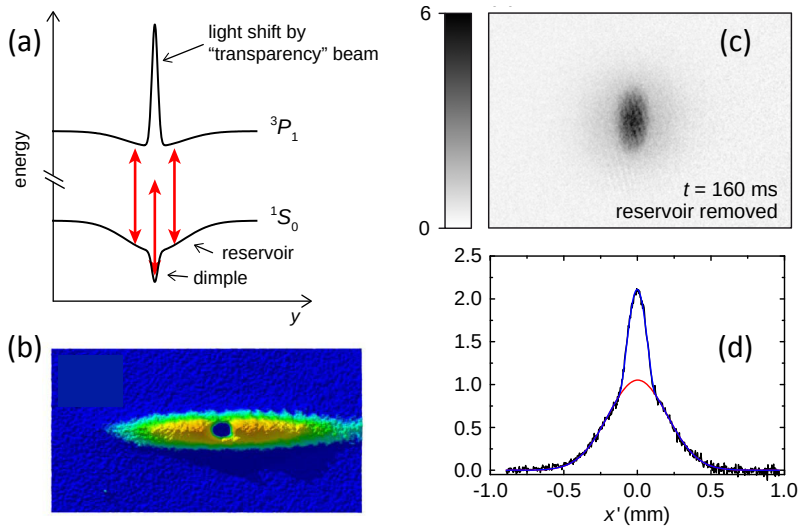

Figure III.19. *Experiment by Stellmer, Pasquiou, et al. (2013) at Innsbruck. (a) ^{84}Sr atoms are Doppler-cooled to a narrow line in a large optical tweezer acting as a reservoir. An optical micro-trap (*dimple*) is superimposed, in which about 10% of the atoms will accumulate. (b) The atoms in the micro-trap are made transparent to the cooling light by an auxiliary beam which strongly displaces the excited level. Conditions are such that a condensate appears in this micro-trap. (c-d) The condensate is observed by eliminating the atoms outside the micro-trap. After time of flight, the usual bi-modal distribution is observed, revealing the condensate (narrow central component) and the non-condensed fraction (wider pedestal). The condensed fraction is of the order of 1%.*

significant light-shift of the $^3P_1$ excited level (more than $1000\,\Gamma$).

The experiment leads to the formation of a Bose-Einstein condensate inside the dimple. The condensed fraction is small ($\sim 1\%$), making the condensate difficult to detect amid the 99% of remaining atoms, essentially confined within the first large optical tweezer. But one can take advantage of the fact that the atoms in the dimple have become transparent to the cooling light to observe this condensate: the radiation pressure of an intense flash of light can push out of the detection zone all atoms except those confined in the dimple. After a time of flight, a bimodal velocity distribution is revealed, the usual signature of a condensate in an anisotropic harmonic trap (figure III.19cd). This formation is reversible, as the dimple can be switched on and off many times, allowing the condensate to form and then disappear.

Although the absolute performance of this experiment in terms of the number of atoms condensed remains below that obtained by evaporation, it represents an important step towards the realization of dissipative quantum systems with cold atomic gases. The condensate is continuously fed by a reservoir of laser-cooled atoms, which can itself be continuously refilled from atomic vapor at room temperature. Transposing this experiment to gases of fermionic atoms would enable one to achieve a situation similar to that of electrons in a metal (normal or superconducting): we would then have a dissipative quantum system, in contact with a thermostat permanently imposing its temperature on the system.

Chapter IV

Hiding in the shadow

The previous chapters were devoted to Doppler cooling, first with a broad line such that the width Γ of the excited level is large in front of the recoil frequency $\omega_{\rm r} = \hbar k^2/2M$, then with a narrow line.

In the first case, we found that the optimum detuning was $\Delta = -\Gamma/2$, leading to the well-known Doppler limit, $k_{\rm B}T = \hbar\Gamma/2$. The variation of the photon scattering rate with atomic velocity is shown in figure IV.1 (left). It is roughly constant throughout the interval from $v = -\Gamma/k$ to Γ/k, and the root-mean-square velocity at equilibrium is large compared with the recoil velocity $v_{\rm r} = \hbar k/M$.

In the second case, we found that the optimum detuning is $\Delta \approx -3\omega_{\rm r}$, leading to a root-mean-square velocity at equilibrium of the order of $v_{\rm r}$. The variation of the photon scattering rate with velocity is then very different from the case of a broad line (see figure IV.1 right): this rate passes through a pronounced minimum around $v = 0$, with atoms accumulating in velocity classes where they scatter very few photons.

The aim of this chapter is to generalize the notion of optical pumping in velocity space that occurs in narrow-line Doppler cooling. We will exploit the idea of interference between quantum paths to cancel the atom's excitation probability when it has reached the desired velocity class. We will discuss two different schemes, leading to the same statistical laws: coherent population trapping and Raman cooling, which uses light pulses of optimized shape to transfer an atom from a given state of the ground electronic level to another, in a velocity-selective manner.

What these two schemes have in common is the use of a Λ configuration of internal levels, with two ground states g_1 and g_2, coupled to a single excited state e (figure IV.2). Despite its apparent simplicity, this is a very rich system, giving rise to many counter-intuitive phenomena. We will start by outlining a number of its properties; we refer the interested reader to the review articles of Arimondo (1996), Harris (1997), and Fleischhauer, Imamoglu, et al. (2005) for a more in-depth study, particularly with regard to its applications concerning electromagnetically induced transparency and quantum information.

1 The Λ system and its dark state

The aim of this first section is to describe some remarkable properties of the Λ system, composed of two states $|g_1\rangle$ and $|g_2\rangle$ of infinite lifetime and an excited state $|e\rangle$. In this section, we will concentrate on the atom's internal dynamics. The study of the atomic center-of-mass motion will be carried out in § 2.

1-1 Reminder of two-level system

Before tackling the Λ system, let us briefly review a few elements we have already encountered for a two-level system, composed of a stable ground

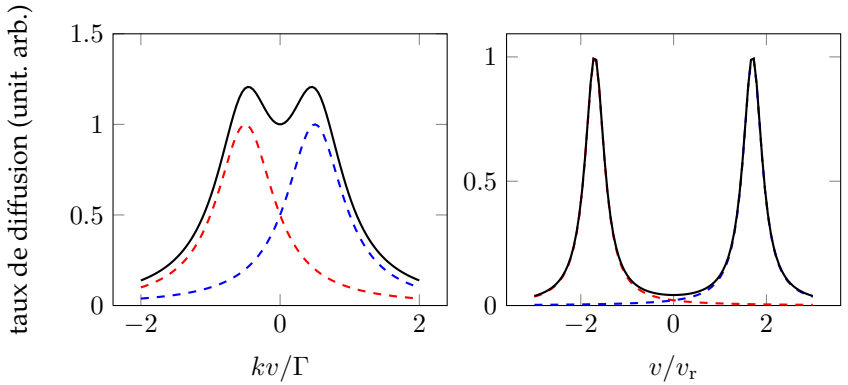

Figure IV.1. *Excitation rate γ of an atom cooled by one-dimensional Doppler effect. Left: broad line case, with $\Gamma \gg \omega_r$ and $\Delta = -\Gamma/2$. Right: narrow line case with $\Gamma = \omega_r$ and $\Delta = -3.4\,\omega_r$. The value of γ is proportional to the light power and its unit here is arbitrary. The dotted curves represent the rates induced by the two running waves creating the cooling, and the solid curve represents the sum of these two rates.*

state g of energy E_g and an excited state e of energy E_e and lifetime Γ^{-1}.

First of all, let us remember that in many calculations we can simply take into account the finite lifetime of the excited state e by adding to its energy the imaginary term $-\mathrm{i}\hbar\Gamma/2$. Indeed, the exponential decay law $P_e(t) = \mathrm{e}^{-\Gamma t}$ is obtained from the evolution of the state vector

$$|\psi(t)\rangle = \mathrm{e}^{-\mathrm{i}E_e t/\hbar}\,\mathrm{e}^{-\Gamma t/2}|e\rangle + \ldots, \tag{IV.1}$$

which is exactly what one would expect for an energy

$$\bar{E}_e = E_e - \mathrm{i}\frac{\hbar\Gamma}{2}. \tag{IV.2}$$

Let us assume now (as in previous chapters) that the levels g and e are coupled by a monochromatic excitation of frequency ω_L detuned by Δ from the atomic resonance $\omega_A = (E_e - E_g)/\hbar$. The coupling is characterized by the Rabi frequency κ, which we will assume here to be small compared with Γ and/or Δ. After switching to the rotating frame or the dressed atom

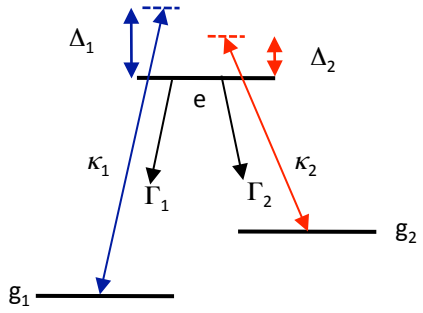

Figure IV.2. *Three-level system, illuminated by two coherent light waves. The spontaneous emission rates from the excited level $|e\rangle$ are assumed to be $\Gamma_1 = \Gamma_2 = \Gamma/2$.*

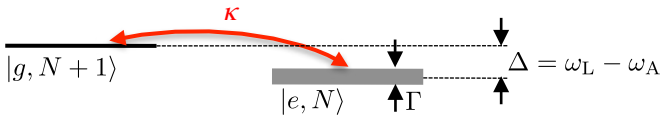

Figure IV.3. *A two-level atom dressed by the photons of a monochromatic light wave. The three frequencies characterizing the problem are the natural width Γ of the excited state, the detuning $\Delta = \omega_L - \omega_A$ and the Rabi frequency κ.*

formalism (figure IV.3), the eigenenergies in the presence of coupling are the eigenvalues of the non-Hermitian matrix describing the Hamiltonian in the $\{|g\rangle, |e\rangle\}$ basis:

$$\bar{H} = \hbar \begin{pmatrix} 0 & \kappa^*/2 \\ \kappa/2 & -\Delta - \mathrm{i}\Gamma/2 \end{pmatrix}. \tag{IV.3}$$

One of its eigenvalues remains close to $-\hbar(\Delta + \mathrm{i}\Gamma/2)$ and corresponds to the state $\bar{e}$, dressed by the coupling with the laser. Since the product of the eigenvalues (matrix determinant) is $-(\hbar|\kappa|/2)^2$, the other eigenvalue is

$$\approx \hbar\frac{|\kappa|^2/4}{\Delta + \mathrm{i}\Gamma/2}. \tag{IV.4}$$

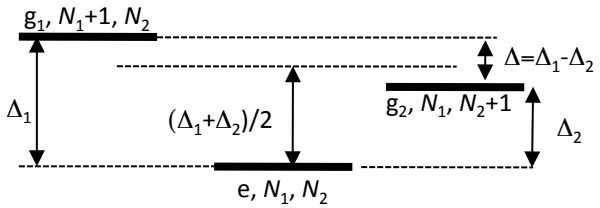

Figure IV.4. *Three-level system of figure IV.2, in dressed-atom representation.*

This gives the complex energy of the state $\bar{g}$, also dressed by the coupling with the laser. The real part of this energy represents the light shift $\delta E(g)$ of $\bar{g}$ with respect to g, and the imaginary part can be written $-\mathrm{i}\hbar\gamma/2$, where γ^{-1} is the finite lifetime of $\bar{g}$ corresponding to photon scattering with rate γ. Explicit calculation of these two terms from (IV.4) gives

$$\delta E(g) = \frac{\hbar\Delta}{2}\, s, \qquad \gamma = \frac{\Gamma}{2}\, s, \qquad \text{with} \quad s = \frac{|\kappa|^2/2}{\Delta^2 + \Gamma^2/4}. \tag{IV.5}$$

The expression for γ corresponds to what we found in Chapter 2 using the optical Bloch equations in the low-saturation limit. The expression for $\delta E(g)$ represents the dipole potential we used in previous lecture series when describing the trapping of atoms by light. We will use it again in the chapter on the Sisyphus effect.

1-2 The Λ system without spontaneous emission

We now switch to the three-level Λ system. We assume that the atoms modelled by this three-level system are illuminated by two monochromatic waves, each driving a $|g_j\rangle \leftrightarrow |e\rangle$ transition. We note κ_j the Rabi frequencies and Δ_j the corresponding detunings (figure IV.2). In a dressed-atom representation (figure IV.4), the state $|e, N_1, N_2\rangle$ is coupled to the two states $|g_1, N_1 + 1, N_2\rangle$ and $|g_2, N_1, N_2 + 1\rangle$ by atom-laser coupling:

$$\hat{V}_{\mathrm{AL}} = \frac{\hbar\kappa_1}{2}|e\rangle\langle g_1| + \frac{\hbar\kappa_2}{2}|e\rangle\langle g_2| + \mathrm{H.c.} \tag{IV.6}$$

By choosing the origin of the energies in the middle of the two states $|g_1, N_1 + 1, N_2\rangle$ and $|g_2, N_1, N_2 + 1\rangle$, the Hamiltonian of this three-level system is written in the basis $\{|g_1, N_1 + 1, N_2\rangle, |g_2, N_1, N_2 + 1\rangle, |e, N_1, N_2\rangle\}$:

$$\hat{H} = \frac{\hbar}{2}\begin{pmatrix} \Delta & 0 & \kappa_1^* \\ 0 & -\Delta & \kappa_2^* \\ \kappa_1 & \kappa_2 & -(\Delta_1 + \Delta_2) \end{pmatrix} \qquad \text{with} \quad \Delta = \Delta_1 - \Delta_2. \tag{IV.7}$$

The quantity Δ represents the detuning of the pair of light beams from the Raman resonance between $|g_1\rangle$ and $|g_2\rangle$.

We will not give the full expression of the eigenstates and associated energies for this Hamiltonian here, but we note a point that will play a crucial role in what follows. The state

$$|\psi_{\mathrm{NC}}\rangle \propto \kappa_2|g_1\rangle - \kappa_1|g_2\rangle = \begin{pmatrix} \kappa_2 \\ -\kappa_1 \\ 0 \end{pmatrix} \tag{IV.8}$$

is not coupled to light:

$$\hat{V}_{\mathrm{AL}}|\psi_{\mathrm{NC}}\rangle = 0 \tag{IV.9}$$

(the subscript "NC" means "not coupled"). If the Raman resonance is satisfied, $\Delta = 0$, then this state is also an eigenstate of the Hamiltonian $\hat{H}$: the atom prepared in this state will not evolve. The fact that this state is not coupled to light results from an interference phenomenon: to go from $|\psi_{\mathrm{NC}}\rangle$ to $|e\rangle$, two paths are possible: $|g_1\rangle \to |e\rangle$ and $|g_2\rangle \to |e\rangle$; however, these two paths have opposite amplitudes and interfere destructively: the total probability amplitude to go from $|\psi_{\mathrm{NC}}\rangle$ to $|e\rangle$ is zero.

In what follows, we will also use the combination state of $|g_1\rangle$ and $|g_2\rangle$ orthogonal to $|\psi_{\mathrm{NC}}\rangle$ which we will call "coupled state":

$$|\psi_{\mathrm{C}}\rangle \propto \kappa_1^*|g_1\rangle + \kappa_2^*|g_2\rangle. \tag{IV.10}$$

1-3 Accounting for spontaneous emission

When we take into account the fact that the excited state has a finite lifetime Γ^{-1}, the study of the system's dynamics must pass through the master equation formalism [or through another formalism that allows dissipative processes to be taken into account, such as the Monte Carlo wave function

method (Mølmer, Castin, et al. 1993)]. The master equation is written in a similar way to what we saw in Lecture 2 for the two-level atom:

$$\frac{\mathrm{d}\hat{\rho}}{\mathrm{d}t} = \frac{1}{\mathrm{i}\hbar}[\hat{H},\hat{\rho}] + \left.\frac{\mathrm{d}\hat{\rho}}{\mathrm{d}t}\right|_{\text{spont. em.}}. \tag{IV.11}$$

The incoherent evolution due to spontaneous emission phenomena generalizes what we have encountered for a two-level system:

$$\left.\frac{\mathrm{d}\rho_{ee}}{\mathrm{d}t}\right|_{\text{spont. em.}} = -(\Gamma_1+\Gamma_2)\rho_{ee}, \quad \left.\frac{\mathrm{d}\rho_{g_jg_j}}{\mathrm{d}t}\right|_{\text{spont. em.}} = +\Gamma_j\rho_{ee} \tag{IV.12}$$

for the populations of the three levels ($j = 1, 2$),

$$\left.\frac{\mathrm{d}\rho_{eg_j}}{\mathrm{d}t}\right|_{\text{spont. em.}} = -\frac{\Gamma_j}{2}\rho_{eg_j}, \tag{IV.13}$$

for optical coherences and

$$\left.\frac{\mathrm{d}\rho_{g_1g_2}}{\mathrm{d}t}\right|_{\text{spont. em.}} = 0 \tag{IV.14}$$

for the coherence between the two ground levels.

For this three-level system, it is possible to give an analytical expression for the steady state of the master equation (Janik, Nagourney, et al. 1985; Lounis & Cohen-Tannoudji 1992). As this analytical treatment is fairly lengthy (without posing any difficulties of principle), we will confine ourselves here to discussing a few physical points that will be useful for what follows.

1-4 Some important results for the Λ system

We consider here the observable corresponding to the stationary population of the excited state P_e. We note immediately that when the Raman resonance condition is satisfied, the uncoupled state (IV.8) proposed above remains a stable state of the system:

$$\hat{\rho}_{\text{NC}} = |\psi_{\text{NC}}\rangle\langle\psi_{\text{NC}}| \quad \Longrightarrow \quad \frac{\mathrm{d}\hat{\rho}_{\text{NC}}}{\mathrm{d}t} = 0. \tag{IV.15}$$

In fact, $\hat{\rho}_{\text{NC}}$ commutes with the Hamiltonian since $|\psi_{\text{NC}}\rangle$ is an eigenstate of this Hamiltonian. Moreover, this state does not evolve by spontaneous emission, since the entire population is concentrated in the ground states. This is an example of a state protected from dissipation (caused here by spontaneous emission processes).

When the Raman resonance condition is not verified, the stationary population of the excited state is non-zero. In figure IV.5, we have plotted the variation of this population with the detuning of one of the light beams (Δ_1) for different parameter regimes.

- When the Rabi frequencies κ_1 and κ_2 are equal, the cancellation of P_e for the Raman resonance $\Delta_1 = \Delta_2$ occurs in a regular manner, with an approximately symmetrical curve in the vicinity of the point where P_e vanishes (figures IV.5 A and B). This strict cancellation of the atom's excitation rate when the Raman resonance is reached will play a key role in the cooling mechanism based on coherent population trapping. Velocity selectivity will be ensured by the dependence of $\Delta_{1,2}$ on atomic velocity via the Doppler effect. We will come back to the typical width of the hole around the Raman resonance when we study this cooling mechanism.

- On the other hand, if the Rabi frequencies are very different (figures IV.5 C and D), the profile around the cancellation point is strongly asymmetrical and takes on the appearance of a line shape of the type predicted by Fano (1961). This type of profile is encountered when interference occurs between a resonant scattering process and a much flatter scattering process. Lounis & Cohen-Tannoudji (1992) proved that Fano's model was indeed realized for the Λ system when $\kappa_1 \ll \kappa_2 \ll |\Delta_{1,2}|$. To recover this result, we start by treating the interaction of beam 2 with the atom exactly. In the case where $\kappa_2 \ll |\Delta_2|$, the "dressing" of the level g_2 induces the light shift found in (IV.5):

$$|g_2\rangle \to |\bar{g}_2\rangle, \quad E(\bar{g}_2) = E(g_2) + \delta E(g_2) \quad \delta E(g_2) = \frac{\hbar\Delta_2}{2}\, s_2. \tag{IV.16}$$

  Starting with the atom in the state $|g_1\rangle$, a photon from the weak laser beam (beam 1) can be scattered either non-resonantly through $|e\rangle$ (figure IV.6, left), or resonantly via a Raman transition that leads the atom transiently into $|\bar{g}_2\rangle$ (figure IV.6, right). The narrow maximum of the

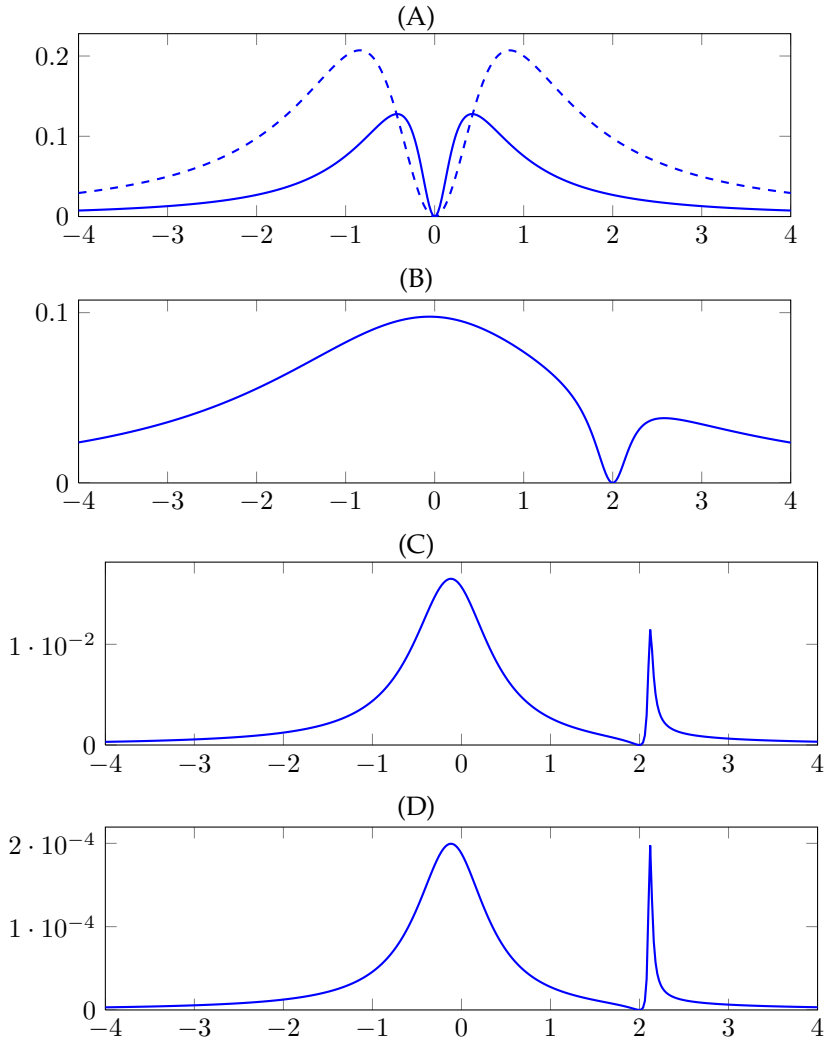

Figure IV.5. *Variation of excited population P_e with detuning Δ_1, measured in units of Γ. The other parameters are (in units of Γ): (A) solid line:$\kappa_1 = \kappa_2 = 0.5$, $\Delta_2 = 0$; dotted line: $\kappa_1 = \kappa_2 = 1$, $\Delta_2 = 0$, (B) $\kappa_1 = \kappa_2 = 1$, $\Delta_2 = 2$, (C) $\kappa_1 = 0.1$, $\kappa_2 = 1$, $\Delta_2 = 2$, (D) $\kappa_1 = 0.01$, $\kappa_2 = 1$, $\Delta_2 = 2$.*

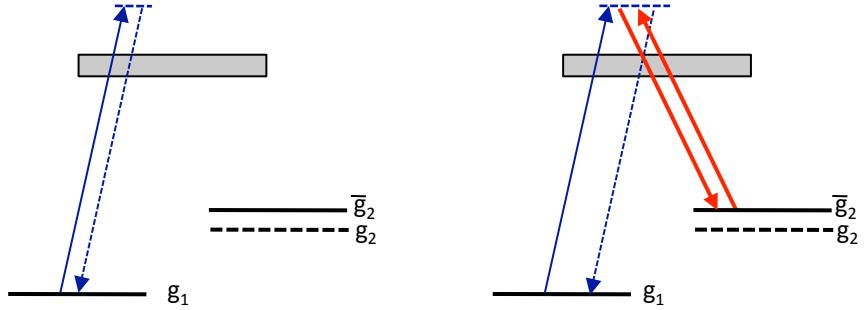

Figure IV.6. *The two scattering processes for a photon from laser 1, leading to the Fano profile of figure IV.5 C and D.*

curve for P_e is obtained when Raman resonance with respect to the dressed state $|\bar{g}_2\rangle$ occurs:

$$\hbar\Delta_1 = \hbar\Delta_2 + \delta E(g_2). \tag{IV.17}$$

We thus obtain a remarkable situation where P_e vanishes for the "bare" Raman resonance $\Delta_1 = \Delta_2$, then passes through a maximum for the "dressed" Raman resonance (IV.17). The width of the resonance is given by the width of the state $\bar{g}_2$, i.e. $\gamma_2 = \Gamma s_2/2$ [IV.5]. We will come back to this Fano excitation profile when we study the reabsorption of scattered photons within a cloud of atoms.

1-5 Beyond the Λ system

The notion of dark state is not limited to a three-level system. Consider a resonance transition from a ground level g with angular momentum J_g to an excited level e with angular momentum J_e. For a dipole transition to be allowed, one must have $J_e = J_g \pm 1$ or $J_e = J_g$. We will assume here that a transition of this type is illuminated with monochromatic light. The atom-laser coupling can be written in the general form

$$\hat{V}_{\mathrm{AL}} = \frac{\hbar}{2} \sum_{m,m'} \kappa_{m,m'} \, |e, m'\rangle\langle g, m| + \mathrm{H.c.} \tag{IV.18}$$

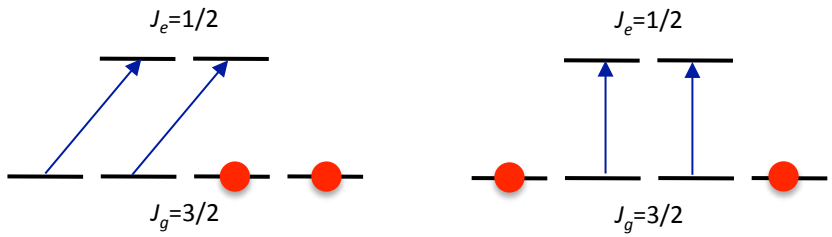

Figure IV.7. *Atom with resonance transition $J_g = 3/2 \leftrightarrow J_e = 1/2$ illuminated by circularly (left) and linearly (right) polarized light. Dark states are indicated by red disks.*

Figure IV.8. *Transition $J_g = 1/2 \leftrightarrow J_e = 1/2$: there is a dark state only if the polarization is strictly circular.*

where the Rabi frequencies $\kappa_{m,m'}$ are non-zero only if $m' = m, m \pm 1$ due to the selection rules for electric dipole interaction. These involve the different polarization components of the elerctromagnetic field ($\sigma_\pm$ and π) and the Clebsh-Gordan coefficients associated with the transitions $|g, m\rangle \leftrightarrow |e, m'\rangle$.

Let us start by noting that there are no dark states in the $J_e = J_g + 1$ case. Whatever the polarization of the laser wave chosen, there is always a non-zero stationary population for the excited level, unless of course the light intensity is strictly zero.

Let us now consider the case $J_e = J_g - 1$. In this case, the ground level has two more Zeeman sublevels than the excited level. Recall that the number of Zeeman sublevels is $2J_{g,e} + 1$. The matrix $\hat{V}_{\rm AL}$ which describes the atom-laser coupling therefore couples a space of dimension $2J_g + 1$ to a space of smaller dimension $2J_e + 1 = (2J_g + 1) - 2$. Its kernel is therefore necessarily of dimension greater than or equal to 2, i.e. there is necessarily a subspace of dimension at least 2 in the space associated with the g level, formed by uncoupled states such as

$$\hat{V}_{\rm AL}|g_\alpha\rangle = 0. \tag{IV.19}$$

These subspaces are shown in figure IV.7 for a transition $J_g = 3/2 \leftrightarrow J_e = 1/2$, in both cases of circular polarization and linear polarization parallel to the quantization axis (π polarization).

Finally, let us move on to the case of a $J_e = J_g$ resonance transition. This case is more subtle. The matrix $\hat{V}_{\rm AL}$ connects two spaces of the same dimension, so there is no obvious reason why we should expect the existence of a dark state. In fact, the existence of these states depends on the integer or half-integer value of J_g and J_e.

- In the half-integer case, there is generally no dark state. For example, for a transition $J_g = 1/2 \leftrightarrow J_e = 1/2$ and linear polarization, we obtain two systems with two independent levels and a non-zero excited population. Only if the light is circularly polarized do we find a dark state in this case (figure IV.8).
- In the case of integer J_g, J_e, there is always a dark state. This is due to the particular values of the Clebsh-Gordan coefficients. If the light is circularly polarized, the dark state is the same as that found for half-integer J_g: $|m_g = \pm J_g\rangle$. If the light is linearly polarized and parallel to the quantization axis, the dark state is $|g, m = 0\rangle$, due to the cancellation of the Clebsh–Gordan coefficient characterizing the $|g, m = 0\rangle \leftrightarrow |e, m = 0\rangle$ transition.

Note: the special case $J_g = 1 \leftrightarrow J_e = 1$. Ol'shanii & Minogin (1992) have obtained in this case a remarkably simple expression of the dark state for a light field of any polarization. Let us choose a quantization axis and characterize a ground state by the three-component complex vector $\vec{g}$:

$$|\psi_g\rangle = \sum_{m=-1}^{+1} \psi_{g,m}|g, m\rangle \quad \leftrightarrow \quad \vec{g} = \begin{pmatrix} \psi_{g,-1} \\ \psi_{g,0} \\ \psi_{g,+1} \end{pmatrix} \tag{IV.20}$$

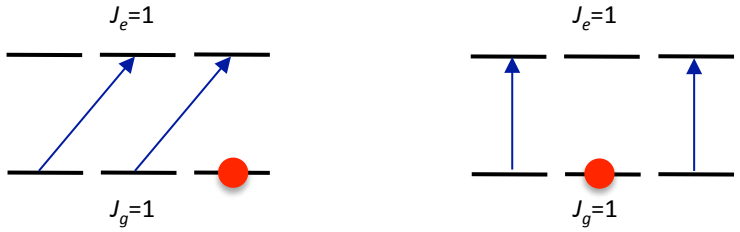

Figure IV.9. *Transition $J_g = 1 \leftrightarrow J_e = 1$: there is a dark state whatever the polarization, although the dimension of the Hilbert space for the excited level is as large as for the ground level.*

and ditto for any excited state, which will be characterized by a vector with three complex components $\vec{e}$. Let us also consider the (complex) polarization vector $\boldsymbol{\epsilon}$ of the laser electric field:

$$\boldsymbol{\mathcal{E}}(t) = \mathcal{E}_0\, \boldsymbol{\epsilon}\, \mathrm{e}^{-\mathrm{i}\omega_L t} + \text{c.c.}. \tag{IV.21}$$

With these notations, Ol'shanii & Minogin (1992) have shown that the absorption of a laser photon sends any ground state characterized by $\vec{g}$ to the excited state characterized by $\vec{e}$ such that

$$\vec{e} \propto \boldsymbol{\epsilon} \times \vec{g}. \tag{IV.22}$$

The expression for the uncoupled state can be deduced immediately: this is the ground state whose components $\psi_{g,m}$ are such that the three-component vector $\vec{g}$ is parallel to the polarization $\boldsymbol{\epsilon}$ of the light beam.

2 Dark state cooling

2-1 A simple picture

We have seen above that the Λ system offers the possibility of obtaining an internal state decoupled from the light:

$$|\psi_{\mathrm{NC}}\rangle \propto \kappa_2 |g_1\rangle - \kappa_1 |g_2\rangle. \tag{IV.23}$$

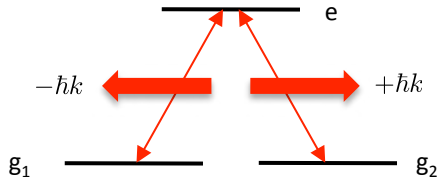

Figure IV.10. *1D configuration for velocity-selective coherent population trapping.*

This state $|\psi_{\mathrm{NC}}\rangle$ is an eigenstate of the Hamiltonian provided that the Raman resonance condition is satisfied.

$$\Delta \equiv \Delta_1 - \Delta_2 = 0. \tag{IV.24}$$

For this effect to be used to cool atoms, it must be made velocity-dependent. Let us work in one dimension of space (z); velocity dependence will be obtained if the two waves propagate in opposite directions, since the Raman detuning $\Delta_1 - \Delta_2$ is then a function of v, the velocity component along the z axis. Let us assume that the wave driving the $g_1 \leftrightarrow e$ transition propagates towards negative z, and that the wave driving the $g_2 \leftrightarrow e$ transition propagates towards positive z (figure IV.10):

$$\Delta_1(v) = \Delta_1(0) + kv, \quad \Delta_2(v) = \Delta_2(0) - kv. \tag{IV.25}$$

Suppose we choose a zero Raman detuning for an atom at rest, $\Delta_1(0) = \Delta_2(0)$, as shown in figure IV.5A. The Raman detuning Δ for an atom with velocity v along Oz will be

$$\Delta = 2kv. \tag{IV.26}$$

We can then propose a simple image for the cooling mechanism exploiting these dark states (figure IV.11). We start with a broad velocity distribution and illuminate the atoms with the two counter-propagating lasers 1 and 2, taking these two lasers to be resonant and with the same coupling $\kappa_1 = \kappa_2$. The variation of the excited-state population with velocity, which also gives the spontaneous emission rate, is shown in figure IV.12. This population shows a marked hole at $v = 0$ as expected: this is called velocity-selective coherent population trapping ("trapping" here refers to

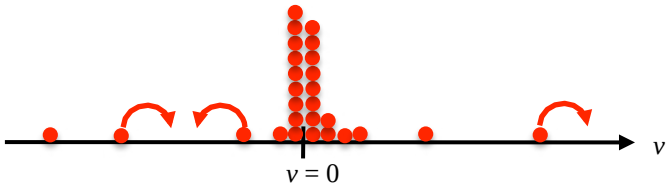

Figure IV.11. *Brownian motion in velocity space with accumulation around zero velocity due to velocity-selective coherent population trapping.*

accumulation in the uncoupled state). Atoms with initially non-zero velocity will absorb laser photons, emit spontaneous photons and thus perform a Brownian motion. When, by chance, they arrive in the vicinity of zero velocity, the probability per unit time that they will absorb a photon falls sharply if they are in the $|\psi_{\mathrm{NC}}(v)\rangle$ state: we therefore expect an accumulation of atoms around $v = 0$, as we saw with narrow-line Doppler cooling. However, there is an important difference between the two types of cooling: in coherent population trapping as described above, there is no friction force to bring the velocity back to around 0: the evolution of velocity here is a purely diffusive phenomenon.

We will see below that this simple reasoning, based on the semi-classical notion of an atom's velocity defined independently of its internal state, is valid, but still needs to be completed. It also raises a number of questions that need to be addressed to assess cooling performance:

- Since the expected cooling depends on the presence of an excitation hole in the vicinity of zero velocity, how does the size of this hole vary with the laser parameters?
- If we want to achieve sub-recoil cooling, we cannot just reason about the atom's velocity without saying whether it is the velocity before or after the last photon. How can we reason in quantum terms, taking into account these elementary changes in velocity?
- The process as we have described it is based on purely diffusive Brownian motion, which from time to time brings the atom's velocity back to the vicinity of $v = 0$. However, the probability of the Brownian motion returning to the origin depends strongly on the dimensionality of the problem. How efficient is this process in 2D or 3D?

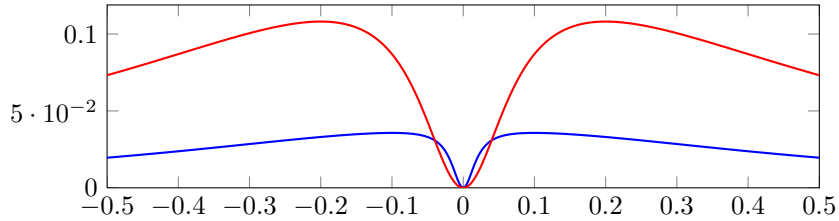

Figure IV.12. *Variation of excited state population P_e with atomic velocity, measured in units of Γ/k. Figure made for $\Delta_1 = \Delta_2 = 0$. Blue: $\kappa_1 = \kappa_2 = 0.2\,\Gamma$, Red: $\kappa_1 = \kappa_2 = 0.4\,\Gamma$.*

2-2 The width of the excitation hole

Let us take a look at the width of the hole in the excitation curve around zero velocity, which will determine the efficiency of the cooling process. We will discuss the influence of dissipation by successively reviewing the three internal states (figure IV.13)

$$|e\rangle, \quad |\psi_{\mathrm{C}}\rangle = \frac{1}{\sqrt{2}}\left(|g_1\rangle + |g_2\rangle\right), \qquad |\psi_{\mathrm{NC}}\rangle = \frac{1}{\sqrt{2}}\left(|g_1\rangle - |g_2\rangle\right). \tag{IV.27}$$

For simplicity's sake, we are interested in the case where both waves have the same Rabi frequency, and we posit $\kappa \equiv \kappa_1 = \kappa_2$, which we will assume to be very small compared to Γ. Our reasoning reproduces that developed by Aspect, Arimondo, et al. (1989).

The state $|e\rangle$ has the width Γ: the atom prepared in this state spontaneously emits a photon after a time $\sim \Gamma^{-1}$.

The state $|\psi_{\mathrm{C}}\rangle$ is resonantly coupled to the state $|e\rangle$ with the Rabi frequency $\sqrt{2}\,\kappa$. This coupling gives the state $|\psi_{\mathrm{C}}\rangle$ the width [*cf.* (IV.5)]:

$$\gamma_{\mathrm{C}} = \frac{2\kappa^2}{\Gamma}, \tag{IV.28}$$

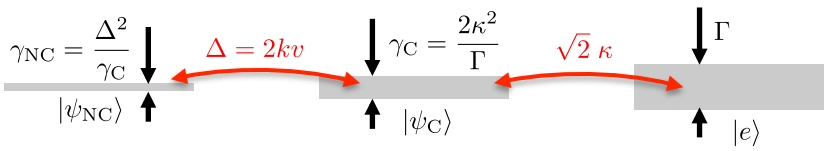

Figure IV.13. *The three coupled states of the problem and their width. The figure is made at resonance $\Delta_1 = \Delta_2 = 0$, with equal Rabi frequencies $\kappa_1 = \kappa_2 = \kappa$.*

which means that an atom initially placed in the state $|\psi_C\rangle$ will scatter a photon after a time of the order γ_C^{-1}.

The state $|\psi_{NC}\rangle$ is by construction uncoupled from the excited state. On the other hand, if the Raman detuning $\Delta = \Delta_1 - \Delta_2$ is non-zero, the states $|\psi_{NC}\rangle$ and $|\psi_C\rangle$ are coupled to each other. Indeed, for $\kappa = 0$, the initial state

$$|\psi(0)\rangle = |\psi_{NC}\rangle = \frac{1}{\sqrt{2}}\left(|g_1\rangle - |g_2\rangle\right) \tag{IV.29}$$

evolves as

$$|\psi(t)\rangle = \frac{1}{\sqrt{2}}\left(\mathrm{e}^{-\mathrm{i}\Delta t/2}|g_1\rangle - \mathrm{e}^{+\mathrm{i}\Delta t/2}|g_2\rangle\right) \tag{IV.30}$$

and thus becomes proportional to $|\psi_C\rangle$ at time $t = \pi/\Delta$. The coupling between $|\psi_{NC}\rangle$ and $|\psi_C\rangle$ is therefore directly given by Δ. A non-zero value of Δ (or a non-zero velocity in our case) will give to the state $|\psi_{NC}\rangle$ the width:

$$\gamma_{NC} = \frac{\Delta^2}{\gamma_C}, \tag{IV.31}$$

which can be rewritten using (IV.28) and $\Delta = 2kv$:

$$\gamma_{NC} = 2\Gamma\frac{(kv)^2}{\kappa^2}. \tag{IV.32}$$

This estimate of γ_{NC} corresponds to the width of the excitation hole in the vicinity of the Raman resonance. In particular, we note that:

- The variation in excitation rate is quadratic with respect to velocity.
- The smaller the Rabi frequency κ, the steeper the quadratic variation. This point is clearly visible in figure IV.12, where we have plotted P_e for two different values of κ.

2-3 Quantum version of the problem

In the foregoing, we have reasoned about the velocity v of the atom without specifying whether this is the velocity before or after the atom has absorbed a photon. This type of reasoning is legitimate when the change in Doppler effect due to the recoil of a single photon, $kv_r = 2\omega_r$, is small compared with all the other frequencies in the problem. On the other hand, it cannot be maintained if we are looking for subrecoil cooling. In this case, we need to be more precise to determine the state in which the atoms will accumulate.

To deal with the atom-radiation interaction in this case, we need to take into account the atom's recoil in the absorption-emission processes. Let us start with the case without spontaneous emission. We can then group the atomic states (internal+external) into families

$$\mathcal{F}(v) = \{\, |g_1, v + v_r\rangle,\ |e, v\rangle,\ |g_2, v - v_r\rangle \,\}. \tag{IV.33}$$

Atom-laser coupling leaves these families globally stable. The Raman resonance condition in a given family is then written:

$$E(g_1) + \hbar\omega_{L,1} + \frac{M(v + v_r)^2}{2} = E(g_2) + \hbar\omega_{L,2} + \frac{M(v - v_r)^2}{2}. \tag{IV.34}$$

As above, let us assume $\Delta_1 = \Delta_2$, i.e. $E(g_1) + \hbar\omega_{L,1} = E(g_2) + \hbar\omega_{L,2}$. The Raman resonance condition (IV.34) is obtained for $v = 0$; the only family exhibiting a truly dark state is therefore the family $\mathcal{F}(v = 0)$, and the corresponding dark state is written as

$$|\psi_{NC}(v = 0)\rangle = \frac{1}{\sqrt{2}}\left(|g_1, +v_r\rangle - |g_2, -v_r\rangle\right). \tag{IV.35}$$

A velocity analysis of this state should show two peaks at $\pm v_r$, on either side of zero velocity.

In the presence of spontaneous emission, the family occupied by the atom will change randomly due to the recoil associated with emission processes. Within each family, the longest-lived state is the uncoupled state $|\psi_{NC}(v)\rangle$ and the estimate made in (IV.32) for its lifetime remains valid.

This more precise treatment therefore confirms the image proposed above for subrecoil cooling, provided that we replace the somewhat vague

notion of atomic velocity by the notion of $\mathcal{F}(v)$ families. The atom's state is indeed a random walk, with the atom jumping from one family to another under the effect of spontaneous emission. When this random walk leads the atom into the uncoupled state $|\psi_{\rm NC}(v)\rangle$ of a family with v very close to 0, the residence time in this family becomes extremely long. We can therefore hope to accumulate a large number of atoms in the vicinity of $|\psi_{\rm NC}(v=0)\rangle$.

2-4 Experimental evidence at 1D

The first one-dimensional subrecoil cooling experiment was carried out by the ENS group using precisely this mechanism (Aspect, Arimondo, et al. 1988). The transition used was the $2^3S_1 \leftrightarrow 2^3P_1$ of helium in its metastable triplet state, illuminated by two polarized counter-propagating waves σ_+ and σ_-. After a few optical pumping processes, the atom reaches the Λ system (figure IV.14, top):

$$|g, m=-1\rangle \leftrightarrow |e, m=0\rangle \leftrightarrow |g, m=+1\rangle \qquad \text{(IV.36)}$$

because the $|e, m=0\rangle$ state has a zero probability of de-exciting to the third ground sublevel $|g, m=0\rangle$. The experiment confirmed the expected effect, and a two-peak velocity distribution was observed (figure IV.14, bottom). This is indeed a cooling effect (and not a simple filtering), as the number of atoms in these velocity classes is higher after interaction with light than before.

3 Scale laws for subrecoil cooling

In this section, we discuss some ideas for assessing the efficiency of subrecoil cooling, taking advantage of a zero in the atom's excitation rate, as shown in figure IV.12. The same reasoning applies to Raman cooling, which we will look at in §4. We want to determine the characteristic width of the narrow velocity peak generated by cooling, as well as the fraction of atoms likely to accumulate in this peak. This is a tricky problem, both because of the multitude of possible situations and because of the complexity

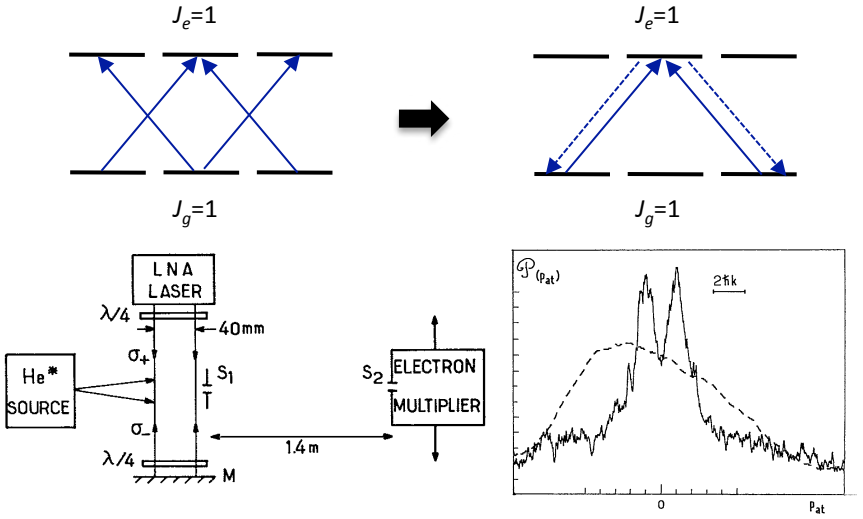

Figure IV.14. *Top: Transition $J_g = 1 \leftrightarrow J_e = 1$ composed of a Λ system and a V system and illuminated with σ_+ and σ_- light. After a few spontaneous emission processes, the atom is optically pumped into the Λ system, and cooling by coherent population trapping can begin. Bottom: figure taken from Aspect, Arimondo, et al. (1988), showing the principle of transverse sub-recoil cooling of a metastable helium atomic beam by coherent population trapping and the observed collimation. The double-peak structure of the final velocity distribution (solid line) is characteristic of the dark state (IV.35) (or its immediate neighbors). The dotted lines represent the initial velocity distribution.*

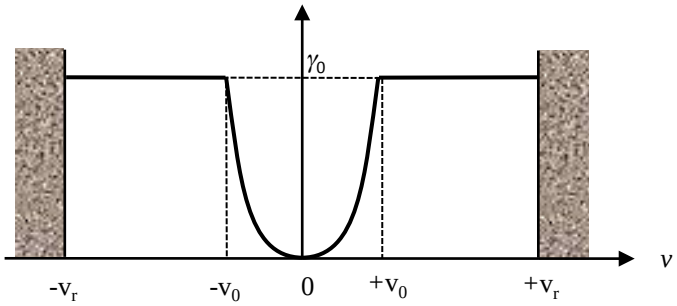

Figure IV.15. *Excitation rate modeling (here at 1D) according to (IV.38), with "walls" in velocity space, located here at* $|v| = v_r$.

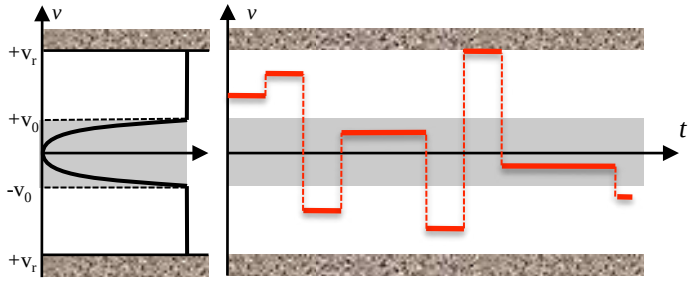

Figure IV.16. *Random walk in velocity space. When the particle arrives in the dark zone, the dwell time on a given velocity class is increased compared to the bright zone.*

of the mathematical and statistical tools to be used. We shall restrict ourselves here to describing a representative case, which will enable us to discuss the influence of two important parameters: (i) the dimensionality of the space and (ii) the variation of the excitation rate around its zero. We refer the reader interested in these notions to Bardou, Bouchaud, et al. (1994) as well as the comprehensive work by Bardou, Bouchaud, et al. (2002).

3-1 Excitation rate model

To simplify the discussion, we will model the problem as follows (figure IV.15): the atom's state is labelled by its velocity $\boldsymbol{v}$ (1D, 2D or 3D), which is used to calculate the excitation rate $\gamma(\boldsymbol{v})$. We describe this rate as follows:

$$\gamma(\boldsymbol{v}) = \gamma_0 \left(\frac{v}{v_0}\right)^{\alpha} \quad \text{if} \quad |\boldsymbol{v}| < v_0, \tag{IV.37}$$

$$= \gamma_0 \quad \text{if} \quad |\boldsymbol{v}| > v_0, \tag{IV.38}$$

the case of the dark state seen above corresponding to the exponent $\alpha = 2$ (cf. IV.32).

We will also assume that, in addition to the subrecoil cooling mechanism that creates the hole in the excitation rate near $v = 0$, there is another cooling mechanism, which we will not detail here, and which may be of the Doppler or Sisyphus type. This other mechanism keeps the atoms in a zone of finite size centered around $v = 0$. It was not present in our discussion in the previous paragraph, nor in the experiment shown in figure IV.14. Insofar as these were one-dimensional situations, this mechanism was not really necessary, as the Brownian motion of the velocity caused by the random recoils due to spontaneous emission was sufficient to bring the atom back to the vicinity of the hole at $v = 0$ from time to time. But in three dimensions, this pure Brownian motion cannot be relied upon, and the atom must be helped to approach $v = 0$ and find the dark zone in velocity space.

To model this other cooling mechanism as simply as possible, we will assume that the modulus of the atom's velocity cannot exceed the recoil velocity: $|\boldsymbol{v}| < v_r$. We therefore place "walls" in velocity space that confine the atom in the central zone. The exact position of these walls is not important, as it acts as a simple multiplicative factor in the calculation. We fix it here at v_r to simplify the analysis.

3-2 Residence time in the dark zone and Lévy's law

We consider the model described above assuming that $v_0 \ll v_r$ and we take the walls into account. As long as the particle is not in the dark zone $|\boldsymbol{v}| < v_0$, it jumps randomly from one velocity to another at a rate γ_0, each step of

this random walk being of the order of v_r (figure IV.16). At each jump, the particle has a chance to fall into the dark zone, which is uniformly sprayed. Once in the dark zone, it takes the particle a time τ of the order of $1/\gamma(v)$ to make another jump.

Let us take a one-dimensional view to evaluate the statistical law $\mathcal{P}(\tau)$ of the residence time τ, the quantity $P(\tau)\,\mathrm{d}\tau$ giving the probability that the particle falling into the dark zone will remain there for a time between τ and $\tau + \mathrm{d}\tau$. We will assume that during its stay in the dark zone, the particle occupies one and only one velocity v. Indeed, the probability of the particle leaving v for another velocity v' also located in the dark zone is low if the width of this zone is small compared with the average size of a jump v_r.

We will take the following expression for the probability density $\mathcal{P}(v)$ that a particle entering the dark zone reaches velocity v:

$$\mathcal{P}(v) = \frac{1}{2v_0}, \tag{IV.39}$$

which means that the dark zone is uniformly "sprayed". Let us assume that the residence time on the velocity class v is exactly equal[1] to $1/\gamma(v)$. Since the velocity classes v and $-v$ correspond to the same residence time, we then have

$$\mathcal{P}(\tau)\,\mathrm{d}\tau = [\mathcal{P}(v) + \mathcal{P}(-v)]\;\mathrm{d}v \qquad \text{with} \quad \tau = \frac{1}{\gamma_0}\left(\frac{v_0}{v}\right)^{\alpha} \tag{IV.40}$$

which leads to

$$\mathcal{P}(\tau) \propto \frac{1}{\tau^{1+\frac{1}{\alpha}}}. \tag{IV.41}$$

In particular, for the case of coherent population trapping, we have $\alpha = 2$ and therefore:

$$\text{Dark resonance in 1D}: \quad \mathcal{P}(\tau) \propto \frac{1}{\tau^{3/2}}. \tag{IV.42}$$

The distribution law (IV.42) is the source of some of the problem's mathematical complexity. It is a broad law which, while normalizable, has no well-defined moments of order 1, 2 or 3. This means, for example, that the central limit theorem does not apply: if we are interested in the total time spent by the atom in the dark zone after N passages:

$$T_N = \tau_1 + \tau_2 + \ldots + \tau_N, \tag{IV.43}$$

we do not find a Gaussian distribution (even though we sum N independent random variables), but a Lévy distribution. More precisely, the usual central limit theorem would indicate that T_N grows as $N\langle\tau\rangle$ plus a correction in $\sqrt{N}$. Here, on the contrary, the sum T_N is dominated by a few events (*cf.* figure IV.17) and we find that T_N grows like N^2 [see for example Bouchaud & Georges (1990)].

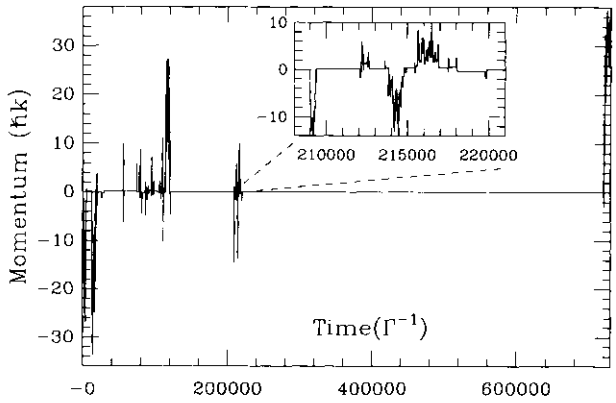

Figure IV.17. *Example of a trajectory in velocity space obtained by a Monte Carlo simulation of dark resonance cooling. We can clearly see that these trajectories are dominated by a few rare events during which the particle velocity reaches a value close to zero [Figure extracted from Bardou, Bouchaud, et al. (1994)].*

We can generalize the above reasoning to the multi-dimensional case. In three dimensions, assuming uniform "spraying" of the sphere $|\boldsymbol{p}| < p_0$, we find instead of (IV.39):

$$\mathcal{P}(v) = \frac{3v^2}{v_0^3} \tag{IV.44}$$

which leads to

$$\mathcal{P}(\tau) \propto \frac{1}{\tau^{1+\frac{3}{\alpha}}}. \tag{IV.45}$$

[1] It would be more correct to write that the residence time τ is itself a random variable with an exponential distribution whose mean is given by $1/\gamma(v)$; however, this does not change the scaling law given in (IV.41) [see Bardou, Bouchaud, et al. (2002), § 3.3.1.2].

More generally, in D dimension, we have

$$\mathcal{P}(\tau) \propto \frac{1}{\tau^{1+\frac{D}{\alpha}}}. \tag{IV.46}$$

3-3 Width of the velocity distribution

The cooling process we are considering here has no stationary state, unlike Doppler or Sisyphus cooling. Let us give ourselves an interaction time t long enough for many jumps to have occurred, at least for the particles that avoided the dark zone:

$$t \gg 1/\gamma_0. \tag{IV.47}$$

Particles that have fallen sufficiently close to $v = 0$ in the course of their evolution have then remained in this zone. More precisely, for a given time t, we can define the velocity $v_t \ll v_0$ such that

$$t = \frac{1}{\gamma(v_t)} \qquad \longleftrightarrow \qquad v_t = \frac{v_0}{(\gamma_0 t)^{1/\alpha}} \tag{IV.48}$$

which defines the radius of a second sphere (in 3D) inside the dark zone sphere of radius v_0 (figure IV.18). In what follows, we will call this second sphere the "black zone"; indeed, particles that arrived inside this zone between 0 and t are still there (with a good probability) at time t. Assuming uniform spraying of the dark zone, we expect the density in this zone to be uniform too.

We therefore expect the velocity distribution $\mathcal{P}(v)$ to have three components, which we schematize in figure IV.18:

- The black zone $v < v_t$: velocity classes in this zone have a population that increases with time, since they are continuously fed, without particles escaping. Note, however, that the size of this zone decreases with time, as $1/\sqrt{t}$ in the case $\alpha = 2$ of dark resonances. The probability density is uniform in this zone.

- The bright zone $v > v_0$ in which particles make frequent jumps in velocity. The probability density is also roughly uniform in this zone.

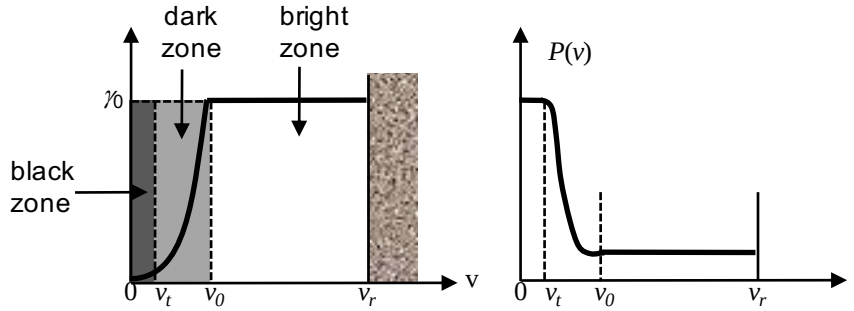

Figure IV.18. *Left: excitation rate and "black zone": for a given interaction time t, we can define a black zone, such that an atom falling into this zone then remained there until time t: $\gamma(v_t)t = 1$. Right: Qualitative diagram of the expected velocity profile; the density inside the black zone increases with time, but the radius v_t of this zone decreases.*

- The intermediate zone $v_t < v < v_0$, located inside the dark zone, but composed of velocity classes with a relatively high rate $\gamma(v)$, such that particles have had time to move in and out of these velocity classes during the time interval t.

This qualitative prediction can be confirmed by a more precise analytical or numerical treatment of the various stochastic processes [Bardou, Bouchaud, et al. (2002), chapter 6].

3-4 Fraction of cooled atoms

The final step in our analysis is to estimate, for a given interaction time t, the fraction of atoms that have reached the dark zone $|\boldsymbol{v}| < v_t$ (figure IV.18). As the size of this zone decreases with time, it is not obvious how large this fraction is. Here again, we will use a qualitative reasoning, which can be confirmed by a much more elaborate quantitative analysis [see Bardou, Bouchaud, et al. (2002), in particular § 6.3 for the 1D case and § 6.4 for the 3D case].

We will assume that over the time interval of duration t, an atom per-

forms the number of attempts $N_{\text{att.}} = \gamma_0 t$ to enter the black zone[2]. At each attempt, the atom evolving in dimension D has a probability

$$p \sim \left(\frac{v_t}{v_\text{r}}\right)^D \tag{IV.49}$$

to arrive in the black zone of radius v_t. The total probability of an atom arriving in the black zone during time t is therefore

$$p_\text{tot} = p\, N_{\text{att.}} \propto\ t\ (v_t)^D \propto\ t^{1-\frac{D}{\alpha}}. \tag{IV.50}$$

In this simple model, the determining parameter is $1 - D/\alpha$:

- If $D/\alpha < 1$, then the probability p_tot given in (IV.50) increases indefinitely with time[3]. This means that a significant fraction of atoms will accumulate in the central peak. This is the case at 1D for dark resonances ($D/\alpha = 1/2$).
- If $D/\alpha > 1$, then the probability of an atom ending up in the central peak tends towards 0 as t increases. The peak around zero velocity may be detectable in an experiment of finite duration, but it will contain only a small fraction of the atoms. This is the case with three-dimensional dark resonances ($D/\alpha = 3/2$).
- The case $D = \alpha$, corresponding to two-dimensional dark resonances, is marginal. Determining the precise value of the fraction of atoms in the dark zone requires a more precise treatment than the simple scaling laws presented here.

3-5 2D and 3D experiments

Experiments carried out at 1D on the metastable helium atom (§ 2-4) were generalized a few years later to 2D and 3D by the ENS group (Lawall, Bardou, et al. 1994; Lawall, Kulin, et al. 1994). The starting point for these

[2]There is an important shortcut here, as some atoms may have spent time in the grey zone $v_t < |\boldsymbol{v}| < v_0$, slowing the rate of their random walk without actually placing them in the desired black zone

[3]Our simple model of summing probabilities as in (IV.50) of course ceases to be valid when the probability p_tot is no longer small in front of 1.

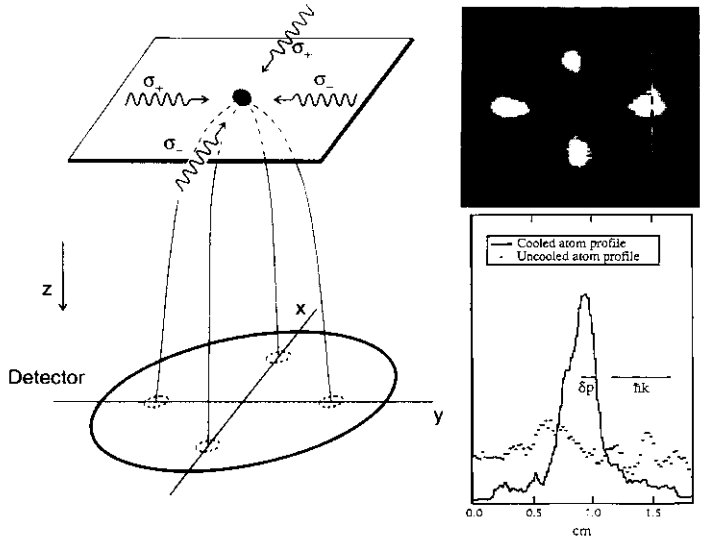

Figure IV.19. *Left: schematic diagram of a two-dimensional dark-state cooling experiment. The dark-state momentum distribution is composed of four peaks, corresponding to the four plane waves illuminating the atoms. This momentum distribution is measured by time-of-flight. Right: example of a momentum distribution. Each peak has a width significantly less than the recoil velocity v_r ($v_\text{r}/4$ for the one shown in the figure). The dotted curve represents the uncooled distribution.*

experiments was a cloud of metastable helium atoms cooled and confined in a magneto-optical trap, operating on the $2^3S_1 \leftrightarrow 2^3P_2$ transition. At a given instant, the magneto-optical trap beams are switched off and the four (2D) or six (3D) beams creating both Sisyphus cooling and coherent population trapping are switched on. The role of Sisyphus cooling is to create the equivalent of "walls" in velocity space, whose presence is essential in 2D or 3D as we saw above. The width of the velocity distribution obtained by Sisyphus cooling, before dark-state cooling becomes significant, is of the order of $1.5\, v_\text{r}$ (Lawall, Kulin, et al. 1994).

Measurement of the velocity distribution of atoms after cooling by coherent population trapping reveals four (at 2D) or six (at 3D) peaks, cor-

responding to the accumulation of atoms in the desired dark state (figure IV.19). The fact that the number of peaks is equal to the number of light beams is a direct consequence of the result of Ol'shanii & Minogin (1992) presented in (IV.20)-(IV.22): when the motion of the atom's center of mass is taken into account, the dark state is a three-component spinor, $\vec{\boldsymbol{g}}(\boldsymbol{r})$, which is proportional to the electric field $\boldsymbol{\mathcal{E}}(\boldsymbol{r})$ of the laser wave (more precisely to the coefficient of $\mathrm{e}^{-\mathrm{i}\omega_{\mathrm{L}}t}$ in the expression of this field). The minimum widths observed for these peaks are of the order of $v_{\mathrm{r}}/4$ at 2D and $v_{\mathrm{r}}/6$ at 3D.

4 A tailor-made shadow: a Raman transition

We have just seen how the use of a dark resonance allows us to obtain a velocity-selective excitation profile, with strict cancellation for a given velocity class. We now explore a second method for obtaining a similar result: this method, also based on a Λ system, consists in using light pulses that transfer atoms between the sublevels $|g_1\rangle$ and $|g_2\rangle$ (figure IV.20). The time profile of the pulse is optimized so that the transfer is also velocity-selective, opening up a second route to cooling well below the recoil velocity v_{r}.

4-1 The principle of Raman cooling

Raman cooling operates by alternating two types of phase:

- At the start of the first phase, the atoms are in the state $|g_1\rangle$, with a velocity distribution that we want to make as narrow as possible (figure IV.21, top). They are illuminated for a time τ with a pair of Raman beams of Rabi frequency κ_j and detuning Δ_j ($j = 1, 2$). The aim is to induce the transition from $|g_1\rangle$ to $|g_2\rangle$ in a velocity-selective manner. If the detunings Δ_j are large compared with the Rabi frequencies κ_j, we can perturbatively eliminate the excited state e and define a Rabi frequency for the Raman transition:

$$\kappa = \frac{\kappa_1 \kappa_2^*}{2\Delta_e}. \tag{IV.51}$$

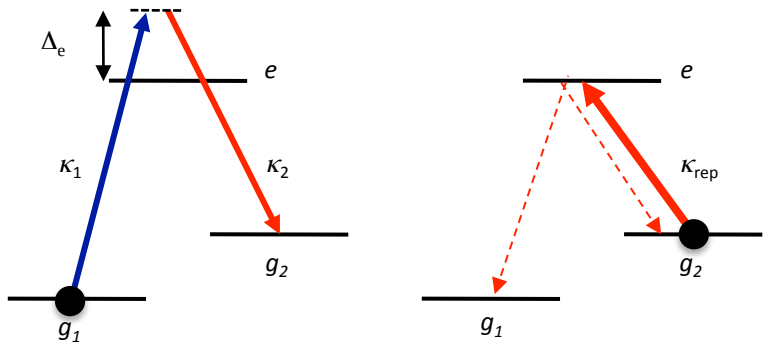

Figure IV.20. *Principle of Raman cooling. Left, first phase: a light pulse transfers atoms of a given velocity class from the state $|g_1\rangle$ to the state $|g_2\rangle$. Right, second phase: a pumping beam send the atoms back to $|g_1\rangle$. The momentum balance over the cycle narrows the width of the velocity distribution.*

The corresponding momentum transfer, $\boldsymbol{q} = \hbar(\boldsymbol{k}_1 - \boldsymbol{k}_2)$, can be adjusted by modifying the angle between the wave vectors $\boldsymbol{k}_1$ and $\boldsymbol{k}_2$. The Raman detuning $\Delta = \Delta_1 - \Delta_2$ and the time variation of the coupling $\kappa(t)$ induced by this pair of beams are chosen so as to excite atoms whose velocity lies within a class determined by energy conservation[4] (to within $\hbar/\tau$):

$$E(g_1) + \hbar\omega_{\mathrm{L},1} + \frac{1}{2}M\boldsymbol{v}^2 \approx E(g_2) + \hbar\omega_{\mathrm{L},2} + \frac{1}{2}M(\boldsymbol{v} + \boldsymbol{q}/M)^2, \tag{IV.52}$$

which simplifies to give

$$\boldsymbol{v}\cdot\boldsymbol{q} = \hbar\Delta - \frac{q^2}{2M}. \tag{IV.53}$$

The momentum transfer $\boldsymbol{q}$ is chosen such that it brings the atom's velocity down to zero ($\boldsymbol{v}\cdot\boldsymbol{q} < 0$): in a one-dimensional model, if the targeted velocity class is negative, atoms in this class will with high probability make a transition that changes their velocity from v to $v + 2v_{\mathrm{r}}$,

[4] Strictly speaking, the energy $E(g_i)$ of the state g_i must include the light shift $\delta E(g_i)$ of this state due to laser i (Moler, Weiss, et al. 1992). However, the contributions of $\delta E(g_1)$ and $\delta E(g_2)$ to (IV.52) offset each other if we take $\kappa_1 = \kappa_2$ and $\Delta_1 \approx \Delta_2$.

accompanied by the transition $|g_1\rangle \to |g_2\rangle$, whereas atoms outside this class will be unaffected and remain in $|g_1\rangle$ (figure IV.21, middle).

- The second phase consists of repumping all atoms from $|g_2\rangle$ to $|g_1\rangle$. A repumping beam resonantly couples the state $|g_2\rangle$ to the excited state $|e\rangle$ (figure IV.20). Once in the state $|e\rangle$, the atom can fall back to $|g_1\rangle$ or $|g_2\rangle$. If it falls on $|g_1\rangle$, the desired pumping is obtained and the process stops. If it falls on $|g_2\rangle$, it can reabsorb a photon from the pumping beam, and so on. The momentum transferred during an optical pumping process is $\hbar(\boldsymbol{k}_{\text{rep.}} - \boldsymbol{k}_{\text{fluo.}})$, where $\boldsymbol{k}_{\text{fluo.}}$ is the wave vector of the spontaneously emitted photon (figure IV.21, bottom).

We repeat this sequence, varying the class of atoms involved in the Raman pulse (figure IV.22): we can address atoms with positive or negative velocity along different spatial axes, closer or further from zero velocity. Ultimately, we hope to accumulate a large number of atoms around $v = 0$.

4-2 Velocity selectivity

To determine precisely the velocity class affected by a given Raman pulse, let us consider a one-dimensional model with $\boldsymbol{k}_1 = -k\boldsymbol{u}_z$, $\boldsymbol{k}_2 = +k\boldsymbol{u}_z$ as shown in figure IV.10. Let us take an atom with initial velocity v and write its internal state as

$$|\psi(t)\rangle = \alpha_1(t)|g_1\rangle + \alpha_2(t)|g_2\rangle, \quad \alpha_1(0) = 1, \alpha_2(0) = 0. \tag{IV.54}$$

As indicated above, we are neglecting the population of the state $|e\rangle$, which is legitimate if the Rabi frequencies κ_j are small compared with the detunings Δ_j. The time evolution of the coefficients α_j is given by the Schrödinger equation

$$\mathrm{i}\dot{\alpha}_1 = \frac{\Delta_v}{2}\alpha_1 + \frac{\kappa^*(t)}{2}\alpha_2, \qquad \mathrm{i}\dot{\alpha}_2 = \frac{\kappa(t)}{2}\alpha_1 - \frac{\Delta_v}{2}\alpha_2, \tag{IV.55}$$

where the velocity-dependent detuning Δ_v is given by:

$$\Delta_v = \Delta + 2k(v - v_{\text{r}}). \tag{IV.56}$$

The general solution to this equation requires a numerical treatment, but an analytical solution can be obtained if we restrict ourselves to the case of

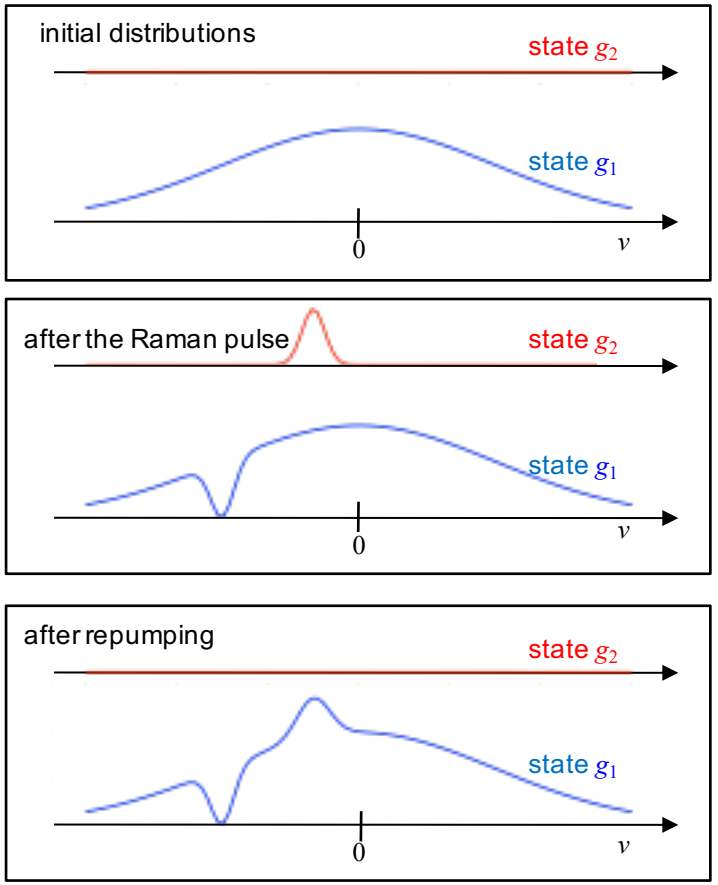

Figure IV.21. *Evolution of the velocity distribution during the two phases of Raman cooling: selective velocity transfer from g_1 to g_2, then repumping from g_2 to g_1.*

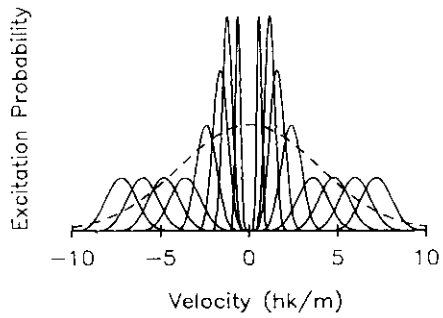

Figure IV.22. *Excitation rates for the different Raman pulses used by Kasevich & Chu (1992). The zero-velocity class remains "protected".*

a weak excitation $|\alpha_1| \sim 1$, $|\alpha_2| \ll 1$ for any velocity:

$$\alpha_1(t) \approx \mathrm{e}^{-\mathrm{i}\Delta_v t/2}, \qquad \alpha_2(t) \approx -\frac{\mathrm{i}}{2}\mathrm{e}^{\mathrm{i}\Delta_v t/2}\int_0^t \kappa(t')\,\mathrm{e}^{-\mathrm{i}\Delta_v t'}\,\mathrm{d}t'. \qquad \text{(IV.57)}$$

Let us take a pulse of duration τ. At the end of this pulse, the excitation probability of an atom of velocity v is:

$$P(v) = |\alpha_2(v)|^2 \approx \frac{1}{4}\left|\int_0^\tau \kappa(t)\,\mathrm{e}^{-\mathrm{i}\Delta_v t}\,\mathrm{d}t\right|^2. \qquad \text{(IV.58)}$$

The variation of this probability with velocity is therefore directly linked to the Fourier transform of the pulse Rabi frequency.

4-3 Which form to choose for the pulse?

The simplest form for the intensity of the Raman pulse is a square function (figure IV.23)

$$\kappa(t) = \kappa \quad \text{if} \quad 0 < t < \tau, \qquad \text{(IV.59)}$$

whose Fourier transform is a cardinal sine, so that

$$P(v) \propto \frac{\sin^2[(\bar{\Delta} + 2kv)\tau/2]}{(\bar{\Delta} + 2kv)^2} \qquad \text{(IV.60)}$$

where $\bar{\Delta} = \Delta - 2kv_\mathrm{r}$ [*cf.* (IV.56)]. We will therefore essentially excite atoms with velocities in the range

$$-\frac{\bar{\Delta}}{2} - \frac{\pi}{\tau} < kv < -\frac{\bar{\Delta}}{2} + \frac{\pi}{\tau}, \qquad \text{(IV.61)}$$

as well as, but to a lesser extent, atoms whose velocity is located in the lateral lobes of the cardinal sine.

We will see later how to take advantage of the well-marked zeros of the cardinal sine. However, as there is a risk that the parasitic excitation created by the side lobes may generate undesirable effects, it is worth exploring the possibility of using other functions $\kappa(t)$, with a Fourier transform that decreases faster on either side of its maximum. This was done in the first series of Raman cooling experiments, carried out at Stanford between 1992 and 1994 (Kasevich & Chu 1992; Davidson, Lee, et al. 1994). The temporal shape of the Raman pulses was a Blackman profile, i.e. the apodization function given by:

$$f(t) = 0.42 + 0.5\cos(2\pi t/\tau) + 0.08\cos(4\pi t/\tau) \quad \text{for} \quad |t| < \tau/2, \qquad \text{(IV.62)}$$

which has the merit of having a Fourier transform with low-amplitude wings (*cf.* figure IV.23): one can thus efficiently excite a velocity class of adjustable center $\bar{v}$ and width at half-maximum Δv, which guarantees an extremely reduced probability (by at least six orders of magnitude) of excitation for any velocity class more than $4\,\Delta v$ away from $\bar{v}$.

This technique led to velocity distributions[5] much narrower than the recoil velocity in one dimension, with $\Delta v \approx 0.2\,v_\mathrm{r}$ (Kasevich & Chu 1992). In two and three dimensions, performance was more modest, with $\Delta v \approx 1.2\,v_\mathrm{r}$ and $\Delta v \approx 2.3\,v_\mathrm{r}$, respectively. Among the reasons given for this drop in performance, we find the point we studied in § 3: filling the velocity class around $v = 0$ is all the slower the higher the dimensionality; a defect that tends to depopulate this velocity class (during the repumping process, for example) will therefore have a more sensitive effect at 2 or 3 D than at 1D. Furthermore, implementing the protocol described above requires, in principle, alternating pairs of Raman beams in all the spatial directions concerned, which is technically complicated to implement. Davidson, Lee,

[5]The widths given in the following are widths at $1/\sqrt{\mathrm{e}}$, which coincide with the r.m.s. width for a Gaussian distribution.

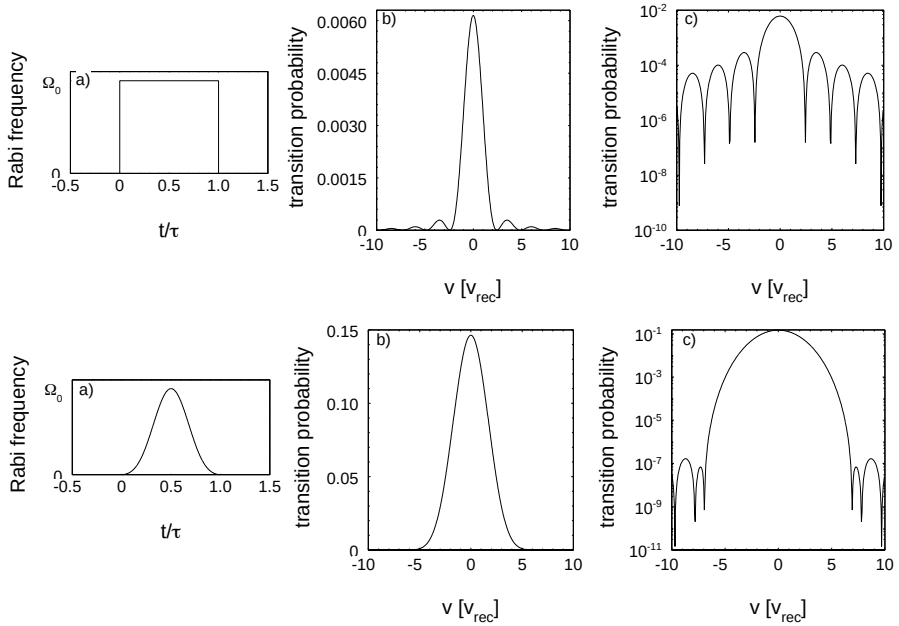

Figure IV.23. *Two possible envelope shapes for Raman pulses, with associated transition probability (IV.58), in linear and logarithmic scale. Top: square pulse with a cardinal sine Fourier transform. Bottom: Blackman pulse, with a Fourier spectrum much tighter than the cardinal sine. Both types of pulses have the same duration $\tau = 1.3\ M/\hbar k^2$. Figures from Jakob Reichel's doctoral thesis, Université Paris 6 (1996).*

et al. (1994) have therefore simplified this procedure by applying several Raman beams simultaneously. This can give rise to spurious non-linear phenomena, which also contribute to increasing the departure rate from the zero-velocity class.

Another way of achieving three-dimensional cooling is to work with trapped atoms. In this case, one can simply cool one direction of space and take advantage of the redistribution of energy with the other two directions due to the ergodicity of the atoms' motion in the trap. Still using Blackman pulses, the Stanford group achieved 3D cooling leading to a velocity width of $0.65\, v_{\rm r}$ (Lee, Adams, et al. 1996; Lee & Chu 1998). A similar experiment was carried out at ENS by Perrin, Kuhn, et al. (1999), using pulses with a frequency sweep. In all these studies, the final phase-space density was of the order of a few 10^{-3}, so still quite far from the Bose-Einstein condensation threshold. However, it should be noted that these experiments were carried out on atoms prepared in levels that we now know are not favorable if we are looking for high spatial densities: sodium in its ground level $F = 2$ or cesium in its ground level $F = 4$. In addition, it seems that heating related to multiple scattering of the photon emitted during the optical pumping process was present in these experiments. This heating could be reduced by using highly anisotropic geometries, favoring rapid photon exit.

Finally, let us return to square pulses and the corresponding excitation law given by a cardinal sine. Since the ultimate goal is to accumulate atoms in the vicinity of $v = 0$, the shape of this cardinal sine, with its marked lobes, is not problematic, provided one takes care to always choose the pair $(\bar{\Delta}, \tau)$ such that the zero-velocity class coincides with the first zero of $P(v)$:

$$|\bar{\Delta}|\tau = 2\pi. \tag{IV.63}$$

This technique has been successfully implemented in both one and two dimensions. In one dimension, the LKB group at ENS (Reichel, Bardou, et al. 1995) obtained a velocity distribution with a width of $0.12\,(1)\, v_{\rm r}$, notably narrower than that measured with Blackman pulses at Stanford ($0.2\,(1) v_{\rm r}$), and which is still a record. Thanks to these very narrow distributions, the ENS group was then able to observe Bloch oscillations in an optical lattice, a phenomenon we described in the 2012-13 lecture series (Ben Dahan, Peik, et al. 1996). In two dimensions, the NIST group produced a distribution of

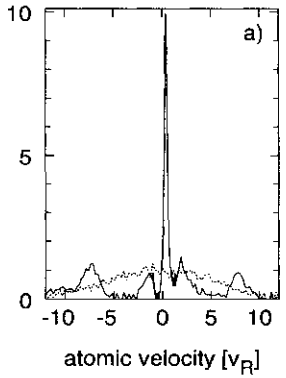

Figure IV.24. *Experimental result by Reichel, Bardou, et al. (1995), showing 1D Raman cooling of cesium atoms with square pulses, such that an atom of zero velocity has probability 0 of being excited by the Raman transition. The equivalent temperature is ∼3 nanokelvin.*

width $0.39\,(5)\,v_\mathrm{r}$ (Boyer, Lising, et al. 2004), which is narrower than the best performances obtained in 2D or 3D with narrow-line Doppler cooling. To our knowledge, this Raman cooling experiment with square Raman pulses has not yet been carried out in three dimensions.

Chapter V

Sisyphus cooling

The first optical molasses was made in 1985 at Bell Labs with sodium atoms (Chu, Hollberg, et al. 1985). Precise temperature measurements were performed at NIST (the National Bureau of Standards –NBS– at the time) on molasses of the same atomic species by Lett, Watts, et al. (1988b) and Lett, Phillips, et al. (1989) (figure V.1). The conclusion of these measurements was clear: Doppler cooling alone could not explain the observed cooling; temperatures were lower than the predicted limit $k_{\rm B}T = \hbar\Gamma/2$, and the variation in temperature with laser detuning was not at all in line with theory. Several cooling models were then developed (Ungar, Weiss, et al. 1989; Dalibard & Cohen-Tannoudji 1989), with in common the idea of taking into account more faithfully the structure of the atomic transition, going beyond the two-level model.

The key point is that for an atom with several ground sublevels, long time constants may appear, linked to the optical pumping time between sublevels. These long time constants can be associated with low energies. In contrast, in the two-level model underlying Doppler cooling, the only relevant time constant is Γ^{-1}, and the associated energy $\hbar\Gamma$ gives the limit of Doppler cooling. Of all the 1D models developed at the time, the most robust is probably the Sisyphus effect, which generalizes almost unchanged to three dimensions [for a review, see e.g. Grynberg & Robilliard (2001)]. It is therefore the one we will discuss now in its initial version, before moving on to recent developments that generalize this type of cooling to other atomic transitions.

1 The standard Sisyphus model

1-1 The $1/2 \leftrightarrow 3/2$ transition

The simplest model for Sisyphus cooling is that of a transition between a ground state $J_g = 1/2$ and an excited state $J_e = 3/2$ (figure V.2). The reason for the choice of this transition is simple: we have seen that the simplest atomic transition $J_g = 0 \longrightarrow J_e = 1$ only gives rise to Doppler cooling, with a temperature bounded by the Doppler limit (for a broad line) $k_{\rm B}T \geq \hbar\Gamma/2$. The appearance of this lower limit can be linked - although it is not absolute proof - to the fact that the only time constant then appearing in the atom's internal dynamics is the lifetime of the excited state Γ^{-1}. By moving on to a more complicated atomic structure, particularly for the ground state, the hope is to see the emergence of new, much longer time constants. These time constants correspond, for example, to the optical pumping time from one ground Zeeman $|g, \pm 1/2\rangle$ state to the other.

To create a non-trivial dynamic between these two ground states, which from now on we will call $|g_\pm\rangle$, it is necessary to place the atom in a situation where the polarization of light varies in space. Let us limit ourselves here to a one-dimensional example, with motion along the z axis. The prototype of such a situation corresponds to the superposition of two running light waves propagating in opposite directions along the z axis, with orthogonal linear polarizations $\boldsymbol{\epsilon}_x$ and $\boldsymbol{\epsilon}_y$ (lin$\perp$lin configuration, figure V.2).

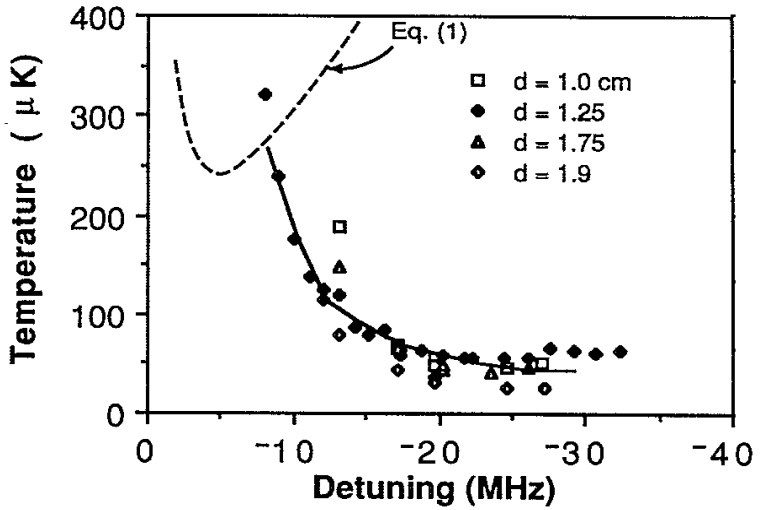

Figure V.1. *First precise temperature measurements in optical molasses (sodium atoms). The dashed curve represents the prediction for Doppler cooling. Figure taken from Lett, Watts, et al. (1988b).*

The two waves are chosen with the same frequency, the same intensity, and a relative phase such that the resulting polarization $\boldsymbol{\epsilon}(z)$ varies in space as follows:

$$\boldsymbol{\epsilon}(z) = \frac{1}{\sqrt{2}}\left(\boldsymbol{\epsilon}_x \mathrm{e}^{-\mathrm{i}kz} - \mathrm{i}\boldsymbol{\epsilon}_y \mathrm{e}^{-\mathrm{i}kz}\right) = \frac{1}{\sqrt{2}}\left(\boldsymbol{\epsilon}_- \cos(kz) - i\boldsymbol{\epsilon}_+ \sin(kz)\right), \quad \text{(V.1)}$$

where the complex unit vectors $\boldsymbol{\epsilon}_\pm = (\mp\boldsymbol{\epsilon}_x - \mathrm{i}\boldsymbol{\epsilon}_y)/\sqrt{2}$ represent the right and left circular polarization basis.

The polarization of light therefore evolves continuously and periodically along the z axis. It is (left-handed) circular ($\boldsymbol{\epsilon}_-$) at points $z = 0$ modulo $\lambda/2$, (right-handed) circular ($\boldsymbol{\epsilon}_+$) at points $z = \lambda/4$ modulo $\lambda/2$, and elliptical between these points. In particular, it is linear at $z = \lambda/8$ modulo $\lambda/4$, along the bisectors of $\boldsymbol{\epsilon}_x$ and $\boldsymbol{\epsilon}_y$.

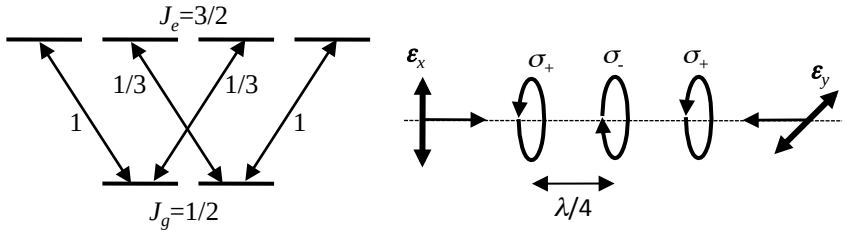

Figure V.2. *Atomic transition $J_g = 1/2 \leftrightarrow J_e = 3/2$ and 1D laser configuration lin⊥lin giving rise to the Sisyphus effect.*

1-2 Light shifts and optical pumping

Assuming that the detuning Δ between the laser beam frequency and the atomic frequency is large compared to the Rabi frequency κ characterizing the atom-light coupling, we know that the atom will be predominantly in one of the two states $g_\pm$, and we can neglect the time spent in the excited level. The effect of light on the atom is therefore twofold:

- Light creates a potential that shifts the energies of $g_\pm$ by an amount that depends on the proportion of $\sigma_\pm$ light at a given point. The result is a differential modulation $V_\pm(z)$ of the energies of $g_\pm$.
- Light induces $g_+ \leftrightarrow g_-$ transitions by spontaneous Raman processes, i.e. absorption of a photon from one of the two laser waves and spontaneous emission of a fluorescence photon. The rate of transition $\gamma_{+\to-}(z)$ from g_+ to g_- involves the local intensity of σ_- light at the point where the atom is located, and is therefore spatially modulated. The same applies to the transition rate $\gamma_{-\to+}(z)$ from g_- to g_+.

Sisyphus cooling will result from the correlation between the potentials $V_\pm(z)$ and the optical pumping rates $\gamma_{+\to-}(z)$ and $\gamma_{-\to+}(z)$. For a more quantitative description, let us start by calculating the light shifts $V_\pm(z)$. To do this, we use the intensity factors (squares of the Clebsch–Gordan coefficients) shown in figure V.2. At a given point z in space, the level g_+ is displaced by a quantity proportional to $I_+(z) + \frac{1}{3}I_-(z)$, where $I_\pm(z)$ are the intensities associated with the polarizations $\sigma_\pm$ at point z. Similarly, the

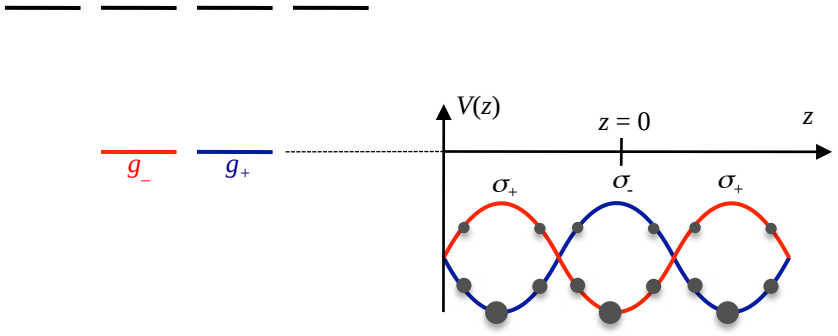

Figure V.3. *Potentials $V_\pm(z)$ created by light on the two ground states $g_\pm$. The dark disks indicate the stationary populations for an atom at rest resulting from optical pumping processes.*

level g_- is displaced by a quantity proportional to $I_-(z) + \frac{1}{3}I_+(z)$. With an additive constant of no importance here, the potentials experienced by $g_\pm$ can be written as follows (figure V.3)

$$V_+(z) = V_0 \cos^2(kz), \qquad V_-(z) = V_0 \sin^2(kz), \tag{V.2}$$

where the energy V_0 is given by $V_0 = \frac{2}{3}\hbar(-\Delta)s_0$. We note here s_0 the saturation parameter for each of the two running waves:

$$s_0 = \frac{\kappa^2/2}{\Delta^2 + \Gamma^2/4} \tag{V.3}$$

where κ is the Rabi frequency associated with each traveling wave, calculated for a Clebsch–Gordan coefficient equal to 1. The quantity V_0 is positive for negative detuning, which is the sign considered here (as for Doppler cooling).

We can similarly calculate the rate $\gamma_{\pm\to\mp}(z)$ at which the atom initially in $g_\pm$ will jump to $g_\mp$. We find

$$\gamma_{+\to-}(z) = \gamma_0 \cos^2(kz), \qquad \gamma_{-\to+}(z) = \gamma_0 \sin^2(kz), \tag{V.4}$$

with $\gamma_0 = \frac{2}{9}\Gamma s_0$. The predicted correlation between light shifts and optical pumping rates is therefore clear.

The equation giving the time evolution of the population P_+ at a given point z is

$$\frac{\mathrm{d}P_+}{\mathrm{d}t} = -\gamma_{+\to-}(z)P_+ \; + \; \gamma_{-\to+}(z)P_-, \tag{V.5}$$

and ditto for P_-. Using $P_+ + P_- = 1$, this evolution equation can also be written as

$$\frac{\mathrm{d}P_+}{\mathrm{d}t} = -\gamma_0 \left[P_+ - P_+^{\mathrm{stat}}(z)\right], \tag{V.6}$$

where the stationary populations $P_\pm^{\mathrm{stat}}(z)$ for an atom at rest in z are given by (figure V.3):

$$P_+^{\mathrm{stat}}(z) = \sin^2(kz), \qquad P_-^{\mathrm{stat}}(z) = \cos^2(kz). \tag{V.7}$$

This result indicates that the most populated level is always the lower of the two states g_+ and g_-. At $z = 0$, for example, light is polarized along $\boldsymbol{\epsilon}_-$ and the atom is optically pumped into the g_- state for which $V_-(z) = 0$, whereas $V_+(z) = V_0 > 0$.

1-3 The Sisyphus mechanism

For an atom at rest, we have just seen that optical pumping tends to move the atom from the top of potential hills to the bottom of valleys. It is this key point that gives the Sisyphus effect its name (figure V.4). It is easy to understand why this effect gives rise to cooling: if the atom moves with a low but non-zero velocity v, it will tend to climb more hills than it descends. Energy conservation is ensured by spontaneous emission: when an atom climbs a hill of potential $V_\pm(z)$, it converts its kinetic energy into potential energy. This energy is then carried away by the fluorescence photons emitted spontaneously during optical pumping processes; these processes transfer the atom from a peak of $V_\pm$ to a valley of $V_\mp$, and the photons have, on average, an energy greater than the energy of incident light wave photons.

This picture generalizes without difficulty to three dimensions, with an intensity and polarization pattern that can be more or less complicated depending on the number, direction, and relative phases of the light waves (Grynberg & Robilliard 2001). The essential point is (i) to maintain the fact that atomic levels are displaced downwards by a space-dependent amount,

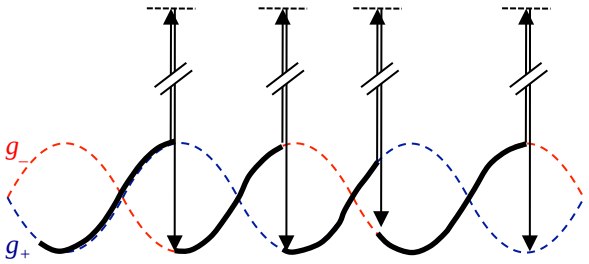

Figure V.4. *Typical evolution of an atom in the bi-valued potential $V_\pm(z)$ for a velocity of the order of γ_0/k.*

and (ii) that optical pumping tends to accumulate the atom in the lowest-energy sublevel. This result is guaranteed if we use a transition $J_g \longleftrightarrow J_e = J_g + 1$ and monochromatic light of negative detuning, $\Delta = \omega_\mathrm{L} - \omega_\mathrm{A} < 0$.

2 Sisyphus cooling limit

To determine the limit of Sisyphus cooling, we take a Brownian motion approach, calculating first the friction force acting on the atom, then the diffusion coefficient for an atom at rest. We will see in the next section (§ 3) how to go beyond this simple linear model.

2-1 Friction force and its linearity range

Our Sisyphus cooling model corresponds to a relatively simple problem of statistical physics: a particle evolves in the bi-valued potential $V_\pm(z)$ by randomly jumping between the two values with rates $\gamma_\pm(z)$. Let us consider an atom of velocity v and determine the force acting on it in steady state. This force is written as a function of the probability $P_\pm(z,v)$ of finding the atom at point z in state $g_\pm$:

$$F(z,v) = P_+(z,v)F_+(z) + P_-(z,v)F_-(z), \tag{V.8}$$

where $F_\pm(z)$ are the forces derived from the potentials $V_\pm(z)$:

$$F_\pm(z) = \pm k V_0 \sin(2kz). \tag{V.9}$$

To calculate the occupancy probabilities $P_\pm(z,v)$, let us take the evolution equation (V.6) and look for its forced regime. The latter is obtained by replacing $\frac{\mathrm{d}}{\mathrm{d}t}$ by $v\frac{\mathrm{d}}{\mathrm{d}z}$, and the solution is written:

$$P_\pm(z,v) = \frac{1}{2}\left(1 \mp \frac{\cos(2kz) + (v/v_c)\sin(2kz)}{1 + v^2/v_c^2}\right) \qquad \text{with} \quad 2kv_c = \gamma_0. \tag{V.10}$$

The force (V.8) averaged over a spatial period is therefore:

$$F(v) = -M\alpha \frac{v}{1 + v^2/v_c^2} \qquad \text{with} \quad M\alpha = k^2\,\frac{V_0}{\gamma_0}. \tag{V.11}$$

This is the friction force we are looking for and we can make three comments about it:

- At low velocities, $v \ll v_c$, we obtain a force linear in velocity $F(v) = -M\alpha v$, as in Brownian motion theory.
- The friction coefficient α is proportional to the ratio of the mean light shift V_0 and the pumping rate γ_0. Both quantities are proportional to light intensity, so α is independent of intensity. More precisely, we find:

  $$V_0 = \frac{2}{3}\hbar|\Delta|s_0, \quad \gamma_0 = \frac{2}{9}\Gamma s_0 \quad \longrightarrow \quad M\alpha = 3\,\hbar k^2\,\frac{|\Delta|}{\Gamma}. \tag{V.12}$$

  This value is to be compared with that obtained for Doppler cooling in the optimum case ($\Delta = -\Gamma/2$):

  $$M\alpha_\mathrm{Dop} = \hbar k^2\, s_0, \tag{V.13}$$

  a result valid only if $s_0 \ll 1$. In practice, the friction coefficient corresponding to the Sisyphus effect can therefore exceed α_Dop by several orders of magnitude.
- The range over which the force is linear in velocity is given by $|v| \ll v_c$, i.e. $kv \ll \frac{1}{9}\Gamma s_0$ or $v/\gamma_0 \ll \lambda/4\pi$. For the force to be linear in

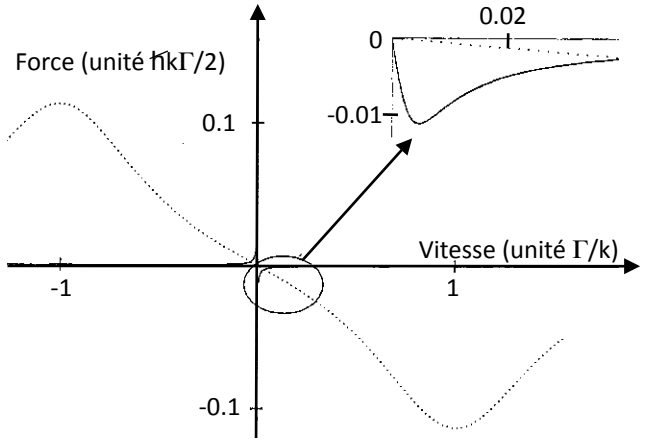

Figure V.5. *Force versus velocity for the Sisyphus effect (solid line) and for the Doppler effect (dashed line), plotted for $\Delta = -\Gamma$ and $s_0 \ll 1$.*

velocity, the atom's displacement during the relaxation time γ_0^{-1} must be very small compared to the spatial period of the light potential. In other words, many optical pumping processes must occur as the atom travels along a wavelength. This linearity range is proportional to the saturation parameter s_0, i.e. the power of the light waves.

The linearity range for Sisyphus cooling is much smaller than that for Doppler cooling, where the result is independent of light power ($kv \ll \Gamma$). For Doppler cooling, on the other hand, the friction coefficient decreases with decreasing power (figure V.5), whereas it is constant (and large) for Sisyphe cooling. In fact, in practice both the Doppler and Sisyphus mechanisms operate simultaneously, taking advantage of both the wide capture range of Doppler cooling and the high friction coefficient of Sisyphus cooling.

The force (V.11) has its maximum $F = kV_0/4$ for $v = v_c$, then decreases as $1/v$ at high velocities. The maximum force for $v = v_c$ corresponds to the situation where about one optical pumping process occurs per potential hill, as shown in figure V.4. This force then corresponds (to within a multiplicative coefficient) to the maximum force felt in the potentials $V_\pm(z)$ (we could not hope for better!).

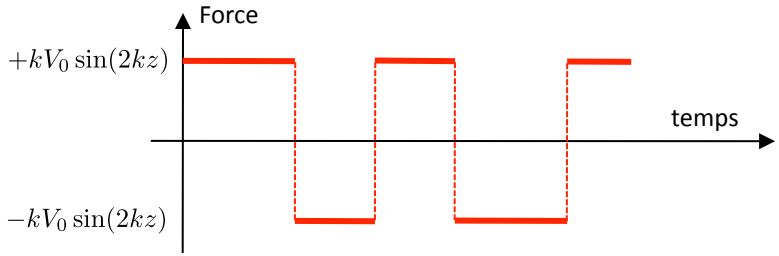

Figure V.6. *Random evolution of the force felt by a stationary atom at the z point as it randomly flips between $g_\pm$ states.*

The $1/v$ behavior of the force at high velocities corresponds to a constant power dissipation $\mathcal{P} = vF(v)$:

$$\mathcal{P} = \frac{1}{4} V_0 \gamma_0, \tag{V.14}$$

i.e. an energy loss of the order of a quarter of the modulation of the potentials $V_\pm$ for each optical pumping process. Again, this corresponds to the optimum that could be expected for this mechanism. This high-velocity regime $F(v) \propto 1/v$ is found in all variants of the Sisyphus effect, whatever the details of atomic dynamics.

In the rest of this paragraph, we will assume that at equilibrium, the atomic velocity distribution is essentially contained in the $|v| \ll v_c$ region, so that the friction force (V.11) is linear in velocity:

$$F = -M\alpha v \qquad \text{with} \quad M\alpha = 3\hbar k^2 \frac{|\Delta|}{\Gamma}, \tag{V.15}$$

as in Brownian motion theory. To determine the equilibrium state, we must also evaluate the momentum diffusion coefficient D_p to deduce the equilibrium temperature $k_B T = D_p/M\alpha$.

2-2 Momentum diffusion

Recall that the momentum diffusion coefficient D_p gives, to within a factor of 2, the growth rate of the momentum variance $\Delta p^2 = \langle p^2 \rangle - \langle p \rangle^2$. To evaluate D_p, let us take an atom at rest at a point z. Due to optical pumping processes, the atom jumps randomly between the levels g_+ and g_-, experiencing a fluctuating force $F(t) = \pm k V_0 \sin(2kz)$ given by the gradients of the potentials $V_\pm(z)$ experienced on each level (figure V.6). This fluctuating force is primarily responsible for the atom's momentum diffusion in Sisyphus cooling, and is therefore what we will be focusing on first. As with Doppler cooling, this contribution is supplemented by heating due to random momentum changes during spontaneous emission processes. We will take this into account later.

By decomposing the force felt by the atom into an average force $\bar{F}(z)$ and a fluctuating force of zero average, the corresponding diffusion coefficient is obtained from the expression (*cf.* chapter 1):

$$D_p(z) = \int_0^{+\infty} \left(\overline{F(z,0)F(z,t)} - \bar{F}(z)^2 \right) \, \mathrm{d}t, \tag{V.16}$$

where the average force $\bar{F}(z)$ is calculated using stationary populations (V.7)

$$\bar{F}(z) = [P_+(z) - P_-(z)] \, k V_0 \sin(2kz) = \frac{1}{2} k V_0 \sin(4kz). \tag{V.17}$$

The expression of $D_p(z)$ can then be calculated without difficulty [cf. Dalibard & Cohen-Tannoudji (1989)] and its average over a spatial period is equal to

$$D_{p,1} = \frac{3}{4} \hbar^2 k^2 \, s_0 \, \frac{\Delta^2}{\Gamma}. \tag{V.18}$$

As mentioned above, to this diffusion coefficient $D_{p,1}$ must in principle be added the contribution $D_{p,0}$ due to the random recoils during spontaneous emission processes. This contribution is of the same order as that found for Doppler cooling:

$$D_{p,0} \approx \hbar^2 k^2 s_0 \Gamma. \tag{V.19}$$

However, in most applications, Sisyphus cooling is used with a detuning significantly greater (in absolute value) than the natural width Γ. We can therefore neglect the contribution of $D_{p,0}$ and concentrate on $D_{p,1}$. We will see $D_{p,0}$ reappear when we try to go beyond the linear model for Brownian motion (§ 3).

2-3 Equilibrium temperature

The equilibrium temperature for Sisyphus cooling is deduced from the friction and diffusion coefficients found above:

$$|\Delta| \gg \Gamma \ : \qquad k_{\mathrm{B}} T \approx \frac{D_{p,1}}{M\alpha} \approx \frac{1}{4} \hbar |\Delta| s_0 = \frac{\hbar \kappa^2}{8|\Delta|}. \tag{V.20}$$

At first glance, it seems that we can obtain an arbitrarily low temperature, by taking the limit of a Rabi frequency $\kappa \to 0$. However, we need to check that the condition $v_0 \ll v_c$ holds for the thermal velocity $v_0 = \sqrt{k_{\mathrm{B}} T / M}$. Since v_0 varies as κ while v_c varies as κ^2, this imposes a lower limit on acceptable Rabi frequencies. For a given detuning Δ, we find that the minimum thermal velocity is

$$\text{Limit of linear model:} \qquad v_{0,\min} \sim v_{\mathrm{r}} \, \frac{|\Delta|}{\Gamma} \qquad \text{with} \quad v_{\mathrm{r}} = \frac{\hbar k}{M}. \tag{V.21}$$

Residual trapping of atoms. The average force (V.17) felt by an atom at rest is derived from the potential $\frac{V_0}{4} \sin^2(2kz)$. The amplitude of this potential $\frac{V_0}{4} = \frac{1}{6} \hbar |\Delta| s_0$ is of the same order as the thermal energy $k_{\mathrm{B}} T$. In this semi-classical model, we therefore expect a slight modulation of atomic density with periodicity $\lambda/4$, the density being slightly greater where light has circular polarization (right- or left-handed).

2-4 First experimental results

The prediction (V.20) corresponds to a very simple scaling law: provided the detuning is taken (in absolute value) to be greater than the natural width Γ, the equilibrium temperature should only depend on the ratio of intensity to detuning.

This prediction is remarkably well verified in practice. We have plotted on figure V.7 the results of measurements made on a 3D cesium optical molasses by Salomon, Dalibard, et al. (1990). The selected detunings ranged from $\Delta/\Gamma = -2$ to -28 and the law found for this 3-dimensional situation can be written:

$$M v_0^2 = k_B T \approx 0.4 \frac{\hbar \kappa^2}{|\Delta|}, \tag{V.22}$$

where v_0 represents the mean square velocity of the distribution and where κ denotes the Rabi frequency for each of the 6 travelling waves making up the optical molasses. A very comparable result was found for the two rubidium isotopes by Gerz, Hodapp, et al. (1993). The change in coefficient from $\frac{1}{8} = 0.125$ to 0.4 is due both to the shift from 1D to 3D and to the fact that the atomic transition involved is considerably more complicated than the $1/2 - 3/2$ model. A quantum Monte Carlo simulation taking these two points into account has made it possible to recover this coefficient with good accuracy (Castin & Mølmer 1995).

On the other hand, for a given detuning Δ, the limit (V.21) obtained within the framework of this linear model is not reproduced experimentally. In fact, the experiment gives a more favourable result: effective Sisyphus cooling continues to be observed even when the velocity distribution falls outside the linear range. The temperature limit reached when the intensity is lowered is in fact the same whatever the detuning chosen: $v_0 \sim$ some v_r, This limit is also verified for sodium ((Lett, Phillips, et al. 1989)) and rubidium (isotopes 85 and 87, Gerz, Hodapp, et al. (1993)). The explanation for this better-than-expected situation lies in the fact that Sisyphus cooling remains effective well beyond the linear regime, as we shall now see.

3 Beyond the linear model

To go beyond the linear Brownian model, we will use the Liouville equation formalism, which is well suited to taking into account the bi-valued potential $V_\pm(z)$ and the jumps between $g_\pm$ levels (Castin, Dalibard, et al. 1991).

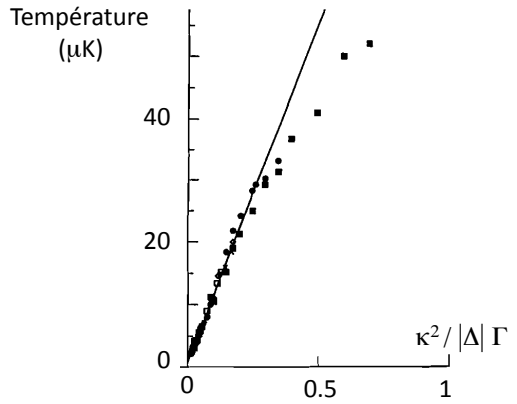

Figure V.7. *Variation of temperature in 3D cesium molasses as a function of the light shift. Figure taken from Salomon, Dalibard, et al. (1990).*

3-1 Coupled Liouville equations

For a particle with no internal structure moving in a force field $F(z)$, the evolution of the distribution $P(z, v, t)$ in phase space is given by Liouville's equation:

$$\frac{\partial P}{\partial t} + v \frac{\partial P}{\partial z} + \frac{F(z)}{M} \frac{\partial P}{\partial v} = 0. \tag{V.23}$$

This is equivalent to Newton's equation of motion for a point particle: $\dot{z} = v$, $M\dot{v} = F(z)$.

For the problem at hand, we need to introduce two distributions $P_\pm(z, v)$ and take account of jumps from one level to the other:

$$\frac{\partial P_+}{\partial t} + v \frac{\partial P_+}{\partial z} + \frac{F_+(z)}{M} \frac{\partial P_+}{\partial v} = -\gamma_+(z) P_+(z, v) + \gamma_-(z) P_-(z, v) \tag{V.24}$$

and a symmetrical equation for $P_-(z, v)$.

Let us look at the steady state of these two coupled equations, which removes the term in $\frac{\partial}{\partial t}$. Let us also consider the total phase space density and the difference between the densities of $g_\pm$:

$$P(z, v) = P_+(z, v) + P_-(z, v), \qquad \delta(z, v) = P_+(z, v) - P_-(z, v). \tag{V.25}$$

Subtracting (V.24) and the equation for P_-, we first find, using $F_- = -F_+$:

$$v\frac{\partial\delta}{\partial z} + (\gamma_+ + \gamma_-)\delta = -\frac{F_+}{M}\frac{\partial P}{\partial v} + (\gamma_- - \gamma_+)P. \tag{V.26}$$

By integrating this equation, we can express the difference $\delta(z,v)$ as a function of the sum $P(z',v)$. Let us then assume that P is independent of position in the steady state: $P(z,v) \equiv P(v)$; we saw earlier (§ 2-3) that this assumption is reasonable, at least in the linear regime. Solving (V.26) is then straightforward and yields

$$\delta(z,v) = \frac{-v/v_c}{1+(v/v_c)^2} \quad \Big[\quad \left(\sin 2kz + \frac{v_c}{v}\cos 2kz\right) P(v) \\ -\frac{kV_0}{\gamma_0}\left(\cos 2kz - \frac{v_c}{v}\sin 2kz\right)\frac{\mathrm{d}P}{\mathrm{d}v}\Big]. \tag{V.27}$$

We then inject this result into the equation of motion for $P(v)$, obtained by summing (V.24) and its equivalent for P_-. The result is written:

$$0 = \frac{\mathrm{d}}{\mathrm{d}v}\left[-F(v)P(v) + \frac{D_p(v)}{M}\frac{\mathrm{d}P}{\mathrm{d}v}\right] \tag{V.28}$$

where the force $F(v)$ is identical to that already found in (V.11) for a motion at constant v velocity:

$$F(v) = -M\alpha\frac{v}{1+v^2/v_c^2} \qquad \text{with} \quad M\alpha = k^2\,\frac{V_0}{\gamma_0}, \tag{V.29}$$

and where the velocity-dependent diffusion coefficient $D_p(v)$ is:

$$D_p(v) = \frac{D_{p,1}}{1+v^2/v_c^2} \qquad \text{with} \quad D_{p,1} = \hbar^2k^2 s_0\frac{\Delta^2}{\Gamma}. \tag{V.30}$$

We recover here the momentum diffusion coefficient $D_{p,1}$, associated with fluctuations in the dipole force when the atom at rest randomly tilts between $g_\pm$, which has already been calculated in (V.18)[1]. Remember that we have so far neglected the diffusion coefficient linked to the random recoil accompanying spontaneous emission processes; this contribution will soon make its reappearance when we come to the question of the ultimate limit of Sisyphus cooling.

[1] There is a $4/3$ factor between the expression found here for D_{p1} and that of (V.18). This factor is linked to the approximation made here of a strictly uniform density (Castin, Dalibard, et al. 1991).

3-2 Stationary state

Solving (V.28) is straightforward:

$$P(v) \propto \exp\left(\int_0^v \frac{MF(v')}{D_p(v')}\mathrm{d}v'\right). \tag{V.31}$$

We note that the $1+v^2/v_c^2$ denominator that appears in the force $F(v)$ outside the linearity range is offset by the same denominator in $D(v)$. The ratio $F(v')/D(v')$ remains a linear function of v', so the stationary distribution remains Gaussian:

$$P(v) \propto \exp(-v^2/2v_0^2) \qquad \text{with} \quad Mv_0^2 = \frac{1}{3}\hbar|\Delta|s_0. \tag{V.32}$$

This result explains why we experimentally find low r.m.s. velocities, of the order of a few recoil velocities, well outside the range of validity (V.21) initially predicted for large detunings.

So what is the true limit of validity of the result (V.32) for the equilibrium temperature of Sisyphus cooling? To determine it, we need to go back to the two heating sources present in this mechanism. In the foregoing, we have taken into account momentum diffusion due to dipole force fluctuations. On the other hand, as we have indicated on several occasions, we have neglected the random kicks of amplitude $\hbar k$ caused by spontaneous emission processes. If we also take this second process into account, we have to replace the diffusion coefficient (V.30) by:

$$D_p(v) = \frac{D_{p,1}}{1+v^2/v_c^2} + D_{p,0} \quad \text{where} \;\; D_{p,0} = \epsilon\,\hbar^2k^2 s_0\Gamma, \tag{V.33}$$

where the value of the multiplicative coefficient ϵ, taking into account the various branching factors between Zeeman sublevels, is $\epsilon = \frac{11}{18}$.

Solving (V.28) is then a little more complicated, but no great difficulty. We find

$$P(v) \propto \frac{1}{(1+v^2/\bar{v}_c^2)^A} \qquad \text{with} \quad \frac{\bar{v}_c}{v_\mathrm{r}} = \xi_1\frac{V_0}{E_\mathrm{r}}, \quad A = \xi_2\frac{V_0}{E_\mathrm{r}} \tag{V.34}$$

i.e. the power of a Lorentzian function. The dimensionless numbers ξ_1 and ξ_2 are respectively equal to $\frac{1}{\sqrt{88}} \approx 0.11$ and $\frac{1}{44} \approx 0.023$. The result is therefore a function of a single physical parameter, the ratio V_0/E_r.

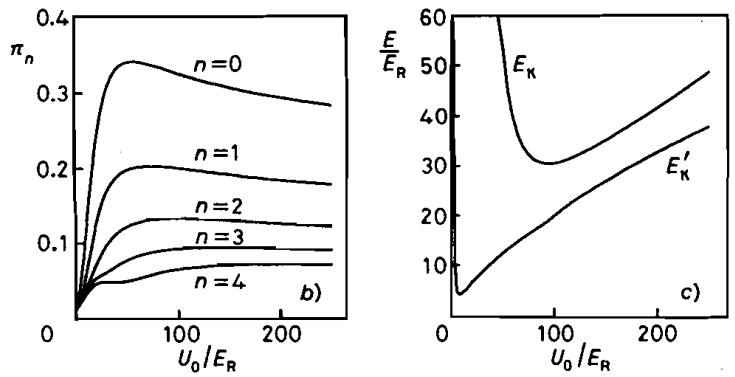

Figure V.8. *Result of a numerical calculation taking into account the quantum character of atomic motion in the bi-valued potential $V_\pm(z)$, with jumps between g_+ and g_- caused by spontaneous emission processes. Left: populations of different energy bands as a function of the ratio V_0/E_r. Right: Variation in mean kinetic energy $M\bar{v}^2/2$ in units of E_r, with two possible definitions for $\bar{v}$: the mean square velocity $\sqrt{\langle v^2\rangle}$ and the width at $1/\sqrt{\mathrm{e}}$ of the velocity distribution. These two quantities coincide for a Gaussian; here, the second definition gives a lower energy than the first. Figure taken from Castin & Dalibard (1991).*

This power-of-Lorentzian distribution is an interesting generalization of the Maxwell-Boltzmann Gaussian distribution. When the power A of the Lorentzian is large in front of 1, i.e. $V_0 \gg E_\mathrm{r}$, the significantly populated velocity classes are small in front of $\bar{v}_c$ and we then recover the Gaussian function of (V.32):

$$(1+v^2/\bar{v}_c^2)^{-A} = \exp\left[-A\ln(1+v^2/\bar{v}_c^2)\right] \approx \exp\left[-Av^2/\bar{v}_c^2\right]. \qquad \text{(V.35)}$$

On the other hand, if we decrease the ratio V_0/E_r, and therefore the exponent A, the wings of the distribution become more pronounced and we finally reach, for $A = 3/2$, a distribution for which the mean kinetic energy $M\langle v^2\rangle/2$ is no longer defined. For $A < 1/2$, the distribution itself can no longer be normalized, which means that there is no stationary regime: particle velocities will increase indefinitely with time, as the Sisyphus molasses is not strong enough to keep them close to zero velocity.

3-3 Quantum approach

To go a step further and get away from the various approximations made above, in particular the assumption of a distribution $P(z,v)$ uniform in z, it is convenient to run a numerical simulation of classical particle motion on this bi-valued potential $V_\pm(z)$. This simulation leads to a minimum r.m.s. velocity of the order of $6\,v_\mathrm{r}$, in good agreement with the previous analytical model (Castin, Dalibard, et al. 1991). However, when the r.m.s. velocity is down to a few recoil velocities, the de Broglie wavelength of the atoms becomes a significant fraction of the optical wavelength λ. This raises legitimate questions as to the validity of the preceding semi-classical treatment, which used the concept of the atom's position z defined to a precision much better than λ.

To go beyond this, a quantum treatment of the atom's motion is required, introducing the energy bands corresponding to the eigenstates in the periodic potential and the transfer rates between bands due to spontaneous emission processes. This treatment performed by Castin & Dalibard (1991) confirmed the conclusions reached here on the limits of cooling, while at the same time refining them. The accumulated population in the ground band is found to be as high as $\sim 30\%$ (figure V.8, left). Moreover, this treatment confirmed the non-Gaussian character of the velocity distribution for relatively low values of V_0/E_r. The minimum root-mean-square velocity is of the order of $5.5\,v_\mathrm{r}$, while the width at $1/\sqrt{\mathrm{e}}$, which should be equal to the previous one for a Gaussian distribution, can be as low as $2.2\,v_\mathrm{r}$ (figure V.8, right).

3-4 Experimental results

We have already described the first experimental results obtained on caesium (figure V.7), which confirmed the general law $k_\mathrm{B}T \propto V_0$. An example of the velocity distribution obtained for a shallow depth V_0 is shown in figure V.9. We can see that this distribution deviates significantly from a Gaussian, and that it is very well fitted by a power of Lorentzian, with $A \approx 2$ here. The width at $1/\sqrt{\mathrm{e}}$ of the velocity distribution is very narrow, of the order of only $2\,v_\mathrm{r}$.

One of the major advantages of Sisyphus cooling, in addition to its very

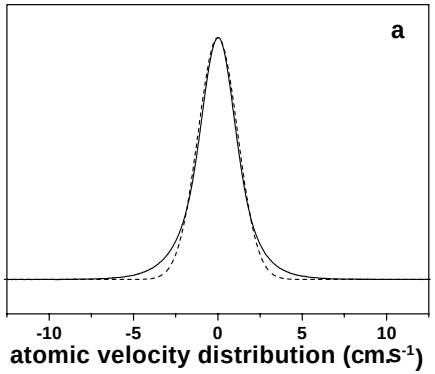

Figure V.9. *Velocity distribution of ^{87}Rb atoms cooled in 3D optical molasses with detuning $\Delta = -5\Gamma$. The effective temperature is $1.2\,\mu$K, i.e. a half-width at $1/\sqrt{\mathrm{e}}$ of only $1.8\,v_\mathrm{r}$. Note, however, that the distribution is clearly not Gaussian: the best fit by a Gaussian is given by the dotted line, while fit by a power of Lorentzian, in this case with exponent $A = 2$, gives a result perfectly superimposed on the experimental curve. Image taken from Sortais, Bize, et al. (2000).*

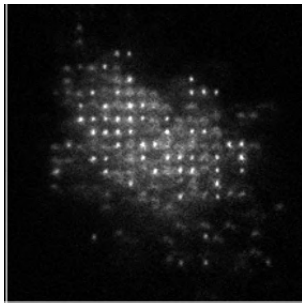

Figure V.10. *Sisyphus cooling of cesium atoms trapped in a large-period optical lattice ($4.9\,\mu$m). Each light point corresponds to a single atom. The estimated temperature is 10 μK and the lattice depth 165 μK. Image extracted from Nelson, Li, et al. (2007).*

low temperature limit, is its robustness. The only requirement is to preserve the essential ingredient - a different modulation of the Zeeman sublevels, with optical pumping preferably towards the lowest level. Sisyphus cooling therefore continues to work when atoms are placed in a magneto-optical trap: measurements by Drewsen, Laurent, et al. (1994) and Cooper, Hillenbrand, et al. (1994) have shown temperatures well below the Doppler limit, albeit with a rapid increase in this temperature with the number of atoms trapped.

Sisyphus cooling also remains operational when the atoms are immersed in an additional optical lattice. The combination of Sisyphus cooling and a lattice that is highly detuned from the atomic resonance makes it possible to create atomic microscopes, i.e. devices that enable the visualization of atoms localized at lattice sites. Sisyphus cooling fulfils two functions: (i) cooling the atoms to a temperature well below the energy barrier between two sites, so that a given atom remains localized at the same site for the duration of the experiment; (ii) ensuring that the atom continuously emits light, which can be detected via a microscope objective and a CCD camera. In this way, the atoms are individually observed, the experiment being limited only by the optical resolution of the microscope objective, which must be able to separate two adjacent sites. An example is shown in figure V.10, for a relatively large-period lattice $\sim 5\,\mu$m (Nelson, Li, et al. 2007). This experiment was then repeated and improved to image atoms in a lattice with a period smaller than $1\,\mu$m (Bakr, Peng, et al. 2009; Sherson, Weitenberg, et al. 2010).

Finally, note that we have concentrated on the case of Sisyphus cooling in a periodic potential. However, this mechanism can also be used as a single-shot process, as in the inelastic bouncing of atoms in an evanescent wave on the surface of a prism (Desbiolles, Arndt, et al. 1996; Ovchinnikov, Manek, et al. 1997). The emission of a single fluorescence photon enables the dissipation of a significant amount of energy, equal to the difference in potential energy between the two internal sublevels under consideration. This type of mechanism has also been used to cool fluoromethane (CH_3F) molecules electrostatically confined by their electric dipole moment (Zeppenfeld, Englert, et al. 2012).

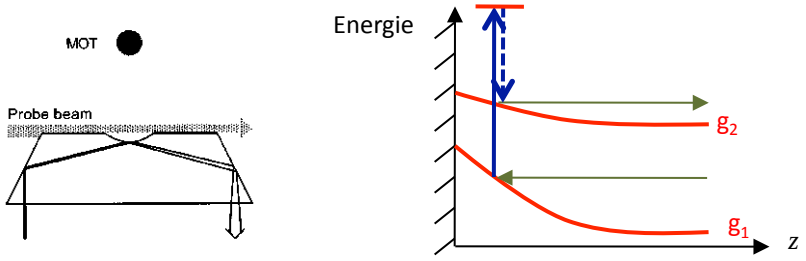

Figure V.11. *Inelastic rebound of atoms on an evanescent laser wave. The two ground sublevels g_1 and g_2 experience repulsive potentials of different values. The atom arrives in the level g_1, which is strongly repelled by the surface. It then undergoes an optical pumping process towards the level g_2 in the vicinity of the surface, and leave on this level g_2, which is more weakly repelled than g_1. The total mechanical energy of the atom has therefore decreased in the rebound process (Desbiolles, Arndt, et al. 1996; Ovchinnikov, Manek, et al. 1997).*

4 Gray molasses

The above description of Sisyphus cooling, with a $J_g = 1/2 \leftrightarrow J_e = 3/2$ transition, took advantage of the correlation between optical pumping rate and light shift. The key point was to accumulate the atomic population at the bottom of the potential valleys. For the $J_g = 1/2 \leftrightarrow J_e = 3/2$ transition, this was ensured by taking a negative detuning, i.e. $\omega_L < \omega_A$ (laser on the red of the atomic resonance). For this configuration $J_g < J_e$, atoms were accumulated in the levels most coupled to light, leading to maximum fluorescence photon emission. We will now look at the opposite situation, $J_g \geq J_e$, where optical pumping tends to accumulate atoms in states weakly coupled to light.

4-1 The transition $J_g = 1/2 \leftrightarrow J_e = 1/2$

To begin with, let us consider a $J_g = 1/2 \leftrightarrow J_e = 1/2$ transition in the same one-dimensional lin⊥lin laser configuration as above. Several results will remain valid; in particular, the light shifts of the two sublevels $g_\pm$ are still spatially modulated, as are the optical pumping rates (figure V.12). However, the modulation of energy levels takes place with an opposite phase to the previous case: at a point where the light is σ_+ polarized, the g_+ level is not displaced, whereas the g_- level is. The phase of the modulation of optical pumping rates is unchanged: σ_+ light always tends to accumulate atoms in the g_+ state.

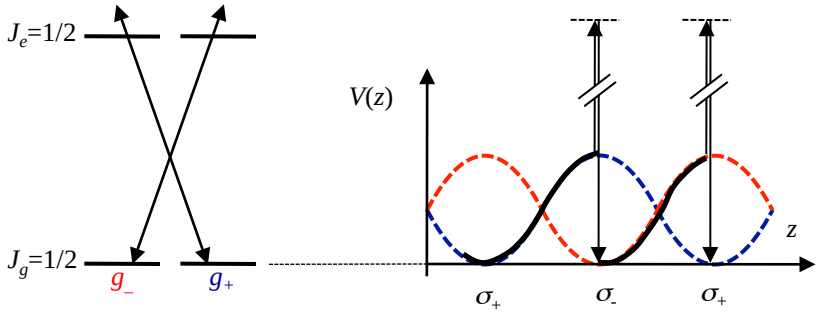

Figure V.12. *Sisyphus cooling for a transition $J_g = 1/2 \leftrightarrow J_e = 1/2$. A positive detuning must be taken and the atoms accumulate in the ground sublevel least coupled to light.*

To achieve Sisyphus cooling, the atoms must accumulate at the bottom of the valleys. At a point where light is σ_+ polarized, the state g_+ must therefore have a lower energy than the state g_-. However, the level g_+ is not displaced by light, whereas g_- is. We deduce that the light shift of g_- must be upwards, which means that the detuning of the laser must now be positive: $\omega_L > \omega_A$.

Once this positive detuning has been chosen, the treatment of Sisyphus cooling for the $J_g = 1/2 \leftrightarrow J_e = 1/2$ transition is in every respect similar to what we saw for the $J_g = 1/2 \leftrightarrow J_e = 3/2$ transition, with a bi-valued potential and optical pumping rates equal (within a numerical factor) to those given in (V.2) and (V.4). The only difference at this stage is that the Sisyphus cooling mechanism will oppose the Doppler mechanism (which is a heating mechanism for $\Delta > 0$), whereas the Sisyphus and Doppler mechanisms work together for a transition with $J_e = J_g + 1$ and a negative detuning Δ. However, this point may be negligible if the velocity ranges associated with the two mechanisms are sufficiently different.

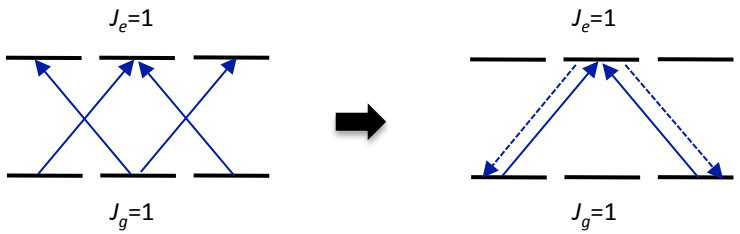

Figure V.13. *A Λ system that emerges in the dynamics of a $J_g = 1 \leftrightarrow J_e = 1$ transition illuminated by $\sigma_\pm$ light.*

4-2 The transition $J_g = 1 \leftrightarrow J_e = 1$

The passage from $J_g = 1/2 \leftrightarrow J_e = 1/2$ to $J_g = 1 \leftrightarrow J_e = 1$ enriches the problem considerably. The reason is that this transition allows the construction of internal states not coupled to radiation, at any point in space.

Here, we present the proposal originally made by Shahriar, Hemmer, et al. (1993) and Weidemüller, Esslinger, et al. (1994). This is a 1D configuration in which the amplitudes of the $\sigma_\pm$ polarizations oscillate in space as before, but not necessarily in phase opposition. This configuration is achieved using two light waves of the same frequency and intensity, counter-propagating, each linearly polarized and such that their polarizations make an angle ϕ (we took $\phi = \pi/2$ in § 1). We will call this configuration lin $\vee$ lin.

As we saw in the previous chapter on coherent population trapping, the fact that light is purely $\sigma_\pm$ polarized means that internal atomic dynamics essentially occur in the Λ system (figure V.13): $|g, m = -1\rangle \leftrightarrow |e, m = 0\rangle \leftrightarrow |g, m = +1\rangle$, with couplings that can be written, for a suitable choice of z-axis origin:

$$\kappa_\pm(z) = \kappa_0 \cos(kz \pm \phi/2). \tag{V.36}$$

Eigenstates and energies for an atom at rest at a point z. We will assume that the Δ detuning of the light waves is large in front of κ_0, so we can restrict our analysis to the two-dimensional subspace of the ground level, made up of linear combinations of $g_\pm$. At any point z in space, we

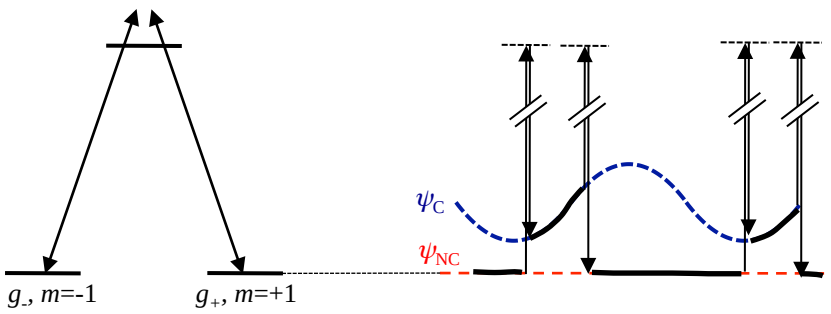

Figure V.14. *Coupled and uncoupled atomic levels in the lin $\vee$ lin configuration. Motional coupling allows the transition from the uncoupled to the coupled state, where the levels are close to each other. A second photon scattering process sends the atom back to the uncoupled state, with a conversion of atomic potential energy into photon energy [Physical image proposed by C. Cohen-Tannoudji in his 1995-96 lecture at the Collège de France].*

can identify a coupled state and an uncoupled state in this subspace, with energies $\hbar\omega_C$ and $\hbar\omega_{NC}$ respectively:

$$|\psi_C\rangle \propto \kappa_+|g_+\rangle + \kappa_-|g_-\rangle, \qquad \hbar\omega_C \approx \frac{\hbar}{4\Delta}\left(\kappa_+^2 + \kappa_-^2\right), \tag{V.37}$$

$$|\psi_{NC}\rangle \propto \kappa_-|g_+\rangle - \kappa_+|g_-\rangle, \qquad \hbar\omega_{NC} = 0. \tag{V.38}$$

Using the expression (V.36) for the Rabi frequencies of the $\sigma_\pm$ waves, the energy of the coupled state is written in this large Δ regime:

$$\hbar\omega_C \approx V_0\left[1 + \cos(\phi)\cos(2kz)\right] \qquad \text{with} \quad V_0 = \frac{\hbar\kappa_0^2}{4\Delta}. \tag{V.39}$$

Here we choose a positive Δ detuning, so that the coupled state is always energetically above the uncoupled state (figure V.14).

Furthermore, as a result of its interaction with the light field, the atom prepared in the coupled state can scatter photons, and the corresponding rate is

$$\gamma_C \approx \gamma_0\left[1 + \cos(\phi)\cos(2kz)\right] \qquad \text{with} \quad \gamma_0 = \Gamma\frac{\kappa_0^2}{4\Delta^2}. \tag{V.40}$$

The photon scattering rate for an atom at rest prepared in the state $|\psi_{\rm NC}\rangle$ is zero by construction, so an atom at rest in z (in a semi-classical approximation) will eventually fall into this state.

The Sisyphus effect in this context. Consider now an atom in slow motion, still in the semi-classical approximation and assume that this atom is initially prepared in the state $|\psi_{\rm NC}\rangle$. Since the expressions of the states $|\psi_{\rm C}\rangle$ and $|\psi_{\rm NC}\rangle$ depend on position, motion will create a coupling between these two states. More precisely, let us take the atom's initial state $|\psi(0)\rangle = |\psi_{\rm NC}[z(0)]\rangle$ and write[2] its state at time t as

$$|\psi(t)\rangle = \alpha(t)\,|\psi_{\rm NC}[z(t)]\rangle + \beta(t)\,|\psi_{\rm C}[z(t)]\rangle, \tag{V.41}$$

with, if the atom moves slowly, $|\beta| \ll |\alpha| \approx 1$. The evolution equation for β is obtained using the Schrödinger equation:

$$\mathrm{i}\dot\beta = \left(\omega_{\rm C} - \mathrm{i}\frac{\gamma_{\rm C}}{2}\right)\beta - \mathrm{i}\alpha\, v\, \langle\psi_{\rm C}|\frac{\mathrm{d}\psi_{\rm NC}}{\mathrm{d}z}\rangle, \tag{V.42}$$

where (i) the complex term $\mathrm{i}\hbar\gamma_{\rm C}/2$ has been added to the energy $\hbar\omega_{\rm C}$ of the coupled state to account for its finite lifetime under the effect of laser irradiation, and (ii) we took into account the fact that the basis vectors $|\psi_{\rm C}\rangle$ and $|\psi_{\rm NC}\rangle$ rotate when the position z varies. Assuming that the atom's displacement over time $1/\gamma_{\rm C}$ is small compared to the spatial period $\lambda/2$ of the problem, the steady state of (V.42) reads

$$|\beta| \approx \frac{k|v|}{\sqrt{\omega_{\rm C}^2 + \frac{\gamma_{\rm C}^2}{4}}}\,\mu \tag{V.43}$$

with

$$\mu = \frac{1}{k}\langle\psi_{\rm C}|\frac{\mathrm{d}\psi_{\rm NC}}{\mathrm{d}z}\rangle = \frac{\sin(\phi)}{1+\cos(\phi)\cos(2kz)}. \tag{V.44}$$

For a moving atom, the contamination of the uncoupled state by the coupled state has the weight $|\beta|^2$. It is maximal at points where the gap $\omega_{\rm C}$ between these two states is minimal: this is where the rotation frequency $kv\mu$ of the vectors $|\psi_{\rm C}\rangle$ and $|\psi_{\rm NC}\rangle$ is greatest. In particular, it is at these points that the atom initially prepared in the state $|\psi_{\rm NC}\rangle$ has the highest probability of scattering a photon, which (with probability $1/2$) can cause it to switch to the state $|\psi_{\rm C}\rangle$.

Once this process has taken place, the usual Sisyphus effect resumes: the atom will climb a fraction of the potential hill in the coupled state, then be optically repumped to the state $|\psi_{\rm NC}\rangle$ after a time $\tau \sim 1/\gamma_{\rm C}$ (figure V.14). In the low-velocity limit, the energy lost in climbing the hill is $E_{\rm C}(z+v\tau) - E_{\rm C}(z)$. The atom can then start a new cycle: switch from $|\psi_{\rm NC}\rangle$ to $|\psi_{\rm C}\rangle$ by photon scattering induced by motional coupling, and back from $|\psi_{\rm C}\rangle$ to $|\psi_{\rm NC}\rangle$ by standard optical pumping.

The velocity-dependent force. Due to the $z \leftrightarrow -z$ symmetry of the problem, the velocity-dependent force is necessarily an odd function of v: $F(-v) = -F(v)$. In the traditional Sisyphus effect leading to the force (V.11), the lowest-order term is linear in velocity, and the corrections are in v^3, v^5, ... In the case we are interested in here, we find from (V.43) a first factor v^2 to obtain a non-zero population in the coupled state. The delay effect in the establishment of the stationary regime, which causes the atom to climb more hills than it descends, brings in an additional factor v (as in § 1) so that the force in the vicinity of zero velocity varies here as v^3. The exact result after spatial averaging over one period is written (Weidemüller, Esslinger, et al. 1994) :

$$F(v) = -\xi\,\hbar k\gamma_0\,\left(\frac{kv}{\gamma_0}\right)^3\,\frac{\Gamma}{\Delta}, \tag{V.45}$$

with the dimensionless numerical coefficient:

$$\xi(\phi) = \frac{16}{5\pi}\sin^2\phi\cos\phi\int_0^{2\pi}\frac{\cos(Z)}{(1+\cos\cos Z)^5}\,\mathrm{d}Z. \tag{V.46}$$

We can see that in order to have a non-zero force, it is necessary that

- $\sin\phi$ must be non-zero; indeed, if $\phi = 0$, $\kappa_\pm$ are equal at every point in space, and coupled and uncoupled states do not depend on position.
- $\cos\phi$ must be non-zero; indeed, if $\phi = \pi/2$ (lin$\perp$lin configuration), the energy of the coupled level $\hbar\omega_{\rm C}$ does not vary in space and there is no energy loss in the Sisyphus process of figure V.14.

[2] To go beyond the semi-quantitative arguments presented here, we refer the reader to C. Cohen-Tannoudji's 1995-96 course where the problem is discussed in detail.

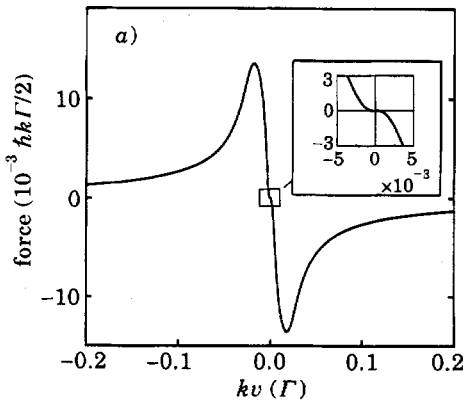

Figure V.15. *Variation of the force $F(v)$ for a transition $J_g = 1 \leftrightarrow J_e = 1$ in a lin $\vee$ lin configuration. Note the variation in v^3 of the force near the origin. Parameters: $\kappa_0 = 0.4\,\Gamma$, $\Delta = +\Gamma$, $\phi = \pi/4$ [figure taken from Weidemüller, Esslinger, et al. (1994)].*

We have extracted from Weidemüller, Esslinger, et al. (1994) the figure V.15 showing the variation of $F(v)$ with velocity v for typical parameters. It clearly shows the variation in v^3 in the vicinity of the origin. When the velocity increases to such an extent that on average one optical pumping cycle occurs as the atom travels through one period of the potential, then the force felt is (to within one numerical coefficient) given by the maximum force $\sim kV_0$ felt on the $|\psi_{\rm C}\rangle$ level. This maximum force is comparable to that found for the standard Sisyphus effect. For even higher velocities, the energy loss due to optical pumping saturates at a fraction of V_0 and the force decreases as $1/v$, as we have seen for the standard Sisyphus effect.

Performance of grey-molasses cooling. To assess the cooling limit, let us start with a semi-classical reasoning. The friction force, in v^3 near the origin, is weaker than the linear velocity force found for traditional Sisyphus cooling. But the velocity diffusion coefficient (which we will not calculate here) is also affected by the same additional v^2 coefficient, so that the velocity distribution, evaluated from (V.31)

$$\mathcal{P}(v) \propto \exp\left(\int_0^v \frac{MF(v')}{D_p(v')}\,{\rm d}v'\right) \qquad \text{(V.47)}$$

remains Gaussian, with an average energy $k_{\rm B}T$ comparable to the modulation of light shift V_0, as in the case of the standard Sisyphus effect.

However, this semi-classical reasoning is insufficient for a transition $J_g = 1 \leftrightarrow J_e = 1$, since we saw in the previous chapter that there is always a dark state for this type of transition. It is expected that a fraction of the atoms will accumulate in this dark state, which will be composed of well-defined peaks in velocity in $\pm v_{\rm r}$. This dynamics; which has a specifically quantum origin, is much slower than the semi-classical dynamics (figure V.16): quantum dynamics results from a random walk in which a given atom must approach the dark state family with a precision much better than the recoil velocity, which requires numerous spontaneous emission processes. Semi-classical dynamics, on the other hand, which brings atoms to within a few recoil velocities of the center, requires only a few spontaneous emission processes if we start from a velocity distribution pre-cooled by the Doppler effect.

4-3 The first gray molasses

The Sisyphus cooling mechanism we have just discussed in the $J_g = 1/2 \leftrightarrow J_e = 1/2$ and $J_g = 1 \leftrightarrow J_e = 1$ cases can be generalized to higher angular momentum transitions of the $J_g \leftrightarrow J_e$ type with $J_e = J_g - 1$ and $J_e = J_g$. For this type of transition, optical pumping is always towards the ground sublevel least coupled to light. A positive detuning Δ must therefore be chosen so that this least coupled state is also the lowest in energy, a necessary condition for the Sisyphus effect to cause cooling and not heating.

Before going into a little more detail, we can highlight two points of comparison with bright molasses:

- A clear advantage of gray molasses is that the fluorescence emitted by the atoms decreases sharply, as the atoms are optically pumped towards the less coupled sublevels, or even a dark state when it exists.

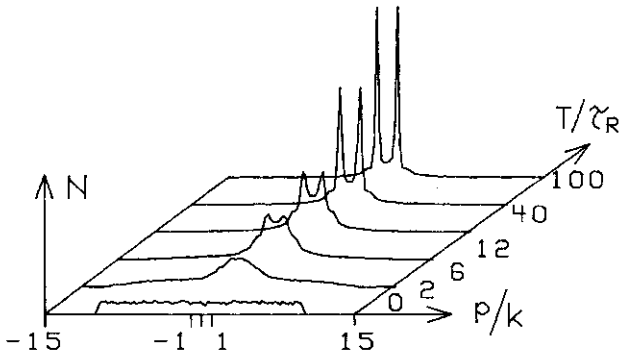

Figure V.16. *Evolution of the atom momentum distribution for a $J_g = 1 \leftrightarrow J_e = 1$ transition in a lin$\vee$lin configuration. Time unit $\tau_{\rm R} = 2M/\hbar k^2$ (parameters for the sodium atom), $\kappa_0 = 0.2\,\Gamma$, $\Delta = +\Gamma$, $\phi = \pi/4$. We can clearly see the two time scales for (i) Sisyphus cooling, (ii) subrecoil cooling [Figure taken from Shahriar, Hemmer, et al. (1993)].*

Some of the harmful effects of fluorescent light can therefore be reduced: repulsive forces between atoms as in the magneto-optical trap and light-assisted inelastic collisions.

- One disadvantage of grey molasses is the sign of the detuning at which it operates; this detuning must be positive, i.e. opposite to that of Doppler cooling. There is therefore a competition between the cooling force due to grey molasses, important for velocities such as $kv \lesssim \gamma_{\rm C}$, and the heating force due to the Doppler effect with a positive detuning, important for $kv \sim \Gamma$. If the parameters of the experiment can be chosen such that the separation between these two velocity scales is well marked, which in practice imposes $kv_{\rm r} \ll \Gamma$, then this competition is not really a problem and Doppler heating can be ignored for atoms cooled around recoil by grey molasses. This will be the case for very broad lines, for which Γ exceeds the recoil frequency $\omega_{\rm r}$ by several orders of magnitude.

The first cooling experiments on a $J_g \leftrightarrow J_e = J_g - 1$ transition were carried out at 1D by Valentin, Gagné, et al. (1992) at the Aimé Cotton laboratory. This involved the $J_g = 3 \leftrightarrow J_e = 2$ component of the D_2 cesium line, which is a closed transition. The extension to 3D was made on the same atomic line by Boiron, Triché, et al. (1995) and Boiron, Michaud, et al. (1996) (see also Hemmerich, Weidemüller, et al. (1995) for a 2D version on a $J_g = 1 \leftrightarrow J_e = 1$ transition). Boiron, Michaud, et al. (1996) measured temperatures in the microkelvin range at low atomic density, which is lower by a factor of two than those measured on the bright transition $J_g = 4 \leftrightarrow J_e = 5$ for the same atom.

4-4 The grey molasses revival

Since 2012, grey molasses have become very popular for cooling certain atomic species such as lithium or potassium (Fernandes, Sievers, et al. 2012; Grier, Ferrier-Barbut, et al. 2013; Nath, Easwaran, et al. 2013; Salomon, Fouché, et al. 2013; Burchianti, Valtolina, et al. 2014; Sievers, Kretzschmar, et al. 2015). These are alkaline atoms, for which we recall that the resonance line, which couples an S state to a P state, is split into two components due to the fine structure of the excited level. This excited level therefore has two sublevels, $P_{1/2}$ and $P_{3/2}$, and the two corresponding lines are called D_1 and D_2.

From the D_2 line to the D_1 line. For Li or K, the traditional Sisyphus cooling on the D_2 line (used successfully for Na, Rb, Cs) works poorly. This D_2 line links the two ground hyperfine sublevels, F and $F-1$, to the four hyperfine sublevels of the $P_{3/2}$ excited state: $F+1$, F, $F-1$, $F-2$ (here $F = I + 1/2$, where I is the spin of the atomic nucleus). Standard Sisyphus cooling works on the closed transition $J_g = F \leftrightarrow J_e = F+1$, and requires a negative detuning Δ (figure V.17, top). An additional repumping beam, tuned to the $J_g = F-1 \leftrightarrow J_e = F$ transition, for example, recycles atoms that would eventually be pumped to the ground $F-1$ level, but this repump plays only a minor role in the problem. This picture is valid if the hyperfine structure between the $J_e = F+1$ and $J_e = F$ sublevels is sufficiently large in front of the natural Γ width. This condition is very well met for heavy alkalis such as rubidium and cesium, but not for lithium and potassium (it is marginal for sodium).

The alternative is to use the D_1 line, which links the two ground hy-

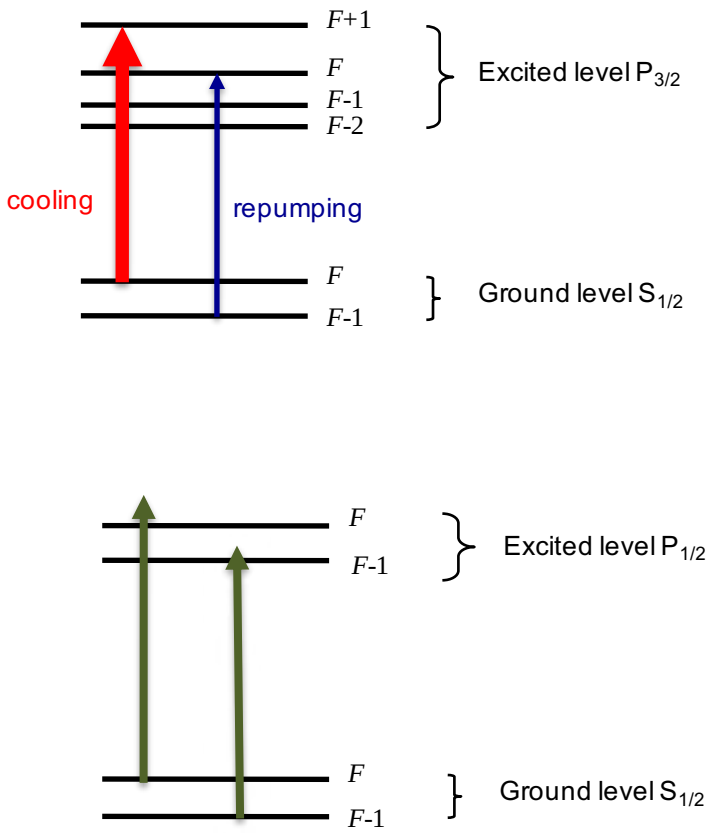

Figure V.17. *Top: D_2 line of an alkali atom and transitions used for standard Sisyphus cooling, with a main laser for cooling and a secondary laser for repumping. Bottom: D_1 line of an alkali atom; the two lasers play comparable roles in cooling. Note that it is possible for the hyperfine levels to be inverted with respect to this scheme, with the F level below the $F-1$ level (this is the case, for example, for ^7Li and ^{40}K). The structure of the D_2 line for ^6Li ($I = 1$, $F = 3/2$) is also slightly different from what is shown here.*

perfine sublevels, F and $F-1$, to the two hyperfine sublevels of the $P_{1/2}$ excited state: F and $F-1$ (figure V.17, bottom). An immediate advantage of this line is that, for a given isotope, the hyperfine structure of the $P_{1/2}$ excited level is significantly larger than that of the $P_{3/2}$ level: the various transitions are therefore better resolved. However, we no longer have a closed transition between a given pair of sublevels: each excited sublevel (F or $F-1$) can de-excite towards the two ground sublevels. We are therefore obliged to consider the problem of atom-light interaction by simultaneously taking into account the two ground levels and the two lasers that excite them. There is no longer one main cooling laser and one repumping laser (with a minor role), but two lasers playing equally important roles.

Raman resonance and Fano profile. A point highlighted by Grier, Ferrier-Barbut, et al. (2013), then by Nath, Easwaran, et al. (2013) and Salomon, Fouché, et al. (2013), is the importance of Raman resonance between the two lasers exciting the $F-1$ and F ground levels respectively. This point is illustrated on the temperature measurement shown in figure V.18 extracted from Sievers, Kretzschmar, et al. (2015), obtained with an intense laser (laser 2) driving the $J_g = 9/2 \leftrightarrow J_e = 7/2$ transition and a weaker laser (laser 1) driving the $J_g = 7/2 \leftrightarrow J_e = 7/2$ transition. When the Raman detuning $|\Delta|$ is greater than Γ, a temperature of the order of 50 μK is measured, which can be interpreted as the result of gray molasses $9/2 \leftrightarrow 7/2$ for the more intense laser, or $7/2 \leftrightarrow 7/2$ for the other. We then have black or gray states obtained by superimposing states of a given ground sublevel ($9/2$ or $7/2$).

When Raman resonance occurs ($\Delta = 0$), the temperature drops by an additional factor ranging from 2 to 4, depending on the atomic species. An unfavorable zone also appears, for a slightly positive Raman detuning. This result can be compared with the profile found in the previous chapter for a Λ system (figure V.19). In the case where the two light waves driving the atom are such that $\kappa_1 \ll \kappa_2$, we found a variation of the excited level population in the vicinity of the Raman resonance very similar to the variation found by Sievers, Kretzschmar, et al. (2015) for temperature. Let us recall here the origin of this asymmetric profile, called *Fano profile*. This form of profile is encountered when interference occurs between a resonant scattering process and a much flatter scattering process. Lounis & Cohen-Tannoudji (1992) proved that the Fano model was indeed realized

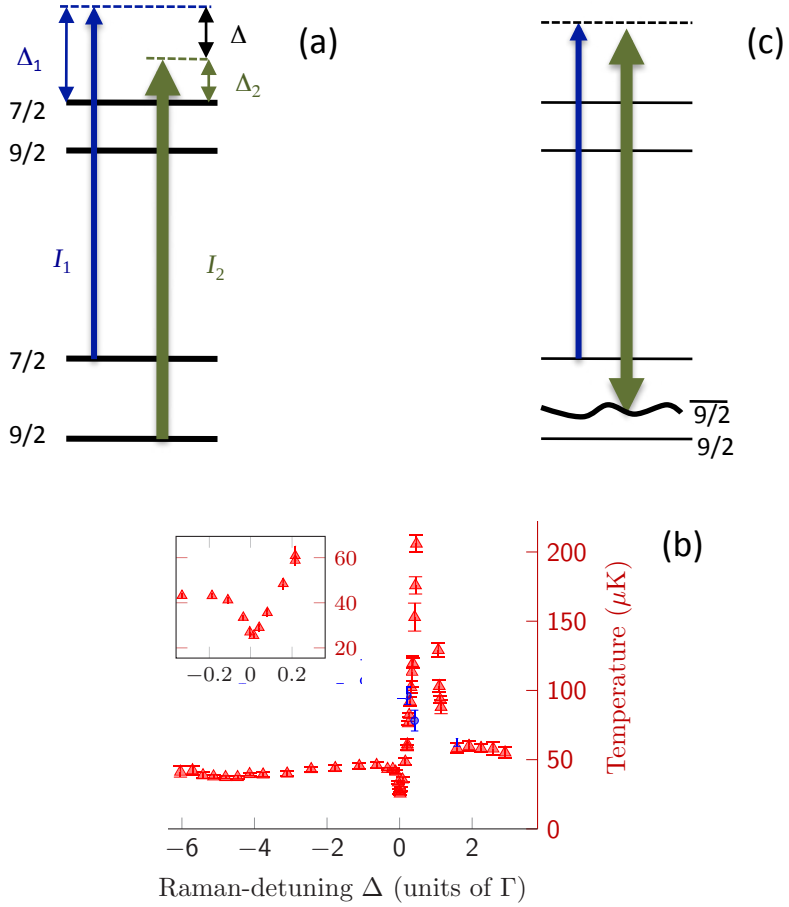

Figure V.18. *a) Schematic of ^{40}K levels and lasers used. b) Temperature in ^{40}K gray molasses, as a function of Raman detuning $\Delta = \Delta_1 - \Delta_2$ ($I_1 = 0.46\, I_{\text{sat}}$, $I_2 = 6\, I_{\text{sat}}$, $\Delta_2 = 3\,\Gamma$) [Figure taken from Sievers, Kretzschmar, et al. (2015)]. c) Explanation of the heating observed for a slightly positive Raman detuning Δ: a resonant Raman transition leads to the excitation of the 9/2 dressed level by photons from the most intense laser.*

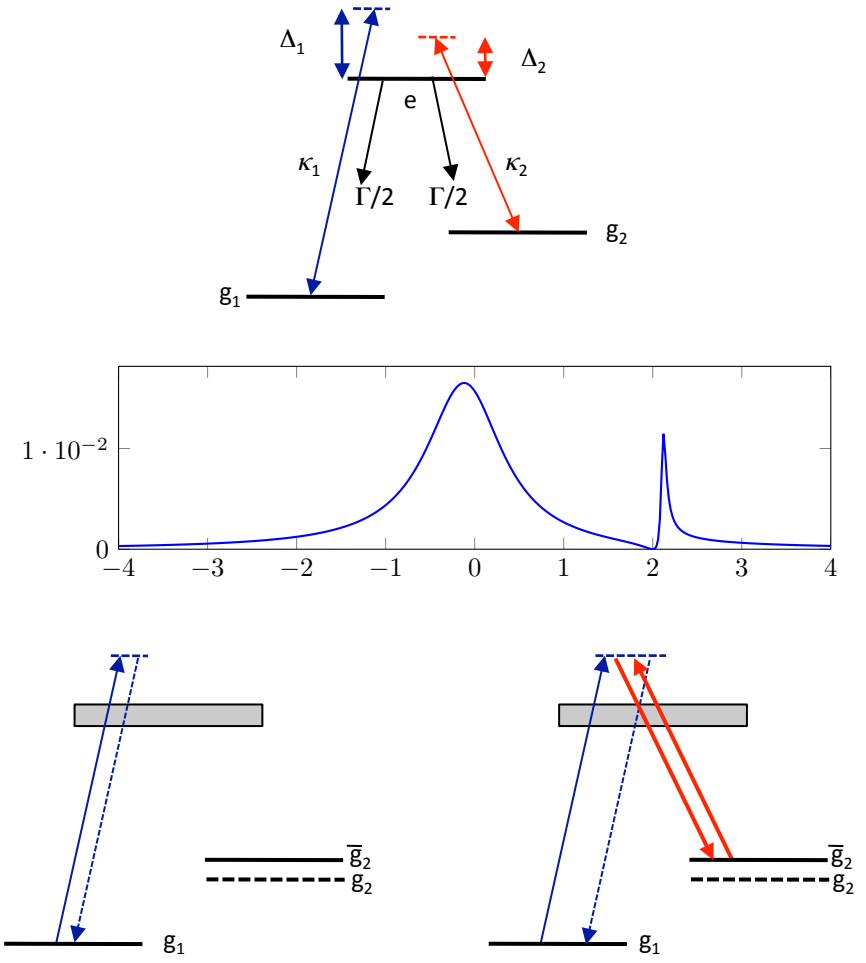

Figure V.19. *Top: Model Λ system. Middle: Variation of excited population P_e with detuning Δ_1, measured in units of Γ. The other parameters are (in units of Γ): $\kappa_1 = 0.1$, $\kappa_2 = 1$, $\Delta_2 = 2$. (Bottom) : The two scattering processes for a photon from laser 1, leading to the Fano profile in the middle figure.*

for the Λ system when $\kappa_1 \ll \kappa_2 \ll |\Delta_{1,2}|$. To demonstrate this, we begin by treating the interaction of beam 2 with the atom exactly. In the case where $\kappa_2 \ll |\Delta_2|$, this dressing of the g_2 level induces the light shift:

$$|g_2\rangle \to |\bar{g}_2\rangle, \quad E(\bar{g}_2) = E(g_2) + \delta E(g_2) \quad \delta E(g_2) \approx \frac{\hbar|\kappa_2|^2}{4\Delta_2}. \tag{V.48}$$

Starting with the atom in the state $|g_1\rangle$, scattering of a photon from the weak laser beam (beam 1) can take place either non-resonantly, passing only through $|e\rangle$ (figure V.19, bottom left), or resonantly via a Raman transition that leads the atom transiently into $|\bar{g}_2\rangle$ (figure V.19, bottom right). The narrow maximum of the curve for P_e is obtained when Raman resonance with the dressed state $|\bar{g}_2\rangle$ occurs:

$$\hbar\Delta_1 = \hbar\Delta_2 + \delta E(g_2). \tag{V.49}$$

We thus obtain a remarkable situation where P_e cancels for the "bare" Raman resonance $\Delta_1 = \Delta_2$, then passes through a maximum for the "dressed" Raman resonance (V.49).

This model of a Λ system is of course a considerable simplification compared with the real case of the D_1 line of potassium, for which 18 ground states are coupled to 18 excited states. But it at least qualitatively accounts for the gain obtained at the bare Raman resonance, which allows robust dark states to appear, linear combinations of the 18 ground states from the two hyperfine levels $F_g = 7/2$ and $F_g = 9/2$. It also helps explain the significant heating observed for slightly positive Raman detuning (figure V.18c).

Conclusion

The Sisyphus mechanism, whether "bright" for a transition such as $J_g < J_e$ or "gray" for a $J_g \geq J_e$ transition, achieves a temperature essentially limited by the recoil of a single photon. It is relatively robust, since it depends only slightly on the quality of the light beams used (polarizations, wavefronts, detuning). The most detailed studies to date of the shape of velocity distributions have been carried out in the bright case. They have shown that the narrowest velocity distribution profiles are notably non-Gaussian, which does not always facilitate comparison between different experiments, as the authors do not systematically use the same convention for measuring their temperature.

	M	λ nm	$\Gamma/2\pi$ MHz	v_r cm/s	$\omega_r/2\pi$ kHz	T_{min} μK	$\bar{v}$ cm/s	$\bar{v}/v_r$
Li	6	671	5.9	9.9	73.5	44*	24.6*	2.5*
Li	7	671	5.9	8.5	63.0	60*	26.6*	3.1*
Na	23	589	9.8	2.9	24.9	25	9.5	3.2
K	39	770	6	1.32	8.6	3*	2.5*	1.9*
K	40	770	6	1.29	8.4	11*	4.8*	3.7*
Rb	87	780	6.1	0.59	3.8	1.2	1.1	1.8
Cs	133	852	5.2	0.35	2.1	2.5	1.25	3.6
Cs	133	852	5.2	0.35	2.1	1.1*	0.83*	2.4*

Figure V.20. *Minimum temperatures obtained by Sisyphus cooling. Data with one star correspond to gray molasses, others to bright molasses. Measured rms velocities $\bar{v}$ are all between 1.8 and 3.7 recoil velocities.*

Nevertheless, we have attempted to summarize the limit obtained by Sisyphus cooling for different species of the alkali-metal family, with either bright or grey Sisyphus cooling, in the table V.20. The essential point to note is that, with the variety of mechanism, one can systematically achieve a rms velocity of the order of a few recoil velocities, typically between 2 and 4 v_r. Finally, it should be noted that the temperatures given here are those measured for very dilute gases, in which collective effects such as multiple scattering play no role. We will return to these effects in the final chapter of this course.

Chapter VI

Optical lattices and sideband cooling

In previous chapters, we explored various cooling mechanisms for free atoms: Doppler cooling, velocity selective coherent population trapping, Raman and Sisyphus cooling. With the exception of Doppler cooling on a broad line, all these mechanisms have a limit, the scale of which is given by the recoil velocity $v_{\mathrm{r}} = \hbar k/M$. Some mechanisms allows one to reach velocity distributions with a width lower than v_{r}, while others like Sisyphus cooling lead to widths of a few v_{r}. These results are obtained for very dilute gases, in which collective effects play a negligible role.

One of the major challenges of experiments with cold atoms is to reach the quantum regime for the gas, in which the different wave packets, of a size given by the thermal wavelength of the gas, overlap. Let us go back to the conditions we need to achieve for this. Consider a gas with r.m.s. velocity $v_0 = v_r$, i.e. $k_{\mathrm{B}}T = Mv_{\mathrm{r}}^2 = \hbar^2k^2/M$. The thermal wavelength λ_T of the gas is related to the optical wavelength $\lambda = 2\pi/k$ by

$$\lambda_T = \frac{\hbar\sqrt{2\pi}}{\sqrt{Mk_{\mathrm{B}}T}} = \frac{\lambda}{\sqrt{2\pi}}, \tag{VI.1}$$

and the quantum degeneracy threshold of the gas is obtained for a density

$$n \approx \lambda_T^{-3} = (2\pi)^{3/2}\,\lambda^{-3}. \tag{VI.2}$$

For an optical wavelength of the order of $0.7\,\mu$m, this corresponds to $n \approx 50$ atoms/μm^3.

Achieving such a high density in the presence of laser cooling beams is a challenge that has never been met for an atomic gas of uniform density. The main obstacles are multiple photon scattering in the gas, as well as inelastic light-assisted collisions between atoms. The only successful strategy so far is that adopted in Innsbruck by Stellmer, Pasquiou, et al. (2013) and described in detail in Chapter 3: a small part of the volume occupied by atoms was confined in a high-stiffness trap and simultaneously made transparent to cooling light; this yielded a Bose-Einstein condensate containing around $1\,\%$ of the total atom number present in the trap.

The aim of this chapter is first to review the limits imposed by collective effects induced by light, in particular the multiple scattering of spontaneously emitted photons. We will examine some of the remedies that have been proposed, such as confinement in a trap with a high oscillation frequency. This leads naturally to the last cooling mechanism we will discuss in this lecture series: sideband cooling, well suited to an assembly of atoms confined to the sites of an optical lattice. And finally, since the major obstacle to obtaining degenerate gases is the multiple scattering of photons emitted spontaneously during cooling, we will end this chapter by tackling a recurring question in the field: is spontaneous emission, which is at the root of the multiple scattering problem, indispensable to laser cooling of atoms?

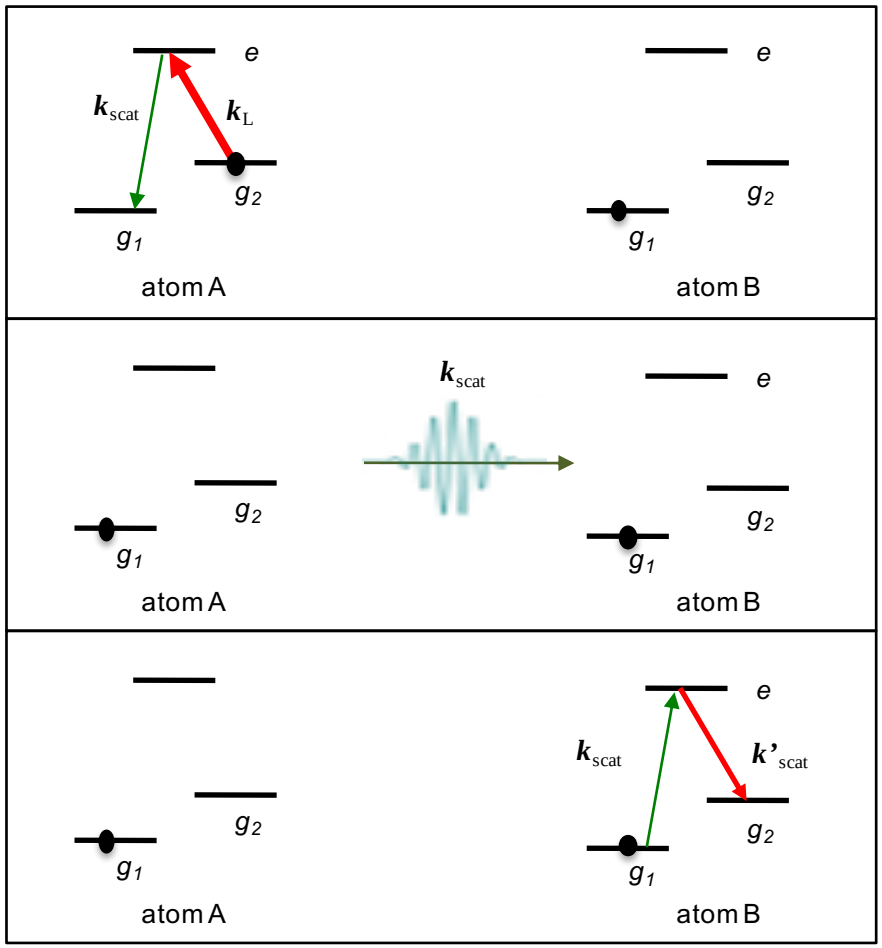

Figure VI.1. *An example of the difficulties associated with multiple scattering in the case of Raman cooling. We start from the situation where an atom B is in the desired state g_1 and we wish to pump the atom A as well. Once the pumping of atom A has taken place, the emitted photon can be absorbed by atom B, thus cancelling out the gain of the first process and causing further heating due to recoil in the scattering process $\boldsymbol{k}_{\rm scat} \rightarrow \boldsymbol{k}'_{\rm scat}$.*

1 Collective effects and multiple scattering

We have already come across the problem of multiple scattering several times in the previous chapters. Let us briefly recall its origins by taking the example of Raman cooling, where atoms have to be optically pumped from one internal state g_2 to another g_1 (figure VI.1). First, an atom A absorbs a photon from the laser in charge of this optical pumping and spontaneously emits a photon through a Raman scattering process:

$$|A : g_2\rangle + \boldsymbol{k}_{\rm L} \longrightarrow |A : g_1\rangle + \boldsymbol{k}_{\rm scat}, \tag{VI.3}$$

In a second step, the emitted photon with momentum $\hbar\boldsymbol{k}_{\rm scat}$ propagates through the gas of atoms and arrives at an atom B in the state $|g_1\rangle$. There, it can be absorbed, giving rise to another scattered photon with momentum $\hbar\boldsymbol{k}'_{\rm scat}$:

$$|B : g_1\rangle + \boldsymbol{k}_{\rm scat} \longrightarrow |B : g_\alpha\rangle + \boldsymbol{k}'_{\rm scat}, \qquad \alpha = 1, 2, \tag{VI.4}$$

and so on until the photon escapes the medium. Note that after scattering the photon, the atom B may be in the internal state g_1 or g_2. In the second case, the repumping process has contributed nothing: an atom initially in the internal state g_1 (atom B) has simply been removed and another atom (atom A) added.

1-1 The dangers of multiple scattering

Multiple scattering has several effects, all of which are detrimental when it comes to approaching the quantum degeneracy threshold, i.e. obtaining low temperatures and high densities :

- It creates an effective repulsive force between the atoms, which tends to destabilize the trapped cloud. We discussed this effect when studying the magneto-optical trap.
- It tends to bring atoms out of the dark state in the coherent population trapping cooling mechanism, by blurring the coherence between the different internal states that enter the wave function of this dark state.
- It disrupts Raman cooling, and more specifically its repumping phase, as mentioned above.

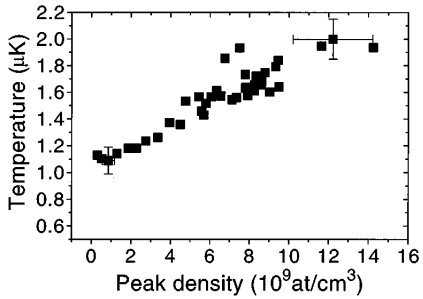

Figure VI.2. *Variation of temperature with atomic density in a Sisyphus cooling experiment with gray molasses. Measurements made on a cloud of cesium atoms by Boiron, Michaud, et al. (1996).*

- It reduces the efficiency of Sisyphus cooling, by breaking the correlation between light shift and optical pumping processes.

In addition, multiple scattering causes random recoil of photon-scattering atoms and creates additional heating. It therefore appears to be a major obstacle to obtaining quantum degeneracy directly from laser cooling (Olshanii, Castin, et al. 1996).

In a number of experiments, an approximately linear variation in temperature with sample density (at a fixed geometry) has been demonstrated. Heating due to multiple scattering is then characterized by the coefficient $\frac{\mathrm{d}T}{\mathrm{d}n}$. For example, for the Sisyphus effect (bright or gray molasses) in a spherical geometry, the typical value for cesium gas is [figure VI.2 and Townsend, Edwards, et al. (1995) and Boiron, Michaud, et al. (1996)]:

$$\frac{\mathrm{d}T}{\mathrm{d}n} \approx 600\ \mathrm{nK}/(10^{10}\ \mathrm{cm}^{-3}), \tag{VI.5}$$

which is considerable [100 times greater than the values given in Chapter 3 for narrow-line Doppler cooling (Katori, Ido, et al. 1999)]. In this regime, starting from a dilute gas that would be cooled at the recoil limit ($v_0 = v_\mathrm{r}$, $T = 200\,\mathrm{nK}$), the temperature would double as soon as the density reaches $3 \times 10^9\ \mathrm{cm}^{-3}$, whereas a density 10^3 to 10^4 times greater would be required to reach quantum degeneracy at this temperature.

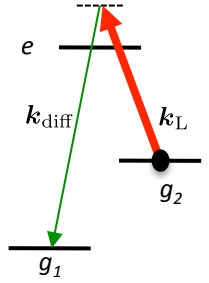

Figure VI.3. *An attempt to reduce the effect of multiple scattering: detuning of the repumping laser beam, which also detunes the spontaneously emitted Raman photons.*

In our study of narrow-line Doppler cooling, we pointed out a (partial) remedy to the problem of multiple scattering: leave the spherical geometry and switch to highly elongated clouds, so that spontaneously emitted photons can rapidly leave the medium by escaping laterally. This remedy also works, at least in part, for Sisyphus cooling: using grey molasses in a very elongated geometry ($600 \times 12 \times 12$ microns), Boiron, Michaud, et al. (1998) obtained a temperature of $\sim 2\,\mu$K for a central density of $10^{12}\,\mathrm{cm}^{-3}$.

1-2 A simple remedy...that does not work

How can we get around the problem of multiple scattering? Consider the Raman cooling process and its optical pumping phase, which brings the atom back from g_2 to g_1, shown in figure VI.1. One might naively think that it would be enough to sufficiently detune the light beam $\boldsymbol{k}_\mathrm{L}$ with respect to the resonance $g_2 \leftrightarrow e$ to diminish the potential harm of the emitted fluorescence photon (figure VI.3). Indeed, by conservation of energy, this photon will also be detuned from the frequency of the $g_1 \leftrightarrow e$ transition. Unfortunately, this remedy does not work: paradoxically, the effective absorption cross-section of the emitted photon by atom B remains equal to the maximum permitted value $\sim \lambda^2$, despite the detuned frequency of this photon relative to the atomic resonance!

The reason for this is shown in figure VI.4, already encountered in pre-

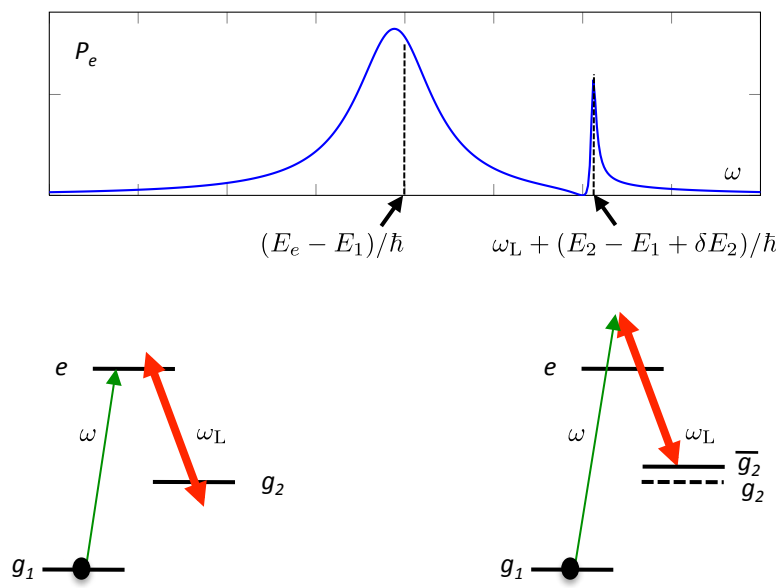

Figure VI.4. *Scattering of a photon of frequency ω in a Λ system when a laser at frequency ω_L drives the transition $g_2 \leftrightarrow e$. The population of the excited state P_e has two maxima as ω is varied: the first corresponds to the simple resonance $g_1 \leftrightarrow e$, the second to resonant Raman scattering involving the state $\bar{g}_2$, i.e. the state g_2 displaced by the laser.*

vious chapters. When a laser beam of frequency ω_L "dresses" the atomic transition $g_2 \leftrightarrow e$ and the transition $g_1 \leftrightarrow e$ is probed with another light at frequency ω of arbitrarily low intensity, the population of the excited atomic state has two maxima. The first, easy-to-understand maximum corresponds to a probe photon in resonance with the transition $g_1 \leftrightarrow e$ (with a slight light shift from the bare transition due to the laser at frequency ω_L):

$$\hbar\omega \approx E_e - E_1. \tag{VI.6}$$

The other, more subtle maximum is obtained for (figure VI.4):

$$\hbar\omega = \hbar\omega_L + E_2 - E_1 + \delta E_2 \tag{VI.7}$$

where δE_2 is the light shift of the level g_2 induced by the laser ω_L. This is the condition for Raman resonance between the state $|g_1\rangle$ and the state $|\bar{g}_2\rangle$, displaced by the laser ω_L. This resonance corresponds to a Fano profile already discussed in Chapter 4 (Lounis & Cohen-Tannoudji 1992). The high population value of the state e corresponds to a large absorption cross-section of the photon ω. This is exactly the frequency at which the photon is emitted in the process shown in figure VI.3.

Finally, for a gas of uniform density, the only (partial) remedies to multiple scattering demonstrated to date are:

- choose a narrow transition and take advantage of the robustness of Doppler cooling to still achieve appreciable phase-space densities,
- take a geometry that limits the mean free path of a photon in the sample, for example very elongated cigar-shaped geometries so that the photon can escape laterally.

We will see in the next paragraph that the situation is favorably modified in a trap.

1-3 The *Festina lente* regime

The *festina lente* regime, initially proposed by Cirac, Lewenstein, et al. (1996) and further developed by Castin, Cirac, et al. (1998), involves placing atoms in a harmonic trap with a high oscillation frequency Ω. More precisely, we consider the situation where

$$\Omega \gg \gamma, \tag{VI.8}$$

γ being the fluorescence rate caused by the cooling and the repumping lasers.

For a pair of trapped atoms, heating during multiple scattering manifests itself as follows: atoms a and b are initially on vibrational levels n_a and n_b (figure VI.5). After an optical pumping process, the atom a is transferred to the level n'_a and a photon is emitted. The atom b can scatter this photon and move to the level n'_b. If $n'_a + n'_b = n_a + n_b$, the energy of the pair of atoms is the same as initially, so nothing serious has happened. On

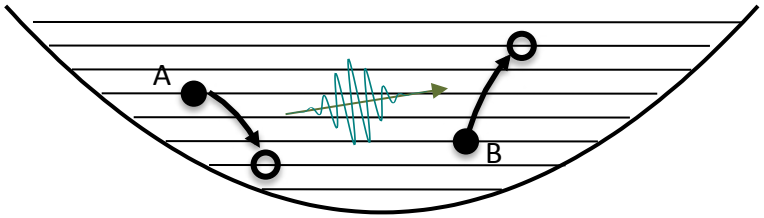

Figure VI.5. *An example of the effect of multiple scattering for trapped atoms. An atom A goes from n_a to n'_a during a cooling process involving the spontaneous emission of a photon. This photon can be scattered by atom B, which passes from n_b to n'_b. If $n'_a + n'_b > n_a + n_b$ (which is the case in this figure), the energy of the pair of atoms A–B has increased, which is unfavorable.*

the other hand, if $n'_a + n'_b > n_a + n_b$, the energy of the pair of atoms has increased, and this heating, if repeated several times before the photon exits the sample, will severely degrade cooling performance.

The argument of Cirac, Lewenstein, et al. (1996) is semi-qualitative: the authors uses a reasoning based on the master equation within the rotating field approximation to justify the fact that heating terms due to reabsorption processes must have a reduced contribution when the condition (VI.8) is realized. More precisely, these terms correspond to a rapid rotation of the coefficients in the master equation, as they oscillate at the frequency $(n'_a + n'_b - n_a - n_b)$ while relaxation takes place at a rate γ. Their contribution therefore becomes negligible in the limit $\Omega \gg \gamma$, except for the secular terms $n'_a + n'_b = n_a + n_b$, which are energetically painless, as mentioned above.

Castin, Cirac, et al. (1998) took up the problem in a more quantitative way; they showed that for two particles placed in an isotropic harmonic trap such as $\gamma \ll \omega \ll \omega_{\rm r}$, the probability of reabsorption $\mathcal{P}$ was strongly decreased in the *festina lente* regime. They considered the case where the average distance between particles r is large in front of the wavelength, i.e. $kr \gg 1$, and found that the result known for free atoms, $\mathcal{P} \sim \sigma/4\pi r^2 \sim 1/(kr)^2$, had to be replaced in the *festina lente* regime by $\mathcal{P} \sim 1/(kr)^3$. The expected gain for the *festina lente* regime is therefore validated by this precise theoretical analysis.

There have been few experimental studies to test, even qualitatively, the predictions made for the *festina lente* regime. We can mention the work of Perrin, Kuhn, et al. (1999), who explored the influence of the power of the repumping beam in a Raman cooling experiment. A temperature reduction of the order of 20% was observed for a variation of γ by a factor of 20. However in this experiment, the pumping rate γ remained higher than the oscillation frequency Ω in the trap: the regime *festina lente* was not yet reached in this experiment.

1-4 Use of an optical lattice

Since the *festina lente* regime requires high oscillation frequencies Ω, it is natural to seek to realize it in an optical lattice formed by superimposing laser standing waves in different directions in space. Depending on the detuning chosen for these waves, atoms are trapped at the nodes or antinodes of the standing waves. The confinement potential of the atoms varies on the optical wavelength scale, and high oscillation frequencies of up to MHz are obtained.

Although the analysis of Castin, Cirac, et al. (1998) does not apply as such to an optical lattice, the intuitively hoped-for gain is indeed present in the experiment: Wolf, Oliver, et al. (2000) studied the Sisyphus cooling of caesium atoms in a deep optical lattice and showed that the heating associated with multiple scattering was greatly reduced (by a factor $\gtrsim 3$) compared with a gas of the same density cooled in free space.

The use of an optical lattice, with the high frequencies Ω it allows, opens the way to the Lamb–Dicke regime, for which

$$\Omega \gg \omega_{\rm r} = \frac{\hbar k^2}{2M}. \qquad \text{(VI.9)}$$

This is a different condition from *festina lente* given in (VI.8), both conditions being in practice realized simultaneously in the lattices we will consider from now on.

2 Sideband cooling

From now on, we consider atoms confined in a harmonic potential $\frac{1}{2}M\Omega^2x^2$ or a periodic potential $V(x) = V_0 \sin^2(kx)$, $V_0 > 0$ (or their equivalent in two or three dimensions). In the case of the periodic potential, the oscillation frequency in the vicinity of a minimum of this lattice is given by $\hbar\Omega = 2\sqrt{V_0 E_\mathrm{r}}$. We assume that the Lamb–Dicke condition

$$\eta \equiv \sqrt{\frac{E_\mathrm{r}}{\hbar\Omega}} \ll 1 \qquad \text{with} \quad E_\mathrm{r} = \hbar\omega_\mathrm{r} = \frac{\hbar^2k^2}{2M} \tag{VI.10}$$

is realized, which imposes the hierarchy of energies in the case of the lattice:

$$E_\mathrm{r} \ll \hbar\Omega \ll V_0. \tag{VI.11}$$

In practice, Lamb–Dicke's condition is easily satisfied in an optical lattice, and it can also be satisfied in an optical tweezer, formed by a highly focused light beam, if it is sufficiently intense. First, we will look at what this condition implies for the absorption and emission of photons by an atom. We will then present the principle of sideband cooling, first for trapped ions, then for neutral atoms.

2-1 The Lamb–Dicke regime

To introduce the important elements that characterize photon absorption and emission processes in the Lamb-Dicke regime, let us consider an elementary process (figure VI.6): an atom (or ion) with two levels, g and e, is prepared in its excited internal state e. We are interested in the final state of the atomic center of mass when the atom has fallen by spontaneous emission into its internal ground state g. We will assume in this paragraph that the atom feels the harmonic potential $\frac{1}{2}M\Omega^2r^2$, independently of its internal state, g or e, the energy levels being (at 1D) $E_n = (n + \frac{1}{2})\,\hbar\Omega$, $n \in \mathbb{N}$.

The initial external state of the atom is an eigenstate of the motion in the trap, characterized by the three vibrational quantum numbers $\boldsymbol{n} \equiv (n_x, n_y, n_z)$. The spontaneous emission of a photon with momentum $\hbar\boldsymbol{k}$ corresponds to

$$|e, \boldsymbol{n}\rangle \longrightarrow |g, \boldsymbol{n}'\rangle + \boldsymbol{k}. \tag{VI.12}$$

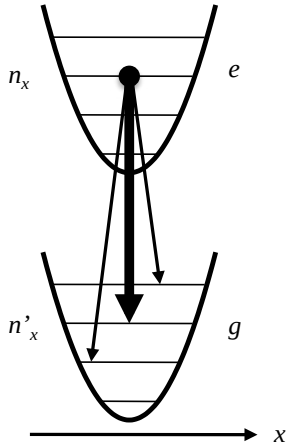

Figure VI.6. *Spontaneous emission of a photon by a two-level atom confined in a harmonic trap. In the Lamb-Dicke limit, the transition with the greatest weight is the line without recoil $n'_x = n_x$. The other two transitions with significant weight correspond to $n'_x = n_x \pm 1$.*

The natural question to ask concerns the possible values of $\boldsymbol{n}'$, for a given triplet $\boldsymbol{n}$. To answer this, we note that the probability of arriving at a level $\boldsymbol{n}'$ involves, via Fermi's golden rule (*cf.* Chapter 1):

$$|\langle \boldsymbol{n}'|\mathrm{e}^{\mathrm{i}\boldsymbol{k}\cdot\hat{\boldsymbol{r}}}|\boldsymbol{n}\rangle|^2, \tag{VI.13}$$

where $\hat{\boldsymbol{r}}$ is the atomic position operator.

The spatial extension of the vibrational state $\boldsymbol{n}$ along a given axis, x for example, is $\approx \sqrt{n_x}\, a_\mathrm{oh}$, where the length

$$a_\mathrm{oh} = \left(\frac{\hbar}{M\Omega}\right)^{1/2} \tag{VI.14}$$

characterizes the extension of the ground state of the harmonic oscillator. Let us restrict ourselves to weakly excited vibrational states, so that $\sqrt{n_x}$ is of order unity. The order of magnitude of the argument of the exponential entering (VI.13), $\boldsymbol{k}\cdot\hat{\boldsymbol{r}}$, is

$$|\boldsymbol{k}\cdot\boldsymbol{r}| \sim ka_\mathrm{oh} \sim \eta \ll 1, \tag{VI.15}$$

where η is defined in (VI.10). We can therefore expand the exponential $\mathrm{e}^{\mathrm{i}\boldsymbol{k}\cdot\hat{\boldsymbol{r}}}$:

$$\mathrm{e}^{\mathrm{i}\boldsymbol{k}\cdot\hat{\boldsymbol{r}}} \approx 1 + \mathrm{i}\boldsymbol{k}\cdot\hat{\boldsymbol{r}}. \tag{VI.16}$$

Let us take a one-dimensional point of view to simplify notation. The position operator $\hat{x}$ is written as a function of the creation and annihilation operators of the harmonic oscillator forming the trap along x:

$$\hat{x} = \frac{a_{\mathrm{oh}}}{\sqrt{2}}\left(\hat{a} + \hat{a}^\dagger\right) \quad \text{hence} \quad k\hat{x} = \eta\left(\hat{a} + \hat{a}^\dagger\right). \tag{VI.17}$$

At order 1 of expansion (VI.16), we only obtain a non-zero matrix element $\langle n'|\hat{x}|n\rangle$ if $|n - n'| = 1$:

$$\langle n+1|\hat{x}|n\rangle = \sqrt{n+1}\,\frac{a_{\mathrm{oh}}}{\sqrt{2}}, \qquad \langle n-1|\hat{x}|n\rangle = \sqrt{n}\,\frac{a_{\mathrm{oh}}}{\sqrt{2}}. \tag{VI.18}$$

From the above we can deduce the type of transitions that are dominant in the Lamb–Dicke regime[1] (figure VI.6):

- Transitions with no change of external state, i.e. $\boldsymbol{n}' = \boldsymbol{n}$, obtained from the first term of (VI.16).
- Transitions with a change of one vibration quantum along one axis, while the other two remain unchanged, for example:

$$n'_x = n_x \pm 1, \quad n'_y = n_y, \quad n'_z = n_z. \tag{VI.19}$$

  These transitions are obtained from the second term of (VI.16), and occur with probability reduced by the factor $\eta^2(n_x+1)$ (for $n'_x = n_x+1$) and $\eta^2 n_x$ (for $n'_x = n_x - 1$) with respect to the transitions $\boldsymbol{n}' = \boldsymbol{n}$.

Note that the predominance of the line $\boldsymbol{n}' = \boldsymbol{n}$ corresponds to a situation formally very close to that of the Mössbauer effect, in which a strongly bound radioactive nucleus in a crystal emits a γ photon with no change in frequency due to recoil.

[1] It can be shown that the average energy increase during the spontaneous emission process is independent of η and always equal to E_{r}.

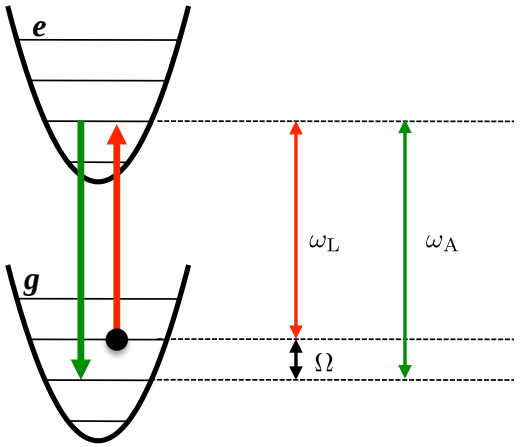

Figure VI.7. *Principle of sideband cooling for a trapped ion. A laser of frequency $\omega_{\mathrm{L}} = \omega_{\mathrm{A}} - \Omega$ causes the ion to change state from $|g, n+1\rangle$ to $|e, n\rangle$. Spontaneous emission occurs preferentially at the $|e, n\rangle \to |g, n\rangle$ transition, so that a quantum $\hbar\Omega$ is dissipated (in the form of photon energy) in this process.*

2-2 Experiments on trapped ions

The first sideband cooling experiment, carried out in Boulder by Diedrich, Bergquist, et al. (1989), succeeded in preparing an ion in the vibrational ground state of the trap. This was a $^{198}\mathrm{Hg}^+$ ion, cooled on the narrow transition $^2S_{1/2} \leftrightarrow {}^2D_{5/2}$ (a long-lived electric quadrupole transition: $\Gamma^{-1} \sim 0.1\,\mathrm{s}$).

The principle of cooling is illustrated in figure 1D. The ion is illuminated by a laser tuned to the transition

$$\text{absorption:} \qquad |g, n+1\rangle \longrightarrow |e, n\rangle, \tag{VI.20}$$

i.e. its frequency is

$$\omega_{\mathrm{L}} = \omega_{\mathrm{A}} - \Omega. \tag{VI.21}$$

This choice gives rise to the name *sideband cooling*: in the ion's rest frame of reference, the absorption frequency is ω_{A}. In the laboratory frame of reference, the ion oscillates at the frequency Ω and its absorption and emission

spectrum is made up of a central band ω_A and sidebands $\omega_A \pm n\Omega$. The cooling laser is tuned to the first sideband on the red side of the resonance.

With the choice (VI.21), the resonant absorption of a photon results in a one-unit decrease in the vibrational quantum number. Once in the excited state $|e, n\rangle$, the ion can fall back into the ground state by spontaneously emitting a photon. In the Lamb–Dicke limit, this emission takes place with a high probability (*cf.* fig. VI.6) on the transition

$$\text{spontaneous emission:} \qquad |e, n\rangle \longrightarrow |g, n\rangle. \tag{VI.22}$$

Each absorption-spontaneous emission cycle thus reduces the vibrational state by one in average, until the ion reaches the vibrational ground state $n = 0$.

The stationary state is characterized by the populations of the different vibrational levels π_n, with $\pi_0 \approx 1$ and $\pi_n \ll 1$ for $n \geq 1$. The ratio between π_0 and π_1 is obtained by equating the fluxes $g, n = 1 \to g, n = 0$ and $g, n = 0 \to g, n = 1$. The first is (figure VI.8, left)

$$|g, n = 1\rangle \to |e, n = 0\rangle \to |g, n = 0\rangle : \qquad \gamma_{1\to 0} \approx \frac{\kappa^2\eta^2}{\Gamma}, \tag{VI.23}$$

where κ is the Rabi frequency of the excitation laser, reduced by the Lamb–Dicke factor η^2 to account for the absorption matrix element $\langle n = 0|\mathrm{e}^{\mathrm{i}kx}|n = 1\rangle$.

The flux $g, n = 0 \to g, n = 1$ is given by non-resonant excitation of the excited states $e, n = 0$ or $e, n = 1$, followed by de-excitation to $g, n = 1$ (figure VI.8, right). The detuning Δ for the excitation process is equal to Ω in the first case and to 2Ω in the second case [*cf.* (VI.21)], so that

$$|g, n = 0\rangle \to |e, n = 0\rangle \to |g, n = 1\rangle \quad : \qquad \gamma^{(a)}_{0\to 1} \approx \frac{\Gamma}{4}\frac{\kappa^2\eta^2}{\Omega^2}, \tag{VI.24}$$

$$|g, n = 0\rangle \to |e, n = 1\rangle \to |g, n = 1\rangle \quad : \qquad \gamma^{(b)}_{0\to 1} \approx \frac{\Gamma}{4}\frac{\kappa^2\eta^2}{(2\Omega)^2}, \tag{VI.25}$$

and the total rate[2] is $\gamma_{0\to 1} = \gamma^{(a)}_{0\to 1} + \gamma^{(b)}_{0\to 1}$. The equality

$$\pi_0\gamma_{0\to 1} = \pi_1\gamma_{1\to 0} \tag{VI.26}$$

[2]The probabilities of the two paths are summed here, not their amplitudes. One can show that this is legitimate since we are taking the average over the momentum carried away by the scattered photon during the optical pumping process.

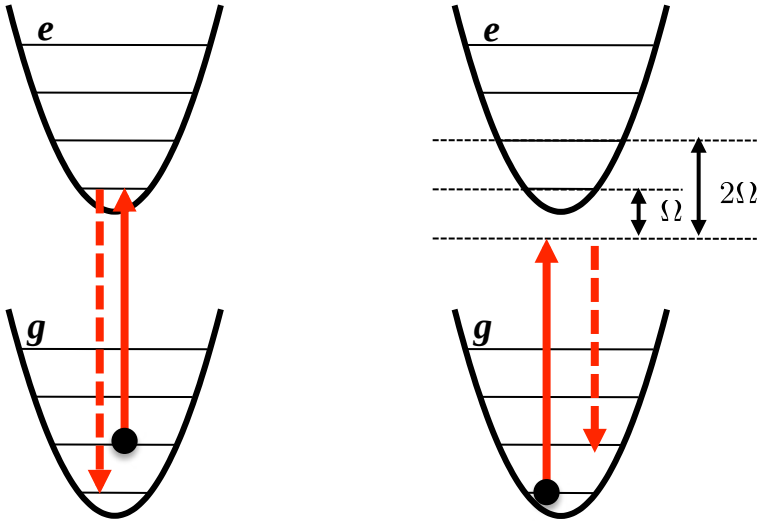

Figure VI.8. *The two processes to consider when determining the steady-state of sideband cooling. Left, flow from $g, n = 1$ to $g, n = 0$. Right, flow from $g, n = 0$ to $g, n = 1$ with two possible relay states.*

then leads to (Wineland & Itano 1979)

$$\frac{\pi_1}{\pi_0} \approx \frac{5}{16}\frac{\Gamma^2}{\Omega^2} \ll 1. \tag{VI.27}$$

The populations of the other excited states ($n = 2, 3, \ldots$) are even smaller than π_1 in the limit $\Gamma \ll \Omega$.

One often uses the value of π_0 to judge the efficiency of sideband cooling, trying to make it as close to 1 as possible. We can also look at the average number of excitations[3]

$$\bar{n} = \sum_n n\pi_n, \tag{VI.28}$$

as well as at equilibrium temperature. It can be shown that the populations

[3]In the limit (VI.27), we have $\bar{n} \approx \frac{\pi_1}{\pi_0} \approx \frac{5}{16}\frac{\Gamma^2}{\Omega^2}$.

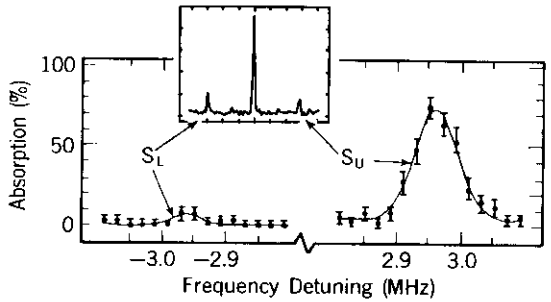

Figure VI.9. *Sideband cooling of a single ion $^{198}Hg^+$. The upper panel shows the spectrum before cooling, with roughly equal weights for the two transitions at $\omega_A \pm \Omega$, corresponding to $|g,n\rangle \longrightarrow |e,n\pm 1\rangle$. The main figure shows the spectrum after cooling: the lower sideband at $\omega_A - \Omega$ is much reduced compared with the upper sideband at $\omega_A + \Omega$. From the relative weight of these two lines, one can deduce the population ratio π_1/π_0 [figure extracted from Diedrich, Bergquist, et al. (1989)].*

π_n follow a Boltzmann law $\pi_n \propto \exp(-n\hbar\Omega/k_B T)$, i.e.

$$\bar{n} = \frac{1}{\exp(\hbar\Omega/k_B T) - 1} \quad \Rightarrow \quad k_B T = \frac{\hbar\Omega}{\ln(1+\frac{1}{\bar{n}})}. \tag{VI.29}$$

In the experiment by Diedrich, Bergquist, et al. (1989), the $^{198}Hg^+$ ion was cooled essentially to the $g, n = 0$ state with $\pi_0 = 0.95$. This was deduced from the absorption spectrum of the trapped ion, which indicated that the first red sideband, corresponding to the $|g,n\rangle \longrightarrow |e,n-1\rangle$ transitions, was much reduced compared with the first blue sideband $|g,n\rangle \longrightarrow |e,n+1\rangle$ (figure VI.9).

The experiment of Diedrich, Bergquist, et al. (1989) required a transition $g \leftrightarrow e$ with a long-lived excited state e, which seems restrictive. However, we have seen in previous chapters that it is possible to replace the direct transition $g \leftrightarrow e$ by a Raman transition $g_1 \leftrightarrow g_2$ via an excited state, and thus obtain an effective two-level system, where the lifetime γ^{-1} of g_2 is adjustable: all that is needed is to change the power of the repumping beam which brings the atoms back from g_2 to g_1. This principle was implemented by Monroe, Meekhof, et al. (1995) following an initial proposal

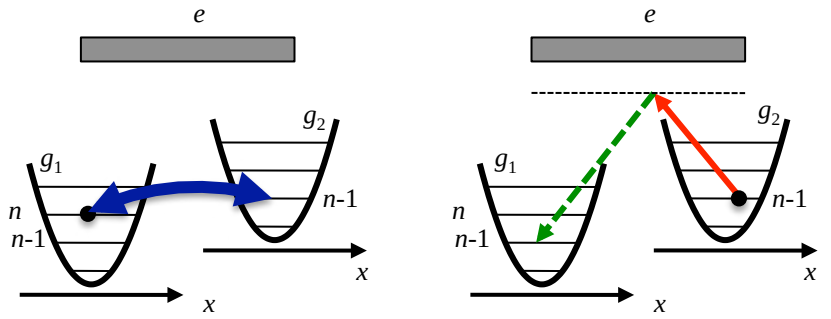

Figure VI.10. *Sideband cooling via a Raman transition. The cooling process has been separated into two phases, although both processes can occur simultaneously. The atom is initially in the internal state g_1 on vibrational level n (1D version). Left: coherent coherent coupling takes it to the internal state g_2 and vibrational level $n-1$. Right: an optical pumping process involving the spontaneous emission of a photon (dotted line) returns the atom to the state g_1. In the Lamb–Dicke regime, this process occurs on average without any change of external state, so that the balance of the cycle is a decrease in the vibrational number by one unit.*

by Heinzen & Wineland (1990). Sideband cooling via a Raman transition is now a standard technique in trapped-ion physics, and leads to an average population of the vibrational ground state greater than 0.99.

2-3 The case of neutral atoms

The principle of sideband cooling for neutral atoms is very similar to that for a trapped ion. The atom is initially in the internal state g_1, which in practice is a Zeeman sublevel of the ground state, and in a vibrational state $\boldsymbol{n} = (n_x, n_y, n_z)$ of the trap confining the atom.

- A coherent coupling, which we will detail in the next paragraph, causes the atom to be transferred to another internal state g_2 and a lower vibrational state, e.g. $\boldsymbol{n}' = (n_x - 1, n_y, n_z)$.
- An optical pumping process brings the atom back from g_2 to g_1 at a rate γ chosen to be small compared with Ω. In the Lamb–Dicke limit,

this optical pumping generally does not modify the vibrational state of the atom, which therefore ends this cycle in the state $|g_1, \boldsymbol{n}'\rangle$: the atom energy has been reduced by the amount $\hbar\Omega_x$, this energy being carried away by the fluorescence photon emitted during the optical pumping from g_2 to g_1.

- This procedure is repeated for the spatial directions y and z.

The main difficulty in implementing this procedure lies in creating a trap of sufficient stiffness. Indeed, the oscillation frequency Ω must be large compared to ω_r and γ, which leads to frequencies $\Omega/2\pi$ of the order of several tens of kHz. As we have already announced, a well-suited method for obtaining such frequencies is to use an optical lattice (see course 2012-13). This lattice can be 1D (Perrin, Kuhn, et al. 1998; Vuletic, Chin, et al. 1998), 2D (Hamann, Haycock, et al. 1998) or 3D (Kerman, Vuletic, et al. 2000; Han, Wolf, et al. 2000).

In all that follows (except in § 2-5), we will treat each lattice site as an independent harmonic well. This approximation is valid when the condition (VI.11) is satisfied, if we restrict ourselves to weakly excited vibrational states: the non-harmonicity of the lattice potential is then negligible, as is tunneling to neighboring wells. A complementary advantage of the optical lattice is that it can cool a large number of atoms simultaneously, in principle up to one atom per lattice site. However, as soon as two atoms are present at the same site, at least in the case of a 3D lattice, light-assisted collisions lead to the loss of this pair of atoms.

It is also possible to achieve sideband cooling in a single well, obtained in an optical tweezer formed by a tightly focused laser beam. Because of the losses just mentioned, at most one atom is present in the tweezer at any time. The first experiments in this direction are recent, and have been carried out in Boulder and at CUA (MIT-Harvard) by Kaufman, Lester, et al. (2012) and Thompson, Tiecke, et al. (2013).

Very recently, the sideband cooling technique has been implemented to image lattice gases (Patil, Chakram, et al. 2014), and observe individual atoms trapped on optical lattice sites in quantum gas microscopy experiments (Cheuk, Nichols, et al. 2015; Parsons, Huber, et al. 2015; Haller, Hudson, et al. 2015) (figure VI.11). These are lithium and potassium atoms (fermionic isotopes) for which Sisyphus-type cooling works poorly due to the hyperfine structure being too small in the excited state (see Chapter 5). Sideband cooling, coupled with high-efficiency imaging, makes it possible to observe individual atoms while freezing their position, to within one period of the optical lattice [4].

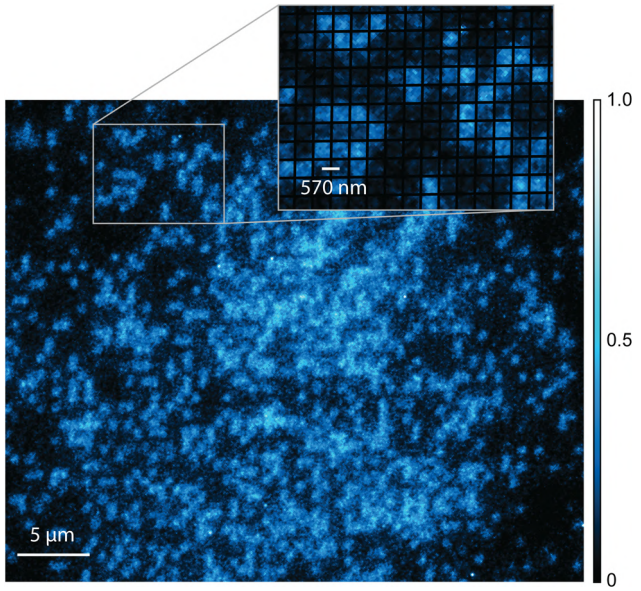

Figure VI.11. *Fluorescence of individual ^{6}Li atoms trapped in a cubic optical lattice and experiencing sideband cooling. The filling factor is about 40% at the center of the cloud [figure extracted from Parsons, Huber, et al. (2015)].*

[4] Haller, Hudson, et al. (2015) uses a variant of sideband cooling, called electromagnetically induced transparency cooling, first proposed by Morigi, Eschner, et al. (2000). There, ones takes advantage of a dark resonance between g_1, n and g_2, n to minimize the influence of transitions without change of the vibrational state, and maximize the desired transitions $g_1, n \to g_2, n-1$.

2-4 How to achieve coherent coupling

Achieving coherent coupling is the trickiest part of implementing sideband cooling for trapped atoms. Let us take a one-dimensional approach to simplify the discussion: we need to find an operator $\hat{W}$ with non-zero matrix elements between $|g_1, n\rangle$ and $|g_2, n-1\rangle$:

$$\langle g_2, n-1|\hat{W}|g_1, n\rangle \neq 0. \tag{VI.30}$$

The operator $\hat{W}$ must therefore change both the atom's internal state ($g_1 \to g_2$) and its external state ($n \to n-1$).

Use of auxiliary laser beams. Conceptually, the simplest way to induce the transition $g_1 \to g_2$ is to use a pair of laser beams inducing a momentum transfer $\hbar\boldsymbol{q}$ (Bouchoule, Perrin, et al. 1999; Han, Wolf, et al. 2000). In this case, the matrix element of the coherent coupling factorizes into

$$\langle g_2, n-1|\hat{W}|g_1, n\rangle = \langle g_2|\hat{W}_{\text{internal}}|g_1\rangle \times \langle n-1|\mathrm{e}^{\mathrm{i}\boldsymbol{q}\cdot\boldsymbol{r}}|n\rangle \tag{VI.31}$$

and the spatial part is simply calculated in the Lamb–Dicke regime. The direction of the vector $\boldsymbol{q}$ must be alternated along to three orthogonal axes to obtain a 3D cooling (Han, Wolf, et al. 2000).

Use of a radio-frequency wave. To change the internal state, a radio-frequency (or microwave) transition can do the trick. But as the wavelength of this radio-frequency is very long compared to the extension of the vibrational states, the action of $\hat{W}$ on the atomic external variables is essentially negligible, so that

$$\text{radio-frequency:} \qquad \langle g_2, n-1|\hat{W}|g_1, n\rangle = \langle g_2|\hat{W}|g_1\rangle \times \langle n-1|n\rangle = 0 \tag{VI.32}$$

because the vibrational states $|n-1\rangle$ and $|n\rangle$ are orthogonal.

However, it is possible to get around this difficulty by spatially shifting the bottom of the potential wells of g_2 with respect to those of g_1, so that the vibrational state $|n\rangle_1$ (for the internal state g_1) is not centered in the same place as $|n\rangle_2$ (for the internal state g_2). We then have:

$$\text{radio-frequency (again) :} \qquad \langle g_2, n-1|\hat{W}|g_1, n\rangle = \langle g_2|\hat{W}|g_1\rangle \times {}_2\langle n-1|n\rangle_1 \neq 0. \tag{VI.33}$$

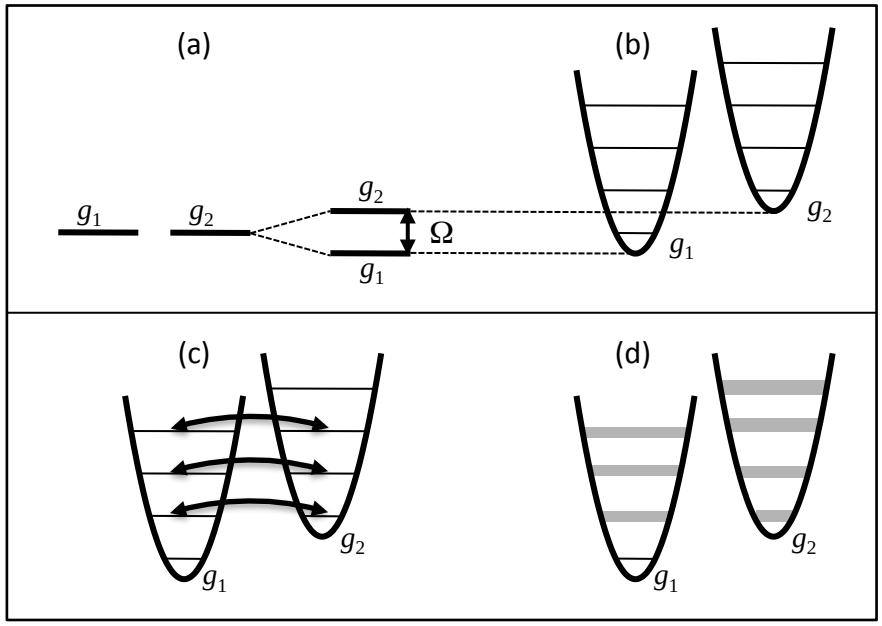

Figure VI.12. *The four steps leading to sideband cooling via the vector component of the light-shift operator (see text). This method has been implemented by Hamann, Haycock, et al. (1998) and Kerman, Vuletic, et al. (2000).*

This method is known as projective sideband cooling and has been implemented[5] in 1D by Förster, Karski, et al. (2009), then in 3D by Li, Corcovilos, et al. (2012). The spatial shift between the potential wells for the two internal states g_1 and g_2 is obtained by taking advantage of the fact that the light-shift operator, which creates the optical lattice potential, has a vector component which, for alkaline atoms, is significant if the laser creating the lattice is not too far from the atomic resonance: the light potential then depends on the internal state, which is the desired condition.

[5] Perrin, Kuhn, et al. (1998) used a Raman transition induced by two laser beams to couple g_1 and g_2, but these beams propagated in the same direction and did not induce spatial coupling. Their action was therefore equivalent to a radio-frequency coupling.

Use of the optical lattice itself. Since the light-shift operator at the origin of the lattice can have a vector component that couples the different Zeeman states, one can take advantage of it in the following way [Hamann, Haycock, et al. (1998) and Kerman, Vuletic, et al. (2000)]:

- One fixes a target value for the oscillation frequency Ω and apply a static magnetic field that shifts the energy of g_2 relative to g_1 by about $\hbar\Omega$. Here, g_1 and g_2 are two Zeeman sublevels of the same hyperfine level, e.g. $|g_1\rangle = |F, m_F = F\rangle$ and $|g_2\rangle = |F, m_F = F-1\rangle$ (figure VI.12a).

- The optical lattice is applied. The scalar component of the light-shift operator, which is the dominant term, creates identical potential wells for g_1 and g_2 with frequency Ω. In combination with the effect of the static magnetic field, the states $|g_2, n\rangle$ are therefore at the same level as the states $|g_1, n+1\rangle$ (figure VI.12b).

- Consider now the vector component of the light-shift operator within a given multiplicity $\{|g_1, n+1\rangle, |g_2, n\rangle\}$: the energy eigenstates in the lattice are not factorized in the form $|g_i, n\rangle$, but are superpositions $\alpha|g_1, n+1\rangle + \beta|g_2, n\rangle$. The only state that remains factorized is the state $|g_1, 0\rangle$, as there is no state involving g_2 in its immediate vicinity (figure VI.12c).

- An optical pumping beam is applied, destabilizing the state g_2 and repumping the atoms back to g_1. The atomic eigenstates in the lattice thus acquire a finite lifetime as they are contaminated by g_2, with the exception of the ground state $|g_1, 0\rangle$ (figure VI.12d). The desired dark state is thus obtained.

Most exploratory experiments on sideband cooling in optical lattices have been carried out with cesium atoms. Performance after optimization is comparable from one experiment to the next. In one and two dimensions, populations $\pi_0 > 95\,\%$ were observed by Hamann, Haycock, et al. (1998), Morinaga, Bouchoule, et al. (1999) and Förster, Karski, et al. (2009). In three dimensions, Kerman, Vuletic, et al. (2000) and Li, Corcovilos, et al. (2012) obtained $\pi_0 \sim 80\,\%$.

2-5 Adiabatic opening of a lattice

The temperature of the atoms after sideband cooling is given by (VI.29). Unless we succeed in producing an average excitation number $\bar{n}$ extremely small in front of 1, this temperature is generally of order Ω. These are therefore relatively high temperatures, since large values of Ω (compared with ω_r, for example) are required for sideband cooling to work properly.

Nevertheless, once the atoms have been cooled in an optical lattice, a simple way of lowering their temperature (without changing the entropy of the gas) is to adiabatically lower the lattice depth (Kastberg, Phillips, et al. 1995; Kerman, Vuletic, et al. 2000). Starting with atoms cooled in the ground state $n = 0$ at the lattice nodes, we show below that this leads to a velocity distribution whose width is below the recoil limit. We will only outline the reasoning here, and refer readers to the 2012-13 course (Chapter 2), where the physics of optical lattices was studied in more detail.

Since the potential of the optical lattice is periodic, the proper tool for analyzing the dynamics of an atom is the formalism deduced from Bloch's theorem. Let us consider once again the 1D case to simplify notation, and write the lattice potential $V(x) = V_0 \sin^2(kx)$, with period $a = \lambda/2 = \pi/k$. Bloch's theorem indicates that we can search for the eigenstates of the single-atom Hamiltonian in the form of Bloch states $\psi_{n,q}(x) = \mathrm{e}^{\mathrm{i}qx}\, u_{n,q}(x)$, where the function $u_{n,q}$ is periodic of period a and the quasi-moment q is chosen in the first Brillouin zone

$$-\pi/a < q \leq \pi/a \quad \Leftrightarrow \quad -k < q \leq k. \tag{VI.34}$$

The index $n = 0, 1, 2, \cdots$ marks, for a fixed quasi-momentum q, the different energy states ranked in ascending order. When q varies in the Brillouin zone, we obtain for a given n an energy band $E_n(q)$ (figure VI.13).

Choosing a high oscillation frequency for the Lamb–Dicke regime [condition (VI.11)] implies that the lattice depth V_0 is large compared to the gap between two consecutive bands, which is of order $\hbar\Omega$ for weakly excited bands. The width of the bands, determined by the tunneling effect from a given well to the neighboring wells, is then very small compared to Ω and these bands are almost flat, with energy equal to $(n+\frac{1}{2})\hbar\Omega$: each lattice site can be treated as a harmonic well in which the atom is trapped, unable to jump to a neighboring site.

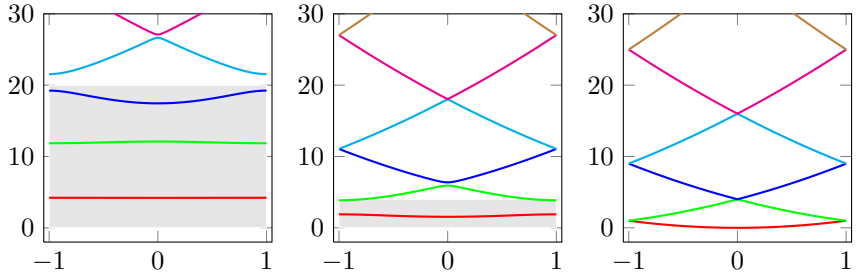

Figure VI.13. *First energy bands $E_n(q)$ (unit $E_\mathrm{r} = \hbar^2k^2/2m$), as a function of q/k for the potential $V(x) = V_0 \sin^2(kx)$. From left to right, V_0/E_r =(20, 4,0). The shaded rectangle represents the energy zone below the height of potential V_0.*

After sideband cooling, let us assume that each atom has been placed in the ground state of a lattice site (our reasoning can easily be generalized to the case $\bar{n} \neq 0$). We make no assumptions about the filling rate of the lattice, and neglect any coherence phenomena between different sites. The density operator describing this situation is a statistical mixture of the different states $\psi_{n,q}(x)$ with $n = 0$ and with q uniformly distributed in the first Brillouin zone:

$$\hat{\rho} \propto \int_{-k}^{+k} |\psi_{0,q}\rangle\langle\psi_{0,q}| \, \mathrm{d}q. \tag{VI.35}$$

When we decrease the depth of the lattice, i.e. vary the amplitude of the potential as $V(x,t) = V_0(t)\sin^2(kx)$, we retain the periodic nature of the problem. This remains true even when the potential is completely extinguished, since the potential $V(x) = 0$ can be seen as a potential of period a and zero amplitude. In the case $V_0 = 0$, the energy bands are obtained simply by starting with the energy of a free particle $E(p) = p^2/2M$, then folding this parabola. To do this, we write the momentum in the form $p = \hbar(q + 2jk)$, with $j \in \mathbb{Z}$ and q in the first Brillouin zone (figure VI.13, right).

Since the potential retains its periodic nature with period a, Bloch's theorem continues to apply at every instant of the decompression. More precisely, starting from a Bloch state $|\psi_{0,q}\rangle$, the atom will remain in a Bloch state $\mathrm{e}^{\mathrm{i}qx}u(x)$, where $u(x)$ is a periodic function: the quasi-moment q is

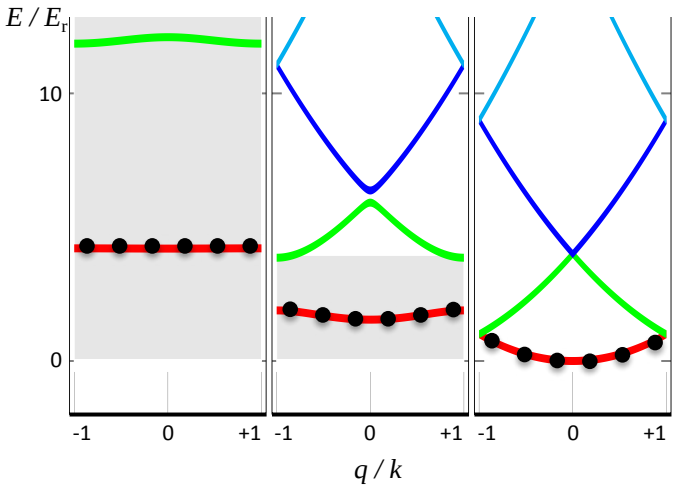

Figure VI.14. *Adiabatic opening of an optical lattice. Atoms initially occupy the ground band of the optical lattice, with all quasi-momenta q equally populated. When the lattice intensity is decreased, the periodicity of the problem entails that the quasi-momentum is conserved. If the intensity variation is sufficiently slow, the atoms remain on the ground band until the lattice is completely extinguished.*

therefore a constant of motion. For decompression to be accompanied by optimum cooling, we simply need to ensure that the lattice is extinguished slowly enough for the transfer from the ground band to the excited bands (at a given q) to be negligible (figure VI.14). The criterion for this, established in the 2012-13 course, is that the extinction time τ should be large in front of $1/\omega_\mathrm{r}$.

When this condition is met, the final state is the same statistical mixture as (VI.35), but with the energy of a state $|\psi_{0,q}\rangle$ corresponding to the case of the free particle $E(q) = \hbar^2q^2/2M$. Since the initial quasi-momentum q is randomly and uniformly distributed in the Brillouin zone, the mean kinetic energy after lattice extinction is:

$$\frac{1}{2}M\langle v^2\rangle = \frac{1}{2k}\int_{-k}^{+k} \frac{\hbar^2q^2}{2M} \, \mathrm{d}q = \frac{1}{6}Mv_\mathrm{r}^2. \tag{VI.36}$$

Cooling the atoms in the ground state of each lattice site therefore offers

the possibility, via adiabatic opening, of producing a gas at subrecoil temperature, with a r.m.s. velocity $v_0 \approx 0.6\, v_\mathrm{r}$.

On a practical level, sideband cooling followed by adiabatic lattice decompression was studied by Kerman, Vuletic, et al. (2000). The fraction of atoms in the ground band after cooling was $\sim 80\%$ and the r.m.s. velocity after adiabatic decompression $1.2\, v_\mathrm{r}$. Kerman, Vuletic, et al. (2000) also measured the variation of temperature with atomic density, and their result clearly illustrates the gain made by the lattice in reducing the adverse effects of multiple scattering. They found

$$\frac{\mathrm{d}T}{\mathrm{d}n} \approx 8\ \mathrm{nK}/(10^{10}\,\mathrm{cm}^{-3}), \tag{VI.37}$$

which is 100 times smaller than the result (VI.5) found for Sisyphus cooling.

Lattice opening and interactions. Our reasoning concerning adiabatic lattice opening has been made in the limit where interactions between atoms play a negligible role during opening. The final state is then a gas of low kinetic energy (below the recoil limit), but not condensed. This is because two atoms initially occupying two distinct lattice sites are in orthogonal quantum states (the Wannier functions associated with each site). In the absence of interaction, they will remain in orthogonal states during the Hamiltonian evolution describing the opening. There can thus be no macroscopic accumulation of particles in an individual state in this case.

The approximation of neglecting interactions is legitimate if the lattice filling factor is low [10^{-3} in the experiment of Kerman, Vuletic, et al. (2000)]. On the other hand, if one starts from a situation with all sites occupied by an atom and in the presence of repulsive interactions, the initial state can be seen as a Mott insulator with unit filling factor. Adiabatic decompression of the lattice in the presence of interactions should then lead to a condensed, superfluid phase with zero temperature.

3 Can we do without spontaneous emission?

In this course, we have reviewed a number of more or less complex mechanisms for increasing the phase-space density of an assembly of atoms, whether free or trapped. Common to all these mechanisms is the phenomenon of spontaneous emission. It is thanks to this that we have been able to reduce the disorder of the gas, entropy being transferred to the modes of the electromagnetic field. But this spontaneous emission also imposes limits on cooling.

- At the fundamental level, several of these mechanisms lead to a r.m.s. velocity v_0 of the order of the recoil velocity v_r, due to the random nature of the recoils taken by the atom when it spontaneously emits a photon.
- On a practical level, spontaneously emitted photons can undergo multiple scatterings before leaving the sample, creating additional heating that can be considerable for dense gases, as we recalled in § 1.

This brings us to a natural question: is spontaneous emission really essential for radiative cooling? Even if the intuitive answer to this question is yes, we shall see that there are nuances to it. On the other hand, some authors believe they have experimentally observed (slight) cooling of a gas of atoms without spontaneous emission (Corder, Arnold, et al. 2015). In the absence of precise information on these very recent experiments, we will not discuss them here in detail, but we will set out in this final section a number of results that restrict the type of effects that can be expected.

3-1 Hamiltonian evolution of a gas without interaction

The Hamiltonian evolution of a gas of N non-interacting atoms cannot lead to an increase in its phase-space density or in the occupancy of any individual quantum state. We have already detailed this point in the introductory chapter of the course [see also Ketterle & Pritchard (1992)]. If the Hamiltonian is written as a sum of one-particle Hamiltonians

$$\hat{\mathcal{H}}(t) = \sum_{n=1}^{N} \hat{H}^{(n)}(t), \tag{VI.38}$$

then the evolution of the single-particle density operator is unitary and its eigenvalues are constant over time: we can neither increase nor decrease

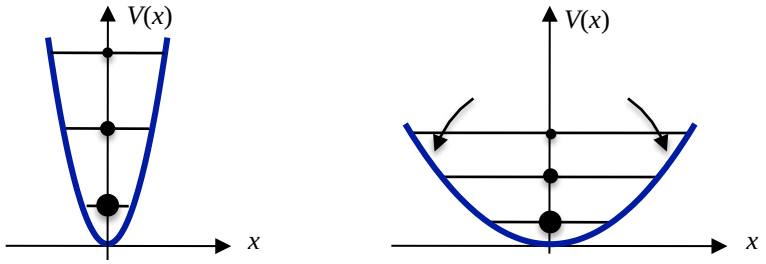

Figure VI.15. *Adiabatic opening of a harmonic trap: the population of each quantum state remains constant.*

the occupancy of a given state, but simply convert one state into another. For example, by adiabatically opening a trap, it is possible to convert states of low spatial extension x_0 and high r.m.s. velocity v_0, into states of large x_0 and low v_0. The temperature, defined by $k_{\mathrm{B}}T = Mv_0^2$, then decreases, but each quantum state in the trap retains its population (figure VI.15).

3-2 Atoms and quantized electromagnetic fields

When a set of atoms is coupled to the quantized electromagnetic field, the Hamiltonian of the system is richer than (VI.38). Let us restrict ourselves to the single-atom case and use the electric dipole approximation to describe the atom-field coupling. The total Hamiltonian is written:

$$\hat{H} = \hat{H}_A + \hat{H}_F - \hat{\boldsymbol{D}} \cdot \hat{\boldsymbol{E}}(\hat{\boldsymbol{r}}), \tag{VI.39}$$

where $\hat{H}_A$ and H_F represent the Hamiltonians of the atom and of the free electromagnetic field. The atom Hamiltonian is

$$\hat{H}_A = \frac{\hat{\boldsymbol{p}}^2}{2M} + \hat{H}_{A,\mathrm{intern}}. \tag{VI.40}$$

In these expressions, $\hat{\boldsymbol{r}}$ and $\hat{\boldsymbol{p}}$ represent the position and momentum operators of the atom center of mass, $\hat{H}_{A,\mathrm{intern}}$ is the Hamiltonian describing the evolution of the atom internal variables and $\hat{\boldsymbol{D}}$ its electric dipole operator. In the simple two-level model of the atom we have used many times in this lecture series, the dipole operator is written as

$$\hat{\boldsymbol{D}} = \boldsymbol{d}\,|e\rangle\langle g| + \mathrm{H.c.} \tag{VI.41}$$

where the vector $\boldsymbol{d}$ represents the reduced dipole of the transition. The field modes are characterized by their wave vector $\boldsymbol{k}$ (with $\omega = ck$) and polarization $\boldsymbol{\epsilon}$, and each mode is indexed by the compact notation $\lambda \equiv (\boldsymbol{k}, \boldsymbol{\epsilon})$. The Hamiltonian of the free electromagnetic field is

$$\hat{H}_F = \sum_\lambda \hbar\omega\ \hat{a}_\lambda^\dagger \hat{a}_\lambda \tag{VI.42}$$

where $\hat{a}_\lambda^\dagger$ and $\hat{a}_\lambda$ are the photon creation and annihilation operators in the mode λ. Finally, the electric field operator $\hat{\boldsymbol{E}}(\boldsymbol{r})$ is written as

$$\hat{\boldsymbol{E}}(\boldsymbol{r}) = \sum_\lambda \mathcal{E}_\lambda\, \boldsymbol{\epsilon}\, \hat{a}_\lambda\, \mathrm{e}^{\mathrm{i}\boldsymbol{k}\cdot\boldsymbol{r}} + \mathrm{H.c.} \qquad \text{with} \quad \mathcal{E}_\lambda = \mathrm{i}\sqrt{\frac{\hbar\omega}{2\epsilon_0 L^3}}, \tag{VI.43}$$

where L^3 represents the quantization volume, and the wave vectors $\boldsymbol{k}$ are $\boldsymbol{k} = \frac{2\pi}{L}\boldsymbol{n}$, $\boldsymbol{n} \in \mathbb{Z}^3$.

When no light beam reaches the atom, the electromagnetic field is the vacuum state, in which no mode is populated:

$$|\mathrm{vac}\rangle = \prod_\lambda |0\rangle_\lambda. \tag{VI.44}$$

When the atom is illuminated by a beam of light, some modes of the electromagnetic field are occupied. The absorption and stimulated emission processes correspond to the destruction and creation of photons in these occupied modes, while the phenomenon of spontaneous emission corresponds to the creation of photons in initially empty modes[6].

3-3 Use of a non-classical field

If no additional constraints are placed on the field state, it is possible to find situations where cooling (in the sense of accumulation in the same quantum state) occurs without populating radiation modes that would initially

[6] More precisely, the probability of creating a photon in a mode λ already containing n_λ photons will be proportional to $n_\lambda + 1$: the term n_λ is due to stimulated emission and the term "1" to spontaneous emission.

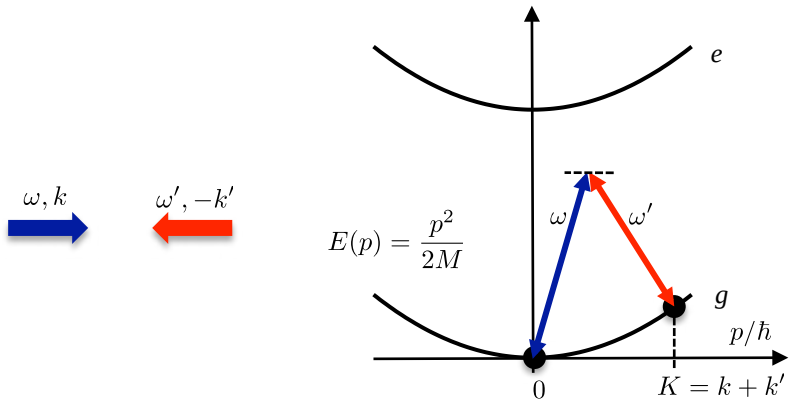

Figure VI.16. *1D laser configuration with two counterpropagating running waves of frequency ω and ω' inducing a resonant transition between the zero momentum state $p = 0$ and the momentum state $p = \hbar K$ with $K = k + k'$.*

be empty. Let us take a 1D example, illustrated in figure VI.16. An atom is illuminated by two counter-propagating beams of frequency $\omega = ck$ and $\omega' = ck'$ chosen such that $\omega - \omega' = \hbar K^2/(2M)$ with $K = k + k'$, so that the Raman transition between the zero momentum state $p = 0$ and the momentum state $p = \hbar K$ occurs resonantly. The detuning from the excited state can be assumed to be large enough to neglect the population of this state. Similarly, for sufficiently weak atom-light coupling, we can neglect the non-resonant processes that would lead to the population of $p = n\hbar K$ states with $n \neq 0, 1$.

First, let us assume that the initial state of the atom + field system is

$$|\psi(0)\rangle = |p = 0\rangle \otimes |N, N'\rangle, \tag{VI.45}$$

with N photons in the mode ω and N' photons in the mode ω'. Note that this notion of explicitly defining the number and momentum of photons in a given mode only makes sense if these modes are defined by a physical (ring) cavity, which we will assume from now on. The state of the system at time t can be written as

$$|\psi(t)\rangle = \alpha(t)|p = 0\rangle \otimes |N, N'\rangle + \beta(t)|p = \hbar K\rangle \otimes |N - 1, N' + 1\rangle \tag{VI.46}$$

since the atom goes from $p = 0$ to $p = \hbar K$ by absorption of a photon in the mode ω and stimulated emission of a photon in the mode ω'. The corresponding matrix element is deduced from the action of the operators $\hat{a}'^{\dagger}\hat{a}$ and is therefore proportional to $\sqrt{N(N'+1)}$. Starting from $p = 0$ at time $t = 0$, the probability of finding the atom in state $p = 0$ at time t can then be written as

$$P(p = 0 : t|p = 0 : 0) = \cos^2\left(\sqrt{N(N'+1)}\,\alpha_0 t\right), \tag{VI.47}$$

where the parameter α_0 is $\alpha_0 = \kappa_0^2/(4\Delta)$, κ_0 being the single-photon Rabi frequency characterizing the atom-light coupling, and Δ the detuning of ω and ω' from the atomic resonance frequency ($|\Delta| \gg \omega_r, \Gamma$).

Now let us assume that the initial state of the atom + field system is

$$|\psi(0)\rangle = |p = \hbar K\rangle \otimes |N, N'\rangle. \tag{VI.48}$$

A similar reasoning indicates that the state at time t is of the form

$$\psi(t)\rangle = \gamma(t)|p = \hbar K\rangle \otimes |N, N'\rangle + \delta(t)|p = 0\rangle \otimes |N + 1, N' - 1\rangle \tag{VI.49}$$

with absorption in the mode ω' and stimulated emission in the mode ω. The probability of finding the atom in the momentum state $p = 0$ at time t, knowing that the atom was in the momentum state $p = \hbar K$ at time 0, is therefore as follows

$$P(p = 0 : t|p = \hbar K : 0) = \sin^2\left(\sqrt{(N+1)N'}\,\alpha_0 t\right). \tag{VI.50}$$

We can then choose a pair N, N' and a value of the parameter $\alpha_0 t$ such that[7]:

- The atom initially in state $p = 0$ has a probability close to 1 of still being in this state at time t:

$$\sqrt{N(N'+1)}\,\alpha_0 t \approx 0 \bmod \pi. \tag{VI.51}$$

- The atom initially in the $p = \hbar K$ state has a probability close to 1 of being in the $p = 0$ state at time t :

$$\sqrt{(N+1)N'}; \alpha_0 t \approx \frac{\pi}{2} \bmod \pi. \tag{VI.52}$$

[7]For example $\alpha_0 t = \pi/10$, $N = 10^2$, $N' = 10^4$.

Starting from a density matrix for the atom corresponding to a statistical mixture with weight $1/2$ for $p = 0$ and $p = \hbar K$, we find at time t a density matrix where the population of the state $p = 0$ has become close to 1. In other words, thanks to the laser field initially prepared in the Fock state $|N, N'\rangle$ (a non-classical state!), we have succeeded (without emitting photons in the initially empty modes) in reducing the initial disorder of the atom's momentum distribution, by transferring this disorder to the light field.

Note. To write that the above process operates without spontaneous emission may be considered as a misuse of language: the argument is based on the difference between N and $N+1$ (or N' vs. $N'+1$). However, the physical origin of this difference corresponds precisely to spontaneous emission in the mode ω (or ω'). It is therefore correct to say that there are no photons created in the empty radiation modes, but abusive to say that spontaneous emission plays no role at all[8].

3-4 And with a coherent state?

The example in the previous paragraph showed us that it was possible, using a well-chosen state of the electromagnetic field, to cool an assembly of atoms without having to rely on spontaneous emission of photons into empty modes of the radiation. However, the generation of Fock states, such as the state $|N, N'\rangle$ in this example, is a delicate operation. In a realistic experiment, we manipulate light fields that originate from laser sources and are well described by coherent (or quasi-classical) states of the electromagnetic field, i.e. eigenstates of annihilation operators:

$$\hat{a}_\lambda|\text{coh}\rangle = \alpha_\lambda|\text{coh}\rangle \tag{VI.53}$$

where α_λ is a complex number.

Let us start with a single mode of the field to simplify notations. The eigenstate of $\hat{a}$ with eigenvalue α, which we will denote $|\alpha\rangle$ from now on, can be written explicitly in different ways:

$$\begin{aligned} |\alpha\rangle &= \exp\left(\alpha\hat{a}^\dagger - \alpha^*\hat{a}\right)|0\rangle = \mathrm{e}^{-|\alpha|^2/2}\mathrm{e}^{\alpha\hat{a}^\dagger}|0\rangle \\ &= \mathrm{e}^{-|\alpha|^2/2}\sum_{n=0}^{\infty}\frac{\alpha^n}{\sqrt{n!}}|n\rangle. \end{aligned} \tag{VI.54}$$

In a realistic situation, several modes of the electromagnetic field are populated, corresponding to different wave vectors, polarizations and frequencies. The state of the field at initial time $t = 0$, before interaction with the atoms has begun, can therefore be written as follows

$$|\psi_C(0)\rangle = \hat{\mathcal{D}}[\{\alpha_\lambda\}]\,|\text{vac}\rangle \tag{VI.55}$$

with the unitary operator $\hat{\mathcal{D}}$, called *displacement operator*, defined by:

$$\hat{\mathcal{D}}[\{\alpha_\lambda\}] = \prod_\lambda \exp\left(\alpha_\lambda\hat{a}_\lambda^\dagger - \alpha_\lambda^*\hat{a}_\lambda\right). \tag{VI.56}$$

We will assume that the state of the total system atom+field $|\Psi(0)\rangle$ is factorized at this initial time (no correlation between the two) so that:

$$|\Psi(0)\rangle = |\psi_A(0)\rangle \otimes |\psi_C(0)\rangle. \tag{VI.57}$$

It is then interesting to perform on the state vector of the total system $|\Psi(t)\rangle$ the following unitary transformation, originally suggested by Mollow (1975) [see also Cohen-Tannoudji, Dupont-Roc, et al. (2012), exercise 17]:

$$|\tilde{\Psi}\rangle = \hat{U}(t)|\Psi(t)\rangle \qquad \text{with} \quad \hat{U}(t) = \left(\hat{\mathcal{D}}[\{\alpha_\lambda\,\mathrm{e}^{-\mathrm{i}\omega t}\}]\right)^\dagger. \tag{VI.58}$$

In this unitary transformation, the Schrödinger equation

$$\mathrm{i}\hbar\frac{\mathrm{d}|\Psi(t)\rangle}{\mathrm{d}t} = \hat{H}|\Psi(t)\rangle \tag{VI.59}$$

becomes

$$\mathrm{i}\hbar\frac{\mathrm{d}|\tilde{\Psi}(t)\rangle}{\mathrm{d}t} = \hat{\tilde{H}}(t)|\tilde{\Psi}(t)\rangle \tag{VI.60}$$

[8] A result similar to (VI.51–VI.52) can be obtained by taking $N = 0$, $N' \neq 0$, a situation in which accumulation in $p = 0$ results from spontaneous emission in the mode ω, via a simple optical pumping process.

with the now time-dependent Hamiltonian

$$\hat{\tilde{H}}(t) = \hat{U}(t)\hat{H}\hat{U}^\dagger(t) + \mathrm{i}\hbar\frac{\mathrm{d}\hat{U}(t)}{\mathrm{d}t}\hat{U}^\dagger(t). \tag{VI.61}$$

Before explicitly calculating this new Hamiltonian, let us immediately point out the interest of this unitary transformation: at initial time, the state after unitary transformation is

$$|\Psi(0)\rangle = |\psi_A(0)\rangle \otimes |\mathrm{vac}\rangle. \tag{VI.62}$$

At the cost of an explicit time dependence of the Hamiltonian, we can therefore consider that the electromagnetic field is initially in its ground state, the vacuum of photons.

The transformed Hamiltonian is easily calculated from the relations:

$$\hat{U}(t)\ \hat{a}_\lambda\ \hat{U}^\dagger(t) = \hat{a}_\lambda + \alpha_\lambda\,\mathrm{e}^{-\mathrm{i}\omega t} \tag{VI.63}$$

$$\tag{VI.64}$$

$$\hat{U}(t)\ \hat{a}^\dagger_\lambda\ \hat{U}^\dagger(t) = \hat{a}^\dagger_\lambda + \alpha^*_\lambda\,\mathrm{e}^{+\mathrm{i}\omega t}, \tag{VI.65}$$

which imply that

$$\hat{U}(t)\ \hat{H}_F\ \hat{U}^\dagger(t) + \mathrm{i}\hbar\frac{\mathrm{d}\hat{U}(t)}{\mathrm{d}t}\hat{U}^\dagger(t) = \hat{H}_F. \tag{VI.66}$$

The atomic Hamiltonian is unchanged in the transformation, and the electric dipole coupling becomes

$$\hat{U}(t)\ \hat{\boldsymbol{D}}\cdot\hat{\boldsymbol{E}}(\hat{\boldsymbol{r}})\ \hat{U}^\dagger(t) = \hat{\boldsymbol{D}}\cdot\hat{\boldsymbol{E}}(\hat{\boldsymbol{r}}) + \hat{\boldsymbol{D}}\cdot\boldsymbol{\mathcal{E}}(\hat{\boldsymbol{r}},t) \tag{VI.67}$$

where the function $\boldsymbol{\mathcal{E}}(\boldsymbol{r},t)$ is given by:

$$\boldsymbol{\mathcal{E}}(\boldsymbol{r},t) = \sum_\lambda \mathcal{E}_\lambda\,\boldsymbol{\epsilon}\,\alpha_\lambda\,\mathrm{e}^{\mathrm{i}(\boldsymbol{k}\cdot\boldsymbol{r}-\omega t)} + \mathrm{c.c.} \tag{VI.68}$$

This expression is none other than the classical time-dependent electric field, for which each mode has been given its initial amplitude α_λ.

In the end, the Hamiltonian of the total system can be written as the sum of two terms, $\hat{\tilde{H}}(t) = \hat{H}_1(t) + \hat{H}_2$. The first is time-dependent and relates only to the atomic variables, coupled to the classical field $\boldsymbol{\mathcal{E}}(\boldsymbol{r},t)$:

$$\hat{H}_1(t) = \hat{H}_A - \hat{\boldsymbol{D}}\cdot\boldsymbol{\mathcal{E}}(\hat{\boldsymbol{r}},t). \tag{VI.69}$$

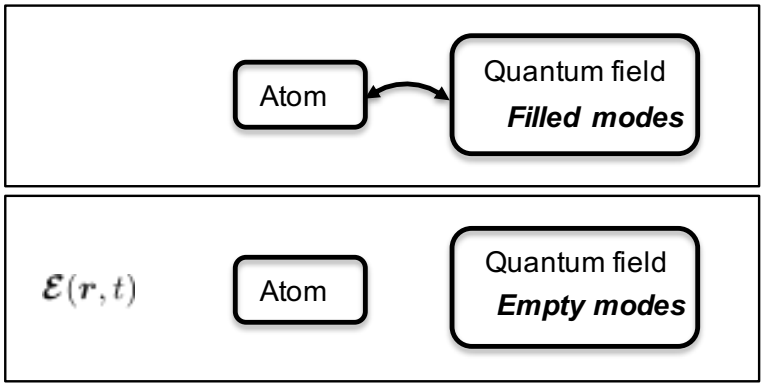

Figure VI.17. *Summary of the unitary transformation (VI.58). The upper figure represents the starting situation, the lower one the situation after transformation.*

The second involves the dynamics of the quantized electromagnetic field and the coupling of the quantum field to the atom:

$$\hat{H}_2 = \hat{H}_F - \hat{\boldsymbol{D}}\cdot\hat{\boldsymbol{E}}(\hat{\boldsymbol{r}}). \tag{VI.70}$$

The outcome of this transformation is therefore remarkable: we arrive at a situation where spontaneous emission phenomena are clearly separated from those linked to absorption and stimulated emission:

- The state of the quantum electromagnetic field after transformation is the photon vacuum (VI.62). The phenomena of absorption and stimulated emission are described by the Hamiltonian $\hat{H}_1(t)$, which involves only the atom's variables, coupled to an externally imposed, time-dependent classical field.
- Spontaneous emission phenomena are described by the Hamiltonian $\hat{H}_2$, with all field modes initially empty and filling up as the atom spontaneously emits photons.

We are then able to answer the initial question of this paragraph for the case of an electromagnetic field initially in a coherent state. If we neglect spontaneous emission phenomena, i.e. the Hamiltonian $\hat{H}_2$, we are back

to a problem of the type considered in (VI.38) via the Hamiltonian $\hat{H}_1(t)$. In this case, we cannot expect to observe an accumulation of atoms in a given quantum state: the eigenvalues of the one-body density operator will be unchanged during the evolution due to atom-field coupling. In other words, spontaneous emission is indispensable for cooling a gas of non-interacting atoms when the radiation is prepared in a coherent state.

4 Conclusions

The first conclusion to be drawn from this course devoted to radiative cooling is the great diversity of mechanisms that have been proposed since the initial idea of Doppler cooling in 1975. Not all of them have been explored experimentally, and we have chosen to describe in this series of lectures only those that have given rise to a detailed and convincing practical study. Despite this restriction, we have not been able to cover all the categories of processes involved in cooling an assembly of atoms with light. Let us mention two of them, which we may return to in subsequent years. Firstly, cavity cooling, which has recently given rise to some spectacular developments [for a review, see for example Ritsch, Domokos, et al. (2013)]. Secondly, mechanisms including a feedback loop on the atoms, inspired by the concept of stochastic cooling widely used in high-energy physics, have been considered, see, for example, the original proposal by Raizen, Koga, et al. (1998).

Nor have we touched on evaporative cooling, which, at the cost of particle losses and relatively long time constants, achieves temperatures comparable to those of optimized radiative cooling (between 0.1 and 1 μK), with spatial densities often considerably greater. The remarkable success of evaporative cooling begs the question: is it worth exploring further the use of cooling mechanisms based on atom-light interaction, which are certainly lossless and faster, but more complicated to implement?

The final conclusion of this course will be a doubly positive answer to this question. Firstly, evaporative cooling, however effective, also has its limitations. A high-energy particle evaporates when it reaches the edges of the sample, which means that cooling is not homogeneous; it is more effective at the periphery of the gas than at the center, which can be a significant bias in certain situations. Moreover, radiative cooling, transposed to assemblies of interacting atoms, can provide a tool for exploring new phases of matter. The principle of dark-state cooling, for example, can be transposed to an assembly of atoms to prepare strongly correlated N-body states that could not be reached by standard Hamiltonian evolution [see, for example, Bardyn, Baranov, et al. (2013)]. Dissipative N-body physics is still in its infancy in the field of quantum gases, but the concepts developed over the last forty years for cooling individual atoms with light will undoubtedly play a key role.

Bibliography

Arcizet, Olivier, P-F Cohadon, Tristan Briant, Michel Pinard & Antoine Heidmann (2006), "Radiation-pressure cooling and optomechanical instability of a micromirror", in *Nature* **444**, pp. 71–74.

Arimondo, E. (1996), "Coherent population trapping in laser spectroscopy", in *Progress in Optics, vol. 35*, ed. by E. Wolf, Elsevier, , p. 259.

Aspect, A., E. Arimondo, R. Kaiser, N. Vansteenkiste & C. Cohen-Tannoudji (1988), "Laser Cooling below the One-Photon-Recoil Energy by Velocity-Selective Coherent Population Trapping", in *Phys. Rev. Lett.* **61**, p. 826.

– (1989), "Laser cooling below the one-photon recoil energy by velocity-selective coherent population trapping: theoretical analysis", in *JOSA B* **6**, p. 2112.

Aspelmeyer, Markus, Tobias J. Kippenberg & Florian Marquardt (2014), "Cavity optomechanics", in *Rev. Mod. Phys.* **86** (4), pp. 1391–1452.

Bakr, W. S., A. Peng, S. Folling & M. Greiner (2009), "A quantum gas microscope for detecting single atoms in a Hubbard-regime optical lattice", in *Nature* **462**, pp. 74–77.

Bardou, F., J.-P. Bouchaud, A. Aspect & C. Cohen-Tannoudji (2002), *Levy statistics and laser cooling*, Cambridge University Press.

Bardou, F., J. P. Bouchaud, O. Emile, A. Aspect & C. Cohen-Tannoudji (1994), "Subrecoil laser cooling and Lévy flights", in *Phys. Rev. Lett.* **72** (2), pp. 203–206.

Bardyn, C-E, M A Baranov, C V Kraus, E Rico, A Imamoğlu, P Zoller & S Diehl (2013), "Topology by dissipation", in *New Journal of Physics* **15**, p. 085001.

Barry, JF, DJ McCarron, EB Norrgard, MH Steinecker & D DeMille (2014), "Magneto-optical trapping of a diatomic molecule", in *Nature* **512**, pp. 286–289.

Ben Dahan, Maxime, Ekkehard Peik, Jakob Reichel, Yvan Castin & Christophe Salomon (1996), "Bloch Oscillations of Atoms in an Optical Potential", in *Phys. Rev. Lett.* **76** (24), pp. 4508–4511.

Bernier, Jean-Sébastien, Corinna Kollath, Antoine Georges, Lorenzo De Leo, Fabrice Gerbier, Christophe Salomon & Michael Köhl (2009), "Cooling fermionic atoms in optical lattices by shaping the confinement", in *Phys. Rev. A* **79** (6), p. 061601.

Bloom, BJ, TL Nicholson, JR Williams, SL Campbell, M Bishof, X Zhang, W Zhang, SL Bromley & J Ye (2014), "An optical lattice clock with accuracy and stability at the 10-18 level", in *Nature* **506**, pp. 71–75.

Boiron, D., A. Michaud, J. M. Fournier, L. Simard, M. Sprenger, G. Grynberg & C. Salomon (1998), "Cold and dense cesium clouds in far-detuned dipole traps", in *Phys. Rev. A* **57**, R4106.

Boiron, D., A. Michaud, P. Lemonde, Y. Castin, C. Salomon, S. Weyers, K. Szymaniec, L. Cognet & A. Clairon (1996), "Laser cooling of cesium atoms in gray optical molasses down to 1.1 μK", in *Phys. Rev. A* **53** (6), R3734–R3737.

Boiron, D., C. Triché, D. R. Meacher, P. Verkerk & G. Grynberg (1995), "Three-dimensional cooling of cesium atoms in four-beam gray optical molasses", in *Phys. Rev. A* **52** (5), R3425–R3428.

Bouchaud, Jean-Philippe & Antoine Georges (1990), "Anomalous diffusion in disordered media: statistical mechanisms, models and physical applications", in *Physics reports* **195**, pp. 127–293.

Bouchoule, I., H. Perrin, A. Kuhn, M. Morinaga & C. Salomon (1999), "Neutral atoms prepared in Fock states of a one-dimensional harmonic potential", in *Phys. Rev. A* **59** (1), R8–R11.

Boyer, V., L. J. Lising, S. L. Rolston & W. D. Phillips (2004), "Deeply subrecoil two-dimensional Raman cooling", in *Phys. Rev. A* **70**.

Burchianti, A., G. Valtolina, J. A. Seman, E. Pace, M. De Pas, M. Inguscio, M. Zaccanti & G. Roati (2014), "Efficient all-optical production of large ^{6}Li quantum gases using D_1 gray-molasses cooling", in *Phys. Rev. A* **90** (4), p. 043408.

Castin, Y., J. I. Cirac & M. Lewenstein (1998), "Reabsorption of Light by Trapped Atoms", in *Phys. Phys. Lett.* **80**, p. 5305.

Castin, Y. & J. Dalibard (1991), "Quantization of atomic motion in optical molasses", in *Europhys. Lett.* **14**, p. 761.

Castin, Y, J Dalibard & C Cohen-Tannoudji (1991), "The limits of Sisyphus cooling.", in *Light Induced Kinetic Effects on Atoms, Ions and Molecules*, ed. by L. Moi, S. Gozzini, C. Gabbanini, E. Arimondo & F. Strumia, Pisa, Italy: ETS Editrice.

Castin, Y., H. Wallis & J. Dalibard (1989), "Limit of Doppler cooling", in *J. Opt. Soc. Am. B* **6**, p. 2046.

Castin, Yvan & Klaus Mølmer (1995), "Monte Carlo Wave-Function Analysis of 3D Optical Molasses", in *Phys. Rev. Lett.* **74** (19), pp. 3772–3775.

Chalony, M., A. Kastberg, B. Klappauf & D. Wilkowski (2011), "Doppler Cooling to the Quantum Limit", in *Phys. Rev. Lett.* **107** (24), p. 243002.

Chang, R., A. L. Hoendervanger, Q. Bouton, Y. Fang, T. Klafka, K. Audo, A. Aspect, C. I. Westbrook & D. Clément (2014), "Three-dimensional laser cooling at the Doppler limit", in *Phys. Rev. A* **90** (6), p. 063407.

Cheuk, Lawrence W., Matthew A. Nichols, Melih Okan, Thomas Gersdorf, Vinay V. Ramasesh, Waseem S. Bakr, Thomas Lompe & Martin W. Zwierlein (2015), "Quantum-Gas Microscope for Fermionic Atoms", in *Phys. Rev. Lett.* **114** (19), p. 193001.

Chu, S., L. Hollberg, J. E. Bjorkholm, A. Cable & A. Ashkin (1985), "Three-Dimensional Viscous Confinement and Cooling of Atoms by Resonance Radiation Pressure", in *Phys. Rev. Lett.* **55**, p. 48.

Cirac, J. I., M. Lewenstein & P. Zoller (1996), "Collective laser cooling of trapped atoms", in *Europhysics Letters* **35**, p. 647.

Cohen-Tannoudji, Claude, Jacques Dupont-Roc & Gilbert Grynberg (2012), *Processus d'interaction entre photons et atomes*, Edp Sciences.

Cooper, C. J., G. Hillenbrand, J. Rink, C. G. Townsend, K. Zetie & C. J. Foot (1994), "The temperature of atoms in a magneto-optical trap", in *Europhys. Lett.* **28**, p. 397.

Corder, Christopher, Brian Arnold & Harold Metcalf (2015), "Laser Cooling without Spontaneous Emission", in *Phys. Rev. Lett.* **114** (4), p. 043002.

Dalibard, J. (1988), "Laser cooling of an optically thick gas: the simplest radiation pressure trap?", in *Optics Comm.* **68**, p. 203.

Dalibard, J. & C. Cohen-Tannoudji (1989), "Laser cooling below the Doppler limit by polarization gradients: simple theoretical models", in *J. Opt. Soc. Am. B* **6**, p. 2023.

Davidson, N., H. J. Lee, M. Kasevich & S. Chu (1994), "Raman Cooling of Atoms in Two and Three Dimensions", in *Phys. Rev. Lett.* **72**, p. 3158.

Desbiolles, Pierre, Markus Arndt, Pascal Szriftgiser & Jean Dalibard (1996), "Elementary Sisyphus process close to a dielectric surface", in *Phys. Rev. A* **54** (5), pp. 4292–4298.

Diedrich, F., J. C. Bergquist, W. M. Itano & D. J. Wineland (1989), "Sideband cooling in an ion trap", in *Phys. Rev. Lett.* **62**, p. 403.

Drewsen, M., P. Laurent, A. Nadir, G. Santarelli, A. Clairon, Y. Castin, D. Grison & C. Salomon (1994), "Investigation of sub-Doppler cooling effects in a cesium magneto-optical trap", in *Appl. Phys. B* **59**, p. 283.

Einstein, Albert (1916), "Strahlungs-emission und absorption nach der quantentheorie", in *Deutsche Physikalische Gesellschaft* **18**, pp. 318–323.

Einstein, Albert (1917), "Zur Quantentheorie der Strahlung [traduction française par F. Balibar, B. Jech et O. Darrigol]", in *Physikaliche Zeitschrift* **18**, p. 121.

Ertmer, W., R. Blatt, J. L. Hall & M. Zhu (1985), "Laser Manipulation of Atomic Beam Velocities: Demonstration of Stopped Atoms and Velocity Reversal", in *Phys. Rev. Lett.* **54**, p. 996.

Fano, U. (1961), "Effects of Configuration Interaction on Intensities and Phase Shifts", in *Phys. Rev.* **124** (6), pp. 1866–1878.

Fernandes, D. Rio, F. Sievers, N. Kretzschmar, S. Wu, C. Salomon & F. Chevy (2012), "Sub-Doppler laser cooling of fermionic 40 K atoms in three-dimensional gray optical molasses", in *EPL (Europhysics Letters)* **100**, p. 63001.

Fleischhauer, Michael, Atac Imamoglu & Jonathan P Marangos (2005), "Electromagnetically induced transparency: Optics in coherent media", in *Reviews of modern physics* **77**, p. 633.

Förster, Leonid, Michał Karski, Jai-Min Choi, Andreas Steffen, Wolfgang Alt, et al. (2009), "Microwave Control of Atomic Motion in Optical Lattices", in *Phys. Rev. Lett.* **103** (23), p. 233001.

Fuhrmanek, A., R. Bourgain, Y. R. P. Sortais & A. Browaeys (2012), "Light-assisted collisions between a few cold atoms in a microscopic dipole trap", in *Phys. Rev. A* **85** (6), p. 062708.

Gerz, C., T. W. Hodapp, P. Jessen, K. M. Jones, W. D. Phillips, C. I. Westbrook & K. Molmer (1993), "The Temperature of Optical Molasses for Two Different Atomic Angular Momenta", in *EPL (Europhysics Letters)* **21**, p. 661.

Gigan, S, HR Böhm, M Paternostro, F Blaser, G Langer, JB Hertzberg, KC Schwab, D Bäuerle, M Aspelmeyer & A Zeilinger (2006), "Self-cooling of a micromirror by radiation pressure", in *Nature* **444**, pp. 67–70.

Gordon, J. P. & A. Ashkin (1980), "Motion of atoms in a radiation trap", in *Phys. Rev. A* **21**, pp. 1606–1617.

Grier, Andrew T., Igor Ferrier-Barbut, Benno S. Rem, Marion Delehaye, Lev Khaykovich, Frédéric Chevy & Christophe Salomon (2013), "Λ-enhanced sub-Doppler cooling of lithium atoms in D_1 gray molasses", in *Phys. Rev. A* **87** (6), p. 063411.

Grynberg, G & C Robilliard (2001), "Cold atoms in dissipative optical lattices", in *Physics Reports* **355**, 335–451.

Haller, Elmar, James Hudson, Andrew Kelly, Dylan A Cotta, Bruno Peaudecerf, Graham D Bruce & Stefan Kuhr (2015), "Single-atom imaging of fermions in a quantum-gas microscope", in *arXiv preprint arXiv:1503.02005*.

Hamann, S. E., D. L. Haycock, G. Klose, P. H. Pax, I. H. Deutsch & P. S. Jessen (1998), "Resolved-Sideband Raman Cooling to the Ground State of an Optical Lattice", in *Phys. Rev. Lett.* **80** (19), pp. 4149–4152.

Han, Dian-Jiun, Steffen Wolf, Steven Oliver, Colin McCormick, Marshall T. DePue & David S. Weiss (2000), "3D Raman Sideband Cooling of Cesium Atoms at High Density", in *Phys. Rev. Lett.* **85** (4), pp. 724–727.

Hänsch, T. W. & A. L. Schawlow (1975), "Cooling of gases by laser radiation", in *Optics Comm.* **13**, p. 68.

Harris, Stephen E (1997), "Electromagnetically induced transparency", in *Physics Today* **50**, pp. 36–42.

Heinzen, D. J. & D. J. Wineland (1990), "Quantum-limited cooling and detection of radio-frequency oscillations by laser-cooled ions", in *Phys. Rev. A* **42** (5), pp. 2977–2994.

Hemmerich, A., M. Weidemüller, T. Esslinger, C. Zimmermann & T. Hänsch (1995), "Trapping Atoms in a Dark Optical Lattice", in *Phys. Rev. Lett.* **75** (1), pp. 37–40.

Huang, K. (1987), *Statistical Mechanics*, New York: Wiley.

Hummon, Matthew T., Mark Yeo, Benjamin K. Stuhl, Alejandra L. Collopy, Yong Xia & Jun Ye (2013), "2D Magneto-Optical Trapping of Diatomic Molecules", in *Phys. Rev. Lett.* **110** (14), p. 143001.

Ido, Tetsuya, Yoshitomo Isoya & Hidetoshi Katori (2000), "Optical-dipole trapping of Sr atoms at a high phase-space density", in *Phys. Rev. A* **61** (6), p. 061403.

Janik, G, W Nagourney & H Dehmelt (1985), "Doppler-free optical spectroscopy on the Ba+ mono-ion oscillator", in *JOSA B* **2**, pp. 1251–1257.

Julienne, P.S., A.M. Smith & K. Burnett (1992), "Theory of Collisions between Laser Cooled Atoms", in *Advances In Atomic, Molecular, and Optical Physics*, ed. by David Bates & Benjamin Bederson, vol. 30, Academic Press, , p. 141.

Kasevich, M. & S. Chu (1992), "Laser Cooling below a Photon Recoil with Three-Level Atoms", in *Phys. Rev. Lett.* **69**, p. 1741.

Kastberg, A., W. D. Phillips, S. L. Rolston, R. J. C. Spreeuw & P. S. Jessen (1995), "Adiabatic Cooling of Cesium to 700 nK in an Optical Lattice", in *Phys. Rev. Lett.* **74** (9), pp. 1542–1545.

Katori, H., T. Ido, Y. Isoya & M. Kuwata-Gonokami (1999), "Magneto-optical trapping and cooling of Strontium atoms down to the photon recoil temperature", in *Phys. Rev. Lett.* **82**, p. 116.

Kaufman, A. M., B. J. Lester & C. A. Regal (2012), "Cooling a Single Atom in an Optical Tweezer to Its Quantum Ground State", in *Phys. Rev. X* **2** (4), p. 041014.

Kerman, Andrew J., Vladan Vuletic, Cheng Chin & Steven Chu (2000), "Beyond Optical Molasses: 3D Raman Sideband Cooling of Atomic Cesium to High Phase-Space Density", in *Phys. Rev. Lett.* **84** (3), pp. 439–442.

Ketterle, W., K. B. Davis, M. A. Joffe, A. Martin & D. E. Pritchard (1992), "High-Densities of Cold Atoms in a Dark Spontaneous-Force Optical Trap", in *Phys. Rev. Lett.* **70**, p. 2253.

Ketterle, W. & D. E. Pritchard (1992), "Atom Cooling By Time-Dependent Potentials", in *Phys. Rev. A* **46**, pp. 4051–4054.

Kim, Kihwan, Heung-Ryoul Noh & Wonho Jhe (2004), "Parametric resonance in an intensity-modulated magneto-optical trap", in *Optics Communications* **236**, pp. 349 –361.

Lawall, J., F. Bardou, B. Saubamea, K. Shimizu, M. Leduc, A. Aspect & C. Cohen-Tannoudji (1994), "Two-Dimensional Subrecoil Laser Cooling", in *Phys. Rev. Lett.* **73**, p. 1915.

Lawall, J., S. Kulin, B. Saubamea, N. Bigelow, M. Leduc & C. Cohen-Tannoudji (1994), "Three-Dimensional Laser Cooling of Helium Beyond the Single-Photon Recoil Limit", in *Phys. Rev. Lett.* **75**, p. 4194.

Lee, H. J., C. S. Adams, M. Kasevich & S. Chu (1996), "Raman cooling of atoms in an optical dipole trap", in *Phys. Rev. Lett.* **76**, p. 2658.

Lee, H. J. & S. Chu (1998), "Atomic spin polarization by Raman cooling", in *Phys. Rev. A* **57**, p. 2905.

Lett, P. D., W. D. Phillips, S. L. Rolston, C. E. Tanner, R. N. Watts & C. I. Westbrook (1989), "Optical Molasses", in *J. Opt. Soc. Am. B* **6**, p. 2084.

Lett, P. D., R. N. Watts, C. I. Westbrook, W. D. Phillips, P. L. Gould & H. J. Metcalf (1988a), "Observation of Atoms Laser Cooled below the Doppler Limit", in *Phys. Rev. Lett.* **61**, p. 169.

– (1988b), "Observation of Atoms Laser Cooled below the Doppler Limit", in *Phys. Rev. Lett.* **61**, p. 169.

Li, Xiao, Theodore A. Corcovilos, Yang Wang & David S. Weiss (2012), "3D Projection Sideband Cooling", in *Phys. Rev. Lett.* **108** (10), p. 103001.

Loftus, Thomas H., Tetsuya Ido, Martin M. Boyd, Andrew D. Ludlow & Jun Ye (2004), "Narrow line cooling and momentum-space crystals", in *Phys. Rev. A* **70** (6), p. 063413.

Lounis, B. & C. Cohen-Tannoudji (1992), "Coherent population trapping and Fano profiles", in *J. Phys II France* **2**, p. 579.

McFerran, J.J., L. Yi, S. Mejri & S. Bize (2010), "Sub-Doppler cooling of fermionic Hg isotopes in a magneto-optical trap", in *Opt. Lett.* **35**, p. 3078.

Minogin, VG & OT Serimaa (1979), "Resonant light pressure forces in a strong standing laser wave", in *Optics Communications* **30**, 373–379.

Moler, Kathryn, David S. Weiss, Mark Kasevich & Steven Chu (1992), "Theoretical analysis of velocity-selective Raman transitions", in *Phys. Rev. A* **45** (1), pp. 342–348.

Mollow, B. R. (1975), "Pure-state analysis of resonant light scattering: Radiative damping, saturation, and multiphoton effects", in *Phys. Rev. A* **12** (5), pp. 1919–1943.

Mølmer, Klaus, Yvan Castin & Jean Dalibard (1993), "Monte Carlo wavefunction method in quantum optics", in *JOSA B* **10**, pp. 524–538.

Monroe, C., D. M. Meekhof, B. E. King, S. R. Jefferts, W. M. Itano, D. J. Wineland & P. Gould (1995), "Resolved-Sideband Raman Cooling of a Bound Atom to the 3D Zero-Point Energy", in *Phys. Rev. Lett.* **75** (22), pp. 4011–4014.

Morigi, Giovanna, Jürgen Eschner & Christoph H. Keitel (2000), "Ground State Laser Cooling Using Electromagnetically Induced Transparency", in *Phys. Rev. Lett.* **85** (21), pp. 4458–4461.

Morinaga, M., I. Bouchoule, J.-C. Karam & C. Salomon (1999), "Manipulation of Motional Quantum States of Neutral Atoms", in *Phys. Rev. Lett.* **83** (20), pp. 4037–4040.

Nath, Dipankar, R Kollengode Easwaran, G. Rajalakshmi & C. S. Unnikrishnan (2013), "Quantum-interference-enhanced deep sub-Doppler cooling of ^{39}K atoms in gray molasses", in *Phys. Rev. A* **88** (5), p. 053407.

Nelson, K. D., X. Li & D. S. Weiss (2007), "Imaging single atoms in a three-dimensional array", in *Nature Physics* **3**, pp. 556–560.

Nicholson, TL, SL Campbell, RB Hutson, GE Marti, BJ Bloom, RL McNally, W Zhang, MD Barrett, MS Safronova, GF Strouse, et al. (2015), "Systematic evaluation of an atomic clock at 2 [times] 10-18 total uncertainty", in *Nature communications* **6**.

Olshanii, M., Y. Castin & J. Dalibard (1996), "Laser Spectroscopy XII", in , ed. by M. Inguscio, M. Allegrini & A. Sasso, Singapore: World Scientific, , pp. 7–12.

Ol'shanii, M.A. & V.G. Minogin (1992), "Three-dimensional velocity-selective coherent population trapping of a (3+3)-level atom", in *Optics Communications* **89**, p. 393.

Ovchinnikov, Y. B., I. Manek & R. Grimm (1997), "Surface trap for Cs atoms based on evanescent-wave cooling", in *Phys. Rev. Lett.* **79**, p. 2225.

Parsons, Maxwell F., Florian Huber, Anton Mazurenko, Christie S. Chiu, Widagdo Setiawan, Katherine Wooley-Brown, Sebastian Blatt & Markus Greiner (2015), "Site-Resolved Imaging of Fermionic ^{6}Li in an Optical Lattice", in *Phys. Rev. Lett.* **114** (21), p. 213002.

Patil, Y. S., S. Chakram, L. M. Aycock & M. Vengalattore (2014), "Nondestructive imaging of an ultracold lattice gas", in *Phys. Rev. A* **90** (3), p. 033422.

Perrin, H, A Kuhn, I Bouchoule, T Pfau & C Salomon (1999), "Raman cooling of spin-polarized cesium atoms in a crossed dipole trap", in *EPL (Europhysics Letters)* **46**, p. 141.

Perrin, H., A. Kuhn, I. Bouchoule & C. Salomon (1998), "Sideband cooling of neutral atoms in a far-detuned optical lattice", in *EPL (Europhysics Letters)* **42**, p. 395.

Pinkse, P. W. H., A. Mosk, M. Weidemüller, M. W. Reynolds, T. W. Hijmans & J. T. M. Walraven (1997), "Adiabatically changing the phase-space density of a trapped Bose gas", in *Phys. Rev. Lett.* **78**, p. 990.

Prodan, John, Alan Migdall, William D. Phillips, Ivan So, Harold Metcalf & Jean Dalibard (1985), "Stopping Atoms with Laser Light", in *Phys. Rev. Lett.* **54** (10), pp. 992–995.

Pruvost, Laurence, Isabelle Serre, Hong Tuan Duong & Joshua Jortner (2000), "Expansion and cooling of a bright rubidium three-dimensional optical molasses", in *Phys. Rev. A* **61** (5), p. 053408.

Raab, E. L., M. Prentiss, A. Cable, S. Chu & D. E. Pritchard (1987), "Trapping of Neutral Sodium with Radiation Pressure", in *Phys. Rev. Lett.* **59**, p. 2631.

Raizen, MG, J Koga, B Sundaram, Y Kishimoto, H Takuma & T Tajima (1998), "Stochastic cooling of atoms using lasers", in *Physical Review A* **58**, p. 4757.

Reichel, J., F. Bardou, M. B. Dahan, E. Peik, S. Rand, C. Salomon & C. Cohen-Tannoudji (1995), "Raman Cooling of Cesium below 3 nK: New Approach Inspired by Lévy Flights Statistics", in *Phys. Rev. Lett.* **75**, p. 4575.

Ritsch, Helmut, Peter Domokos, Ferdinand Brennecke & Tilman Esslinger (2013), "Cold atoms in cavity-generated dynamical optical potentials", in *Reviews of Modern Physics* **85**, p. 553.

Salomon, C., J. Dalibard, W. D. Phillips, A. Clairon & S. Guellati (1990), "Laser Cooling of Cesium Atoms Below 3 μK", in *EPL (Europhysics Letters)* **12**, p. 683.

Salomon, G., L. Fouché, P. Wang, A. Aspect, P. Bouyer & T. Bourdel (2013), "Gray-molasses cooling of 39 K to a high phase-space density", in *EPL (Europhysics Letters)* **104**, p. 63002.

Schliesser, Albert, Pascal Del'Haye, Nima Nooshi, KJ Vahala & TJ Kippenberg (2006), "Radiation pressure cooling of a micromechanical oscillator using dynamical backaction", in *Physical Review Letters* **97**, p. 243905.

Sesko, David W, TG Walker & Carl E Wieman (1991), "Behavior of neutral atoms in a spontaneous force trap", in *JOSA B* **8**, pp. 946–958.

Shahriar, M. S., P. R. Hemmer, M. G. Prentiss, P. Marte, J. Mervis, D. P. Katz, N. P. Bigelow & T. Cai (1993), "Continuous polarization-gradient precooling-assisted velocity-selective coherent population trapping", in *Phys. Rev. A* **48** (6), R4035–R4038.

Sherson, Jacob F., Christof Weitenberg, Manuel Endres, Marc Cheneau, Immanuel Bloch & Stefan Kuhr (2010), "Single-atom-resolved fluorescence imaging of an atomic Mott insulator", in *Nature* **467**, 68.

Sievers, Franz, Norman Kretzschmar, Diogo Rio Fernandes, Daniel Suchet, Michael Rabinovic, Saijun Wu, Colin V. Parker, Lev Khaykovich, Christophe Salomon & Frédéric Chevy (2015), "Simultaneous sub-Doppler laser cooling of fermionic ^{6}Li and ^{40}K on the D_1 line: Theory and experiment", in *Phys. Rev. A* **91** (2), p. 023426.

Sortais, Y, S Bize, C Nicolas, A Clairon, Ch Salomon & C Williams (2000), "Cold collision frequency shifts in a 87 Rb atomic fountain", in *Physical Review Letters* **85**, p. 3117.

Stamper-Kurn, D. M., H.-J. Miesner, A. P. Chikkatur, S. Inouye, J. Stenger & W. Ketterle (1998), "Reversible formation of a Bose–Einstein condensate", in *Phys. Rev. Lett.* **81**, p. 2194.

Stefano, Andrea di, Marie Fauquembergue, Philippe Verkerk & Daniel Hennequin (2003), "Giant oscillations in a magneto-optical trap", in *Phys. Rev. A* **67** (3), p. 033404.

Stellmer, Simon, Benjamin Pasquiou, Rudolf Grimm & Florian Schreck (2013), "Laser Cooling to Quantum Degeneracy", in *Phys. Rev. Lett.* **110** (26), p. 263003.

Terças, Hugo, J Tito Mendonça & Robin Kaiser (2010), "Driven collective instabilities in magneto-optical traps: A fluid-dynamical approach", in *EPL (Europhysics Letters)* **89**, p. 53001.

Thompson, J. D., T. G. Tiecke, A. S. Zibrov, V. Vuletic & M. D. Lukin (2013), "Coherence and Raman Sideband Cooling of a Single Atom in an Optical Tweezer", in *Phys. Rev. Lett.* **110** (13), p. 133001.

Townsend, C. G., N. H. Edwards, C. J. Cooper, K. P. Zetie, C. J. Foot, A. M. Steane, P. Szriftgiser, H. Perrin & J. Dalibard (1995), "Phase-space density in the magneto-optical trap", in *Phys. Rev. A* **52**, p. 1423.

Ungar, P. J., D. S. Weiss, E. Riis & S. Chu (1989), "Optical molasses and multilevel atoms: Theory", in *J. Opt. Soc. Am. B* **6**, p. 2058.

Valentin, C., M.-C. Gagné, J. Yu & P. Pillet (1992), "One-Dimension Sub-Doppler Molasses in the Presence of Static Magnetic Field", in *EPL (Europhysics Letters)* **17**, p. 133.

Van Kampen, Nicolaas Godfried (1992), *Stochastic processes in physics and chemistry*, vol. 1, Elsevier.

Vuletic, Vladan, Cheng Chin, Andrew J. Kerman & Steven Chu (1998), "Degenerate Raman Sideband Cooling of Trapped Cesium Atoms at Very High Atomic Densities", in *Phys. Rev. Lett.* **81** (26), pp. 5768–5771.

Walker, T., D. Sesko & C. Wieman (1990), "Collective Behavior of Optically Trapped Neutral Atoms", in *Phys. Rev. Lett.* **64**, p. 408.

Wallis, H & W Ertmer (1989), "Broadband laser cooling on narrow transitions", in *JOSA B* **6**, pp. 2211–2219.

Weidemüller, M., T. Esslinger, M. A. Ol'shanii, A. Hemmerich & T. W. Hänsch (1994), "A Novel Scheme for Efficient Cooling below the Photon Recoil Limit", in *EPL (Europhysics Letters)* **27**, p. 109.

Wilkowski, David, Jean Ringot, Daniel Hennequin & Jean Claude Garreau (2000), "Instabilities in a Magneto-optical Trap: Noise-Induced Dynamics in an Atomic System", in *Phys. Rev. Lett.* **85** (9), pp. 1839–1842.

Wineland, D. J. & H. Dehmelt (1975), "Proposed $10^{14}\Delta\nu < \nu$ laser fluorescence spectroscopy on TI^{+} mono-ion oscillator III", in *Bulletin of the Americal Physical Society* **20**, p. 637.

Wineland, D. J. & Wayne M. Itano (1979), "Laser cooling of atoms", in *Phys. Rev. A* **20** (4), pp. 1521–1540.

Wohlleben, W., F. Chevy, K. W. Madison & J. Dalibard (2001), "An atom faucet", in *Eur. Phys. J. D* **15**, pp. 237–244.

Wolf, Steffen, Steven J. Oliver & David S. Weiss (2000), "Suppression of Recoil Heating by an Optical Lattice", in *Phys. Rev. Lett.* **85** (20), pp. 4249–4252.

Zeppenfeld, Martin, Barbara GU Englert, Rosa Glöckner, Alexander Prehn, Manuel Mielenz, Christian Sommer, Laurens D van Buuren, Michael Motsch & Gerhard Rempe (2012), "Sisyphus cooling of electrically trapped polyatomic molecules", in *Nature* **491**, pp. 570–573.